AGARD-R-800

AGARD

ADVISORY GROUP FOR AEROSPACE RESEARCH & DEVELOPMENT
7 RUE ANCELLE, 92200 NEUILLY-SUR-SEINE, FRANCE

AGARD REPORT 800

The Design, Qualification and Maintenance of Vibration-Free Landing Gear

(la Conception, la qualification et la maintenance des trains d'atterrissage sans vibration)

Papers presented at the 81st Meeting of the AGARD Structures and Materials Panel, held in Banff, Canada 4-5 October 1995.

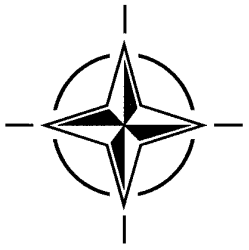

NORTH ATLANTIC TREATY ORGANIZATION

Published March 1996

Distribution and Availability on Back Cover

AGARD-R-800

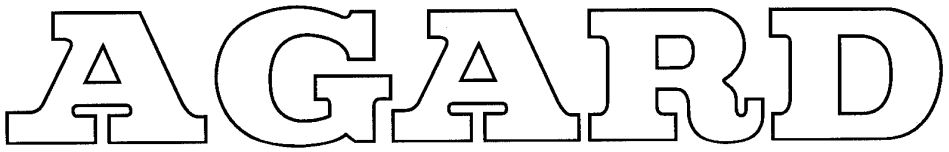

ADVISORY GROUP FOR AEROSPACE RESEARCH & DEVELOPMENT
7 RUE ANCELLE, 92200 NEUILLY-SUR-SEINE, FRANCE

AGARD REPORT 800

The Design, Qualification and Maintenance of Vibration-Free Landing Gear

(la Conception, la qualification et la maintenance
des trains d'atterrissage sans vibration)

Papers presented at the 81st Meeting of the AGARD Structures and Materials Panel, held in Banff, Canada 4-5 October 1995.

North Atlantic Treaty Organization
Organisation du Traité de l'Atlantique Nord

DISCLAIMER NOTICE

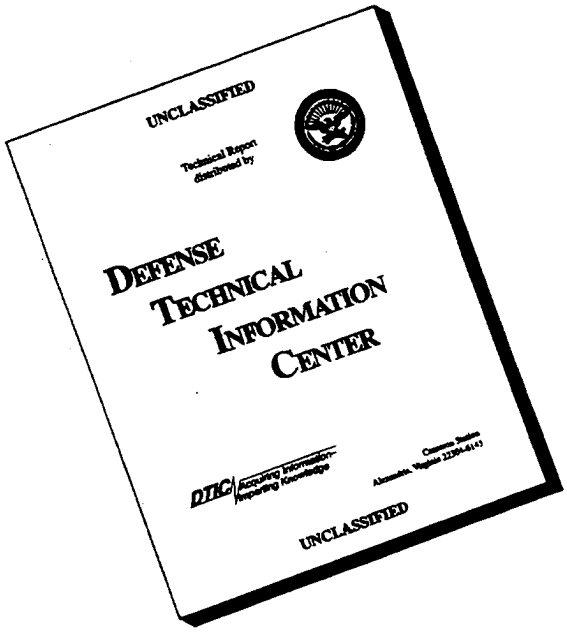

THIS DOCUMENT IS BEST QUALITY AVAILABLE. THE COPY FURNISHED TO DTIC CONTAINED A SIGNIFICANT NUMBER OF PAGES WHICH DO NOT REPRODUCE LEGIBLY.

The Mission of AGARD

According to its Charter, the mission of AGARD is to bring together the leading personalities of the NATO nations in the fields of science and technology relating to aerospace for the following purposes:

- Recommending effective ways for the member nations to use their research and development capabilities for the common benefit of the NATO community;
- Providing scientific and technical advice and assistance to the Military Committee in the field of aerospace research and development (with particular regard to its military application);
- Continuously stimulating advances in the aerospace sciences relevant to strengthening the common defence posture;
- Improving the co-operation among member nations in aerospace research and development;
- Exchange of scientific and technical information;
- Providing assistance to member nations for the purpose of increasing their scientific and technical potential;
- Rendering scientific and technical assistance, as requested, to other NATO bodies and to member nations in connection with research and development problems in the aerospace field.

The highest authority within AGARD is the National Delegates Board consisting of officially appointed senior representatives from each member nation. The mission of AGARD is carried out through the Panels which are composed of experts appointed by the National Delegates, the Consultant and Exchange Programme and the Aerospace Applications Studies Programme. The results of AGARD work are reported to the member nations and the NATO Authorities through the AGARD series of publications of which this is one.

Participation in AGARD activities is by invitation only and is normally limited to citizens of the NATO nations.

Published March 1996

ISBN 92-836-1032-6

Printed by Canada Communication Group
45 Sacré-Cœur Blvd., Hull (Québec), Canada K1A 0S7

The Design, Qualification and Maintenance of Vibration-Free Landing Gear

(AGARD R-800)

Executive Summary

Aircraft landing gears are crucial for safety, comfort (both for passengers and pilots) and for weight considerations. As the element responsible for safely moving the aircraft on the ground, the landing gear has to fulfill several, sometimes conflicting, requirements.

Landing gears that shimmy (shimmy can be defined as a self-excited instability during take-off, landing or taxiing, involving up to three vibration motions: angular wheel motions about a vertical axis - yaw -, and a fore and aft axis - roll -, and lateral displacement of the wheel) are unacceptable. In fact, a severe occurrence of shimmy can damage the landing gear and its attaching structure, resulting in significant repair costs and airplane down time. Some assurance is therefore needed that landing gear designs will be free from shimmy under all operating conditions including the normal wear and tear experienced in service.

One of the difficulties of shimmy analysis is that real landing gear systems exhibit many non-linear characteristics. Tests on life-size aircraft are obviously expensive and risky, and tests on test-rigs (namely drop-test facilities) allow only for limited information about the landing gear's dynamics; the interaction between aircraft and landing gear is especially difficult to assess. On the other hand, simulation offers a means to examine the behaviour of the landing gear as part of a complex system at a reasonable cost. Both rigid and elastic body motions can be modelled.

In view of the problems involved in correcting landing gear vibrations emerging late in the design process or even after delivery of the aircraft to service, the Workshop participants concluded that the state of the art of analyzing landing gear vibrations is not quite up to other similar subjects and that the cooperation of experts across aircraft, landing gear and tyre industry institutions is badly needed.

Workshop participants did not expect rapid progress unless there was a well planned and coordinated approach to the problem. They unanimously identified AGARD as the only institution which had enough power and authority to promote such a coordinated effort in the interest of NATO member nations.

L'étude, l'homologation et la maintenance des trains d'atterrissage à amortissement

(AGARD R-800)

Synthèse

Le train d'atterrissage d'un aéronef est un élément déterminant pour la sécurité et le confort des passagers et des équipages, en plus des considérations de coefficient de chargement. C'est le train d'atterrissage qui autorise le déplacement de l'avion au sol dans des conditions de sécurité acceptables. Il doit, par conséquent, satisfaire à plusieurs critères, qui sont parfois contradictoires.

Les trains d'atterrissage sujets au shimmy sont inacceptables (le shimmy étant défini comme une instabilité auto-excitée qui se produit lors du décollage, de l'atterrissage ou du roulement au sol et qui comprend jusqu'à trois mouvements: les mouvements angulaires de roue autour d'un axe vertical, c'est à dire de lacet, les mouvements autour d'un axe longitudinal, c'est à dire le roulis, et le déplacement latéral de la roue). En effet, un phénomène grave de shimmy peut occasionner l'endommagement du train d'atterrissage et de ses points de fixation, nécessitant des réparations coûteuses entraînant l'immobilisation de l'appareil. Par conséquent, certaines assurances sont recherchées pour que les trains d'atterrissage soient exempts du shimmy dans toutes les conditions du service, y compris l'usure normale.

L'un des problèmes posés par l'analyse du shimmy vient de ce qu'en pratique, les trains d'atterrissage présentent un certain nombre de caractéristiques non-linéaires. Des essais effectués sur avions réels seraient, bien entendu, trop coûteux et trop dangereux, tandis que les essais effectués sur des installations fixes (et notamment les épreuves de chute) ne donnent que des informations limitées sur les caractéristiques dynamiques du train; l'interaction entre l'aéronef et le train d'atterrissage est particulièrement délicate à évaluer. En revanche, la simulation permet d'étudier le comportement du train d'atterrissage en tant qu'élément constitutif d'un système complexe, et ce, pour un coût abordable. La simulation permet la modélisation des mouvements rigides et élastiques du fuselage.

Etant donné les problèmes posés par l'élimination des vibrations des trains d'atterrissage qui ne se manifestent que tardivement dans le processus de conception voire même après la livraison de l'appareil, les participants ont conclu que l'état de l'art de l'analyse des vibrations des trains d'atterrissage n'est pas tout à fait comparable aux progrès réalisés dans d'autres domaines analogues et qu'il est urgent d'obtenir la coopération des spécialistes des différents secteurs de l'industrie aéronautique, et en particulier les fabricants des cellules, des trains d'atterrissage et des pneumatiques.

Pour les participants à l'Atelier, des progrès rapides dans ce domaine ne seraient réalisables que moyennant une approche du problème bien planifiée et bien coordonnée. Ils étaient unanimes à reconnaître l'AGARD comme étant la seule instance ayant la capacité et l'autorité nécessaires à la promotion d'un tel effort coordonné pour le plus grand bien des pays membres de l'OTAN.

Contents

Preface

Fully reliable procedures for designing vibration-free landing gear still do not exist. This is in large part due to the absence of accurate dynamic models for describing the tyres in ground contact, the complexity of the (generally non-linear) dynamic behaviour of the structural systems involved as well as the dynamic interactions with steering and braking systems which are contributing stability factors.

The Workshop focused on the various vibrational and stability problems (e.g. shimmy, antiskid induced vibrations) that must be considered in the early design phase of landing gear systems, thereby especially addressing problems which are related to vibrations of the combined structural system formed by the landing gear, its tyres and the flexible aircraft structure. The intention was to indicate the impact of (combined) landing gear/aircraft vibration problems on aircraft design and operations. A further aim of the Workshop was to bring together specialists from aircraft, landing gear and tyre manufacturers to discuss the state-of-the-art technology in this area and to define possible future steps of development.

Dr. R. Freymann
Workshop Chairman

Structures and Materials Panel

Chairman: Prof. O. Sensburg
Chief Engineer
Daimler Benz Aerospace
Militaerflugzeuge LM2
Postfach 80 11 60
81663 Munich
Germany

Deputy Chairman: Prof. S. Paipetis
Prof. of Applied Mechanics
School of Engineering
Dept. of Mechanical Engineering
University of Patras
26110 Patras
Greece

SUB-COMMITTEE MEMBERS

Chairman: Dr. R. Freymann
Ministère de la Force Publique, LU
Bahnhofstrasse 27
85386 Eching
Germany

Members:						
D. Chaumette	—	FR	H. Perrier	—	FR
L. Chesta	—	IT	C. Perron	—	CA
M. Curbillon	—	FR	O. Sensburg	—	GE
H.H. Ottens	—	NE			

PANEL EXECUTIVE

Dr. J.M. CARBALLAL, SP

Mail from Europe:
AGARD-OTAN
7, rue Ancelle
92200 Neuilly-sur-Seine
France

Mail from US and Canada:
AGARD-NATO/SMP
PSC 116
APO AE 09777

Tel: 33 (1) 4738 5790 & 5792
Telefax: 33 (1) 4738 5799
Telex: 610175F

Technical Evaluation Report

A. Krauss

Daimler-Benz Aerospace AG
Military Aircraft LME24
81663 Munich
Germany

INTRODUCTION

Landing gear is an invaluable aircraft system, albeit quite unpopular with most aircraft designers:
In extended position, it spoils the aerodynamic shape of the aircraft. Retracted, it uses internal space which "could much better have been devoted to fuel or other useful things". Moreover, its dead weight impairs flight performance. Looking at landing gear from a structure point of view, it produces large concentrated loads and provides for a lot of difficulties by requiring voluminous landing gear bays and doors interrupting the smooth flow of loads and stress. There is also the possibility that the optimal position of the landing gear with regard to e.g. nosewheel liftoff differs from that required for a satisfactory behaviour as a ground vehicle, and both positions might be unfavourable with regard to structural attachment. Another stanza to this lamentation could be devoted to the themes of wheel size, brake accommodation, tyre size, tyre mechanical characteristics, and tyre pressure.

Present author has spent almost thirty years of his professional life in aircraft and landing gear design and analysis. It appeared to him that to arrive at a design satisfying straightforward and clearly written physical requirements was hard enough. It was even harder to defend such design from the particular interests of other design disciplines. However, at least in military landing gear performance and design requirements the situation with regard to "vibration-free" landing gear was even more difficult. There was not only a lack of guidance with regard to acceptable methods of design and analysis, the requirement for a vibration-free landing gear itself was compromised by accepting "shimmy" to the extent that pilots could still control the aircraft, that shimmy loads did not exceed structural limits, and that the phenomenon was adequately taken into account in fatigue analysis (see for instance British requirements). What wonder that budgets for shimmy analyses were limited at best and that an analytical prediction of landing gear shimmy was not considered a hard fact. Hence the landing gear designer did not get much support in striving for a landing gear free of shimmy, especially not if this aspect would have led to aircraft interface or even redesign problems.

Therefore, the idea brought forward by AGARD SMP to perform a workshop on **"THE DESIGN, QUALIFICATION AND MAINTENANCE OF VIBRATION-FREE LANDING GEAR"** was highly appreciated and widely supported. Present author then volunteered for "Recorder", hoping to be able to draw up a fairly consistent picture of the state of the art as well as of a viable path to be followed from early design to trouble-free operation of vibration-free landing gear. The author's initial intention was to arrange this technical evaluation report in parallel to the workshop title. However, having browsed through the papers several times, it appeared more appropriate to concentrate on crucial technical subjects along all the development process and to provide a view on more general subjects along with a summary of the Round Table Discussion.

TYPE AND CAUSE OF VIBRATION

In summary, most attention was paid to conventional shimmy, which implies a combined lateral / torsional / tilting motion of the wheel (3 degrees of freedom). In particular, [2], [8], and [10] concentrate on this type of landing gear vibration. Cases of fore/aft oscillations (1 d.o.f.) were presented at [3] and [4]. Though not a case of self-induced oscillations, there was a study on the use of semi-active landing gear technology (control of stroke damping force coefficient) to damp fuselage vertical bending oscillations of a passenger transport aircraft [5]. A view on forced (vertical) potentially resonant aircraft/landing gear oscillations on rough ground is given at [1]. In one of the two classical shimmy cases presented at [7], the analytical model included a stick model of the wing which the landing gear is attached to. At [2], there is also evidence that a predictedly stable landing gear exhibited shimmy because of neglecting attachment/fuselage flexibility in the analysis. Starting from isolated front wheel shimmy of motorcycles, [6] also considers oscillations of the complete vehicle.

It became evident that the classical problem of shimmy is becoming increasingly complex due to coupling with other aircraft systems. [5] indicates that a fully active landing gear could cause stability problems in vertical (stroking) direction; in view of [1], [3], [4], [6],and [7] present author expects a lot of additional problems if a fully active landing gear were to be proven to be vibration-free, notwithstanding ground coupling of flight control system. The coupling of the flexible dynamics of landing gear and antiskid feedback dynamics to cause fore-aft vibrations ("gearwalk")is studied at [4]. A related case of strong braking force oscillations (involving virtually rigid wheel suspension) is being described at [3]. At [7] there is indicated a case involving feedback from the steering actuator.

The author's conclusion is that latest at the time of qualification the designer will have to substantiate that the landing gear is vibration-free in all possible degrees of freedom. Furtheron he will have to show this for all active systems with direct or indirect coupling with the landing gear.

To prepare for this task he should have at his disposition a wide range of proven and accepted models and he should start to apply these models as early as possible in the design stage. However it appears that the development of vibration-free landing gear is still far from that.

TYRE MODELS

Without any doubt, a well proven tyre model along with a reliable set of tyre parameters for this model is of vital importance for expedient and successful development of vibration-free landing gear. However there appears to be no commonly accepted, much less a validated dynamic tyre model for application to a full-size analysis of all kind of landing gear vibration (viz. 6 d.o.f. wheel motion with arbitrary deviations from steady state). As a natural consequence of this situation, there is an almost complete lack of routinely measured and published (e.g. along with a tyre catalogue) tyre model parameters.

[2] is an example where linearized tyre models (3 d.o.f.) attributed to von Schlippe and Moreland are applied to study shimmy stability of three different aircraft landing gear data sets. Both Moreland and von Schlippe tyre models were used by [7] to represent tyre dynamic properties in solution of one existing and one predicted shimmy problem. [7] prefers the von Schlippe model due to difficulties encountered in defining the Moreland tyre time constant. Paper [10] refers to the Moreland point-contact tire model in a study on shimmy problems on a service aircraft. [8] presents a derivation of a 6 d.o.f. unsteady dynamic tyre model which in its puristic version would require measurement of 36 transfer functions at a number of well defined working points of the tyre. A comprehensive comparison of published theories (v. Schlippe + Dietrich, Smiley, Pacejka, Rogers + Brewer) with regard to their definition of model parameters is also presented at paper [8]. [9] contains a very short description of a dynamic tyre frequency domain model which was conveyed by the tyre manufacturer together with 9 elementary transfer functions derived from manufacturer dynamic tyre tests. With application to motorcycles, [6] not only deals with more than 3 d.o.f. but also reviews so-called "tire magic formulas" (i.e. fitting mathematical functions to graphical representations of (nonlinear) physical tyre behaviour). Besides, [6] discusses a number of tyre transfer functions measured on 2 each motorcycle and passenger car tyres. A review of models and methods for the wheel simulation is presented at [4], also including a view on "Magic Formula" tyre models. The bulk of paper [4] deals with development and discussion of "brush models" for application to numerical investigation on "gear walk".

In summary, there is definitively a lack of consistent tyre dynamic models for arbitrary wheel motion, both in the nonlinear and linearized field. As long as this lack persists, shimmy calculations proper will be blind to e.g. gear walk and vice versa. Present author's impression is, that of the existing limited models none has ever been subject to a comprehensive and formal process of validation.

NONLINEARITIES

One of the great difficulties in landing gear vibration analysis is the large number of nonlinear effects. Not only that these effects impede use of straightforward linear models, the large scatter of every single nonlinearity (e.g. friction, freeplay) in combination with scatter of all the other model parameters (both linear and nonlinear) does certainly not increase reliability of analytical predictions. As a consequence, practically all papers presented deal with problems posed by the extraordinary accumulation on landing gear of nonlinear physical phenomena (most prominent: Coulomb friction and freeplay, but also velocity-squared damping, tyre out-of-round, etc.).

Paper [2] treats the relative influence of model parameter variations on shimmy stability predictions; it also presents practical experience w.r.t. prediction/reality discrepancies and reasons thereof. Paper [3] treats a case of apparent shimmy (which,

according to the explanation given in the paper, is rather a case of camouflaged gear walk), which vanishes at increased speed presumably due to nonlinearity of tyre circumferential force characteristics. Also in [3] there is descripted a rig test case (virtually rigid) where tyre and brake/antiskid system nonlinearities prohibit linear treatment. [4] describes a similar phenomenon observed on aircraft, and embarks on development of a nonlinear (time domain) model for calculation of tyre longitudinal force. [5] discusses feasibility of linearization in context with control optimization of a semi-active nose landing gear. Both linear and nonlinear differential equations are developed at [6] for the wobble (shimmy) of a motorcycle front wheel; nonlinear effects arise from inclusion of wheel unbalance and periodic tyre radial force variation. In studying shimmy having occurred in flight trials, nonlinear effects were also accounted for by [7] in time domain analyses. Paper [8] presents a complete set of nonlinear equations of unsteady tyre dynamics. Paper [9] discusses influence of nonlinearities on shimmy, presenting models for typical nonlinearities as stick-slip friction and freeplay. Inclusion of nonlinearities in a simulation model of a cantilevered landing gear geometry is presented at [10].

From a scan of the subject of nonlinearities, present author got the impression that there is widespread concern about the reliability of linearized landing gear models. However, increased modelling effort and cost of computation appear to impede application of nonlinear models except in cases when shimmy occurred on existing hardware, notwithstanding cases where linearization is inappropriate (landing, braking).

Interesting enough to present author none of the papers mentioned shimmy under nonsymmetric basic conditions, e.g. a wheel running at a geometrically or elastically induced pre-set slip angle ("toe-in") or tilt angle.

CORRECTIVE MEASURES

In spite of all effort spent on design of supposedly vibration-free landing gear, the workshop was presented with some practical examples of landing gear shimmy ([2], [3], [7], [10]). It was interesting to note that in most cases the landing gear affected could not really be cured. Rather in most instances the burden had to be put on maintaining close tolerances w.r.t. freeplay and tyre pressure, on costly early tyre replacement, on frequent checks of tyre unbalance and out-of-round, and on pilots having to observe special operating procedures. In some instances there has also mass been added to the landing gear, either in form of landing gear reinforcement for increased stiffness or in form of mass balance for changing vibration modes and/or frequencies.

There was not one serious attempt reported to modify geometry of a landing gear affected, for instance to implement a more suitable leg inclination and/or trail arm. It appears that volume and form of landing gear bays are being defined to the last millimeter at a much too early time in the development process, leaving landing gear designers at both airframe and landing gear manufacturers at a loss to re-establish a truly vibration-free landing gear. This again emphasizes the necessity of preparation and as early as possibly application of qualified and commonly accepted methods of design for vibration-free landing gear.

ROUND TABLE DISCUSSION

The Workshop was concluded with a Round Table Discussion led by Dr. R. Freymann. The discussion was characterized by deep concern about present state and future development of **"THE DESIGN, QUALIFICATION AND MAINTENANCE OF VIBRATION-FREE LANDING GEAR".** Compared with effort spent on aero-(servo)elasticity it is obvious that the field of landing gear vibrations has been neglected badly for a long time. There was also some discussion about the reasons therefor. However, in view of the cost involved in correcting landing gear vibration problems emerging late in the design process or even not before aircraft delivery to service, discussion turned to future. It became clear that the state of the art of treating landing gear vibrations was not quite up to other similar subjects and that cooperation was needed of experts widely distributed across aircraft, landing gear and tyre industry (the latter was not represented at the workshop), institutions, and authorities. Workshop participants did not expect the rapid progress needed, unless there was a well planned and coordinated approach to the problem. Unanimously, AGARD was identified the only institution which had enough power and authority to promote such a coordinated effort in the interest of NATO member nations. The format of a Working Group was considered most suitable to achieve the progress necessary within a reasonable time. Dr. Freymann was asked to convey this proposal to the appropriate AGARD body. It was considered useful to have tentative "Terms of Reference" written for this task. John Glaser of de Havilland, William E. Krabacher of Wright Laboratory, and Arnulf Krauss of Daimler-Benz Aerospace were nominated for an informal "Point of Contact" group.

PAPERS PRESENTED AT THE WORKSHOP

[1] "Preliminary Design Optimization of Carrier and Land Based Fighter Landing Gears", B. M. Crenshaw and Susan C. Brown, Lockheed Martin Aeronautical Systems, 86 South Cobb Drive, Marietta Ga. 30063 USA

[2] "A Review of Aircraft Landing Gear Dynamics", William E. Krabacher, WL/FIVMA, Wright Laboratory, Wright Patterson AFB, Ohio 45433 USA

[3] "Self-Induced Oscillations of Landing Gear as an Integral Landing Gear Aircraft System Problem", W. Luber, G. Kempf, A. Krauss, Daimler-Benz Aerospace AG, Military Aircraft LME24, D-81663 Munich, Germany

[4] "Analysis and Control of the Flexible Dynamics of Landing Gear in the Presence of Antiskid Control Systems", E. Denti and D. Fanteria, Dipartimento di Ingegneria Aerospaziale, Università di Pisa, Via Diotisalvi 2, 56126 Pisa, Italy

[5] "Fuselage Vibration Control Using Semi-Active Front Gear", H. Wentscher, W. Kortüm, W. R. Krüger, DLR - Deutsche Forschungsanstalt für Luft- und Raumfahrt, Institut für Robotik und Systemdynamik, D-82234 Wessling, Germany

[6] "Dynamic Behaviour of Motorbikes", F. Böhm and H. P. Willumeit, Department of Traffic Engineering and Applied Mechanics, Technical University Berlin, Germany. Paper was presented by P. Bannwitz.

[7] "Landing Gear Shimmy - DE HAVILLAND's Experience", John Glaser and George Hrycko, Structural Dynamics Group, de Havilland Inc., 123 Garratt Blvd., Downsview, Ontario, M3K1Y5, Canada

[8] "Unsteady Tire Dynamics and the Application Thereof to Shimmy and Landing Load Computations", Klaus Koenig, Daimler-Benz Aerospace Airbus GmbH, Hünefeldstraße 1-5, Bremen, Germany

[9] "Influence of Nonlinearity on the Shimmy Behaviour of Landing Gear", P. Woerner and O. Noel, Messier-Dowty S.A., Vélizy, France

[10] "A Nonlinear Model for Landing Gear Shimmy with Applications to the McDonnell Douglas F/A-18A", Jeff Baumann, Senior Engineer, Structural Dynamics and Loads, McDonnell Douglas Aerospace, P.O. Box 516, St. Louis, MO 631666-0516, USA

PRELIMINARY DESIGN OPTIMIZATION OF CARRIER AND LAND BASED FIGHTER LANDING GEARS

B. M. Crenshaw
Susan C. Brown
Lockheed Martin Aeronautical Systems
86 South Cobb Drive, Marietta Ga. 30063 USA

SUMMARY

The differences in requirements of land based (LB) and carrier based (CB) aircraft landing gear are reviewed with respect to landing impact and ground surface roughness. Frequently the issue of operational roughness requirements vs. "taxi" requirements arises. More often, it seems, attention is being focused on operational runway roughness requirements. The MIL-SPEC roughness amplitudes and wavelengths may not represent the operational capability of an aircraft when combined sources of loading are considered. There are severe loads on both main and nose gears during landing rollout on a rough runway surface if braking is used; however, levels of braking and roughness combinations are not always clearly defined in procurement specifications.

The more robust landing gears sized for carrier operations are examined to determine their potential operational performance for land based roughness levels when combined loads from rollout braking are considered. While the weight penalty associated with carrier qualified landing gears is commonly recognized, and weight efficiency requirements of fighter aircraft may ultimately outweigh cost considerations for commonality of landing gear components, it is nevertheless worthwhile to consider methods for reducing costs through multiple application designs and parts usage. Although without great previous success, multi-service application of designs has long been an attractive concept. If severe runway roughness capability is considered as an operational requirement for land based gears, the weight obstacles to common landing gears may diminish.

A hypothetical future fighter aircraft is utilized to compare runway roughness capability of gears sized for carrier landing and arrestment loads with gears sized exclusively for land based use, to compare relative landing gear weights, and to develop concepts of landing gears with the potential of multi-service usage. A simple forward retracting vertical post strut arrangement has been examined from a conceptual standpoint for low cost production in two stroke lengths.

LIST OF SYMBOLS

g	acceleration of gravity -in./sec. squared
L	aerodynamic lift (per strut) - lb.
N	load factor - nondimensional
S	strut stroke - in.
V	sink speed - in./sec.
W	weight per strut - lb.
δ_t	tire deflection - in.
η_S	strut efficiency - nondimensional
η_t	tire efficiency - nondimensional

1. INTRODUCTION

An effective general approach to minimizing vibration effects on landing gear and preventing transmission of ground generated high frequency loads into other aircraft structure is to utilize the lowest practical tire pressures, and to keep the strut airspring constants low. To achieve these goals, thorough preliminary analysis is needed to avoid later "fixes" which can make the gears marginal energy absorbers for ground operations.

All too frequently, landing gears and their retraction/extension mechanisms become overly complicated or compromised because the implications of structural requirements were not studied thoroughly enough during the initial aircraft layout to lay claim to the space and volume necessary to accommodate all landing gear needs. Sometimes inevitable aircraft growth or mission changes can require a tire size change or stroke adjustment, only to have an interfering bulkhead preclude a straightforward change. In the tightly packed wheel wells of fighter aircraft, any unconservative gear sizing may even prevent such changes as slight caster/camber adjustments to improve tire wear life or trail adjustment to optimize shimmy stability. It is therefore important to exercise all available computing and simulation techniques early in the aircraft preliminary design stage to ensure sufficient gear stroke and wheel well clearances to support the aircraft design maturing process without undue cost penalties to the landing gear or the necessity for compromise solutions.

For a long period, landing gear load/stroke characteristics were determined primarily by landing impact energy absorption requirements. Taxi loads

Paper presented at the 81st Meeting of the AGARD SMP Panel on "The Design, Qualification and Maintenance of Vibration-Free Landing Gear", held in Banff, Canada from 4-5 October 1995, and published in R-800.

were defined by a 2.0g requirement. Presently, specifications MIL-A-8862 and MIL-A-8863 include roughness definitions in terms of (1-cosine) dips or bumps plus requirements for steps and other obstacles.

Transport aircraft designers usually concentrate on maximizing step bump capability and operations from semi-prepared surfaces. Because of the low landing and takeoff speeds of large transports, only the shorter (1-cosine) wavelengths (below perhaps 100 ft.) usually produce a speed/wavelength combination near enough to resonance to produce high gear and wing loads. At these short wavelengths, amplitudes are low. There is little published information available indicating how designers have addressed the longer wavelength roughness that becomes important at the higher landing and takeoff speeds of modern fighters. It is particularly perplexing how gears are designed with enough damping to meet the MIL-A-8863 requirement if the aircraft is assumed to operate through resonant speed on a surface of "continuous" (1-cosine) bumps.

Conversations with procurement representatives, with design and structures personnel, with test pilots, and with potential users have not indicated a consensus of opinions with respect to "design roughness" as contrasted with "operational capability." In almost all instances, current specification wording is generally vague in this respect, in some places using the term -- "operate to and from --" and in other places referring to taxi only, without braking.

With this uncertainty as to operational requirements vs. aircraft capability in mind, it was decided to select two sets of landing gears, one sized for carrier operation, and one sized for conventional land based operations for studying potential roughness capability as a function of strut stroke and design load level. The ground rules for carrier based gears and land based gears have been generally followed at a preliminary design level, concentrating on vertical strut loads. Thus other load sources such as turning, pivoting, jacking, etc. have been ignored as they can be determined in connection with establishing gear strength, setting wall thicknesses, lug sizes, etc. No study of launch bar or holdback mechanisms has been made. Vertical struts have been assumed for computational simplicity. Non-vertical or articulated struts are expected to yield similar results for equivalent vertical axle strokes.

2. SINK RATES AND LANDING GEAR ENERGY ABSORPTION

The first step in sizing a landing gear is to establish the stroke length. For vertical struts, Currie, (Reference 1, p35) shows that:

$$\delta_t \eta_t N + S \eta_S N = \frac{V^2}{2g} + \frac{(W - L)(S + \delta_t)}{W} \quad (1)$$

To calculate the gear stroke required vs. sink speed and load factor, the landing impact is assumed to occur at 1g wing lift, and the term:

$$\frac{(W - L)(S + \delta_t)}{W}$$

goes to zero. If it is further assumed that a tire will be selected to produce 40% as much deflection as the shock strut, and that strut and tire efficiencies are 85% and 45% respectively, Equation 1 becomes:

$$S + 0.4\, S \frac{\eta_t}{\eta_S} = \frac{V^2}{2gN\eta_S} \quad (2)$$

$$S = \frac{V^2}{1 + 0.4\left(\frac{0.45}{0.85}\right)(2)(386)(0.85)N} \quad (3)$$

$$S = \frac{V^2}{795.16\, N} \quad (4)$$

Using Equation 4, a plot of stroke requirements for several load factors and sink rates can be developed as shown in Figure 1.

Figure 1 may be used as a guide in selecting strut strokes; however, a carrier based gear with a sink rate requirement of 20-25 fps. would not be designed for the lowest load factor shown because the stroke would be excessive, nor would a land based gear with a sink rate requirement of 10 fps. be designed to the highest load factor shown, because of the lack of sufficient stroke to absorb runway roughness. In keeping with current acceptable aircraft strut sizing, a preliminary design 25 inch stroke for carrier gears and a 12 inch stroke for land based gears was selected for further study.

Once preliminary stroke values are obtained, tires must be chosen. Reference 2 suggests that tires should have a deflection capability from static to fully compressed equal to the step bump height to be traversed; however, this is only practical for steps and short wavelength bumps. For longer roughness wavelengths with their large amplitudes, it is believed to be reasonable to choose a tire with a total deflection capability of around 40 percent of the strut stroke as used in Equation 4.

During preliminary designs, it is usually sufficient to consult tire manufacturers' handbooks and select an existing tire if possible. For single tire struts, the tire must have the required maximum static load rating. A little more freedom exists for multiple tires in that there may be more sizes available which together will have the necessary load rating. It is desirable to utilize as much tire deflection capability as practical, yet keep the volume occupied by the tires small enough to fit in a minimal size and crowded wheel well.

For this preliminary study, an F-111 main tire was the only listed size found with both reasonable tire diameter and the required static load rating for the main gear. Dual C-130 size nose tires were selected, keeping in mind the heavy nose gear loading resulting from the carrier loading condition of free-flight engagement by the arresting cable. To maximize roughness amplitude capability of the study gears, the same tire sizes are used for both carrier and land based designs.

3. RUNWAY ROUGHNESS

Once strut stroke lengths and tire sizes have been selected, runway roughness response must be addressed. The procurement authority specifies roughness requirements, usually in terms of existing military specifications. In the future the requirements will likely be those in MIL-A-87221. Figure 2 compares portions of these specifications for (1-cosine) discrete bumps for surfaces defined as either prepared or semi-prepared at wavelengths up to 400 ft. Further breakdowns in speeds below and above 50 knots are are made in MIL-A-87221; however, only speeds above 50 knots are considered in this study. Takeoff or landing dictates responses for higher speeds; but at 50 knots and lower "taxi" conditions, speed limitations are feasible for controlling roughness induced loads. Table 1 summarizes several requirements in addition to amplitude and wavelength.

Of the three specifications considered (References 3-5), only MIL-A-8863 explicitly requires combined braking simultaneously with loads from the rough surfaces; however, it does not specify a level of braking to be used. MIL-A-8862 defines the profiles as "acceptable runway roughness" but does not mention braking. In addition, an alternative 2.0 x MLG static load and 3.0 x NLG static load criteria is allowed by MIL-A-8862. These alternate load levels allow very little energy absorption reserve to be used for braking.

MIL-A-87221 is also considered ambiguous because it specifies taxi analysis without braking in the taxi load section, but requires consideration of runway roughness in the braking section. A review of the structural design criteria for several modern fighter aircraft did not reveal any allowance for combined braking with taxi loads.

It should not come as a surprise, with the pressure to minimize landing gear weight, that gears designed to these specifications provide little braking capability over the defined runways, and "operational" roughness capability today remains largely an undefined quantity. It is recommended that procurement documents in the future provide more specific definitions as to the level of "operational" runway roughness capability required.

Any additional roughness capability above that achieved by current land based aircraft must come with some weight penalty. The next section of this paper attempts to quantify this penalty by comparisons with a gear sized for MIL-A-8863 carrier landing criteria based on a hypothetical aircraft. This comparison is done only at a preliminary design level and is intended to help quantify the potential weight penalty. It remains a customer's decision to accept higher landing gear weight to achieve increased operational capability.

4. AIRCRAFT AND LANDING GEAR CONFIGURATION

A hypothetical aircraft has been configured for this landing gear comparative study. The aircraft is not representative of any existing aircraft; however, an effort was made to achieve realistic proportions, weights, and size anticipated for future fighters. In addition to landing gear characteristics, the required parameters are landing and takeoff weight, pitching moment of inertia, wheel base, and main gear tread width. Tread width was chosen to ensure turnover requirements are met. An artist's concept of the aircraft is shown in Figure 3.

Two single tire, forward retracting main gear struts are used. A dual tire nose strut is used for compatibility with carrier nose gear catapults. These configurations are illustrated in Figure 4. Both struts have simple forward retraction mechanisms, and are mounted laterally between spherical bearings to reduce bending loads transmitted to the airframe. On each gear, one bearing is locked. The lateral positioning of the side brace should isolate any spin-up/springback and

antiskid vibrations from transmission into the aircraft structure through installed bearing tolerances. No details were considered for catapult attachment. Pertinent aircraft data is shown in Table 2.

Figure 5 shows the struts in more detail. Gas separator pistons are used in each strut to minimize any pressure loss potential from gas going into solution in the hydraulic oil. There is no significant pressure differential across this separator to cause leakage. Although metering pins are shown, computations were carried out assuming a constant orifice size. Metering pins should offer some improvement in efficiency, with resultant lower loads, but would not be expected to affect relative comparisons of gear capability. Rebound damping using a flap valve below the strut upper bearing is used in all gears. Rebound damping generally follows recommendations given in Reference 6.

Both main and nose struts are assumed to be of the same diameter for computational convenience. For a given load/stroke curve, the strut diameter does not determine vertical load, it establishes strut internal pressures.

5. LANDING LOADS

Landing impact loads for land based gears are established for 10 fps sink rates. Sink rates for carrier landing gears are based on the multivariate analysis outlined in MIL-A-8863. For the study aircraft, this analysis results in a sink rate of 24.5 fps as shown by Figure 6, based on an approach speed of approximately 125 knots. Besides the landing impact loading, allowance must be made for tire encounters with carrier deck obstructions. Thus, additional tire deflection capability equal to the deck obstruction height needs to be provided.

The main gear drop weight is calculated for an aft c.g. at design landing weight. The nose gear drop weight is calculated for the most forward c.g. plus a forward acting c.g. acceleration of 10 fps squared, to account for pitching following impact with a tail down aircraft attitude.

Carrier nose gears are very highly loaded by the "free-flight engagement" condition where the tail hook catches an arresting cable at the instant of main gear contact while at low sink speed and a high angle of attack. For this design point, the nose gear must react impact loads plus absorb a large amount of aircraft rotational energy introduced by hook loads.

Figure 7 shows landing impact load/stroke calculations for both land based and carrier based nose and main gears along with nose and main tire load deflections.

Figure 8 shows drop test simulations for nose and main gears and free flight engagement simulation loads for the nose gear. Since aerodynamic characteristics of the hypothetical aircraft were not defined, a conservative tail down angle of 16 degrees was used for the free flight engagement simulation.

6. LANDING GEAR GROUND ROUGHNESS CAPABILITY COMPARISONS

Evaluations of the roughness capability of these gears during landing rollout have been based on techniques developed for evaluating existing aircraft to operate from bomb damage repaired runways as reported in Reference 7. In this method, a matrix of aircraft velocity and roughness wavelength combinations is simulated and the maximum landing gear vertical loads are tabulated. For purposes of this comparison, the runway roughness amplitude is defined by the equations of MIL-A-8862 that express the roughness amplitude as a function of the wavelength. Velocity increments of five knots were used from 50 to 150 knots, along with wavelengths from 50 ft. to 400 ft. in 50 ft. increments. MIL-A-8862 specifies use of single and two bumps. In this study, two bumps were assumed. Also only dips were simulated as dips are usually found in other studies to produce higher loads than corresponding bumps of equal amplitude.

From the resultant 3-dimensional table of velocity, wavelength, and maximum gear load, contours of constant load level can be drawn, producing a graphical description of load trends. Contours of loads equal to or higher than limit load define combinations of roughness wavelength and airplane speed that must be avoided. For full capability over the entire speed/wavelength range, no load contour can exceed the limit vertical load of the landing gear. If limit load exceedances are found, the bump amplitude can be reduced until the gear loads are within the limit load envelope. To minimize the number of computer simulations required, the amplitudes have been reduced by an equal percentage over the entire wavelength range studied. Thus when the results are discussed in terms of a percentage of the specification roughness amplitude, the quoted percentage represents the point at which the highest load occurred, and more capability exists for other noncritical combinations of speed and wavelength.

Initial simulations were made using conventional static to compressed 3:1 compression ratio strut sizing. The land based gears sized for the alternate 2g/3g criteria could not achieve more than approximately 55% of the semi-prepared roughness requirement based on single bumps and the carrier based gear could not reach 100% of the semi-prepared surface single bump requirements. The airspring curves were then recomputed using

increased inflation pressures and lower compression ratio values. Because of high preload pressures, these modifications represent what is believed to be the maximum capability for conventional single chamber gears with these stroke lengths.

Figure 9 shows strut capability for these gears where sufficiently high roughness levels have been used to produce at least limit gear load over some portion of the speed/wavelength range studied. Unrestricted operations would require a lower roughness level where no limit loads would occur.

Figure 9 (a) shows the land based 12-inch stroke gear results without braking. The roughness level was 45% of the MIL-A-8862 semi-prepared surface. High load levels were produced for both main and nose gears in the wavelength range above 300 ft.

Since only limited semi-prepared surface roughness capability exists for the land base gear, braking simulations were made assuming only prepared surface roughness as shown in Figure 9 (b). A braking coefficient of 0.4 was assumed. Main gear loads were well below limit, but nose gear loads did exceed limit at the highest speeds around a wavelength of 100 ft.

As configured in this study, the carrier sized 25-inch stroke gear could not achieve 2-bump capability to 100% of the MIL-A-8862 roughness level at all speeds and wavelengths. Figure 9 (c) shows that limit loads are reached in the 300 ft. and above wavelength range at 75% of the semi-prepared surface roughness level without braking. The carrier sized gear does have substantial braking capability over roughness as compared to the land based design. Figure 9 (d) shows that limit loads are just reached at 50% of the MIL-A-8862 roughness level.

Undoubtedly, additional changes could provide some improvement in the roughness tolerance of these gears; however, it is not believed that the changes would affect the relative capabilities of the carrier and land based designs. One potential method of obtaining additional roughness capability is the use of double chamber struts. In recognition of objections to double chamber struts by maintenance and gear overhaul personnel, this survey was limited to single chamber gears only.

7. WEIGHT COMPARISONS

It is not possible to estimate accurate landing gear weights until all load components, including drag, side, and miscellaneous loads are known and the gear design has progressed at least through the detail layout task. Consequently, parametric weight estimating techniques have been used to compare these gears as shown in Figure 10. For quantifying the weights, it is believed that the conventional land based design would be in the range of 2.2% of aircraft weight. The 0.9% relative increment shown for the carrier based design is believed to approximate the additional landing gear weight necessary for 25 inch stroke gears to achieve full takeoff/landing/RTO capability on MIL-A-8862 paved runways and limited operational capability on semi-prepared surfaces. Full operational capability with braking over MIL-A-8862 semi-prepared surfaces with two bumps or over the MIL-A-8863 continuous (1-cosine) bumps could not be achieved with these struts as configured on the hypothetical aircraft.

8. REDUCING ROUGH FIELD LANDING GEAR COSTS

Escalating costs of aircraft procurement requires that all possible methods of cost reduction be examined. For landing gears, this means design simplicity and commonality wherever possible. Cost and weight optimization must be considered jointly.

Forging costs represent as much as 5 - 10% of total cost of modern landing gears. Applying design initiatives to maximize commonality of forgings between land and carrier based gears, and possibly between nose and main gear components can reduce production costs. To do so, the general arrangements of the land based and carrier based gears should be as similar as is practical. Using the same basic geometry and trunnion attach points can facilitate commonality of components and maximize interchangeability.

Major structural components such as the shock strut cylinder and piston could perhaps be machined from common forgings. Forging dies cut to produce forgings for a 25 inch stroke gear could have excess material removed when producing 12 inch stroke gears. Common strut diameters could be achieved by machining to different wall thicknesses as necessary for higher carrier landing loads. Navy requirements now indicate Aermet 100 material, and this steel is presently a significant cost factor. Aermet 100 material removed during machining can be recovered to recoup some raw material cost.

Minor structural components such as drag and side braces may also be made from common forgings, again being sized for the heavier gear design. Allowances for wider lugs should be made during the design process. Common trunnion pins may be used with a larger inner diameter for the land based gears and a smaller diameter for the carrier based gears. Retract and steering actuators may also be made from common forgings, allowing for larger piston areas for heavier gears.

Many nonstructural components may be designed to be interchangeable from carrier based to land based designs. By using equal piston diameters, common components such as separator pistons, gland nuts, and strut bearings may be incorporated. Also, system type components such as steering valves may be completely common.

To benefit from design commonality, both carrier based landing gear requirements and the maximum operational runway/taxiway roughness should be considered at the beginning of the design process. History has shown that landing gears initially designed for land base use are impractical for carrier operations and entirely new designs are required. If carrier requirements are considered initially, the landing gear may be more easily adapted to multi role uses in the future and at the same time much higher roughness tolerance potential can be achieved.

9. CONCLUSIONS

Specifications for landing gear design ground loads are not always explicit in describing operational requirements on rough runways. The lack of clarity of operational requirements with respect to braking levels while on rough surfaces can lead to designs with reduced operational capability, i. e. limited to unbraked taxi or free rollout where the possibility of roughness resonance exists.

Navy carrier based aircraft specifications (MIL-A-8863) require landing/takeoff operations from lower amplitude rough surfaces than the corresponding MIL-A-8862 surfaces; however, additional capability is inherent over corresponding Air Force gears from other requirements associated with Navy shipboard operations. When severe roughness combined with other load sources is considered, weight differences in Navy and Air Force landing gears may diminish.

Airfield roughness capability of two landing gears with different stroke lengths using MIL-A-8862 roughness specifications have been compared for a hypothetical aircraft. The landing gears were sized by Air Force and Navy Landing Impact Criteria. The landing gear weight penalty to provide operational capability with braking to Air Force gears has been estimated from this comparison at approximately 0.9 percent of aircraft weight.

10. Recommendations

Landing gear design and user technical personnel need to improve, clarify, and develop realistic ground roughness performance requirements definitions to avoid potential problems in landing gear/vehicle integration. Wheel well sizing should be based on the maximum stroke lengths and tire sizes that could be anticipated for future, perhaps multi service usage of the airframes.

Future studies should focus on the inherent capabilities of gears designed for shipboard operations to establish benefits for use on rough runways.

Additional work is needed to rapidly quantify landing gear weight as a function of required capability through improvements in automated loads and stress analysis. Modeling tools of this type must be available and utilized from the earliest design stages.

It is recommended that cost reduction methods, including simplified gear retraction geometry, be given high priority in the initial gear design. Sizeable cost savings might be realized, both in development and manufacturing with more progress toward standardized gear arrangements, and by reduced gear complexity which enable the use of common parts and forgings.

11. REFERENCES

1. Currie, Norman S., "Aircraft Landing Gear Design: Principles and Practices," AIAA Education Series, American Institute of Aeronautics and Astronautics, Inc. , Washington, D. C., 1988, p.35.

2. Williams, W. W., Williams, G. K., and Garrard, W. C. J., "Soft and Rough Field Landing Gears," SAE Paper 650844, October, 1965.

3. Airplane Strength and Rigidity, Landplane Landing and Ground Handling Loads, MIL-A-8862A, March,1971.

4. Airplane Strength and Rigidity, Ground Loads for Navy Acquired Airplanes, MIL-A-8863B(AS), 6 May 1987.

5. Aircraft Structures, General Specification For, MIL-A-87221, 28 February, 1985.

6. Conway, H. G., "Landing Gear Design," Chapman and Hall Ltd., London, 1958. , p. 184

7. Anon, "Aircraft Operation on Repaired Runways," Report of Working Group 22 of the Structures and Materials Panel, NATO/AGARD, Paris France, AGARD-R-731, August, 1990.

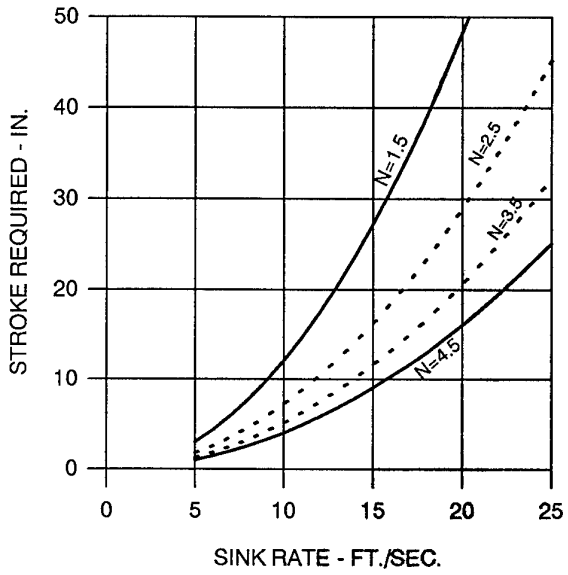

Figure 1. Stroke Requirements as a Function of Sink Rate and Load Factor.

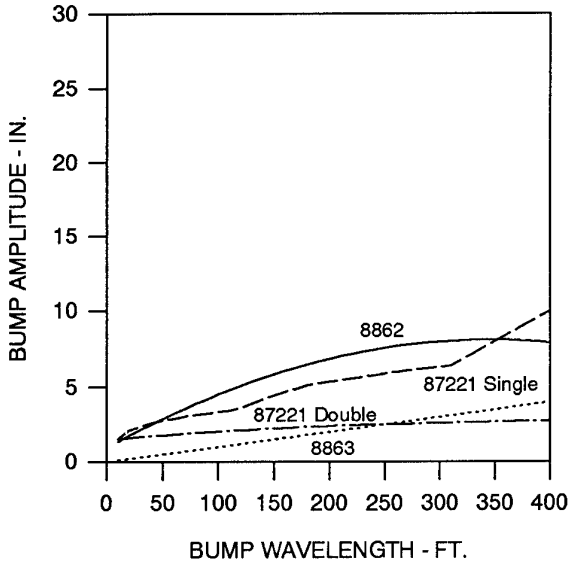

(a) Prepared Surfaces

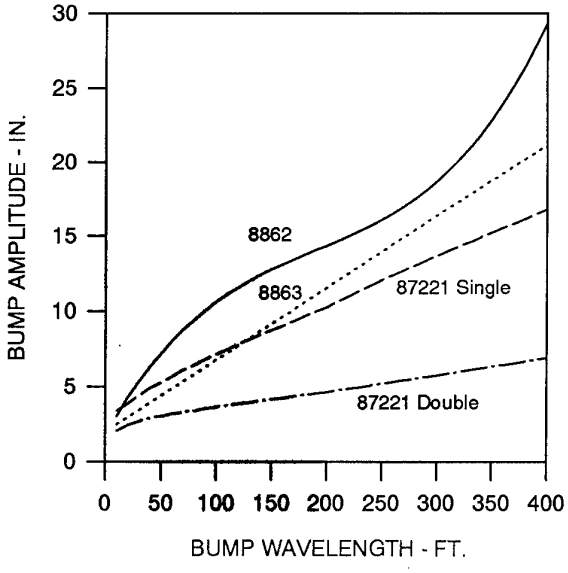

(b) Semi-Prepared Surfaces

Figure 2. Military Specification Roughness for Prepared and Semi-Prepared Surfaces.

TABLE 1.

ADDITIONAL RUNWAY ROUGHNESS REQUIREMENTS

MIL-SPEC	Number of Bumps or Dips	Braking Plus Roughness	Landing Impact on Roughness
8862	1 or 2	None Defined	No
8863	Continuous	Yes	Yes
87221	Different Amplitude Requirements for Single and Double Bumps	2 Definitions: Taxi without Braking Braking over Roughness	No

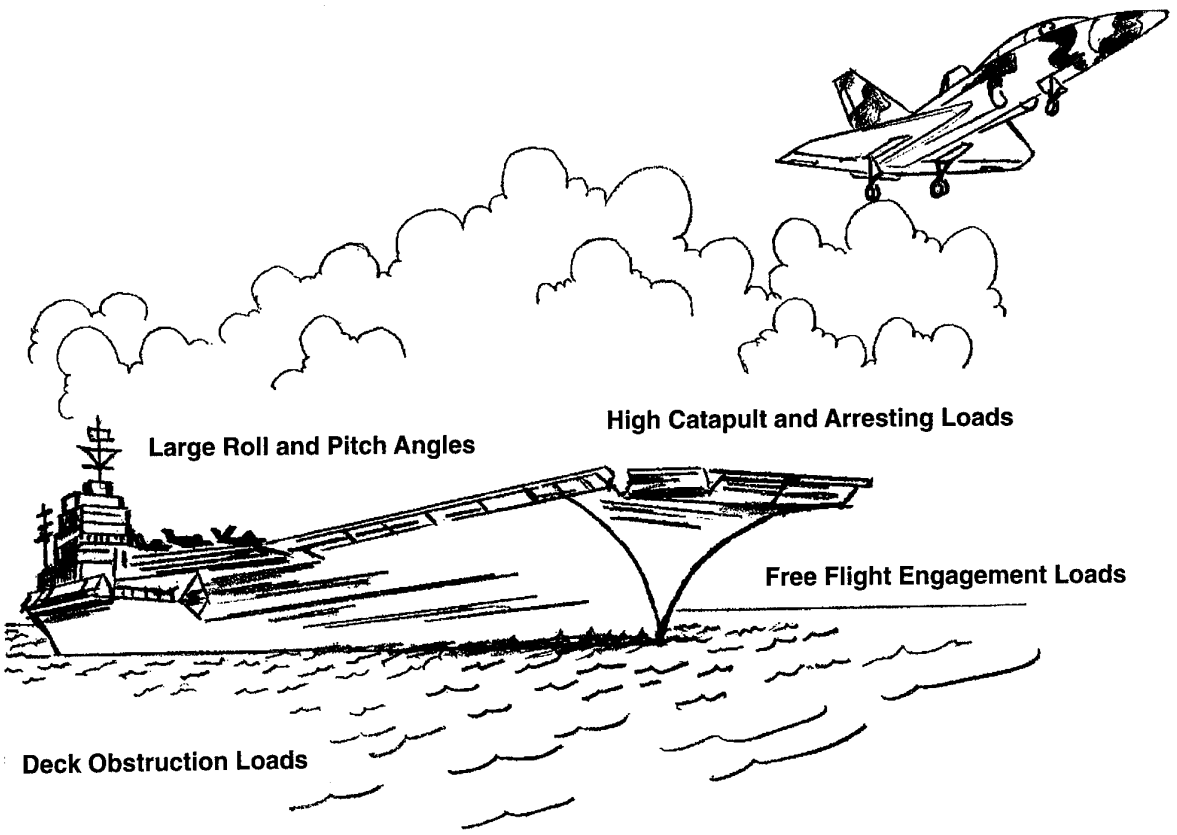

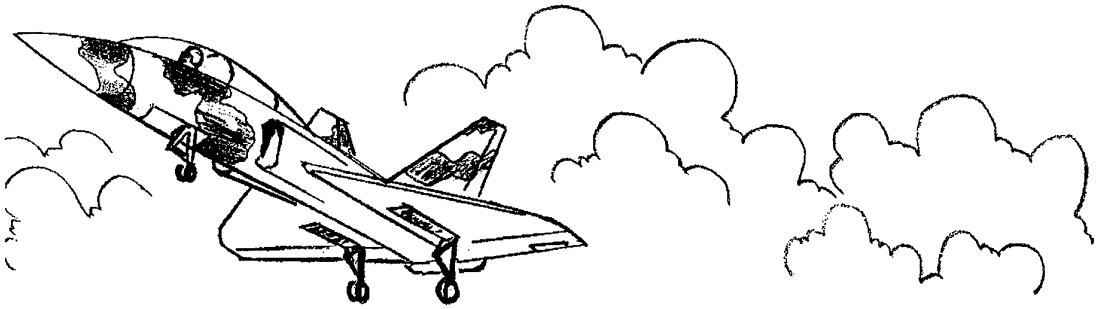

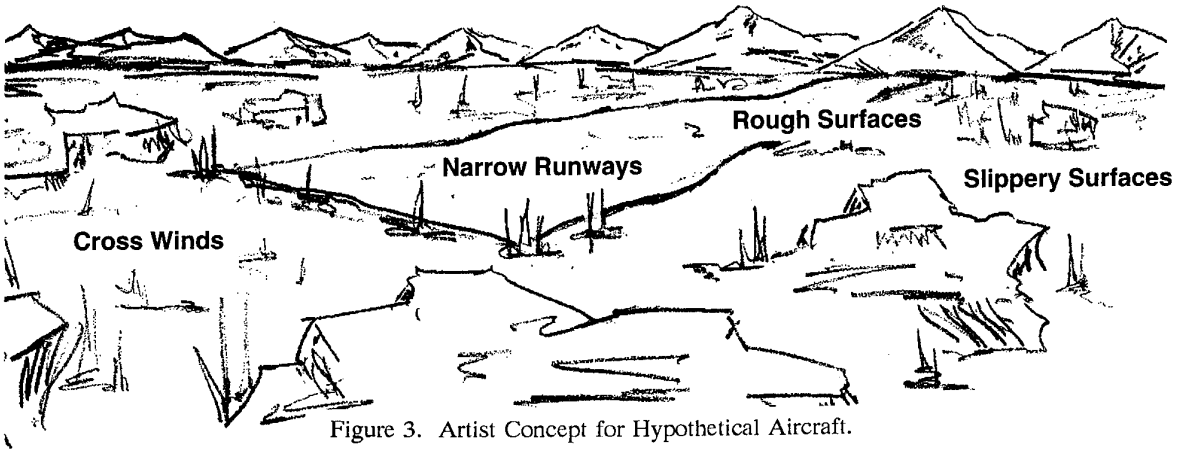

Figure 3. Artist Concept for Hypothetical Aircraft.

TABLE 2.

STRUCTURAL DETAILS OF HYPOTHETICAL AIRCRAFT

Maximum Weight	100,000 Lb.
Landing Weight	75,000 Lb. (65,000 CB)
Maximum Weight Pitch Inertia	1.13 E+09 Lb.-in.^{2}
Landing Weight Pitch Inertia	0.848E+09 Lb. in.^{2}
Longitudinal Distance, Nose Gear to Main Gear	330 in.
Main Gear Tread Width	180 in.
Forward C. G. Position	61.8 in. forward of Main Gear
Aft C. G. Position	26.8 In. forward of Main Gear.
C. G. Height Above Ground	100.78 in.
Tailhook Location	190.76 in. aft of C. G., 32.34 in. below C. G.
Tipback Angle	15 Degrees
Turnover Angle (Forward C. G.)	53.819 Degrees
Minimum Static Nose Gear Load	8,121 Lb.
Maximum Static Nose Gear Load	18,727 Lb.
Nose Gear Load with Braking (10 ft./sec.^{2} Decel.)	28,211 Lb.

ITEM	MIL-A-8863, Soft Strut Single Chamber, Gas/Oil Separated		MIL-A-8862, Soft Strut Single Chamber, Gas/Oil Separated	
	MAIN GEAR	NOSE GEAR	MAIN GEAR	NOSE GEAR
Stroke	25 in.	25 in.	12 in.	12 in.
Piston Dia./Area	6 in./28.274 in.^{2}	6 in./28.274 in.^{2}	6 in./28.274 in.^{2}	6 in./28.274 in.^{2}
Extended Pressure	844 psi	426 psi	886 psi	313 psi
Extended Volume	903 in.^{3}	794 in.^{3}	466 in.^{3}	402 in.^{3}
Tire Size/Number	47 x 18 36PR/1	39 x 13 22PR/2	47 x 18 36PR/1	39 x 13 14PR/2
Unsprung Wt. (Est.)	650 lb.	275 Lb.	600 Lb.	200 Lb.
Orifice Coefficient	2.65	1.43	4.6	2.9
A_1 Tire Coefficient	9918.0	17,710 (2 Tires)	7406.5	4742. (2 Tires)
A_2 Tire Coefficient	1.259	1.022	1.237	1.269
Tire Pressure	245 psi	165 psi	160 psi	60 psi
Strut Preload	23,863 Lb.	12,045 Lb.	25,051 Lb.	8,850 Lb.
Strut Bottoming Load	109,857 Lb.	109,736 Lb.	92,128 Lb.	56,729 Lb.
Tire Static Load Rating	54,000 Lb.	24,600 Lb./Tire	54,000 Lb.	24,600 Lb./Tire

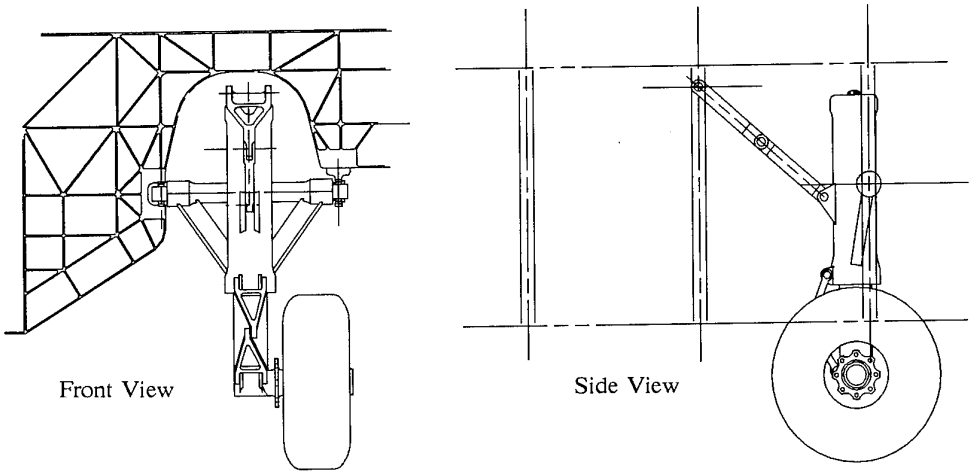

(a) Main Gear

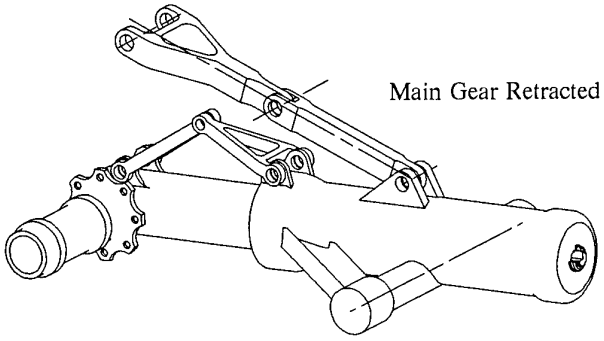

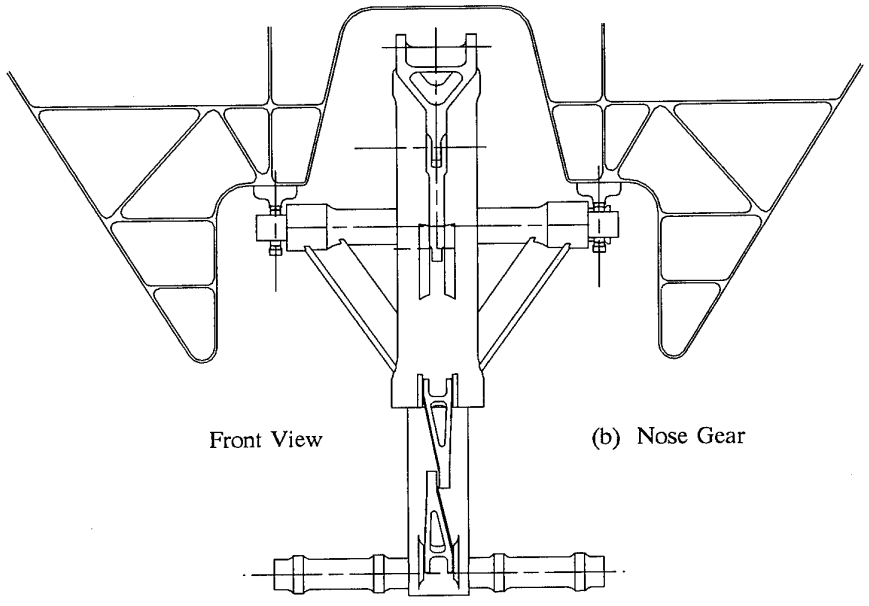

Figure 4. Landing Gear Arrangement.

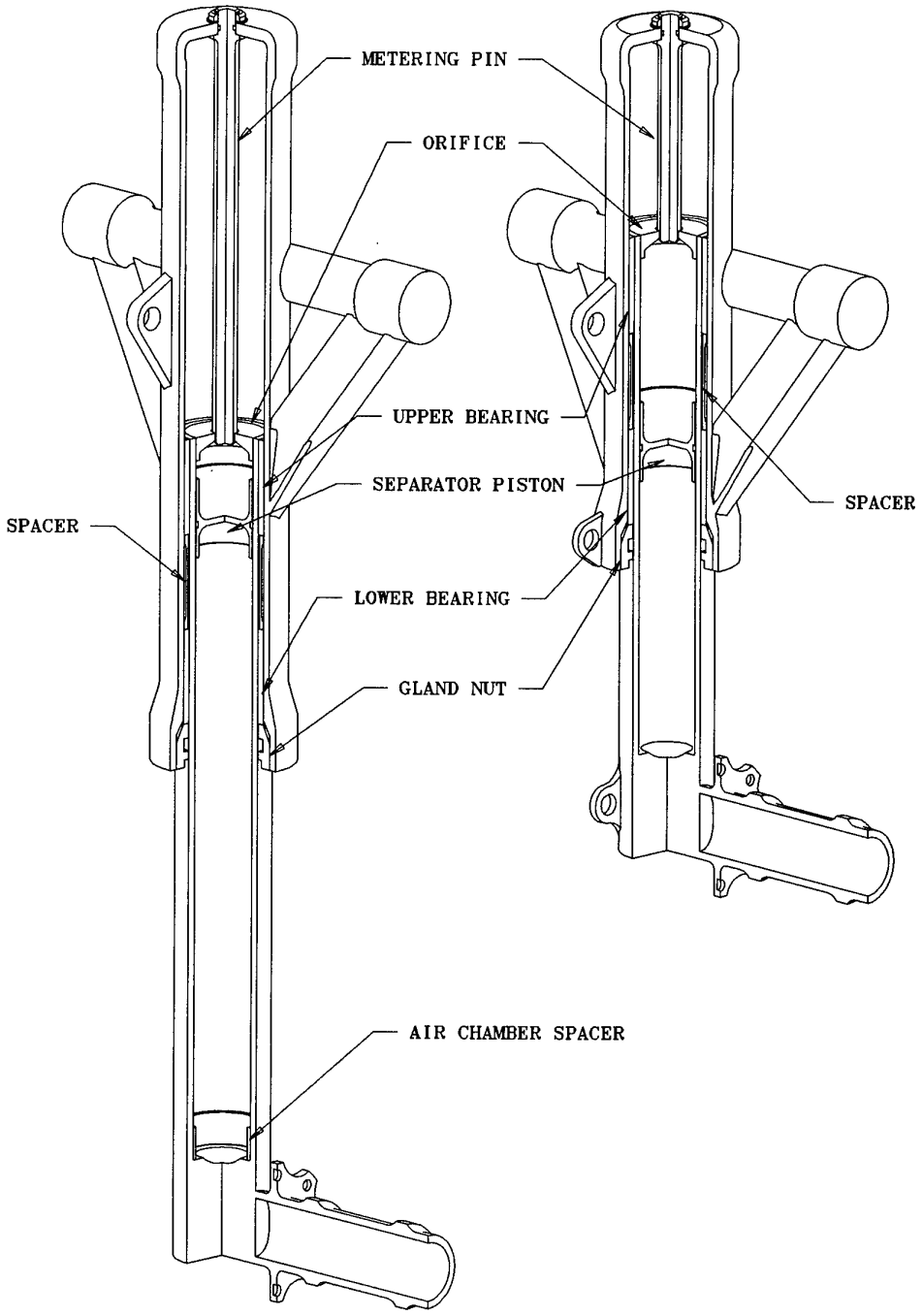

Figure 5. Landing Gear Strut Concepts.

Figure 6. Carrier Based Sink Speed as a Function of Approach Speed.

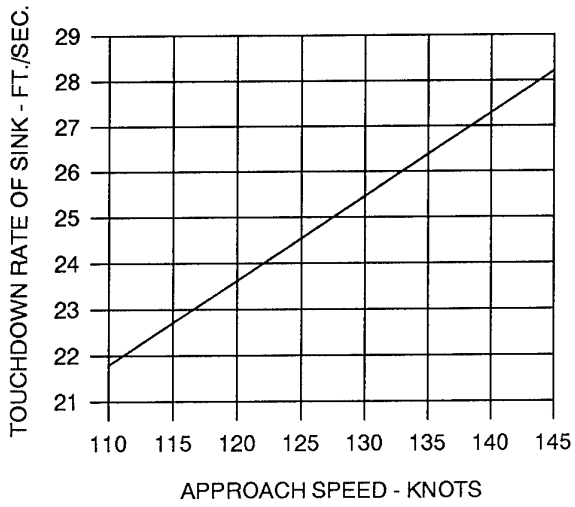

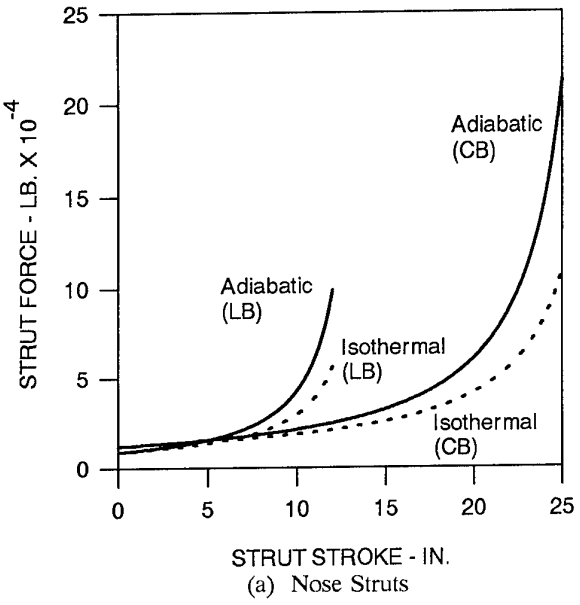

(a) Nose Struts

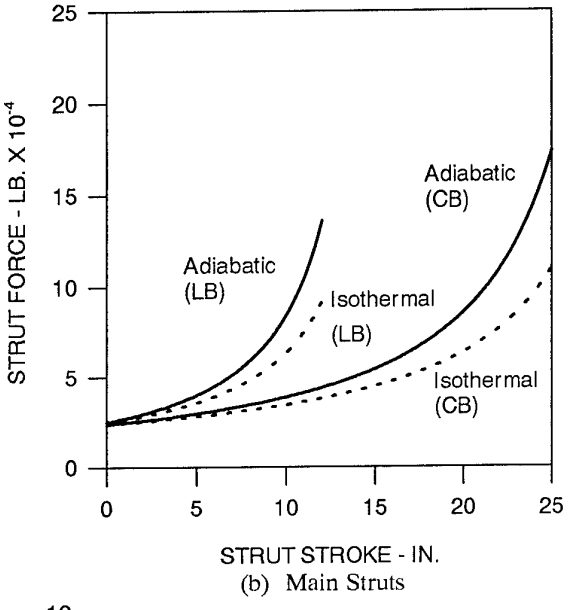

(b) Main Struts

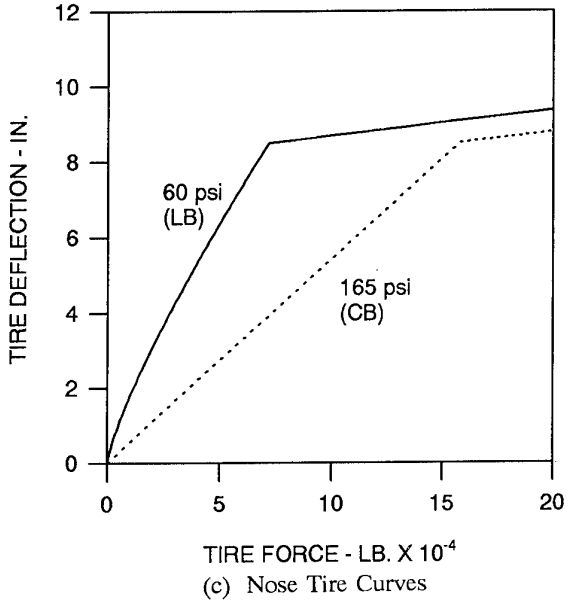

(c) Nose Tire Curves

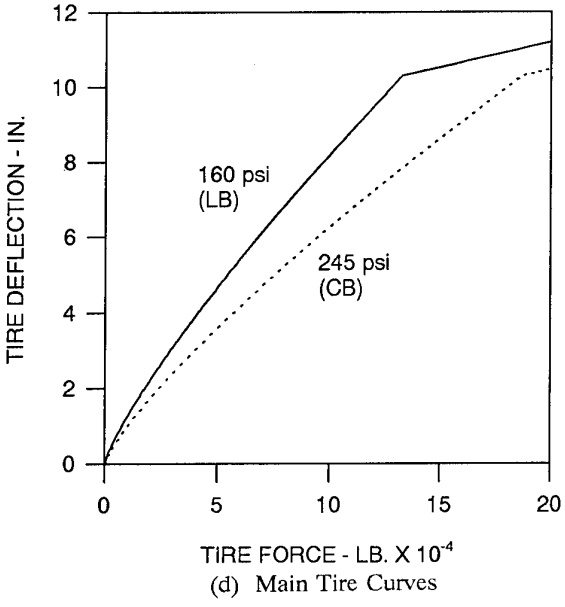

(d) Main Tire Curves

Figure 7. Strut and Tire Load-Deflection Characteristics.

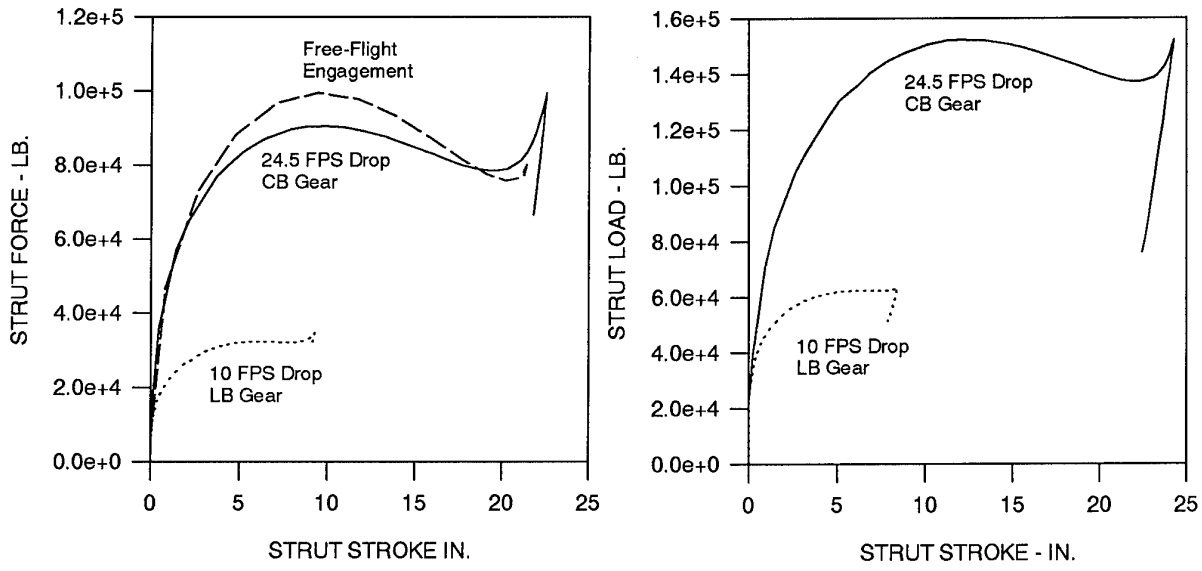

(a) Nose Gear

(b) Main Gear

Figure 8. Drop Test and Free-Flight Engagement Simulations.

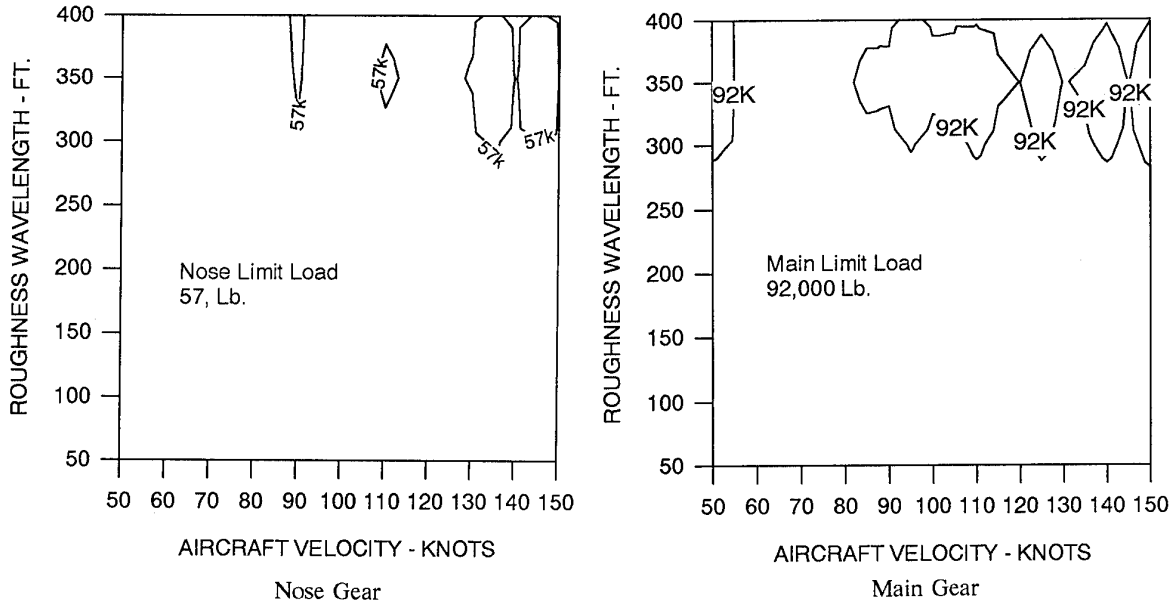

Nose Gear

Main Gear

Figure 9 (a). Land Based Gear Capability over Two Bumps at 45 Percent MIL-A-8862 Semi-Prepared Roughness.

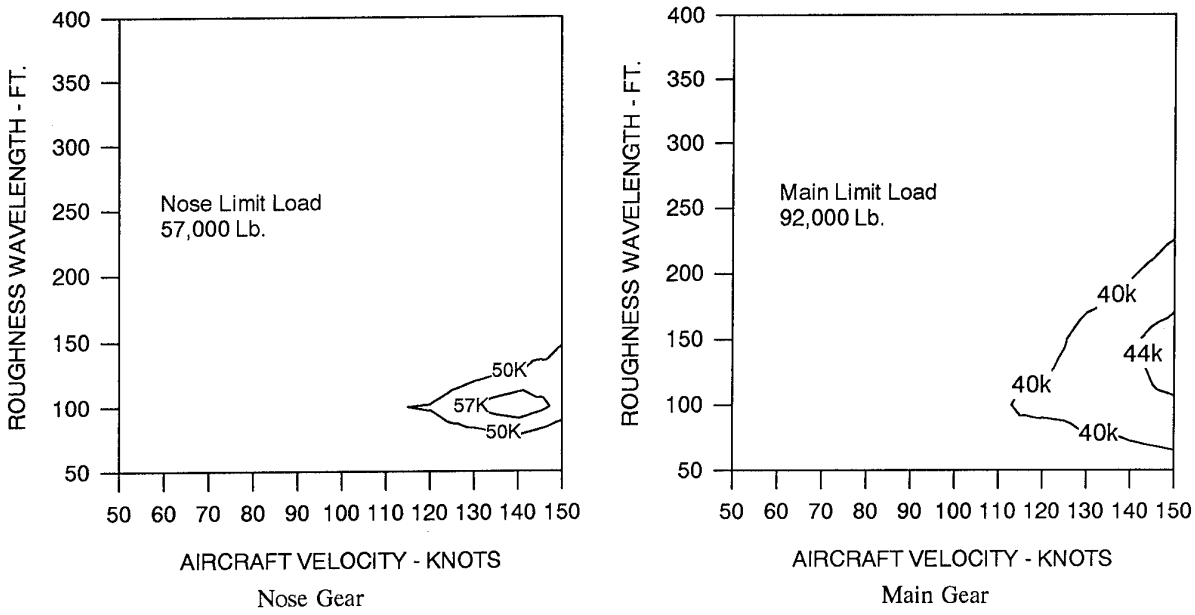

Figure 9 (b). Land Based Gear Capability over MIL-A-8862 Prepared Surface Roughness with 0.4 Braking Coefficient.

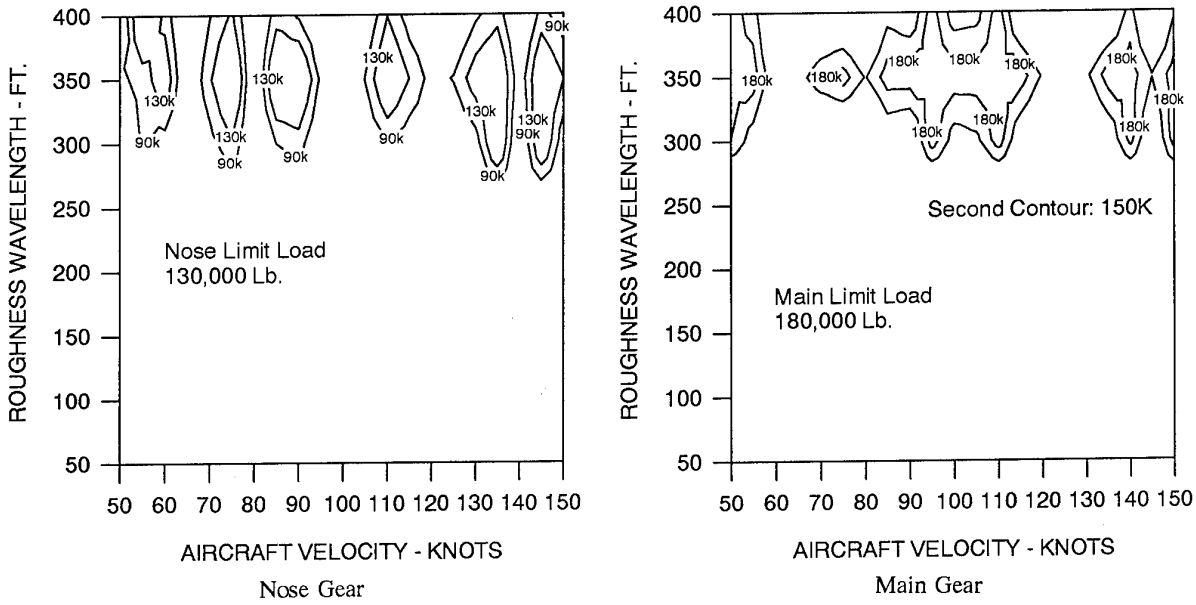

Figure 9 (c). Carrier Based Gear Capability over 75 Percent MIL-A-8862 Semi-Prepared Roughness.

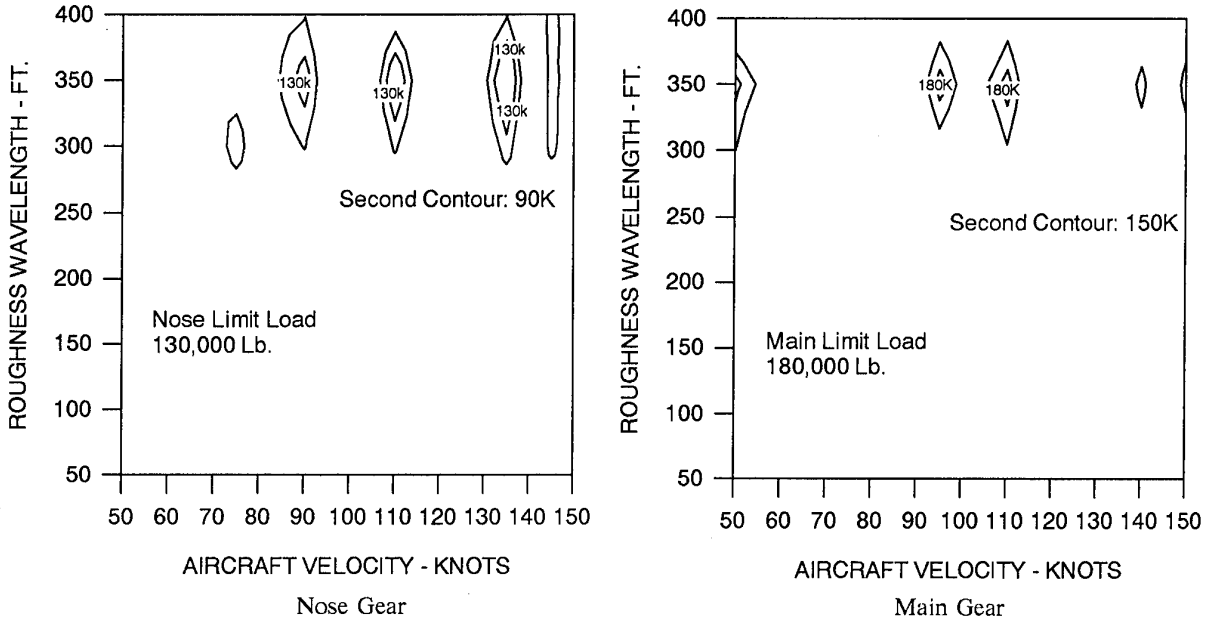

Figure 9 (d). Carrier Based Gear Capability over 50 Percent MIL-A-8862 Semi-Prepared Roughness with 0.4 Braking Coefficient.

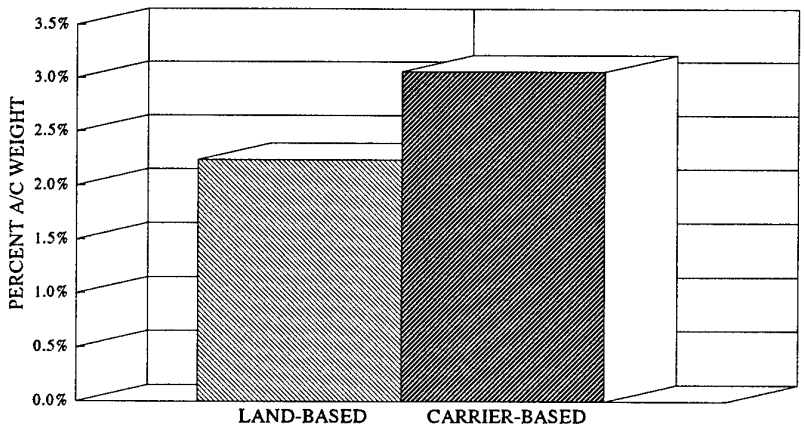

Figure 10. Landing Gear Weight Comparisons.

A REVIEW OF AIRCRAFT LANDING GEAR DYNAMICS

WILLIAM E. KRABACHER
WL/FIVMA Building 45
WRIGHT LABORATORY
WRIGHT PATTERSON AFB
2130 Eighth Street, Suite 1
Ohio 45433-7542, USA

SUMMARY

A review of two different landing gear shimmy mathematical models is presented. One model uses the Moreland tire model and the other model uses the Von Schlippe-Dietrich tire model. The results of a parametric study using these models is presented indicating the sensitivity of various parameters to numerical variation. An identification of stability critical parameters in the models is given. Three different aircraft landing gear shimmy data sets are reviewed and model stability predictions are discussed. A comparison is made with actual experimental results. One of these data sets indicates the nonlinear variation of various input parameters as a function of strut stroke. In the course of the presentation some design rules and cautions are suggested.

LIST OF SYMBOLS

The definitions of the various parameters used in the mathematical models are defined below. Except as noted, the parameters are used in both the Moreland and the Von Schlippe-Dietrich models.

C - Tire Yaw Coefficient (rad/lb) (Moreland Model Only)

C_1 - Moreland Tire Time Constant (sec) (Moreland Model Only)

h - Half Length of the Tire Ground Contact Patch (in) (Von Schlippe-Dietrich Model Only)

L_R - Tire Relaxation Length (in) (Von Schlippe-Dietrich Model Only)

C_3 - Structural Rotation Damping Coefficient (Rotation of Mass about the Trail Arm Axis) (in-lb-sec/rad)

C_D - Tire Lateral Damping Coefficient (lb-sec/in)

C_S - Structural Lateral Damping Coefficient (lb-sec/in)

C_T - Rotational Velocity Squared Damping Coefficient (Rotation about the Strut Vertical Axis) (in-lb-sec^2/rad^2) OR Linear Viscous Damping Coefficient (in-lb-sec/rad)

CF1 - Friction Torque (in-lb)

CF2 - Coefficient of Friction Torque as a Function of Side Load at the Ground (in-lb/lb)

FP - Peak to Peak Torsional Freeplay of the Gear about the Strut Vertical Axis (rad)

I - Mass Moment of Inertia of the Rotating Parts about the Axle (in-lb-sec^2/rad)

I_F - Equivalent Mass Moment of Inertia of the Lumped Mass System about the Trail Arm Axis (in-lb-sec^2/rad)

I_S - Equivalent Mass Moment of Inertia of the Lumped Mass System about the Strut Vertical Axis (in-lb-sec^2/rad)

K_3 - Rotational Spring Rate about the Trail Arm Axis Measured at the Wheel/Axle Centerline (in-lb/rad)

K_4 - Cross Coupled Spring Rate (lb)

K_D - Tire Lateral Spring Rate (lb/in)

K_S - Lateral Spring Rate of the Structure at the Trail Arm and Strut Vertical Centerline Intersection (lb/in)

K_T - Torsional Spring Rate of the Structure about the Strut Vertical Centerline with the Damper Locked (in-lb/rad)

Paper presented at the 81st Meeting of the AGARD SMP Panel on "The Design, Qualification and Maintenance of Vibration-Free Landing Gear", held in Banff, Canada from 4-5 October 1995, and published in R-800.

K_{TI} - Torsional Spring Rate of the Steering Actuator about the Strut Vertical Centerline (in-lb/rad)

L - Mechanical Trail Length, defined as the Normal Distance from the Axle Centroid to the Strut Vertical Centerline (in)

L_G - Geometric Trail = R*sin(γ)

m - Equivalent Lumped Mass of the Wheel, Tire, and Fork (lb-sec^2/in)

m_a - Equivalent Lumped Mass of the Fork (lb-sec^2/in)

R - Rolling Radius of the Wheel/Tire (in)

V - Aircraft Forward Taxi Velocity (in/sec)

W - Landing Gear Vertical Reaction (lb)

μ_t - Tire Moment Coefficient (in-lb/rad)

γ - Attitude of the Gear, Positive Wheel Forward (rad)

Other symbols used in the analysis

F_N - Ground Reaction Normal to the Wheel Plane (lb)

T - Torque Moment about the Strut Vertical Axis due to Torsional Spring Rate of the Structure (in-lb)

1. INTRODUCTION

In an earlier paper (1), a rudimentary outline was presented for the development of an international standard for dealing with various types of landing gear dynamics problems such as shimmy, gear walk, judder, antiskid brake induced vibrations, dynamic response to rough runways, tire-out-of-round, and wheel imbalance. The purpose of the present paper is to sharpen the focus of the previous paper by presenting a detailed analysis of the specific problem of landing gear shimmy. The main content of this paper will be to review two different landing gear mathematical models, to present the results of a parametric study performed on a fighter aircraft nose gear indicating the sensitivity of various parameters in the model to variation[1], to discuss a few parameters critical to gear stability, to review some aircraft landing gear data sets indicating in one case the non-linear variation of the various input parameters as a function of strut stroke, and to review mathematical model stability predictions for these data sets.

2. THE MATHEMATICAL MODELS

Seventeen years ago the author developed a mathematical analysis for determining the shimmy stability boundaries of an aircraft nose landing gear. Over the intervening years, this analysis has evolved into a user friendly, robust computer program that has been quite useful in the prediction of aircraft landing gear shimmy problems. In presenting these mathematical models, it should be made clear that no claim is made to these models being the best or most sophisticated ones that can be used. The only claim made is that these models have been consistently successful in the prediction of shimmy problems on the aircraft studied.

From the landing gear structural standpoint, the two models to be presented are completely identical. The only difference between the two models is that one uses the Moreland tire model (2) and the other uses the Von Schlippe-Dietrich tire model (3)(4). The mathematical equations of motion for the Moreland tire model are given by

1. $m*d^2y/dt^2 - (m - m_a)*L*d^2\Theta/dt^2 = F_N - K_S*y - K_4*\alpha - C_S*dy/dt$

2. $I_S*d^2\Theta/dt^2 = T + (V/R)*I*d\alpha/dt - \mu_t*\psi - F_N*(L + L_G) + (m - m_a)*L*d^2y/dt^2 - W*(\Delta - R*\alpha)*\sin(\gamma)$

3. $I_F*d^2\alpha/dt^2 = - K_3*\alpha - K_4*y - C_3*d\alpha/dt - (V/R)*I*d\Theta/dt - F_N*R*\cos(\gamma) - W*(\Delta - R*\alpha)*\cos(\gamma)$

4. $C_1*d^2\Delta/dt^2 = - dy/dt - d\Delta/dt + R*d\alpha/dt + (L + L_G)*d\Theta/dt - V*\Theta - C_1*d^2y/dt^2 + C_1*R*d^2\alpha/dt^2 + C_1*(L + L_G)*d^2\Theta/dt^2 - C_1*V*d\Theta/dt - V*C*F_N$

[1] Due to space limitations, a discussion of how each parameter in the mathematical models is obtained will be deferred to another paper.

(Note: For a general layout of the coordinate system used refer to Figure 1 below. Both models use the same coordinate system.)

5. $T = -K_T*[\,|\Theta - \Theta_1| - FP]*[\Theta - \Theta_1]/[\,|\Theta - \Theta_1|\,] - [\,CF1 + CF2*F_N]*[d\Theta/dt]/[\,|d\Theta/dt|\,]$

6. $C_T*d\Theta_1/dt*|d\Theta_1/dt| = K_T*[\,|\Theta - \Theta_1| - FP]*[\Theta - \Theta_1]/[\,|\Theta - \Theta_1|\,] - K_{T1}*\Theta_1$

7. $F_N = K_D*\Delta + C_D*\,d\Delta/dt$

8. $\psi = (1/V)*[dy/dt + d\Delta/dt - R*d\alpha/dt - (L_c + L_G)*d\Theta/dt + V*\Theta\,]$

where the degrees of freedom of the model are

y - Strut Lateral Deflection at the Intersection of the Strut Vertical Centerline and the Centerline of the Trail Arm

Θ - Torsional Rotation about the Strut Vertical Centerline

Θ_1 - Torsional Rotation at the Steering Actuator /Damper

α - Tire Roll Rotation about the Fore-Aft Axis through the Trail Arm

ψ - Tire Torsional Rotation about the Vertical Axis through the Axle Centerline

Δ - Tire Contact Patch Centerline Lateral Deflection with respect to Wheel Center Plane Intersection at the Ground

The mathematical equations of motion for the Von Schlippe-Dietrich tire model are given by

1. $m*d^2y/dt^2 - (m - m_a)*L*d^2\Theta/dt^2 = F_N - K_S*y - K_4*\alpha - C_S*dy/dt$

2. $I_S*d^2\Theta/dt^2 = T + (V/R)*I*d\alpha/dt - \mu_t*\psi - F_N*(L + L_G) + (m - m_a)*L*d^2y/dt^2 - W*(y_0 - y + (L + L_G)*\Theta - R*\alpha)*\sin(\gamma)$

3. $I_F*d^2\alpha/dt^2 = -K_3*\alpha - K_4*y - C_3*d\alpha/dt - (V/R)*I*d\Theta/dt - F_N*R*\cos(\gamma) - W*(y_0 - y + (L + L_G)*\Theta - R*\alpha)*\cos(\gamma)$

4. $\{[(3*L_R + h)*h^2]/[\,6*V^3\,]\}*d^3y_0/dt^3 = -y_0 + y - (L + L_G)*\Theta + (L_R + h)*\Theta - [(L_R + h)/V]*dy_0/dt - [(2*L_R + h)/(2*V^2)]*d^2y_0/dt^2$

5. $T = -K_T*[\,|\Theta - \Theta_1| - FP]*[\Theta - \Theta_1]/[\,|\Theta - \Theta_1|\,] - [\,CF1 + CF2*F_N]*[d\Theta/dt]/[\,|d\Theta/dt|\,]$

6. $C_T*\,d\Theta_1/dt*|d\Theta_1/dt| = K_T*[\,|\Theta - \Theta_1| - FP]*[\Theta - \Theta_1]/[\,|\Theta - \Theta_1|\,] - K_{T1}*\Theta_1$

7. $F_N = K_D*(y_0 - y + (L + L_G)*\Theta) + C_D*(dy_0/dt - dy/dt + (L + L_G)*d\Theta/dt)$

8. $\psi = [1/V]*[\,dy_0/dt - R*d\alpha/dt + V*\Theta]$

It is noted for reference (See Figure 1) that a special equation can be derived which connects the Moreland Tire Model parameter Δ with the Von Schlippe-Dietrich parameter y_0. This equation is

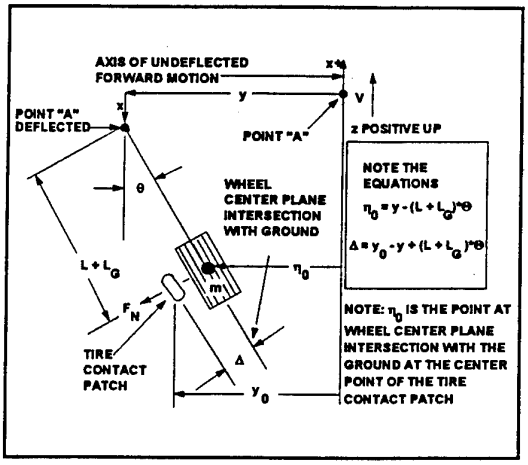

FIGURE 1

$\Delta*\cos(\Theta) = y_0 - y + (L + L_G)*\sin(\Theta)$

or, making the small angle assumptions, $\cos(\Theta) = 1.0$ and $\sin(\Theta) = \Theta$, it follows that

$\Delta = y_0 - y + (L + L_G)*\Theta$

The degrees of freedom of this model are

y - Strut Lateral Deflection at the Intersection of the Strut Vertical Centerline and the Centerline of the Trail Arm

Θ - Torsional Rotation about the Strut Vertical Centerline

Θ_1 - Torsional Rotation at the Steering Actuator/Damper

α - Tire Roll Rotation about the Fore-Aft Axis through the Trail Arm

ψ - Tire Torsional Rotation about the Vertical Axis through the Axle Centerline

y_0 - Lateral Distance from the Fore-Aft Axis of Undeflected Forward Motion to the Center Point of the Ground Contact Area

The method of initial excitation in both models is to give Θ an initial value of 5.0 degrees.

In comparing these two mathematical models, it will be noted that the only difference between them is essentially which equation is used to describe the tire motion. When this shimmy analysis was originally developed, only the Moreland Tire Model was used and most of the landing gears analysed with this analysis had Moreland tire data available. About ten years after the original analysis was developed, a landing gear needed to be analysed for which only Von Schlippe-Dietrich tire data was available. Due to the prior success of the original analysis, it was decided to retain the original structural analysis portion and only modify the tire model portion. The result is the Von Schlippe-Dietrich version presented in this paper.

An important result of obtaining this second analysis is that now a direct comparison of the accuracy of the two tire models can be obtained since all structural considerations are exactly identical for the two analyses. Recently, it became known that an empirical procedure existed which could approximate either tire model's shimmy parameters from the knowns of tire size and inflation pressure (5). The availability of this procedure lends itself to providing a basis for a direct comparison of the two models' prediction capabilities. Some preliminary comparisons of analysis predictions have been conducted on a fighter known to have shimmy problems. However, at this time it is felt that these comparisons are too few to make any general statements on trends found in these comparisons.

To provide examples of the type of output obtained from the two computer analyses based upon the above two sets of differential equations, reference is made to Figures 2, 3, 4, and 5 below. These four graphs are plots of the y - L*Θ variable for the cases of a stable landing gear, a gear in limit cycle oscillation, a gear in divergent shimmy, and a gear in severe divergent shimmy. The two computer analyses also output the Θ, Θ_1, α, Δ or y_0, and torque T variables in similar graphical plots.

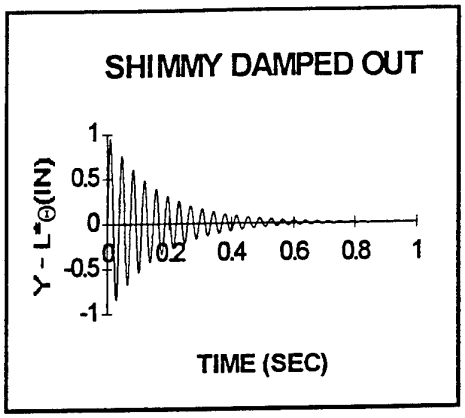

FIGURE 2

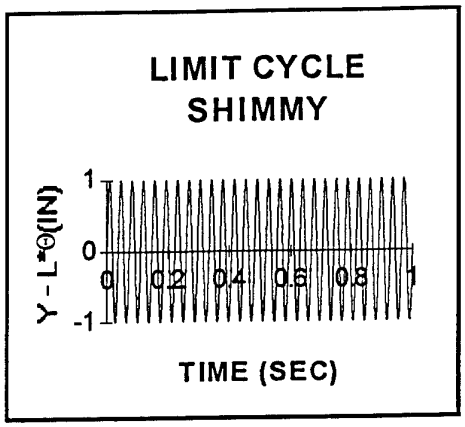

FIGURE 3

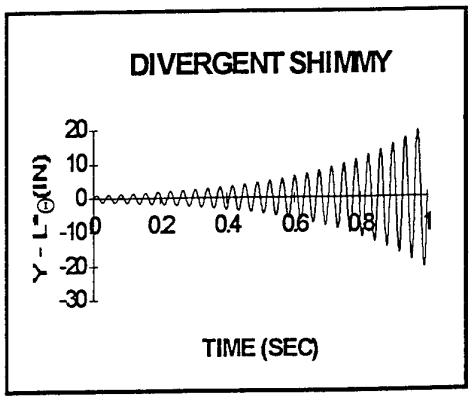

FIGURE 4

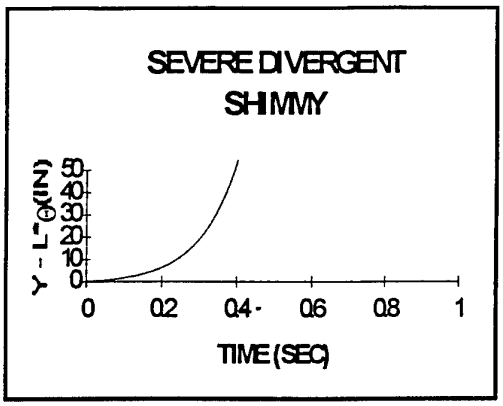

FIGURE 5

3. SENSITIVITY ANALYSIS OF PARAMETER VARIATION

About fifteen years ago, a sensitivity analysis was conducted using some fighter nose landing gear data and the Moreland Tire Model version of the shimmy analysis. While the results of this study are only totally accurate for the aircraft analysed, it has been found that the general trends in this study have been a valuable guide in analysing other nose landing gear. The data defining this nose landing gear from a shimmy standpoint is presented in Table 1 under the column for Fighter A.[2]

Defining the values in this table as the nominal values of the gear, the parametric study was conducted by incrementally varying one parameter at a time and increasing its value until its value was 1.5 times its nominal value. The computer output from the variation of each parameter was reviewed for stability effects and graded according to the scale: greatly increases stability, increases stability, slightly increases stability, no change, slightly decreases stability, decreases stability, greatly decreases stability. Using this scale the following results were obtained.

C - Increases Stability
C_1 - Increases Stability
C_D - Slightly Increases Stability
C_S - Increases Stability
C_T - Increases Stability
C_3 - Slightly Decreases Stability
I - Decreases Stability until I = 1.6 and then Increases Stability
I_F - Decreases Stability
I_S - Decreases Stability until I_S = 2.25 and then Increases Stability
K_D - Greatly Increases Stability
K_S - Decreases Stability
K_T - Increases Stability
K_3 - Increases Stability
K_4 - Greatly Decreases Stability
L - Greatly Decreases Stability[3]
γ - Greatly Increases Stability
m - Decreases Stability until m = .225 and then Neutral Stability
R - Increases Stability
W - Slightly Decreases Stability
FP - Greatly Decreases Stability
CF1 - Greatly Increases Stability
CF2 - Slightly Increases Stability
μ_T - Slightly Increases Stability
K_{T1} - Decreases Stability

4. LANDING GEAR STABILITY CRITICAL PARAMETERS

In one particular shimmy investigation involving a trainer nose landing gear a problem was uncovered that identified stability critical parameters[4,5]. Specifically, the vendor supplied a complete set of

[2] The some of the original values used in the parametric study were accidentally lost. The values listed in Table 1 are approximately correct. However, they should not be used in the analysis in an attempt to reconstruct the results cited here. The results of this study should be viewed simply as a general indicator of how dynamic response may change as a parameter value is altered.

[3] Since the nominal value of L for this landing gear is 0.8 inches, the maximum value used in this sensitivity study is 1.2 inches. Therefore, greatly decreasing stability makes physical sense in this case. Generally, positive trail values below 3 inches tend to be destabilizing.

[4] The term stability critical parameter is taken to mean that this parameter will produce greatly varying analysis prediction results for small changes in the parameter value.

[5] The actual experimentally measured data for this trainer is presented in Table 1.

landing gear shimmy analysis data which was entered into a data file for the shimmy analysis. When the analysis was executed, the analysis indicated the gear would shear off in the first quarter-cycle. (Refer to Figure 5 above for a plot of the actual dynamic response predicted by the analysis.) Since this level of unstable dynamic response had never been encountered before, it was determined that something must be wrong with the data. After the vendor supplied four additional data sets, all of which also predicted the gear would shear off in the first quarter-cycle, an investigation was conducted by comparing the values of the data in these five data sets with the data sets from other aircraft nose landing gears to determine the physical realism of the data. Using the above introduced parametric study as a guide, focus quickly narrowed onto the value of the parameter K_4 since its variation greatly alters the analysis predictions. The result determined was that in all five data sets supplied the value of K_4, relative to the values of K_4 for other landing gears was in error by being two orders of magnitude too large.

It was decided to measure the stiffness values of K_T , K_S , K_3 , and K_4 as well as the torsional freeplay of the gear on an actual aircraft (6). The outcome of this measurement process was that in all five sets of vendor supplied data, these four stiffnesses were grossly at odds with what was experimentally measured on the actual aircraft. The experimentally measured values of K_T, K_S, and K_3 were approximately one order of magnitude smaller and the K_4 parameter was two orders of magnitude smaller than the values supplied in the data sets.

While this particular vendor did not have a finite element analysis capability for determining these parameters, it should be pointed out that subsequent encounters with these parameters on other aircraft nose landing gears has generally established that finite element analyses tend to error on the high side in determining these four parameters. Therefore, since these parameters are stability critical, considerable caution should be used in determining values for them in the design stage of the gear. As an additional caution, a band around each such determined value should be established and investigated in the analysis to insure no stability boundaries are crossed within this band or in the combination of bands of these parameters.

5. REVIEW OF LANDING GEAR DATA SETS AND STABILITY PREDICTIONS

Table 1 below provides the shimmy data sets for two different fighter (Fighter B and Fighter C) and one trainer aircraft that have been analysed for shimmy behavior. These three aircraft were selected

	FIGHTER A	TRAINER	FIGHTER B	FIGHTER C 4 IN STROKE
NOSE LANDING GEAR SHIMMY MODEL PARAMETERS				
C (MORE)	7.5E-05	2.40E-04	CHART 1	4.49E-05
C1 (MORE)	2.05E-04	4.20E-03	CHART 2	1.29E-03
h (VSD)	N/A	N/A	N/A	N/A
LR (VSD)	N/A	N/A	N/A	N/A
C3	0.0	21.92	0.0	0.0
CD	6.0	4.41	CHART 3	3.45
CS	2.5	0.9455	3.55	4.82
CT (SEE NOTE)	200.0	120.0	6124.0	2325.0
CP1	200.0	200.0	CHART 4	360.0
CP2	0.0	0.8194	0.0	0.575
FP (DEG)	1.0	1.97	0.5 - 1.2	0.76
I	1.554	1.43	5.155	5.76
IF	1.99	1.015	3.422	3.37
IS	2.192	0.498	4.519	5.34
K3	654000.0	347282.19	CHART 5	2009000.0
K4	30600.0	27037.53	CHART 6	1000000
KD	2857.0	858.0	CHART 7	2672.0
KS	3150.0	2552.61	CHART 8	7504.0
KT	89000.0	117974.0	CHART 9	493200.0
KT1	65000.0	22800.0	2815000.0	6.00E+05
L	0.8	1.25	3.0	3.00
LG	0.96	0.72124	VARIED	1.1753
m	0.0965	0.04378	0.163	0.154
mA	0.0359	0.0134	0.041	0.037
R	7.88	6.9	CHART 10	10.0
W	3000.0	970.0	VARIED	7300.0
μT	10000.0	3900.0	CHART 11	35361.0
γ	7.0	6.0	1.0	6.75
LOAD - STROKE CURVE			CHART 12	
LOAD - GROUND SPEED CURVE			CHART 13	
NOTE: CT FOR FIGHTER A AND THE TRAINER ARE LINEAR DAMPING VALUES CT FOR FIGHTER B AND FIGHTER C ARE VELOCITY SQUARED VALUES				

TABLE 1

because of a desire to provide examples of both shimmying and non-shimmying landing gear. Each of these data sets will be reviewed and their shimmy characteristics discussed.

The Trainer data set is an example of a stable

landing gear when the values listed in Table 1 are used in the shimmy analysis. An example of the typical dynamic response of this landing gear is provided in Figure 6 below for the Θ variable. (Note: Θ in this figure is in degrees.) It is noted that this gear is very stable as there is little dynamic response to the initial 5 degree deflection of Θ.

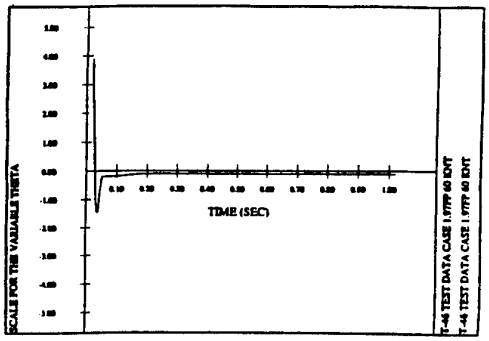

FIGURE 6

The Fighter B data set is one of the most complete data sets for a landing gear that the author possesses. This set contains 11 charts that show the nonlinear variation of 11 of the input parameters to the shimmy analysis. Also included are charts 12 and 13 which show the load stroke curve of the shock strut and the load on the gear as a function of aircraft forward ground speed.

In an earlier paper (7), an investigation was conducted to determine the overall effect of these nonlinear variations on the predicted stability boundaries of the analysis in comparison to the experimentally determined shimmy stability boundaries of the gear. The manner in which this investigation was conducted was to have the analysis execute 5 knot increment runs starting with 15 knots and incrementing up to 150 knots. At each speed increment, the analysis would determine the load on the gear from chart 13. Depending on the particular parameter, the analysis would either then calculate the parameter directly or it would determine the stroke position from chart 12 and then calculate the desired parameter. After all 11 parameters were so calculated, the analysis would execute and the dynamic response of the gear would be determined. From the analysis results, the shimmy speed was then taken to be the lowest speed at which the analysis indicated sustained limit cycle oscillation of the gear. This procedure was repeated at increments of 0.05 degrees of torsional freeplay from 0.5 to 1.2 degrees.

As a comparison, a static analysis of the gear was also performed to evaluate the prediction variations. The static analysis was conducted by selecting the 11 parameter values at the static stroke position of the gear and incrementing the taxi speed in 5 knot increments from 15 to 150 knots while holding these 11 parameters constant. Again the shimmy speed was taken as the lowest speed at which the analysis indicated sustained limit cycle oscillation of the gear. The comparison between the dynamic and static analyses predictions are shown in chart 14. Also included in this chart are the actual experimentally determined shimmy boundaries of the gear. The lower experimental boundary shows when shimmy onset occurred in the gear and the upper experimental boundary indicates strong limit cycle oscillation shimmy.

It is particularly interesting to note that the dynamic analysis boundary follows the contour of the shimmy onset boundary quite closely and consistently errors slightly on the conservative side. Whereas, the static analysis boundary lies above the shimmy onset curve below 0.85 degrees of freeplay and errors increasingly on the conservative side as the torsional freeplay increases from 0.85 degrees to 1.20 degrees. Both the dynamic and static analyses indicated the shimmy frequency to be 27 HZ and this was confirmed in experimental measurement.

The overall implication of these findings seems to suggest that the dynamic modelling of the gear as described above will significantly improve the accuracy of the analysis predictions and that nonlinear parameter variation is an important consideration in obtaining an accurate shimmy analysis of a landing gear.

The Fighter C data set in Table 1 is provided for the 4 inch stroke position which corresponds to the static stroke position of the gear. Figures 7, 8, 9, 10, 11, 12, 13, and 14 show typical dynamic response of this nose gear. Figures 7, 8, 9, and 10 are plots of the y - L*Θ or lateral displacement variable at the point A for the taxi speeds of 80, 90, 95, and 100 knots respectively. (Note: In these figures what is called the x - L*Θ variable is identical to what is referred to as the y - L*Θ variable in this paper.) Figures 11, 12, 13, and 14 are the plots of the Θ or torsional rotation about the strut vertical axis variable at these same taxi speeds. (Note: Θ in degrees.)

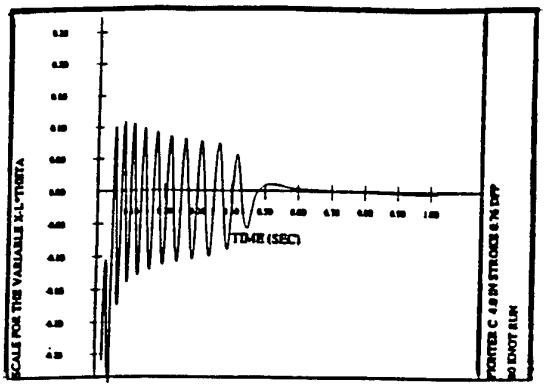

FIGURE 7

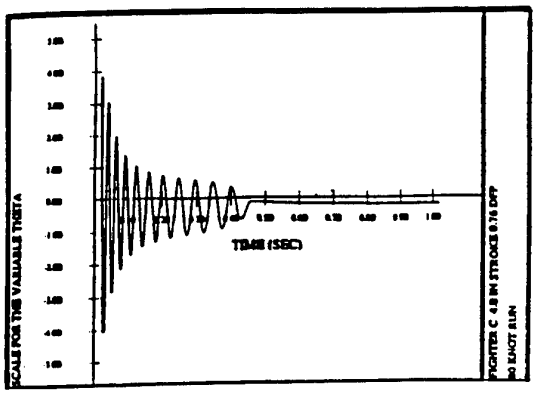

FIGURE 11

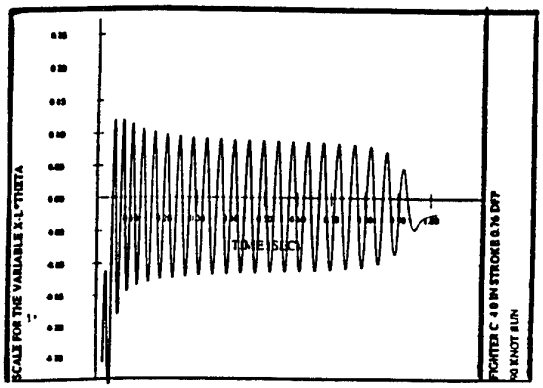

FIGURE 8

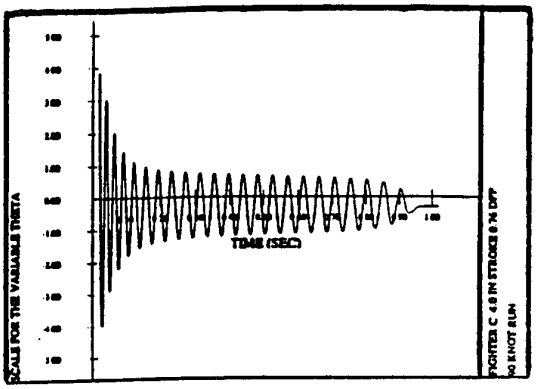

FIGURE 12

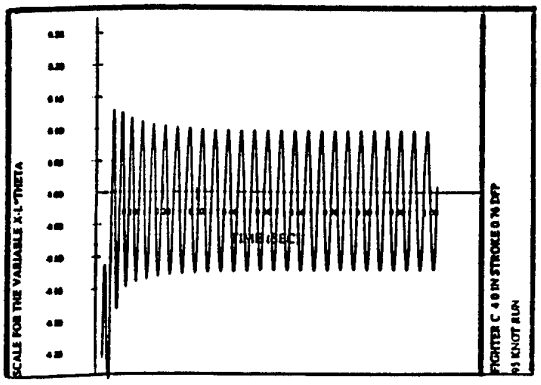

FIGURE 9

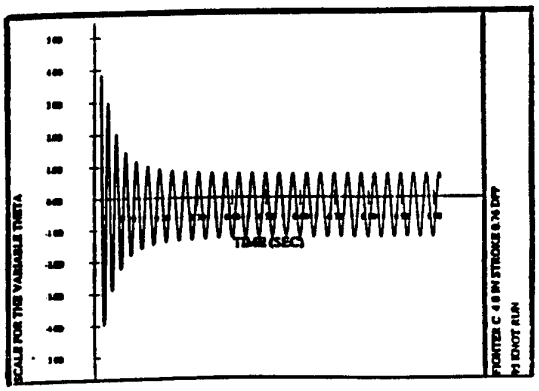

FIGURE 13

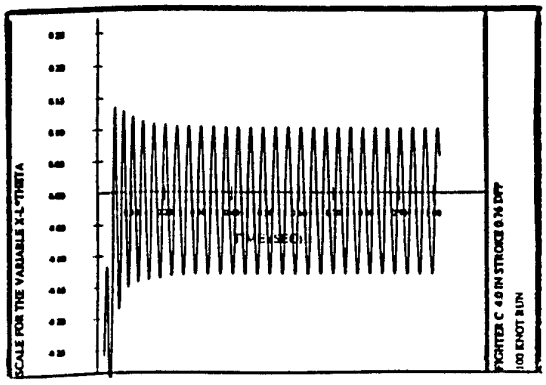

FIGURE 10

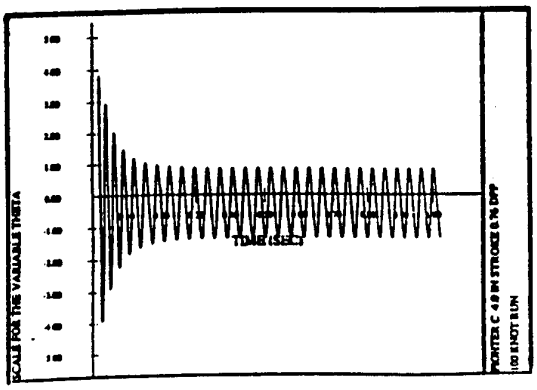

FIGURE 14

In comparing these graphs it is noted that as the taxi speed increases from 80 to 90 knots a progressively longer period of time is required for the vibration to damp out. At 95 knots the gear has the onset of limit cycle shimmy. At 100 knots the limit cycle shimmy is definitely established. From these time histories it is seen that the shimmy oscillation frequency is about 27.06 HZ at 95 knots. When the actual aircraft was tested, it was found that the nose gear went into a sudden onset of shimmy at 92 knots and had a frequency of 27.5 HZ. Repeated testing of this landing gear, yielded reasonably consistent repeatability at this shimmy speed and frequency.

In the course of the shimmy investigation for Fighter C, one very important point came to light concerning the measurement of landing gear shimmy parameters. The vendor's original analysis consistently indicated that this landing gear was stable at all taxi speeds. The analysis provided by the author indicated the 95 knot shimmy event at 27.06 HZ. The question arose as to what was different between the two analyses. After review of the input data a primary cause of this difference was established. The stability critical parameters K_T, K_S, K_3, and K_4 used in the vendor's analysis were obtained by rigidly mounting the landing gear in a fixture and measuring the resulting parameters. Whereas, the author's analysis took into consideration the softening effects of the landing gear mounted in a flexible fuselage and reduced the stiffness values supplied by the vendor. The amount of this reduction was largely based on experience with other landing gear.

The reason for taking fuselage flexibility effects into consideration was based on some data obtained in another landing gear shimmy investigation.

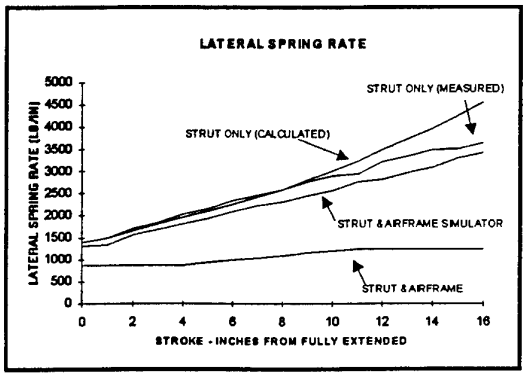

FIGURE 15

Referring to Figure 15, it is seen that the lateral stiffness values obtained for a landing gear rigidly mounted in a fixture (in the chart, strut only (measured)) vary from one and a half to three times the values of the lateral stiffness actually measured on a landing gear mounted on the aircraft. This comparison establishes the fact that backup structural flexibilities of the airframe must be taken into consideration when the four stability critical stiffness values are determined.

In addition to this primary cause of the difference between analysis predictions, a secondary cause was also established. The vendor's analysis assumed a value of 6% of critical damping as the magnitude of the structural damping available. Whereas, based upon personal experience with the variablity of available structural damping, the author decided to assume that the maximum amount of available damping was 1% of critical. At the time, the main reason for this selection was a desire to select a damping value that would expose any potential sensitivities the gear may have toward shimmying. Further support for this position was established after the fact when Denis J. Feld published his results on an analytical investigation of landing gear shimmy damping (8). The essential conclusion of the analytical investigation was that the amount of available damping at any instant during a taxi run could vary from 1% to 10% of critical viscous damping. Therefore, at the beginning of any landing gear shimmy investigation an assumption of 1% critical damping is a reasonable starting point.

Before departing from Figure 15, another subject is in need of mention. In the discussion of landing gear stability critical parameters above in section 4, it was pointed out that caution should be exercised when obtaining stability critical stiffness values because the finite element analysis predictions for these values tend to error on the high side. The proof of this error is established in the above figure for the strut only (calculated) case where it is seen that the largest error in stiffness values occurs between the calculated values and the strut mounted on an actual airframe.

6. CONCLUSIONS

In conclusion, a detailed analysis of the specific problem of landing gear shimmy was presented in which the two mathematical models described have been consistently successful in the prediction of landing gear stability characteristics to date. One of

these models uses the Moreland Tire model and the other uses the Von Schlippe-Dietrich Tire model. A classification of the various types of analysis output was given which consisted of a stable gear, a gear with limit cycle oscillation shimmy, a gear with divergent shimmy, and a gear with severe divergent shimmy. The results of a sensitivity study based on Fighter A's landing gear data was given. The parameters K_T, K_S, K_3, and K_4 were identified as being stability critical in the analysis of gear shimmy. The Trainer data set described a stable landing gear. The Fighter B data set described a gear with limit cycle oscillation shimmy at a frequency of 27 HZ which was verified experimentally. Finally, the Fighter C data set analytically described a gear also with limit cycle oscillation shimmy at 95 knots with a frequency of 27.06 HZ. Experimentally, this gear went into limit cycle oscillation at 92 knots with a frequency of 27.5 HZ.

In the course of the presentation a number of important points were made. First, the Fighter B data set indicated the nonlinear variation of 11 input parameters to the shimmy analysis and suggested that dynamic modelling of the gear will significantly improve the accuracy of the overall analysis predictions. The Fighter C data set established the importance of taking into consideration the backup fuselage flexibilities when determining the stability critical parameters K_T, K_S, K_3, and K_4. This data set also suggested that an initial assumption of 1% of critical viscous damping is a good manner in which to expose the potential senstivities of a landing gear to shimmy. Lastly, the tendency of finite element analyses to error on the high side when calculating the stability critical parameters was established.

BIBLIOGRAPHY

1. AIRCRAFT LANDING GEAR DYNAMICS PRESENT AND FUTURE, William E. Krabacher, SAE Technical Paper Series 931400 (1993).

2. THE STORY OF SHIMMY, William J. Moreland, Journal of the Aeronautical Sciences, pp. 793-808 (1954).

3. SHIMMYING OF A PNEUMATIC WHEEL, B. Von Schlippe and R. Dietrich ATI-18920 (1941) Subsequently printed as NACA TM 1365

4. CORRELATION, EVALUATION, AND EXTENSION OF LINEARIZED THEORIES FOR TIRE MOTION AND WHEEL SHIMMY, Robert F. Smiley NACA TR 1299 (1957)

5. EMPIRICAL ESTIMATION OF TIRE PARAMETERS, Raymond J. Black, paper presented at SAE Committee A-5 Meeting, 28 April 1980, Renton, Washington

6. THE EXPERIMENTAL MEASUREMENT OF THE T-46 NOSE LANDING GEAR SHIMMY PARAMETERS, William E. Krabacher, ASD/ENFSL, Wright Patterson AFB, OH (1986) (In-House Publication)

7. A DYNAMIC SHIMMY ANALYSIS, William E. Krabacher, ASD/ENFSL, Wright Patterson AFB OH (1981) (In-House Publication).

8. AN ANALYTICAL INVESTIGATION OF DAMPING OF LANDING GEAR SHIMMY, Denis J. Feld, SAE Technical Paper Series 902015 (1990).

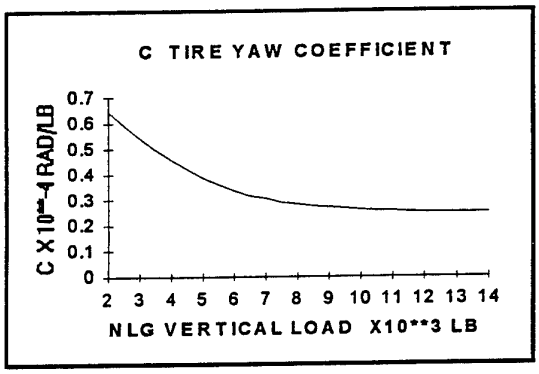

CHART 1

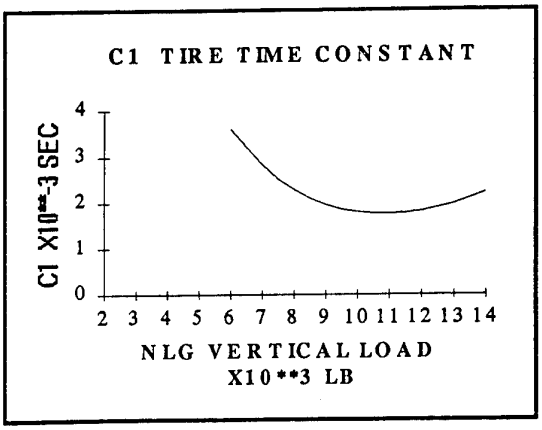

CHART 2

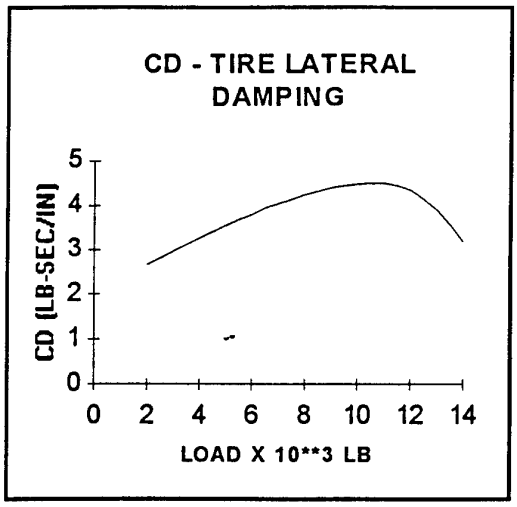

CHART 3

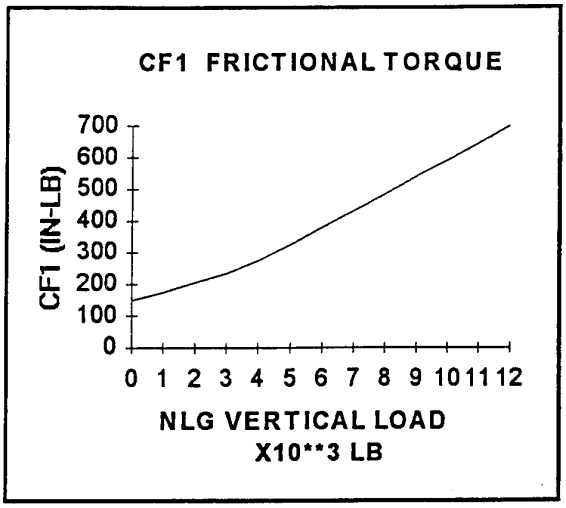

CHART 4

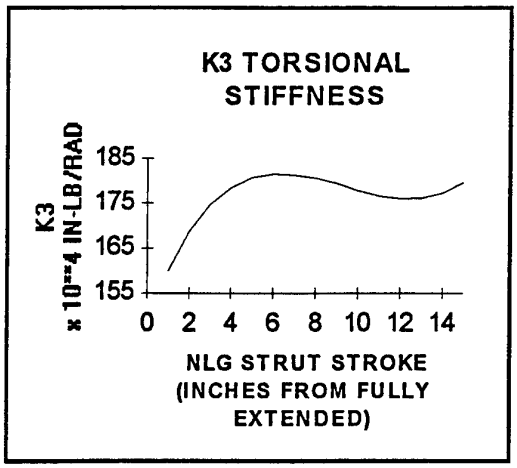

CHART 5

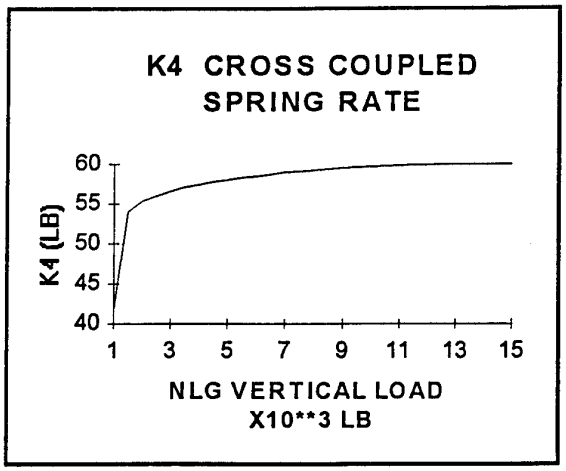

CHART 6

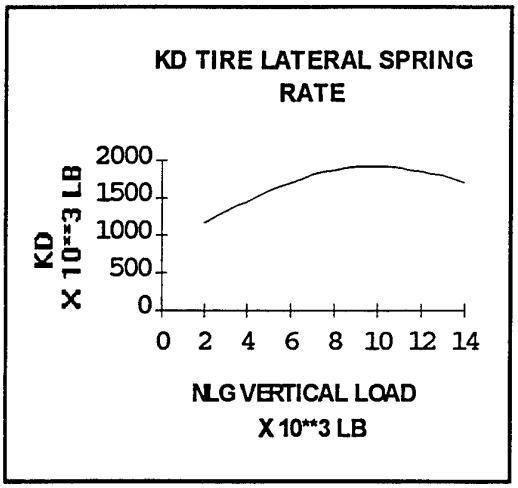

CHART 7

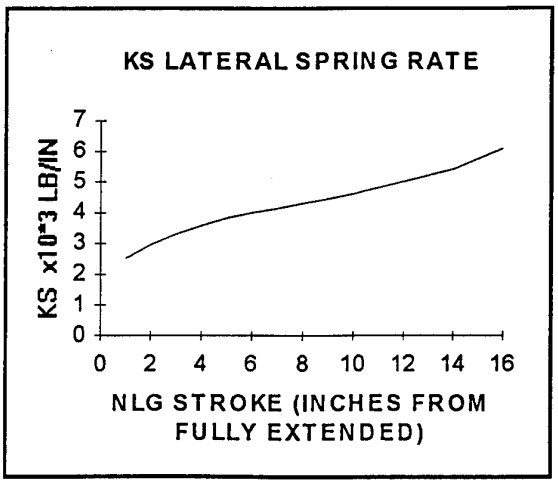

CHART 8

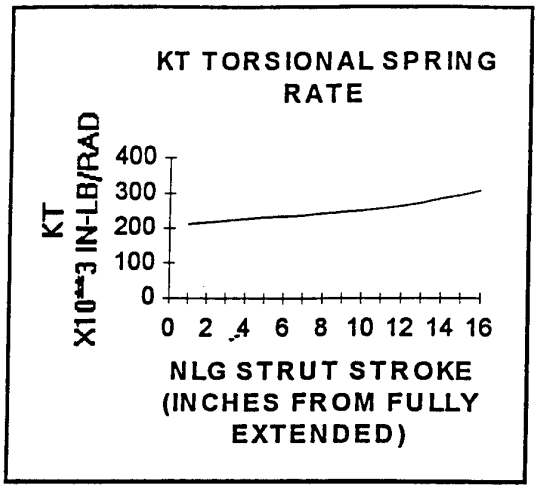

CHART 9

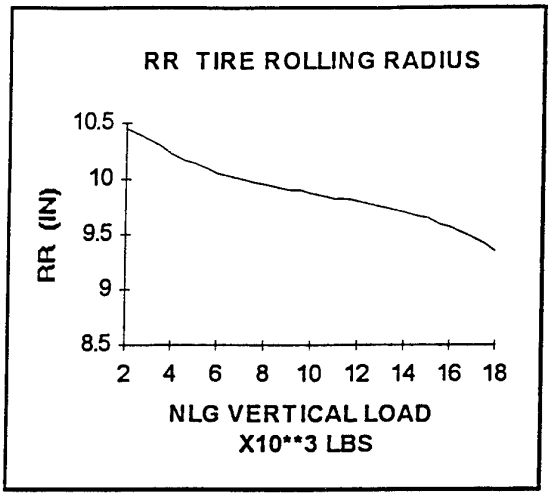

CHART 10

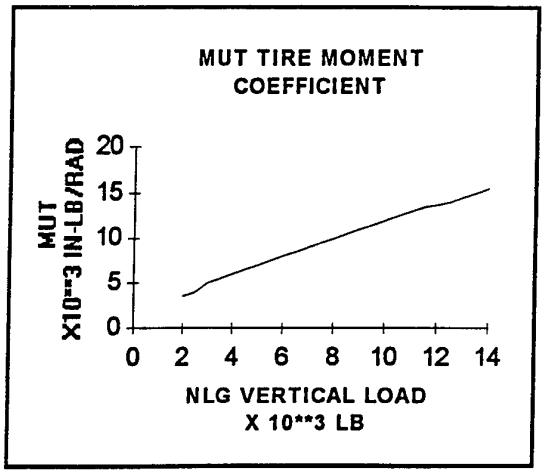

CHART 11

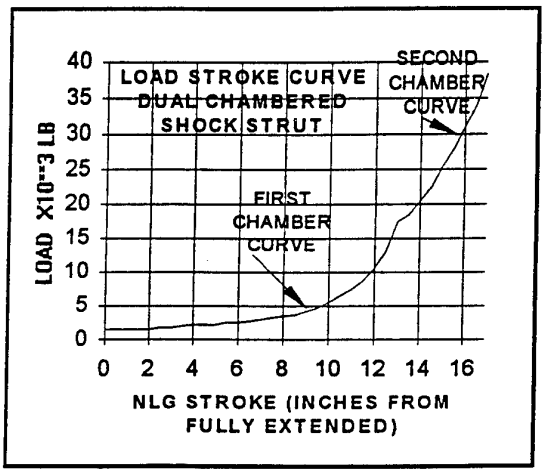

CHART 12

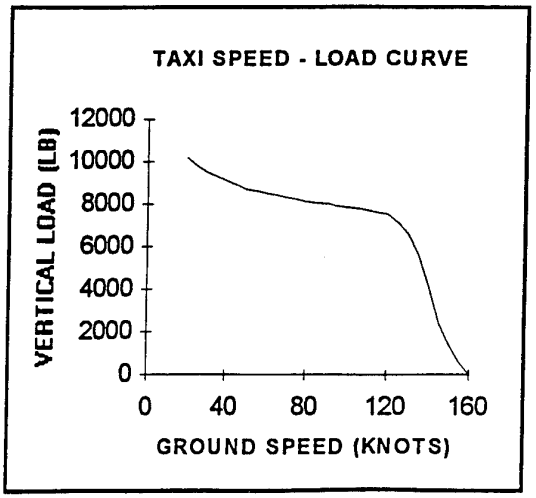

CHART 13

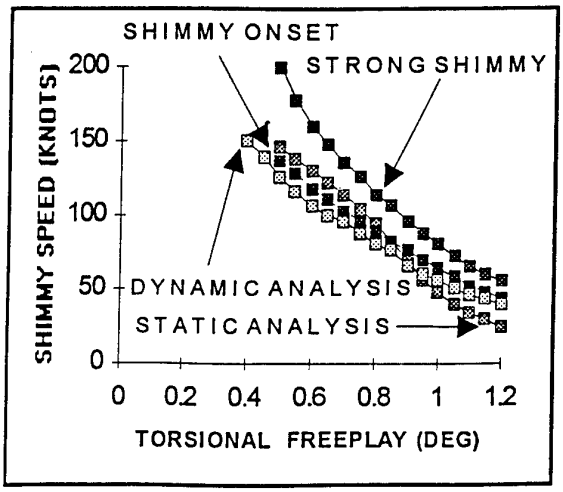

CHART 14

Self-Induced Oscillations of Landing Gear as an Integral Landing Gear Aircraft System Problem

W.Luber, G.Kempf, A.Krauss

Daimler-Benz Aerospace AG
Military Aircraft LME24
81663 Munich
Germany

SUMMARY

Present paper is treating three topics:

Two of the topics deal with seemingly self-induced oscillations observed during aircraft and subsystem development tests. The third topic gives a short overview on procedures to treat shimmy as a "flexible landing gear on flexible aircraft" problem.
The topic treated in section 2 (Shimmy on Nose Landing Gear) presents a case observed in taxi tests of a prototype aircraft. Although specific shimmy calculations were not performed for this case, there are indications that a purely lateral/torsional tyre model would possible not have shown the instability observed. Appendix A gives some evidence therefor.
Section 3 (Brake Torque Oscillations at Brake Initiation) treats a case, where quasi self-induced oscillations are caused by interaction of tyre circumferential force characteristics with the brake control system. Usual means to suppress shimmy (e.g. dampers, modification of landing gear geometry) are ineffective in this case.
Landing gear vibrations may cause a variety of problems in the rest of the aircraft. Section 4 (Integral Landing Gear/Aircraft Problem) presents a summary of potential problem ramifications. It also gives a short overview on a viable approach to treat landing gear shimmy in context with aircraft structure.

1. INTRODUCTION

An aircraft landing gear system has to be designed to meet various requirements covering all ground-based operations. It is a complex non-linear system which incorporates many sub-components often procured of sources which can produce structural dynamics and loading effects on the gear as well on the aircraft.
The landing gear must be capable to carry heavy weight for take off operations, hard impact of the landing as well as the kinetic energy of forward motion on landing to bring the aircraft safely to rest. Due to the long terms of developing an aircraft reducing the risk of redesign and the cost of testing it is desirable to be able to predict the dynamic behaviour of landing gear systems.
In the past methods were used to calculate via mathematical criteria, Ref. 1-1 and 1-2, the stability of the nose landing gear against shimmy. Since landing gear are very non-linear systems a time domain simulation code must be applied to show the behaviour of the landing gear itself and also the involved subsystems. An integrated approach to the modelling of the subsystems of the landing gear and the interaction of the elastic aircraft is required to accomplish the task. To get reliable results, which can also be validated by tests various components must be considered and introduced in the calculations like tyre, wheel, bogie, leg, oleo, braking system, anti skid control, steering and flexible aircraft.
This report presents the straight forward trial to integrate the elastic aircraft into the shimmy investigation for nose landing gear of a fighter type aircraft development phase.

2. SHIMMY ON NOSE LANDING GEAR

A prototype training aircraft is depicted in Fig.2-1 and the major design data are presented in the table 1 below.

Wing Span	10.46 m
Total Length	10.90 m
Height	3.91 m
Wing Area	15.51 m^2
Gross Weight	3540 kg
Maximum Cruise Speed	330 KEAS
Maximum Dive Speed	390 kts
Approach Speed Landing Config.	105/120 kts
Range	800 nm
Operation Ceiling	31,000 ft
Load Factor	+6/-3 g
Static Thrust at Take Off	14.2 kN

Table 1 Technical Data Advanced Training Aircraft

The aim of the development was to take part on the competition of the next generation of the Air Force and Navy training aircraft. The design of the aircraft was

Paper presented at the 81st Meeting of the AGARD SMP Panel on "The Design, Qualification and Maintenance of Vibration-Free Landing Gear", held in Banff, Canada from 4-5 October 1995, and published in R-800.

therefore based on the requirements of the " Joint Primary Advanced Training - System ".
To keep the development of the A/C in time attention was paid to a new aerodynamic design with good handling and performance quality. Reducing the risk of redesign proven components of similar aircraft were used for fast prototyping. Therefore the nose landing gear from T-46A training aircraft was used. The modified nose landing gear is shown in Fig. 2-2 with the most specific data. This paragraph describes the investigation to prove the modified nose landing gear on the advanced training aircraft is free of shimmy.

2.1 THEORETICAL ANALYSIS MODEL

For structural dynamics analysis a NASTRAN finite element model (FEM) with about 9000 degrees of freedom for the half aircraft was established (Ref. 2-1). This model does not include the elasticity of the undercarriage for shimmy investigations due to the large variety of possible state variables.
The major eigenmodes with respect to nose landing gear shimmy are vertical and lateral fuselage bending modes due to the displacements of x- and y- direction on the attachment points as well as the fuselage torsion mode which generates camber angle of the nose landing gear.
Some important eigenmodes are summarised in table 2.

Mode	Frequency [Hz]
Elevator Rotation	3.65
Rudder Rotation	3.55
Fin 1st Bending	7.02
Wing 1st Bending Symmetric	8.85
Fuselage 1st Vertical Bending	12.62
Aileron Rotation Antisymmetric	15.37
Wing 1st Bending Antisymmetric	16.15
Fin 1st Torsion	20.16
Aileron Rotation Symmetric	26.20
Wing 1st Torsion	36.59
Fuselage 2nd Vertical Bending	51.40

Table 2 Major Eigenmodes and Frequencies

2.2 NOSE LANDING GEAR

The nose landing gear strut is a single axle forward retracting gear with an oil filled, nitrogen charged shock strut. The gear was originally developed for the Fairchild Republic T-46A Trainer A/C. It was designed for a sink rate of 13 fps limit and 16.2 fps ultimate cases. To maintain the same trail of the nose landing gear as on T - 46A aircraft the original actuator rod end has been modified by Daimler Benz Aerospace. The nose landing gear wheel and tyre is from the Pilatus PC-9 and delivered via BFGoodrich, Ohio, because the original wheel and tyre was not more available.

2.3 TAXI TEST

Several taxi tests were performed on the smooth runway at Dasa flight test centre Manching to show that the nose landing gear is free of shimmy. During the test no special equipment for shimmy excitation was installed on the runway. The aircraft was equipped with 13 transducers on wing and tail to measure the important dynamic eigen modes. Two additional transducers were installed on the nose landing gear to measure the x- and y- acceleration (Fig. 2-2). The result of a low taxi test is shown in Fig. 2-3. This time history reveals a heavy oscillation in x- and y- direction at a frequency of 25.7 Hz.

2.4 EXPLANATION

Shimmy onset was measured at an aircraft speed of 35 kts during deceleration of the aircraft. The speed was stabilised and the aircraft was moving straight forward with no pilot input on the stick .
Fig. 2-3 shows the time history of the measured nose landing gear transducers as well as the wing tip and ailerons. The analysed frequency is at 25.7 Hz and the maximum recorded accelerations are ± 10g in x-direction and ±7g in y-direction. From these accelerations it is suspected that a primary fore/aft oscillation induces y-oscillations due to asymmetry of nose wheel suspension (see Fig. 2-2 and Appendix). All other pick ups show no change in the time history before and during shimmy. The oscillation lasted about 2.4 seconds.
The speed of the aircraft was slightly decreased to 32 kts.
A more detailed sketch of the pure shimmy, only the x- and y- behaviour of the nose landing gear is depicted in Fig. 2-4 .
It should be mentioned that a rigid body mode of about 3 Hz is overlapped this shimmy oscillation. This aircraft mode were always measured during taxi tests and is not responsible for this landing gear oscillation.
Fig. 2-5 shows the Power Spectral Density of the ailerons. The dominant frequencies are the fuselage bending , aileron rotation.

2.5 SOLUTION OF THE PROBLEM

To avoid shimmy on the nose landing gear the following points were considered:

a) Change of trace line
Comparison of the original nose landing gear on T-46A aircraft shows that the inclination of training aircraft landing gear leg is the same. To change the inclination of the nose landing gear either the actuator rod end or the attachments of the strut must be modified.

b) Influence of elastic fuselage modes
Due to the shimmy frequency of 25.7 Hz it is assumed that the eigen-modes of the fuselage, 1st(12.6 Hz) and

2nd (51.4 Hz) vertical bending are not involved in this oscillation problem.

c) Tyre Pressure
Under the circumstances that the original tyre was not available and the used tyre has a different characteristic, an increase of pressure could solve the problem due to shorten the relaxation line.

d) Installation of shimmy damper
The shimmy damper is a hydraulic unit which reduces the tendency of the wheel to oscillate from one side to side. This dampers are usually constructed in one of two general designs, piston type and vane type, both of which might be modified to provide power steering as well as shimmy damper actions.

e) Mounting of massbalance
Tuning the eigenfrequencies of the landing gear massbalance weights have to be mounted on an arm forwards or rearwards on the strut. Massbalance is a useful tool if there is enough space to mount the weights.

f) Landing gear torsion stiffness
Possible effects of torsional backlash is a reduced effective torsional stiffness of the strut. Generally there is an undue sensitivity by reduction in torsional stiffness.

Taxi tests after increasing the tyre pressure reveals no shimmy. Fig. 2-6 shows this sufficient improvement because the nose landing gear is almost free of oscillation.
No further changes were investigated.

It should be noticed that worn and cold tyres made undercarriages less stable than it was with new tyres. This was reported by pilots during taxi tests and is likely due to the change in tyre stiffness as the tread wears away. There is also a possibility that out of balance forces in the worn tyre induces high frequency oscillations which nullifies the effect of friction in the landing gear.

3. BRAKE TORQUE OSCILLATIONS AT BRAKE INITIATION

The case following demonstrates that not only unsuitable combinations of structural stiffness, damping, and pneumatic tyre characteristics may lead to unexpected vibration problems on landing gears. Rather, an unlucky combination of brake system design with the peculiarities of circumferential force development by a tyre can also produce a serious vibration problem.

3.1 THE SITUATION

In a series of development rig tests for a fighter aircraft brake system, some test, were scheduled to demonstrate fastest possible brake force rise at high speed. A fast brake force rise was considered to yield, at least in theory, shortest possible landing ground run distance.

The test set-up "dynamometer"consisted of one main wheel with brake running within a heavy drum, where the rotational inertia of the drum was to represent respective mass per braked wheel of the aircraft. This arrangement not only gives a representative picture of aircraft deceleration by the brake but also provides correct kinetic energy to be dissipated by the brake. The brake was actuated by representative hydraulic components. Brake control was performed by one lane of the brake control computer, pilot's pedal input being replaced by a synthetic signal. Anti-skid functions of the brake control computer were implemented and active.

3.2 DESCRIPTION OF THE PHENOMENON

At brake initiation ("pilot" quasi "jumping" onto brake pedal) there was not the expected crisp yet steady rise of brake force with eventual subsequent anti-skid system activity. Rather there was a sequence of rapid on/off switching of the brake which lasted for about 1.5 seconds at a frequency of about 6 Hz. Thereafter the system stabilised to a normal behaviour.

Fig. 3-1 shows a principal sketch of those three test measurement traces which are considered essential for description and explanation of the phenomenon. From top to bottom, these are Wheel Speed, Brake Pressure (i.e. pressure on brake piston face), and Brake Torque.

The very first increase of brake pressure is needed to overcome the piston lifting spring. To arrive at the net pressure acting on the brake pad, that "spring pressure" is to be subtracted from the value measured; thus, at the first three troughs in Brake Pressure trace, brake pads are practically unloaded. This becomes apparent in Brake Torque trace, where for all practical purposes torque reduces to zero at the corresponding non-zero troughs of Brake Pressure.

The initial phase of Brake Pressure deserves a further comment: While brake servo valve output pressure (not shown) follows solenoid current with negligible delay, this is not true for the brake pressure proper as long as brake pistons are moving to close the gaps between rotor and stator disks of the brake package. The flow of hydraulic fluid from servo valve to brake is restricted by a quite narrow Restrictor orifice which limits loss of hydraulic fluid in case of e.g. rupture of a flexible hose. The Restrictor leads to a pressure drop between servo valve output and brake piston as long as the piston is moving. This pressure drop is the larger the faster the pilot tries to actuate the brake. However, when fluid flow stops, pressure drop across the Restrictor vanishes and full servo valve brake pressure gets through to brake

pistons within fractions of a second. Thus indirectly the safety feature "Restrictor" is responsible for the extremely steep brake pressure rise following on the brake filling phase.

3.3 EXPLANATIONS

From measurement traces not shown here it became apparent that oscillations observed were produced by anti-skid system action. However, given the software and the parameters for skid identification installed in the control algorithm, the anti-skid system worked correctly. The real reason for that disagreeable and inappropriate series of anti-skid actions at brake initiation is a mismatch of brake system control and tyre physics.

3.3.1 Physics of Tyre Braking Force

Explanations following aim for a basic understanding of tyre mechanics with regard to developing circumferential force.

When a tread element of a straight-rolling tyre enters the ground contact patch it will stick to that ground element. On a tyre rolling exactly at the forward speed of the wheel axle, the position in space of tyre tread element and ground element will be practically identical at entry to and exit from ground contact patch. Nevertheless within the patch there will be slight distortion due to the tyre tread being forced from originally circular shape to straight (ground) shape. Contact patch distortion changing sign at half patch length leads to approximately zero net circumferential force on the wheel.

Non zero net circumferential force develops when wheel circumferential speed differs from axle ground speed. Due to speed difference the tread point and the ground point which coincided at entry to the contact patch depart from each other on their travel through the contact patch. As long as the relative distance of the two points is not too large, tread rubber will adhere to the original entry ground point; elastic deformation of the tread element increases on its travel through the contact patch, thereby increasing the local circumferential load on the tyre. If wheel circumferential speed is sufficiently less than ground speed, at some point along the contact patch shear force on the tread element will exceed adhesive friction capacity of the element. As a consequence, the tread element will start to slide on the ground. Sliding friction of rubber in quite complex manner depends, amongst other parameters, on sliding distance covered and sliding speed. In general it may gradually fall well below adhesive friction with increasing sliding distance and speed. This admittedly coarse view of rubber tyre mechanics leads to the following conjectures about circumferential force on a braked wheel:

a) At low speed differences, circumferential force on the tyre should be approximately proportional to the distance between corresponding tread and ground points at exit from the ground contact patch. This "exit" distance d_e is, under stationary speed conditions, calculated to be

$$d_e = (v_g - v_c) \cdot \frac{l_p}{v_c}$$

where v_g ground speed
v_c wheel circumferential speed
l_p length of ground contact patch

Please note that circumferential force in this regime is dependent on a speed ratio rather than on actual speed.

b) At increasing speed difference, adhesive friction capability will be exceeded in small portions of the footprint mainly at the exit end of the ground contact patch. Within the footprint spots affected, rubber will start to slip relative to ground albeit at a very low slip speed and for very short distance. This means that circumferential force will still increase with increasing speed difference. However, rise rate will decrease with friction limited areas covering increasing portions of the tyre footprint.

c) At speed difference approaching ground speed practically all of the rubber in the footprint will be skidding at nearly ground speed and for extended distance. Since skidding friction depends on skidding speed and distance covered, circumferential force of a non-rotating tyre (full skid) will be less at high ground speed than at low ground speed. Furthermore, at fixed ground speed circumferential force of a skidding tyre will also be less than the maximum achievable at a lower differential speed, where almost all of the footprint area may also be skidding yet at a higher coefficient of friction.

Circumferential coefficient of friction (μ_c) of a tyre usually is presented as a function of "Slip Ratio" (SR), where

$$SR = \frac{v_g - v_c}{v_g}$$

This presentation compresses all tyre angular rates from rolling at ground speed (SR = 0) to full skid (SR = 1) into an abscissa from 0 to 1. However, as shown above μ_c with an increase of slip ratio becomes increasingly dependent on ground speed. Hence there will be different μ_c vs. SR curves for different values of ground speed. Fig. 3-2 presents a qualitative picture of this speed effect on circumferential coefficient of friction.
Figures concerning tyre circumferential force are in essence modifications of figures presented at Ref. 3-2.

Ref. 3-2 treats this subject in much more detail than it is done in present paper.

3.3.2 Conclusions with Regard to Sensible Brake Control

3.3.2.1 Brake Control during Braking

Fig. 3-3 is an somewhat exaggerated variation of Fig.3-2. However, the ordinate has been renamed "Wheel Torque" after, in ideas, having multiplied circumferential friction coefficient with wheel load and ground-to-axle distance.

Best possible deceleration of the aircraft by wheel braking could certainly be achieved if retarding moment produced by the brake ("brake torque") was just equal to the maximum driving moment achievable by the tyre ("wheel torque"). However, this maximum point will move around very quickly due to wheel load fluctuation on uneven ground, due to fluctuation of ground to tyre friction on varying ground roughness, due to variation of ground-to-axle distance, and due to other effects (e.g. side load on a braked wheel).

Although brake torque is measurable directly, wheel torque is not. Hence it is virtually impossible to exploit 100 percent of achievable wheel torque throughout the braked ground run. Therefore, brake control systems in general are aiming for a working point below the maximum wheel torque on the left (stable) branch of the wheel torque vs. slip ratio curve. However, if by chance maximum wheel torque falls below brake torque or if brake torque is increased beyond maximum achievable wheel torque, this statically unbalanced torque difference will decelerate the wheel and thereby increase slip ratio. Provided torque difference is large enough and is acting for sufficiently long time, slip ratio will be increased to the unstable part of the wheel torque curve.

In order to avoid this critical situation it is necessary in the first place to timely recognise an incipient skid and to reduce brake torque fast enough such that slip ratio is kept on the stable side.

However, a backup procedure is needed in case that slip ratio has eventually reached the unstable side of the wheel torque vs. slip ratio curve. If this happened the wheel would continue to decelerate to an eventual standstill as long as brake torque is larger than actual wheel torque, even if maximum achievable wheel torque had meanwhile recovered beyond actual brake torque. To recover from this "deep skid" the safest way is to lift brake completely until wheel speed has returned to the stable part of the wheel torque vs. slip ratio curve.

For better understanding of the case presented it is necessary to explain the principal method applied here to recognise an incipient skid: Wheel angular deceleration is the most important parameter used for skid detection.

During perfectly steady braking wheel angular deceleration is proportional to aircraft linear deceleration. Hence, on first view one could assume that any wheel deceleration beyond this value could be interpreted as an incipient skid. In theory this assumption holds only if the brake is operating at the maximum wheel torque transmittable to ground, because any loss of transmittable wheel torque will drive the working point to the right (unstable) side of the curve (Fig.3-3 and 3-4).

If the brake operates on the stable side somewhere below maximum transmittable wheel torque a reduction of transmitted wheel torque will be followed by a "useful" increment of wheel deceleration which brings transmitted wheel torque back to brake torque. Therefore, anti-skid action should only be triggered on exceedance of this "useful" wheel deceleration increment. As stated above, admittable trigger level is zero if brake torque equals transmittable wheel torque; trigger level rises (progressively) with the ratio of transmittable wheel torque to brake torque.

Assumed that a brake control system in its anti-skid branch contains a fixed wheel deceleration trigger criterion, the control system should also provide for the appropriate torque reserve between brake torque and maximum transmittable wheel torque. Since maximum transmittable wheel torque is not measurable directly, anti-skid systems of the type considered here contain algorithms which reduce brake pressure output from the servo valve according to frequency and intensity of previous anti-skid actions. Brake pressure will be cautiously re-increased (eventually to the level corresponding to pilot's command) if no more anti-skid action was triggered in a sufficiently long time interval.

3.3.2.2 Brake Initiation

Up to the point of brake initiation, the wheel rolls freely at negligible wheel torque just balancing rolling drag. Therefore at brake initiation, rise of brake torque cannot immediately be counteracted by wheel torque. Rather, momentary difference between wheel torque and brake torque leads to angular deceleration of the wheel. This effects an increase of slip ratio and wheel torque. If brake torque is limited to a value below maximum transmittable wheel torque, slip ratio will eventually tune in to stationary balance of brake torque by wheel torque.

Wheel deceleration occurs during brake initiation as well as during a skid. Hence, if during brake initiation wheel deceleration exceeds the threshold set for skid detection, anti-skid control will unnecessarily lift the brake. The wheel will recuperate to or nearly to freely rolling conditions. When brake pressure is re-applied by anti-skid control another undue skid prevention cycle may occur.

For sake of a vibration-free brake onset it appears useful to gain insight into the factors influencing wheel angular

deceleration during brake initiation. To this end quite basic considerations may be helpful:

a) Step increase of brake torque: If brake torque is assumed to follow a step function then extremum wheel deceleration will occur at t = 0 and will equal brake torque divided by wheel moment of inertia.

b) Creeping increase of brake torque: If brake torque is applied very slowly, this will lead to low wheel deceleration values as well, because the wheel is being given ample time to adapt to the slowly increasing demand on slip ratio.

c) Influence of "brakes on" aircraft speed: In a diagram showing wheel torque versus slip ratio (see e.g. Fig. 3-3) the initial linear part is virtually independent of ground speed. However, analysis of the equation defining slip ratio, viz.

$$SR = \frac{v_g - v_c}{v_g}$$

indicates that wheel torque rise rate over time will reduce with an increase of ground speed.

Assumed wheel torque is linearly dependent on slip ratio, i.e.

$$WT = K \cdot SR = K \cdot \frac{v_g - v_c}{v_g}$$

or

$$WT = K \cdot (1 - \frac{\omega_w \cdot r_w}{v_g})$$

then wheel torque rise rate becomes

$$\dot{WT} = -\frac{K \cdot r_w \dot{\omega}_w}{v_g}$$

From this equation it is easily concluded that wheel deceleration will increase proportionally to "brakes on" ground speed (brake torque rise rate assumed independent of speed).

It is also concluded that wheel deceleration may vary with tyre type, e.g. if different tyre construction and/or tread material changes the slope K of the wheel torque vs slip ratio, K may also change with operating conditions, e. g. dry or wet ground (Ref. 3-2)

Furtheron, wheel deceleration increases on transition from the quasilinear part of the wheel torque slope into the degressive part while approaching maximum transmittable wheel torque.

Fig. 3-5 shows simulation results of a braked wheel during brake initiation. The model used is quite simple. It contains just one degree of freedom representing rotation of a wheel moving at constant ground speed. Brake torque is assumed to form a ramp type function of time while K is assumed constant, i.e. brake torque is assumed to not exceed the linear part of wheel torque vs slip ratio function. Eventual dynamic deviations of wheel torque vs slip ratio from quasi-stationary behaviour were not taken into account.

Numerical results from simulation confirmed principal considerations presented above. Hence a systematic evaluation of simulations was performed and summarised in Fig. 3-6. This figure presents kind of a design chart. With maximum design "brake on" speed given it shows which brake torque rise rate is at best admissible if skid detection threshold shall not be exceeded during brake initiation. This type of diagram can easily be set up for a specific aircraft using its tyre and wheel characteristics (mainly moment of inertia and wheel torque curve) in combination with brake and anti-skid control characteristics (primarily skid detection threshold).

In developing Fig. 3-6 it was tacitly assumed that brake torque shall not exceed the straight part of the wheel torque vs slip ratio curve. However, in reality this is rather improbable, because maximum brake torque achievable is mostly close to or even beyond maximum wheel torque achievable on dry runways. If brake torque ceiling is below maximum wheel torque achievable, wheel angular deceleration will increase on the degressive slope and fall sharply off to the value corresponding to aircraft deceleration when brake torque ceiling is reached. If brake torque ceiling is beyond maximum wheel torque achievable, then wheel deceleration will not fall off at brake torque reaching its ceiling; rather it will progressively increase on the negative slope of the wheel torque vs slip ratio curve. Unless skid detection level had been exceeded already on the degressively positive slope of the curve, it will be exceeded here, provided it is small enough. In addition, since brake torque rise rate is not at all perfectly controllable (e.g. due to brake temperature influence on brake torque vs brake pressure characteristics), variations of rise rate will also lead to variations of wheel deceleration.

Assumptions taken for Fig. 3-6 are therefore on the optimistic side. It is advisable to apply more realistic assumptions (especially on wheel torque vs slip ratio) in developing brake and anti-skid control system algorithms and parameters.

Nevertheless, the simplified approach which was taken here yields sufficient insight into the oscillation problem observed during dynamometer tests of rapid brake application at high aircraft speed.

3.4 RECOMMENDATIONS AND CONCLUSIONS

In the case treated here, both brake pressure and brake torque rise at enormous rates. Brake torque rise rate alone would have been sufficient to trigger anti-skid action. In addition, presumably due to slight time delays in the system, brake torque is allowed to by far overshoot maximum wheel torque achievable. Although in the next cycle the brake torque ceiling is lowered it is still too high due to the excessive overshoot in the previous cycle. In cycles following it is hard to decide whether sharp rises of brake torque or brake torque overstressing wheel torque capacity lead to further anti-skid actions.

In any case, a substantial reduction of brake pressure and brake torque rise rates during initial brake application would be beneficial in two ways: First, undue anti-skid action could be reliably avoided thereby. Second, eventual brake torque overshoot could be drastically reduced with the effect that brake pressure ceiling could adapt to wheel torque capacity within a single step and with significantly less pressure amplitude. In summary, reduced brake torque rise rate is suited to overcome the brake torque / brake force oscillation treated here.

From all insight gained into the problem there is no solution to be expected from any kind of bolt-on structural damping device.

3.5 POINTS OF IMPROVEMENT IN THE BRAKE SYSTEM

The brake torque oscillations observed in dynamometer tests at extreme "brakes on" speed and at extreme step input to the system can be avoided through improvement by design as well as through improvement by operation.

Improvement by operation means that pilots are instructed to initiate brakes such that brake torque rise rate is kept below critical values. Improvement by operation is viable as long as an average pilot is not overcharged by the operation required. At best, oscillations should not occur if the pilot just avoids "jumping" onto brake pedals.

Nevertheless there are aspects of the problem rendering improvement by design a desirable alternative.

- Experience shows that aircraft get heavier in course of time. As a consequence maximum "brakes on" speed shows tendencies to increase, too. If safety margins against oscillations shall be kept constant then brake torque rise rate and/or skid detection threshold must be changed. If brake torque rise rate is a hardware constant then the necessary lifting of skid detection threshold will lead to reduction of skid detection quality. In turn, reduced skid detection quality reduces anti-skid system efficiency throughout all braked ground roll. Ground roll distance lost at soft yet non-oscillatory brake initiation is only a fraction of that which can be gained by improvement of brake efficiency by correspondingly lower skid detection threshold.

- Quickest possible brake reaction at braking onset appears desirable with regard to flight performance. However, nose diving provoked by abrupt braking will eventually produce critical loads and/or reduce aircraft capability to cope with rough ground (e.g. aircraft operation on bomb damaged and provisionally repaired runways)[Ref.3.1]. If brake torque rise rate is reliably controlled by brake system control then this can be advantageously used in structural design (Fig. 3-7).

Adjustable control of brake torque rise rate is considered a sensible means not only to avoid oscillatory anti-skid action at brake initiation but also to improve aircraft ground handling and performance.

4. INTEGRAL LANDING GEAR/AIRCRAFT PROBLEM

Sustained (e.g. self-induced) landing gear vibrations often are considered to form an exotic and rather local class of dynamic stability problems. However, the ramifications of a vibration problem on landing gear may well extend across the entire aircraft.
First of all, that vibrations can present severe problems with regard to dynamic loads on landing gear and its attachments.
Even if oscillatory landing gear loads do not exceed loads determined by quasi-static load cases, they may well become a problem with regard to structural fatigue (e.g. Ref. 4.1).
Furtheron, landing gear vibrations may impair pilot's ability to control the aircraft.
Excessive aircraft on landing gear vibrations deteriorate passenger comfort.
Early and comprehensive consideration of landing gear vibration is therefore an indispensable part in the development of a successful aircraft.

"Shimmy" is not the only but one of the most frequent and most dangerous sources of landing gear vibration. Shimmy is an oscillatory wheel mode induced by a mechanism similar to that of a wing in flutter.
The shimmy mode is important because it can lead to a dynamic stability problem.
Primary source of the phenomenon is the flexibility between tyre footprint and the wheel plane. Other factors such as wheel speed, tyre geometry and torsional constraints have a contributing effect. From flutter calculations we know that a component investigation show general existence of instability. Total aircraft analysis reveal always the same flutter mode as component calculation but very often at lower speed.

Through interference of aerodynamic and interaction of coupled components new flutter modes are possible. Similar to this flutter behaviour it is believed that the eigenmode of the flexible aircraft can influence the stability of landing gear.
The aim of the landing gear dynamic behaviour programme is to obtain dynamic data to support the design specification of an aircraft. To do this sufficiently the code must be capable to reconcile different subsystems (structure, flight control system, hydraulic etc.) and improve data with test results.
At the beginning of a project the data available for sub systems are very limited. The analysis can be used to obtain preliminary results by assumed or old data and can be updated with more detailed information during the development. The analysis at Dasa is now organised as a series of individual modules for dynamic investigation for components and subsystems. This system allow easy but time intensive upgrading of modules and trend calculation by using generalised modes.

Each full analytical model of the leg has about 50 eigenmodes, depending on the configuration selected. The high order of the model is a direct consequence of including all the features that are necessary to represent the interactions with other sub-systems during landing and ground roll simulation.

Lower order models are required to permit efficient time response evaluation. Reduction in modal order is achieved by removing the dynamics with the higher frequencies modes. This can be achieved by dynamic condensation of the mass and stiffness matrix. For this application, with relatively small finite element models, the method is preferable to that of R. Guyan, because the dynamic condensation or also the residual flexibility methods preserves the mode shapes very well and permits a simple procedure for the selection of modes. Up to the lowest five modes of the leg model, selected in the manner described above are retained by transforming the equations into modal coordinate system. It is also possible to determine the lowest eigenmodes on a free Ground Vibration Test (GVT) with retracted undercarriage. With those derived modes a stiffness matrix can be calculated, which corresponds to the mass matrix but is not useable for static calculations.
A damping matrix corresponding to the generalised co-ordinates can be easily established, because each mode is selectable. This generalised matrices are used as input to the stability criteria of R. Smiley in connection with the linearised tyre characteristic and the applicable ground force.
Generally speaking it turned out that the most important parameter in the shimmy investigation is the relaxation length of the tyre, because changes of this length results in large changes of the landing gear stability.
Second, the torsion (friction) damping of the piston against the cylinder, which is derived from measurement of the landing gear producer has also an imminent influence to shimmy.

Third, it turned out that the elastic fuselage modes are not important , if the leg mode frequencies are well separated from the aircraft mode frequencies.

5. REFERENCES

[1.1] Smiley R.F.
Correlation, Evaluation and Extension of Linearized Theories for Tyre Motion and Wheel Shimmy
NACA TR 1299; 1957

[1.2] Pacejka H. B.
The Wheel Shimmy Phenomenon
A Theoretical and Experimental Investigation with Particular Reference to the Non Linear Problem
Technical University Delft, Netherlands

[2.1] Schweiger J., Weiss F., Dobbs S.
Aeroelastic Design and Flight Test Evaluation of the RANGER 2000 Training Aircraft
International Forum on Aeroelasticity and Structural Dynamic 1995 Manchester U.K.

[3.1] Krauss, A. J.
Considerations on Optimality of Landing Gear Arrangement and Design.
Paper #8 from AGARD Conference Proceedings 484: Landing Gear Design Loads

[3.2] Brewer, H. K.
Parameters Affecting Aircraft Tire Control Forces.
AIAA Paper No. 74-966

[4.1] McBrearty, J. F.
A Review of Landing Gear and Ground Loads Problems.
AGARD Report 118

[4.2] Guyan,R.
Reduction of Stiffness and Mass Matrices
AIAA Journal February 1965

APPENDIX

Consider a wheel equipped with a pneumatic tyre. The wheel axle shall be connected to a straight guiderail by a linear spring/damper element. This guiderail shall be moved across the ground at constant speed; furtheron the guiderail shall be inclined against the ground.

Motion of the wheel axle relative to the guiderail is influenced by radial tyre force (also represented by a linear spring/damper element) and by circumferential tyre force. Modeling of circumferential force depends on assumptions made.

A1. "Cog-Wheel" Assumption

The wheel is assumed to rotate at that angular velocity which is defined by the ratio of ground speed to deflected tyre radius. Circumferential force is then defined by rotational acceleration of the wheel enforced by tyre radius variations. Since this radius depends only on the coordinate of the wheel axle relative to the guiderail, the equation of motion reflecting the "Cog-Wheel" assumption has one degree of freedom, viz the linear displacement of the wheel axle on the guiderail.

With regard to potential self-induced oscillations of this system it is interesting to study the various damping terms in that equation of motion.

With

DC Damping coefficient of the guiderail spring
DT Damping coefficient of tyre radial spring
IW Wheel moment of inertia
VG Ground speed
XB Axle displacement relative to guiderail
RR Distance axle to ground
ρ Inclination of guiderail (positive front end up)

the complete damping term reads

$$D = DC + DT \cdot \sin^2 \rho - \frac{IW \cdot \sin \rho \cdot \cos \rho \cdot (VG + XB \cdot \cos \rho)}{(RR + XB \cdot \sin \rho)^3}$$

The damping term resulting from the "Cog-Wheel" assumption is negative (destabilizing). Since it increases approximately proportional to ground speed, the equation indicates that there might exist a critical ground speed at which overall damping becomes negative.

This critical speed can be increased by a "hardware" modification to the model by reducing inclination of the guiderail. In reality this would mean a reduction of landing gear leg forward rake.

Improvement can also be achieved by a quasi "software" modification, i.e. by pumping up the tyre to increase RR.

A2. The "Slip Ratio" Assumption

As already discussed in present paper, circumferential force on an almost freely rolling tyre is approximately proportional to slip ratio SR.

If this assumption is introduced to the model then linear displacement of the wheel axle and rotation of the wheel are two separate degrees of freedom which are coupled by the circumferential force.

This system is not as readily analyzed as the "Cog-Wheel" system. However, from the main part of this paper it is concluded, that one and the same axle linear velocity relative to the guiderail will effect different slip ratio rates, slip ratio rates becoming smaller with increasing ground speed. That means that the ratio of circumferential force oscillation amplitude to axle displacement amplitude reduces with increasing ground speed.

Apart from any phase shift effects it is therefore expected that an eventual destabilizing effect of tyre circumferential force on axle fore/aft motion will cease with speed.

A3 Conclusion

Comparation of the "Cog-Wheel" model and the "Slip Ratio" model perception lead to the conclusion that sustained fore/aft bending oscillations may well occur under unfavourable landing gear design parameters. However, this type of self-induced oscillation should be limited to the low to medium aircraft speed range.

In a realistic analysis of the phenomenon, care should be taken that all important effects are included in the model. For instance, effective "guiderail" inclination can be influenced by fuselage bending and / or by stroking motion of the oleo strut.

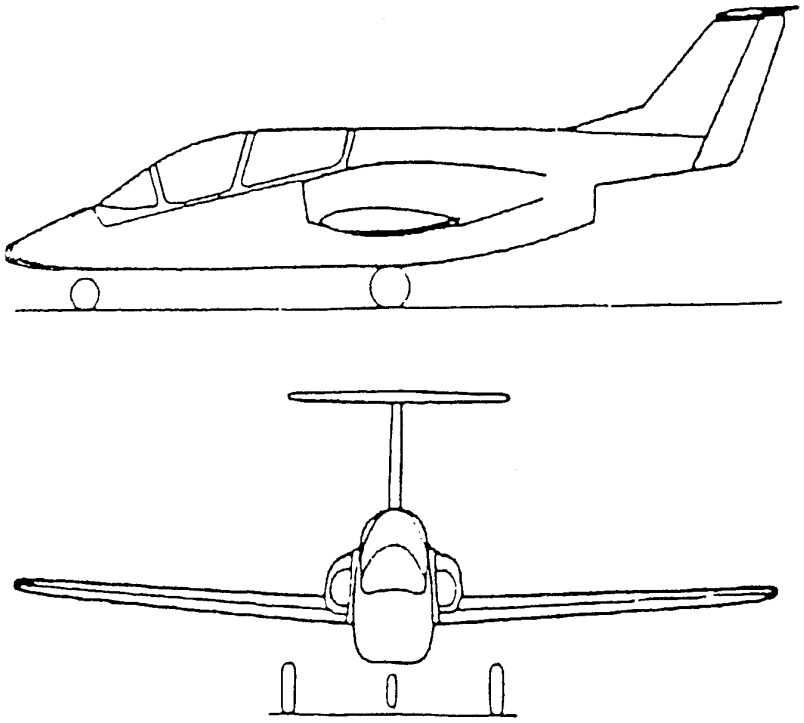

Fig. 2-1 Advanced Training Aircraft

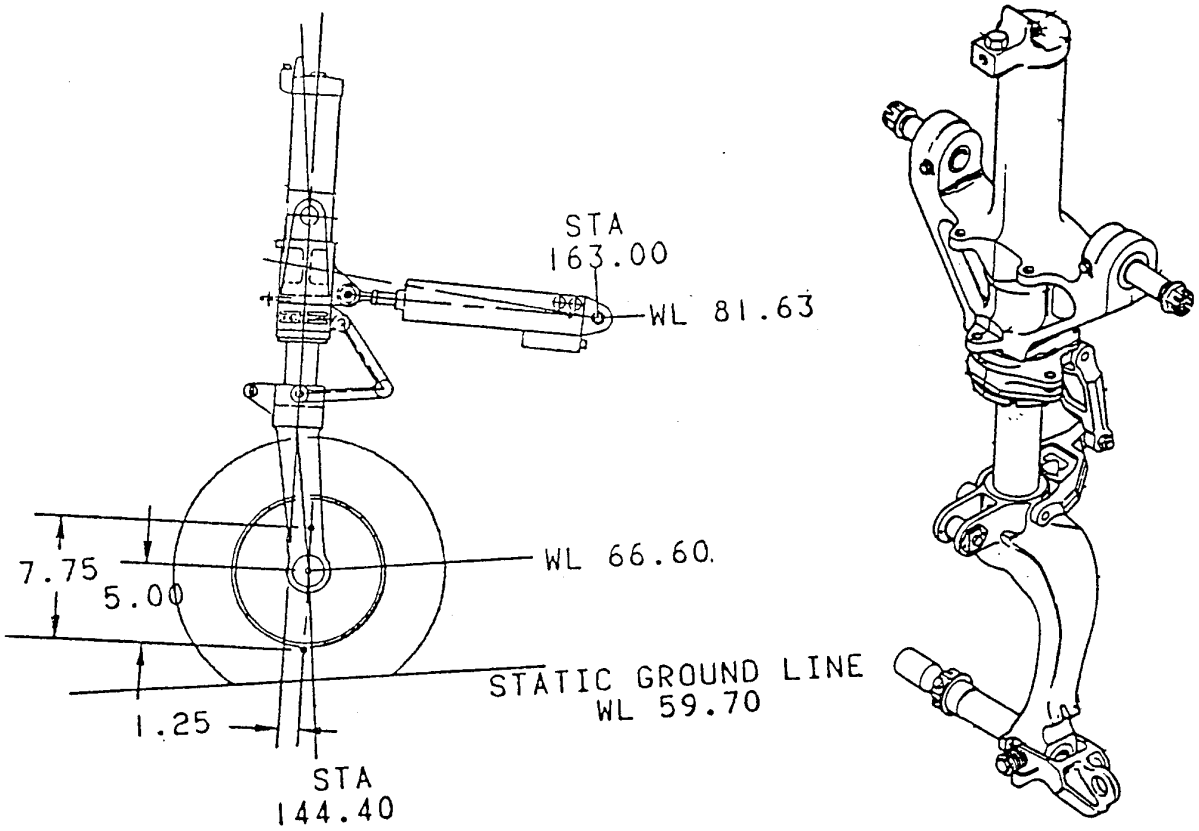

Fig. 2 - 2 Nose Landing Gear

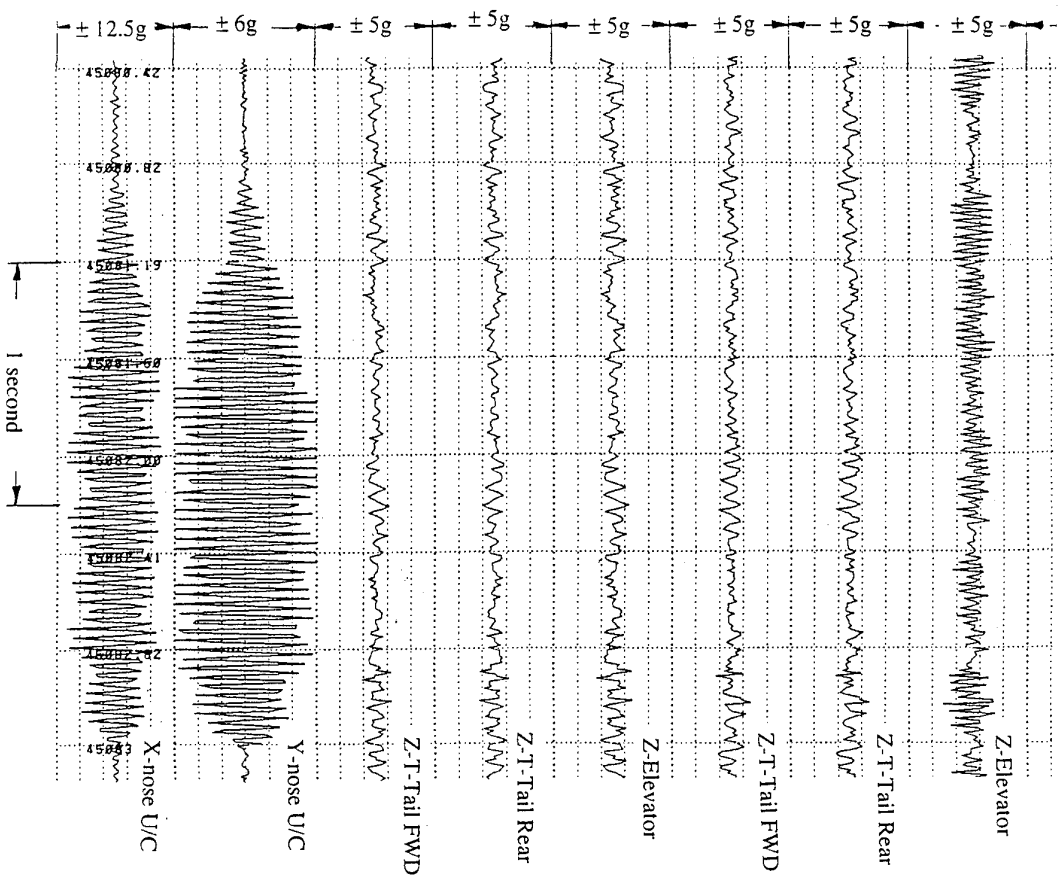

Fig. 2 - 3 Time History Nose Undercarriage

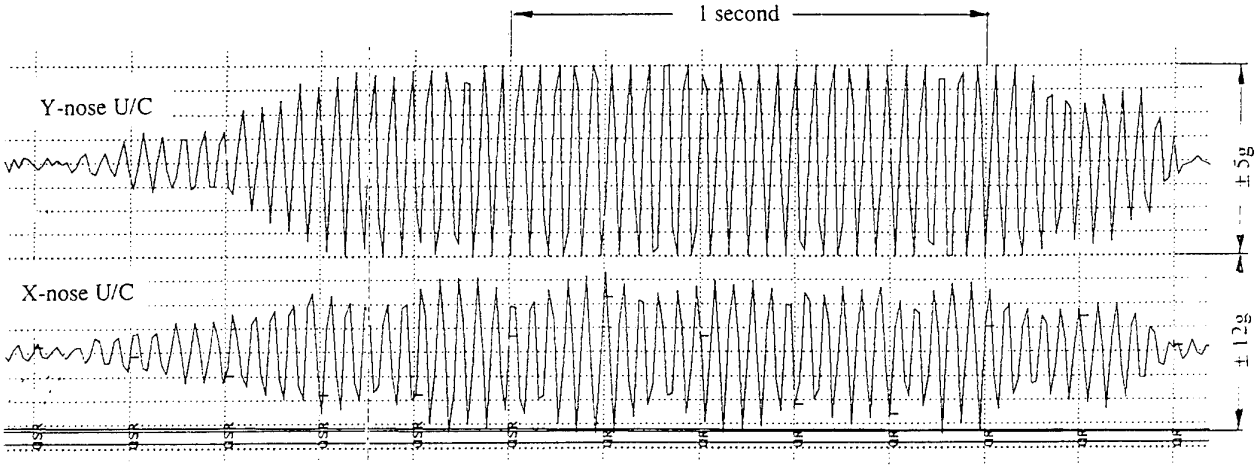

Fig. 2 - 4 Shimmy

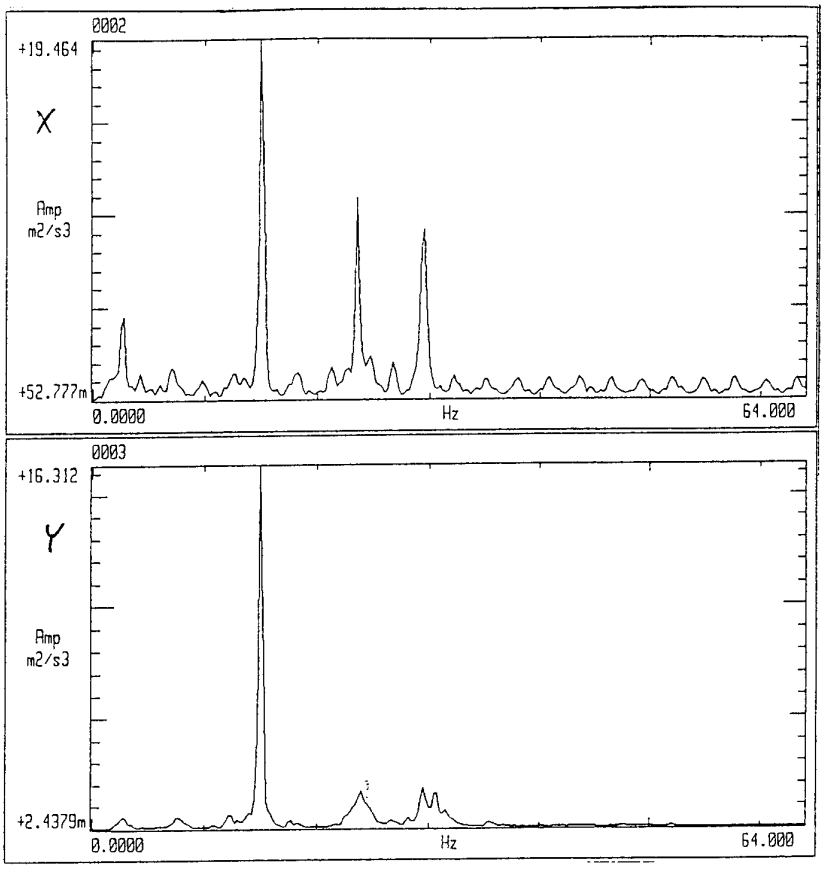

Fig. 2 - 5 Power Spectral Density

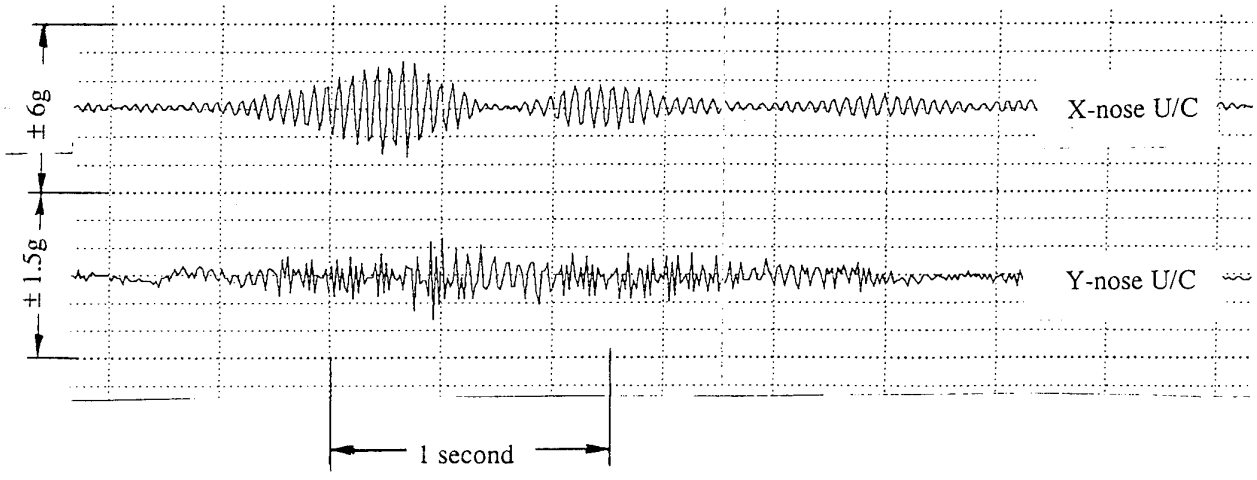

Fig. 2 - 6 Time History after Modification

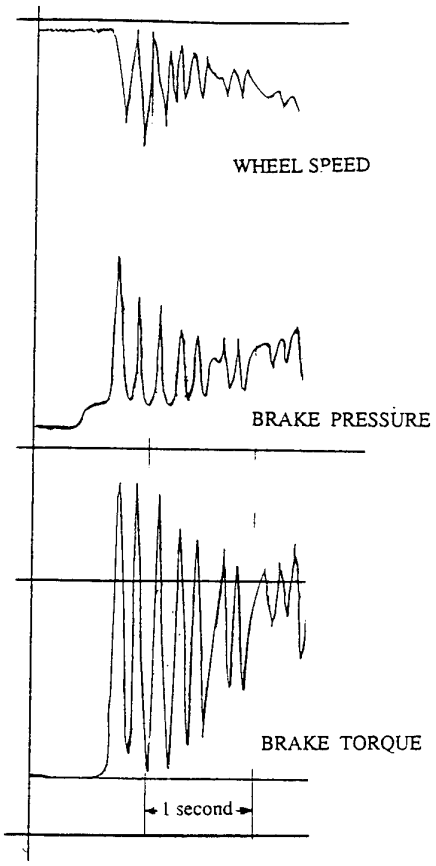

Fig. 3-1 Measurement Traces from Brake Dynamometer Test

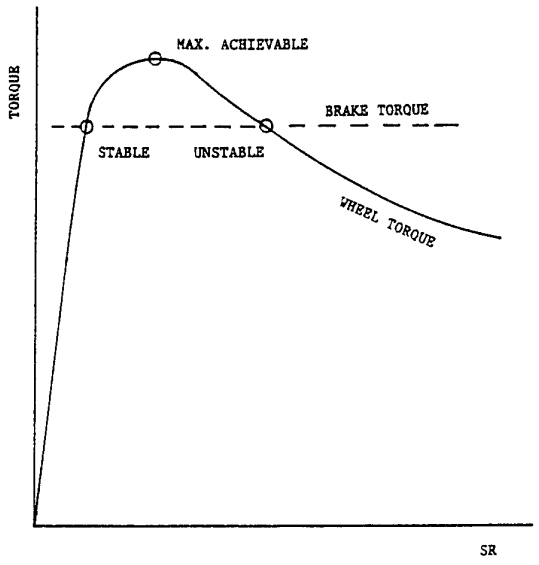

Fig. 3-3 Brake Working Points in Relation to Wheel Torque versus Slip Ratio

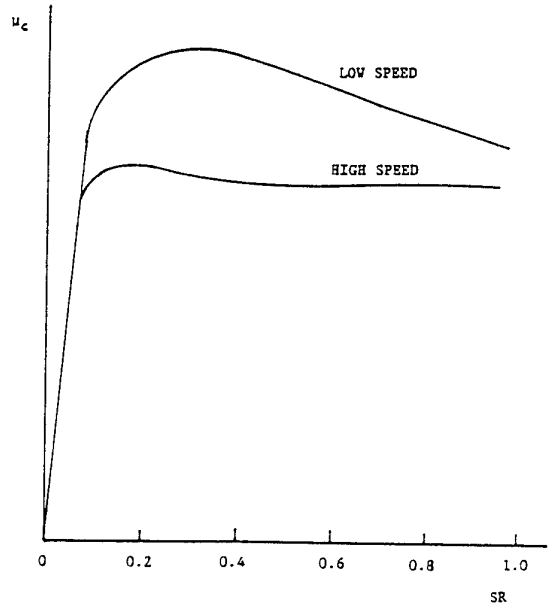

Fig. 3-2 Circumferential Friction Coefficient Dependence on Slip Ratio and Speed

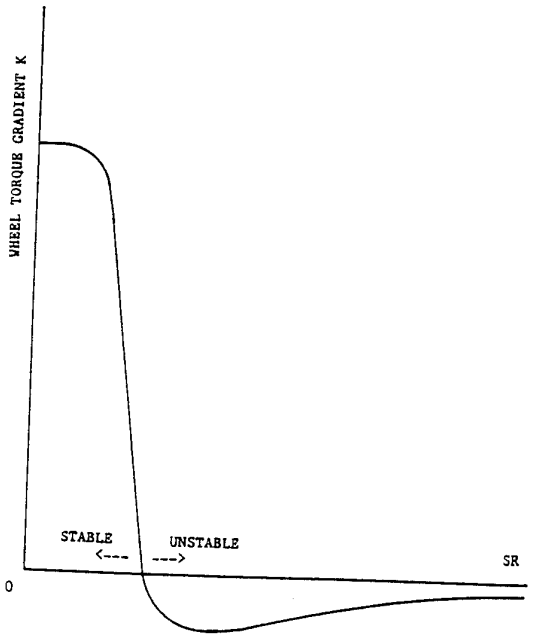

Fig. 3-4 Wheel Torque Gradient K versus Slip Ratio

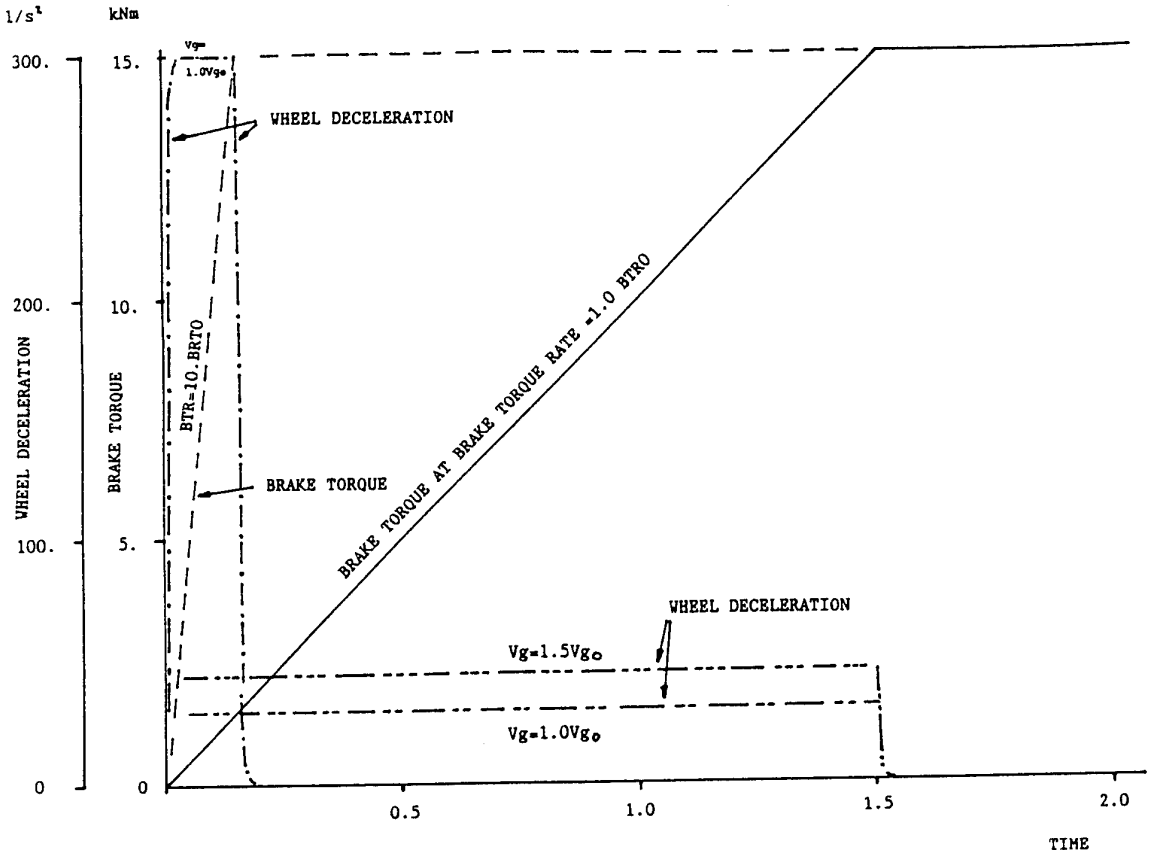

Fig. 3-5 Histograms of Wheel Deceleration

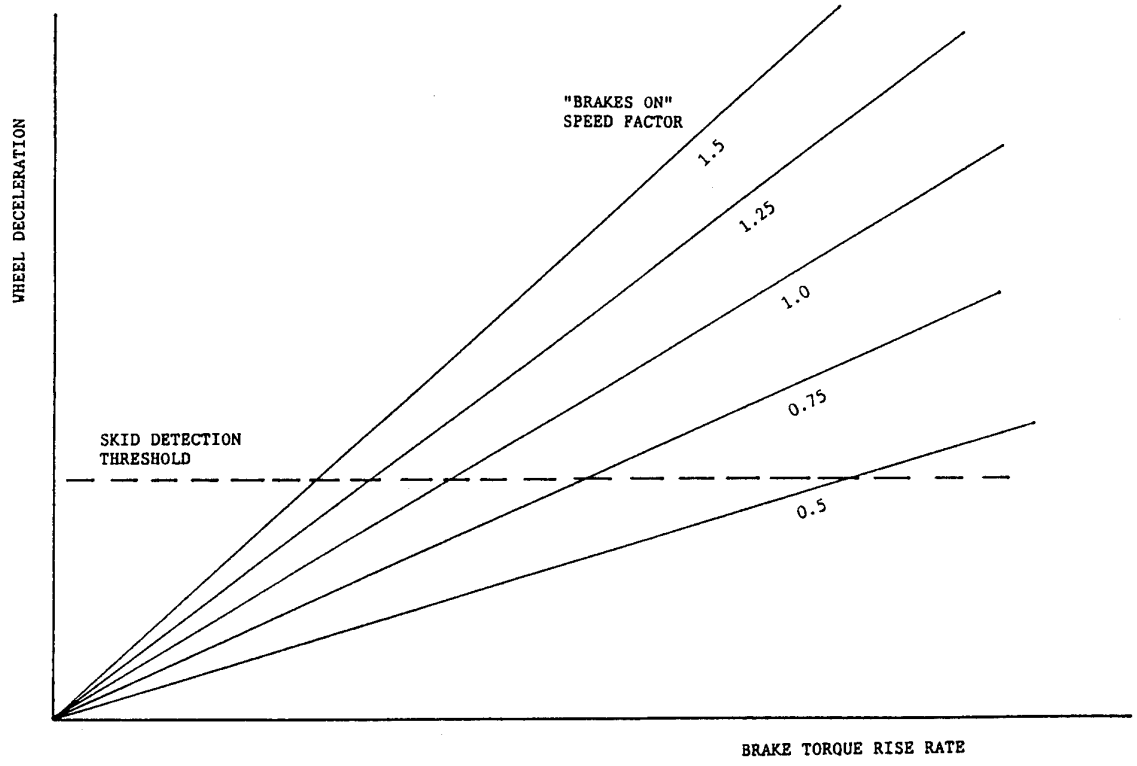

Fig. 3-6 Design Chart for Brake Torque Rise Rate

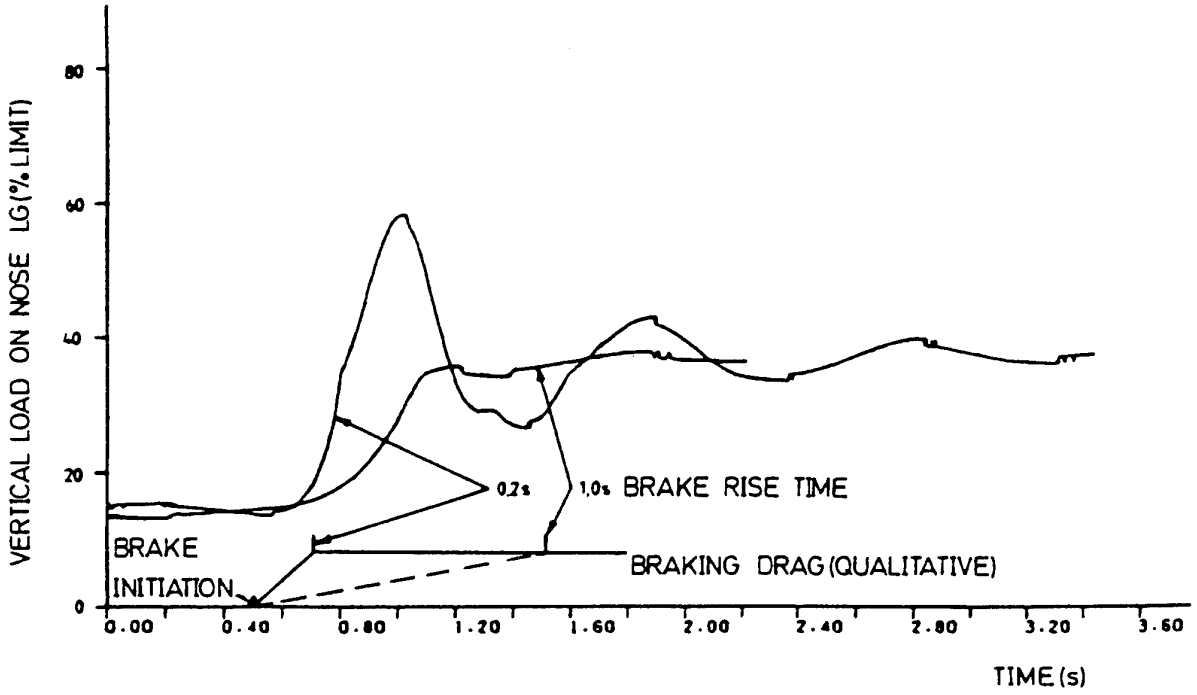

Fig. 3-7 Nose Landing Gear Histograms from Dynamic Braking Analyses

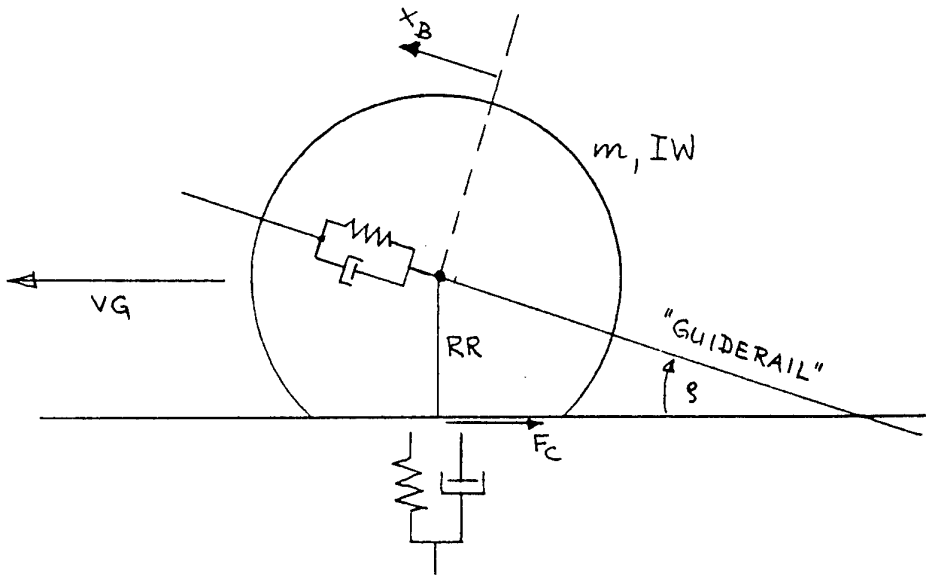

Fig. A-1

ANALYSIS AND CONTROL OF THE FLEXIBLE DYNAMICS OF LANDING GEAR IN THE PRESENCE OF ANTISKID CONTROL SYSTEMS

E. Denti, D. Fanteria
Dipartimento di Ingegneria Aerospaziale, Università di Pisa
Via Diotisalvi 2, 56126 PISA, Italy
Tel. +39.50.550200 - Fax +39.50.553654

SUMMARY

This work is part of research carried out to investigate the vibration problems due to coupling between the flexible dynamics of aircraft landing gear and the dynamics of antiskid control systems. The last objective is the development of new antiskid devices for the suppression of landing gear vibrations during braking.
In the paper the above mentioned problems are described together with the models and methods available for their investigation. Preliminary results of the research are also presented. Namely, an analytical and numerical model of the tyres in runway contact dynamics, that is one of the most critical models involved, is developed. A linearized model of the system composed of the wheel and the landing gear is developed and the system poles are investigated.

LIST OF SYMBOLS

F_N	Vertical ground force
F_x	Longitudinal ground force
P_N	Vertical ground load distribution
R_e	Effective rolling radius
s_x	Slip coefficient
T	Braking torque
V_A	Aircraft speed
V_C	Wheel centre speed
V_r	Wheel circumferential speed
V_S	Wheel slip speed
V_{SL}	Local sliding velocity
x_G	Long. deflection of landing gear leg
μ	Tyre friction coefficient
σ	Theoretical slip coefficient
Ω	Wheel spin velocity

1. INTRODUCTION

The growth in aircraft size and landing speed has led to the development of braking control systems to protect tyres from skid damage and to reduce the stopping distance. Early antiskids were "on-off" systems developed only as "tyre savers" to prevent lock-up skids; later, with the introduction of the proportional servo-valve, it became possible to develop improved systems with modulated braking control. Modern antiskids are complex electronic systems that can actually improve landing performance on dry and wet runways. This performance may however be compromised by the coupling of the flexible dynamics of landing gear and antiskid feedback dynamics that may cause large wheel-hub acceleration and landing gear vibrations known as "gear walk".
The subject of the present paper is the development of mathematical and numerical models for the study of this phenomenon, with the final aim of developing new antiskid control laws for the reduction of vibrations and loads on landing gear during braking.
To achieve this objective a numerical code, for the dynamic simulation of the whole system (antiskid-landing gear-aircraft), is needed. Accurate analytical models of system components are also fundamental in order to design new control laws. In literature models and methods are mainly developed around automotive problems while few specific works on aircraft braking are available. The difference between the automotive and the aeronautical point of view is mainly in the elasticity of the link between the vehicle and the wheel; wheel-hub vibration due to the elastic motion of the aircraft's landing gear has in fact a great influence on the dynamic behaviour of the wheels.
This paper is composed of three parts. In the first part (sec. 2, 3, 4) the above mentioned problems are described, together with a review of the literature on available models and methods for their investigation. Suitable models for numerical simulation are also critically discussed. The second part (sec. 5, 6) is focused on the tyres in runway contact dynamics. A "dynamic brush" numerical model, based on a Lagrangian point of view, is developed and investigated. The "Eulerian version" of the basic equations is analytically solved and a method to obtain the transfer function of braking force for small parameter variations, both at free rolling and in generic conditions, is given. Finally (sec. 7) a linearized model of the landing gear-wheel system is developed and a preliminary investigation into the system poles is presented.

2. COUPLING PROBLEMS

On aircraft equipped with antiskid devices a dynamic instability phenomenon, known as "gear walk", may occur. This is reported in detail in [MOSEL] and [ENRIG]. The gear walk consists in strong vibration of the landing gear, typically below 20 Hz, that involves large wheel-hub accelerations and seems due to a negative matching between the frequency spectrum of the longitudinal ground force and the natural frequencies of the gear. Further documentation on gear walk, collected during a braking test on a turboprop executive, is given in Fig. 2-1 and Fig. 2-2; when the antiskid current sharply decreases (and the braking torque rises) strong undamped

Paper presented at the 81st Meeting of the AGARD SMP Panel on "The Design, Qualification and Maintenance of Vibration-Free Landing Gear", held in Banff, Canada from 4-5 October 1995, and published in R-800.

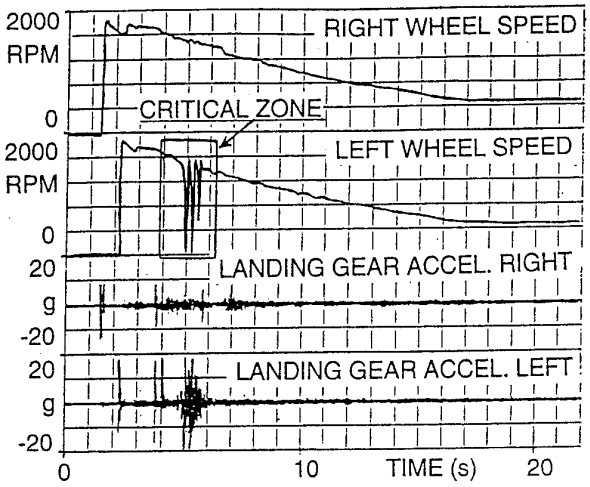

Fig. 2-1 An example of the gear walk phenomena

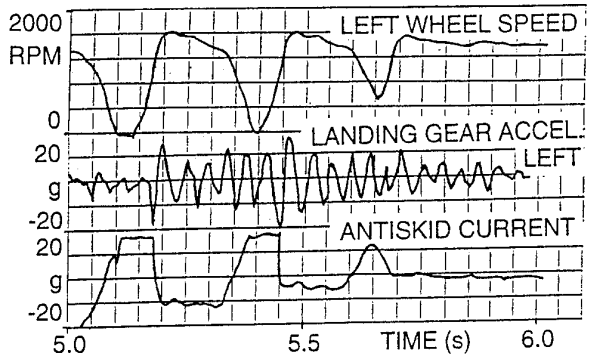

Fig. 2-2 Zoom of the critical zone

wheel-hub vibration starts. In [MOSEL] the gear walk also occurred in tests where the braking level was below the antiskid working threshold. The hypothesis put forward in [MOSEL] is that the wheel-hub fore-aft elastic motion causes high wheel angular speed variations that can be interpreted as an impending wheel skid by the antiskid system. Another problem can be the lag between the real angular speed of the tread and the angular speed measured at the rim; this lag is due to the torsional elastic mode of the tyre whose natural frequency is of the order of 30 Hz. A further possible cause of gear walk may be brake torque oscillations, due to the random behaviour of brake friction [TANNE, MOSEL]. In any case, a possible solution might be an antiskid with a feedback on aircraft and wheel-hub longitudinal acceleration, in addition to wheel spin parameters. This allows evaluation of the real slip conditions and in any case makes the synthesis of a control on landing gear acceleration possible.

Investigation into these phenomena is quite difficult. The collection of experimental results is expensive and critical from the point of view of correct data measurement and interpretation. Furthermore numerical simulation needs a very accurate modelling of all system components because physical reasons for gear walk are unknown and it might be impossible to simulate gear walk if it is due to neglected details of the behaviour of these components. On the other hand accurate analytical and numerical models of system components are also fundamental for analysis and synthesis of new antiskid laws for the suppression of gear walk.

3. SYSTEM MODELLING

The dynamic system to be studied is composed of: aircraft, landing gear, wheels, the braking system and the antiskid control system, connected as shown in Fig. 3-1. Starting from the simulation code described in [DENTI], a computer program has been developed for the numerical simulation of the system. This program is based on the following preliminary choices. The dynamics of the aircraft is represented by a 3 degrees of freedom (DOF) rigid model. The elastic dynamics of the landing gear is represented by a 1 DOF second order linear model. The vertical and horizontal ground forces are computed as functions respectively of tyre deformation and slip coefficient; these functions are supplied to the program by tables as input data. The dynamic model of the wheel spin takes into account the horizontal ground force, the rolling friction and the braking moment. The braking system model takes into account only the servo-valve dynamics, represented by a second order linear model, while the braking moment is assumed to be proportional to the output pressure of the servo-valve. The antiskid control box implements a basic control strategy and it is possible to build other strategies of the user's choice. The time history of the pilot's braking command is an input datum.

All these models are discussed in the following.

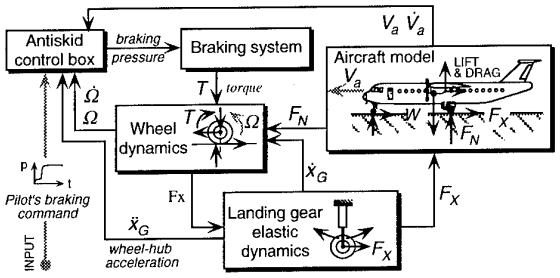

Fig. 3-1 Antiskid-landing gear-aircraft system

• *Aircraft dynamics* has been taken into account in order to evaluate the time histories of aircraft speed and vertical ground loads, so as to consider the modifications of the working conditions of the antiskid control system. For this purpose the model chosen seems adequate. Note that the aircraft pitch model gives the vertical loads, on nose and main landing gear, as a function of the longitudinal braking force, working as a low-pass filter.

• *The landing gear elastic dynamics* model mentioned above seems adequate for research purposes [ENRIG]. Anyhow, if previous modal analysis of the landing gear is possible, a n-DOF second order linear model based on modal superimposition can be used.

• *Braking system.* Literature on brakes and braking systems is limited. Useful data about braking systems are to be found in [GERDE, GILES, TANNE] and about brakes in [ENRIG, MOSEL, PERRO, TARTE]. However, these papers contain little information for the system modeller, especially on the physical phenomena that

govern the dynamic generation of the braking moments. Friction is a non linear phenomenon depending upon temperature, with histeresis and random components. So a lot of work would seem necessary to improve the simple model chosen. In any case, the way of modelling this system is not essential for the present work because it does not affect the dynamics of the wheel-landing gear subsystem. However it becomes fundamental when the antiskid control loop is eventually closed.

• *Antiskid control box.* The antiskid system is a dynamic box that allows simulation of both basic and newly designed antiskid control laws.
Recent research on antiskid control systems mainly concerns ground vehicles (cars, bikes and trucks). For example new antiskid control laws are studied in [LINDO, MIYAS, WATAN], where experimental and simulation results are given, too, and in [TANCH, YEH_1, YEH_2] from a more theoretical point of view. In [HOHNO, MAUER] systems based on Fuzzy Logic and Neural Networks are presented. Practical data for car antiskid device simulation are also available in [BOWMA, FANCH].
In the aeronautical field the development of antiskid, from the early antilock "on-off" systems (1950) to the modern digital antiskid devices, is described in [CURRE, HIRZE] and NASA research on antiskid is reviewed in [TANNE]. But the strategic importance of the matter leads to a virtually total lack of recent research and detailed information and data about commercial antiskid devices. So, an accurate simulation of these devices may be difficult and may need a new synthesis based on what is known about their control logic.

• *Wheel.* The classical wheel model adopted so far is quite good for the evaluation of the ground behaviour of aircraft, but not for the simulation of wheel transient dynamics; so, improvements are necessary for the study of gear walk phenomena. In the following a review of the literature on this subject is given and improved models are developed and examined.

4. REVIEW OF MODELS AND METHODS FOR WHEEL SIMULATION

Ample literature exists in which several tyre models are developed from different points of view. Recent developments in classical models and advanced models are briefly reviewed in the following. Advanced models are divided in two classes: the first concerns models of contact forces, the second load transfer from contact patch to wheel hub. Global models resulting from the integration of the above mentioned aspects are described too.

• *Classical models.* In classical modelling it is assumed that tyre structure conveys the whole load, from contact patch to wheel hub, without any lag [CLARK, DUGOF, PACE2, SAKA1]. Longitudinal forces, arising in the wheel contact patch, closely depend upon the distribution of the local sliding velocity of the tread in relation to the ground. Steady state experiments show that, at free rolling, the absolute velocity of the tread in contact is zero and the *Effective Rolling Radius* (R_e) may be defined [CLARK, PACE2] as the ratio between wheel hub velocity (V_C) and spin velocity (Ω), that are both measurable quantities; R_e depends upon V_C, vertical load on the hub (F_N) and tyre features. In generic braking conditions, circumferential velocity (V_r) is defined as the product ΩR_e, while slip velocity is given by the relationship: $V_S = V_C - V_r$ (Fig. 4-1).

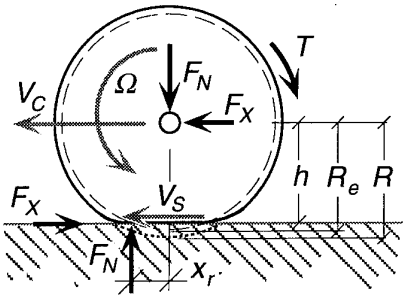

Fig. 4-1 Classical model

Local sliding velocity and longitudinal global force are linked to wheel dynamic variables such as V_C, Ω, F_N, braking torque (T) and time; so, in steady state conditions, we have $\mu=\mu(F_N,T,V_C,\Omega)$ with $F_x=\mu F_N$. Since F_x, T and Ω are linked by the wheel spin equation of motion, the previous relationship may be written again as $\mu=\mu(F_N,V_C,\Omega)$ or $\mu=\mu(F_N,V_C,V_S)$. In literature [CLARK, PACE2, SAKA1] global friction coefficient μ is given as a function of F_N, V_C and slip coefficient $s_x=V_S/V_C$ (or of F_N, V_C and theoretical slip coefficient $\sigma=V_S/V_r$). These curves, known as "tyre stationary characteristics", depend upon working conditions such as: inflation pressure, environmental temperature, soil status. They can be used to evaluate longitudinal forces in quasi stationary vehicle dynamics simulation, but their experimental evaluation is heavy work and need adequate tools.

• *Recent developments.* In order to synthesise tyre stationary characteristics an empirical formulation has been proposed in [BAKK1, BAKK2], whose coefficients have a physical meaning. Since this model, known nowadays as the "Magic Formula" tyre model, gave good results and was easy to use, it has been improved upon [OOSTE, PACE1] and implemented in computer simulation facilities [SHURI]. Recently, in [SLAGM] a Magic Formula tyre model was suggested to represent wheel dynamics in computer simulation for landing gear parameter estimation and ground load prediction.

• *Contact and Force Generation Models (Brush Models)* are divided into two main categories: *Steady State (or quasi steady state)*, for slowly varying conditions, and *Unsteady state*, capable of simulating high frequency phenomena.
- *The steady state brush model* is an idealised representation of the tyre contact region that results from the following basic hypotheses [CLARK, PACE2, SAKA1]:
1) the vertical ground load distribution is an input data evaluated experimentally or numerically by means of other models;
2) rolling resistance is disregarded nor is the model

itself able to predict it;
3) belt and tread are considered to be flat in the contact zone and tread is undeformable orthogonally to the ground;
4) the belt velocity, in the contact zone, is assumed to be uniform and equal to slip velocity V_S;
5) at free rolling (V_S=0) the tread is longitudinally undeformed and no shear stress exists;
6) in generic braking conditions ($V_S \neq 0$), for the adhering part of the contact patch, the horizontal shear stress is assumed to be linearly dependent on the local longitudinal tread deformation, while for the sliding part, shear stress depends on the local sliding velocity (V_{SL}) on the basis of the dynamic friction law [PACE2].

To discretize the problem the tread in contact may be regarded as a brush (Fig. 4-2) whose "bristles" are attached to the belt and move through the contact zone with the relative velocity V_r. At least one bristle is always adhering at the beginning of the contact patch and the adhering zone extension is determined by the static friction threshold.
The brush model, whose first formulation can be found in [DUGOF] (1970), gives good results and is widely used, both in its simplest form [DUGOF, PACE2] and with experimental or empirical improvements [SAKA1, SAKA2, SAKA3, SAKA4].

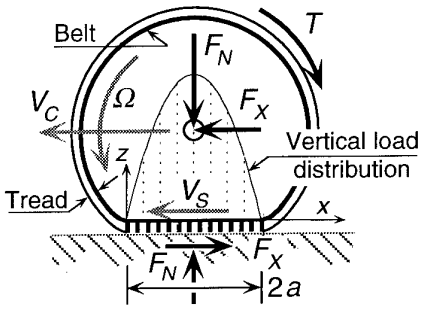

Fig. 4-2 Brush model

- *Unsteady Models* of contact force generation are rare in literature. Examples can be found in [ZANT1] and [ZANT2] where the model adopted for computer simulation is an unsteady brush model, implemented from an "Eulerian" point of view, which gives very good matching between experimental and numerical results. It was developed from the above mentioned basic hypothesis extended to unsteady motion by [CLARK].
An interesting point of view on the subject appears in [ZEGEL] where a simplified unsteady contact model is presented.
Finally it should be noted that all contact models and their results are closely connected to the modelling of rubber-soil *friction phenomena*. Reviews on this subject are to be found in [SAKA2] and [CLARK]; furthermore in [PACE2] simplified models for analytical studies or for reducing the computational load in numerical simulation are discussed.

• *Tyre Structure and Transmission Property Models* may be divided into the following main categories:
A elastic link between elastic belt & rim
B elastic link between rigid belt & rim
C elastic link between rigid belt & rim + residual stiffness

A) An elastic ring tyre model was developed by [SGONG, ZEGEL] to solve the problem of correctly representing the high frequency vibrational phenomena of the tyre belt. Particularly, the need for a model capable of simulating the observed "Standing Waves" phenomena was felt [CLARK, HUAN1, HUAN2]. The model consists of an elastic ring, treated as a circular elastic beam, a mass, representing the wheel rim, and radial and torsional springs, connecting the ring to the rim, whose aim is to reproduce tyre side-wall and pressurised air behaviour ("foundation stiffness"). The ring is assumed to have the radius of the belt and ground loads are concentrated at the intersection between the ring itself and a straight line perpendicular to the ground and passing by the undeformed ring centre. The model gives good results [SGONG, ZEGEL] and makes it possible to take into account the fundamental elastic in-plane dynamics of the wheel. On the other hand, if one is not interested in high frequency modes, only translational and rotational rigid displacements of the belt with respect to the rim are really important and the model becomes too sophisticated.
B) In this case the ring modelling the tyre belt is linked to the rim by radial and torsional springs as in the previous model but it is assumed to be rigid [CLARK, SAKA1, ZANT1, ZANT2]. The ring radius is assumed to be equal to the effective rolling radius [ZANT1, ZANT2] to fit the kinematic relationships at free rolling [PACE2] and the previous hypotheses about load introduction are retained. The rigid ring model provides good results in wheel dynamics simulation as demonstrated in [ZANT1] and [ZANT2].
C) Recently, an intermediate model has been proposed in [ZEGEL]. The first test results show a good agreement with experimental data for medium range frequency phenomena. The ring is rigid and it has the radius of the undeformed belt, but, between the load introduction point and the ring, more elasticity has been introduced. Such elasticity (referred to as "residual stiffness") consists of vertical, longitudinal and torsional springs whose stiffnesses are calibrated on the basis of experimental wheel elastic properties [ZEGEL].

• *Integrated Global Models*
Combining the previously described *Tire Structure Models* and the *Contact Models*, integrated global models capable of describing the whole tyre-wheel system can be obtained. Several steady state models are described in Pacejka's 1991 review [PACE2]. At one extreme, there are detailed physical models with both tyre structure and tread-ground interaction represented [SAKA1, SAKA2, SAKA3, SAKA4], while at the other, there are classical tyre and Magic formula models. In the middle a simple physical model can be found, essentially obtained by combining the wheel spin equation of motion with the above cited Brush Model.
Unsteady models combining a "B" or "C" tyre structure model with the unsteady brush model give a very good fit between simulation and unsteady experimental results [ZANT1, ZANT2, ZEGEL]. Recently, a global dynamic

tyre model has been proposed in [NEGRU]; it consists of a complex representation of the elastic and dumping features of tyre structure (Fig. 4-3) with detailed contact modelling. It makes it possible to evaluate the vertical ground load distribution and to take into account rolling resistance phenomena disregarded in all physical models reviewed. The price to pay is in terms of computational load and complexity in the interpretation of results.

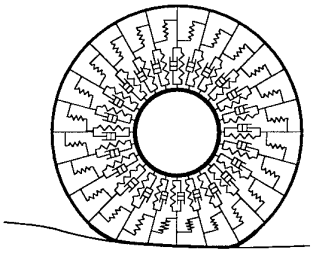

Fig. 4-3 Radial spring-damper model

• *Conclusions*

For the numerical analysis of gear walk, a "B" or "C" tyre structure model coupled with the unsteady brush model (Fig. 4-4) seems to give a fairly good representation of the physical phenomena.

From the point of view of the analytical modelling of the system, in all the works reviewed, a constant wheel forward speed V_C is assumed. Since such a hypothesis cannot be accepted if the wheel hub is connected to an elastic landing gear leg, improvements are then necessary to obtain dynamic characteristics of the system (zeroes and poles). The poles of the brush subsystem are given in [ZEGEL] but only at free rolling; so, poles in generic braking conditions must be determined in order to synthesise antiskid control systems.

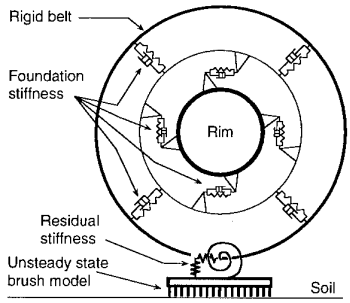

Fig. 4-4 The model selected

5. A LAGRANGIAN BRUSH MODEL FOR CONTACT DYNAMICS SIMULATION

5.1 Bristle models

The first step in order to build a Lagrangian brush model is to make certain dynamic models of the bristles available. A sketch of the bristle is shown in Fig. 5.1-1 together with the physical model being considered.

Three possible parameter choices, referred to as the "MCK Model" (with $M,C,K\neq 0$), the "CK Model" (with $M=0$) and the "K Model" (with $M=0,C=0$), have been investigated by numerical simulation. The K Model is

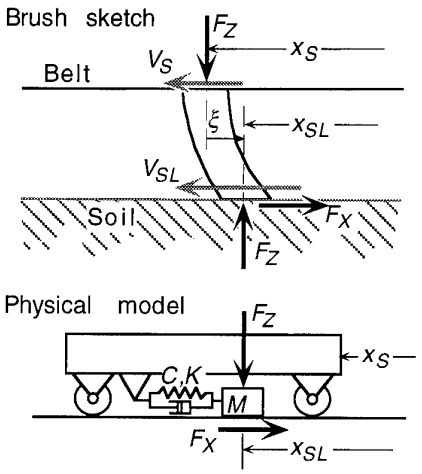

Fig. 5.1-1 Bristle sketch and physical model

analogous to that usually used for brush modelling [ZANT1]. The equations governing bristle dynamics are summarised in the following table, where $\mu(V_{SL})$ is the friction law (see sec. 5.3).

	Sliding bristle	Non sliding bristle
MCK Model	$\dot{V}_{SL}=\left(\frac{C}{M}\right)\dot{\xi}+\left(\frac{K}{M}\right)\xi+\frac{\dot{F}_x}{M}$ $F_x = F_z\,\mu(V_{SL})$	$V_{SL}=0\,;\dot{\xi}=V_S$ $F_x = K\xi + C\dot{\xi}$
CK Model	$V_{SL}=V_S-\left(\frac{K}{C}\right)\xi-\frac{F_x}{C}$ $F_x = F_z\,\mu(V_{SL})$	$V_{SL}=0\,;\dot{\xi}=V_S$ $F_x = K\xi + C\dot{\xi}$
K Model	$V_{SL}=V_S\,;\,\xi=\frac{F_x}{K}$ $F_x = F_z\,\mu(V_{SL})$	$V_{SL}=0\,;\dot{\xi}=V_S$ $F_x = K\xi$

Discontinuities in bristle dynamic behaviour have been handled as shown in the flow chart in Fig. 5.1-2. The adhering bristle starts sliding, with respect to the ground, if the sum of the elastic and dumping forces becomes greater than the static friction threshold. The sliding bristle stops moving when a change in velocity sign occurs and the sum of the elastic, dumping and inertial forces (if any) is below the static friction threshold.

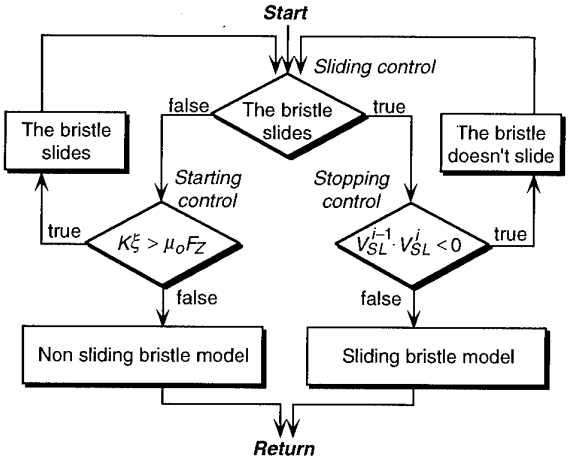

Fig. 5.1-2 Bristle K-model management

In Fig. 5.1-3 qualitative responses to a step in slip velocity (V_S) are shown for the three models presented above. The K Model (Fig. 5.1-3 a) behaves in a rather simple way even if it is quite "unphysical"; as bristle sliding happens, the sliding velocity V_{SL} suddenly reaches its steady state value (V_S), while the relative displacement of the bristle shows a discontinuity due to the fact that the spring force (proportional to the relative displacement of the bristle) must balance ground friction which decreases as V_{SL} increases. The CK Model (Fig. 5.1-3 b) avoids the discontinuity of the kinematic quantities, by introducing a V_{SL} dynamic transient before the steady state value V_S is gained. The MCK Model (Fig. 5.1-3 c) shows very complex dynamics whose effects in a dynamic brush model simulation are not valuable a priori.

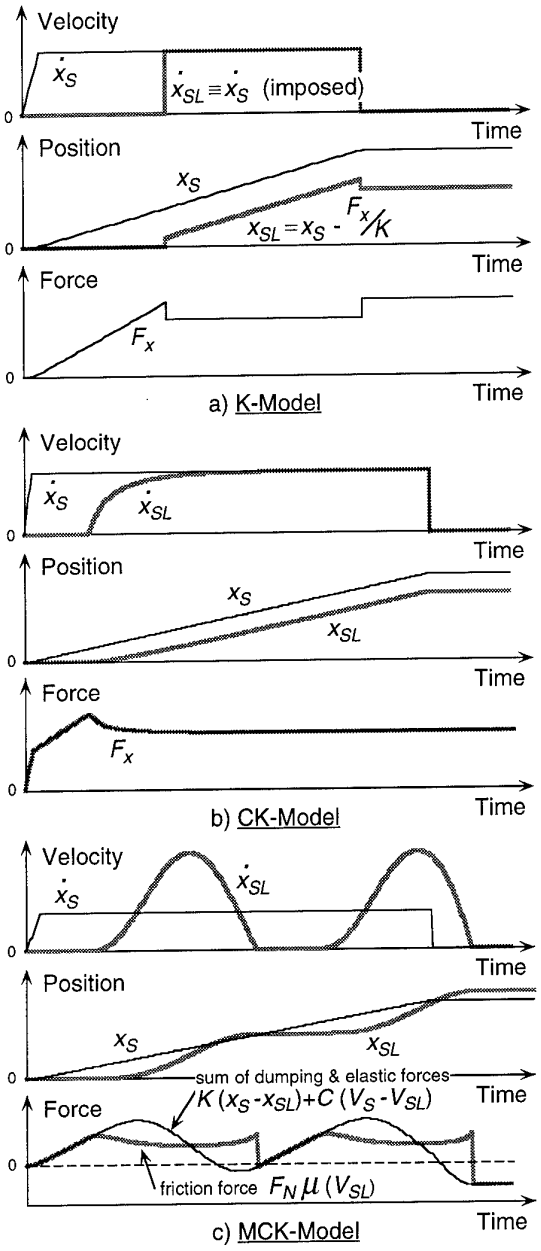

Fig. 5.1-3 Bristle responses

5.2 Brush models and software structure

The software represents a brush built with a set of bristles behaving according to one of the three previously described models. The basic hypotheses are the same as those mentioned in sec. 4 for brush models, with the assumption of a parabolic distribution of vertical forces (see Fig. 4-2). The simulation is performed by means of a Lagrangian approach; each bristle is followed as an independent dynamic system during its motion along the contact patch. The roots of the bristles are attached to the belt and equally spaced; they move all together with the slip velocity (V_S) that is one of the two inputs of the system, the other being wheel centre velocity (V_C). When a bristle exits from the contact patch, a new bristle enters, at the same time, from the other side.

5.3 Results from the Brush K Model

In this section the numerical results obtained with the brush model based on the bristle K Model are reported.

• *Data for simulation* were taken from various sources [CLARK, SAKA2, ZEGEL] constituting a set describing a reasonable tyre. The values used for the tyre parameters are listed below while the function giving rubber friction versus sliding velocity is shown in Fig. 5.3-1:

- Vertical force (F_N) = 3200 N/m
- Footprint half length (a) = 0.08 m
- Bristle stiffness (K) = $1.0\ 10^6$ N/m^3

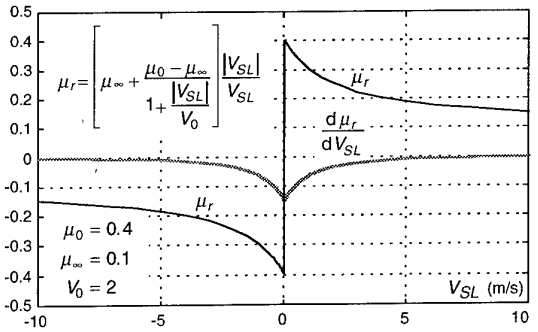

Fig. 5.3-1 Rubber-soil friction law

• *Braking test.* Fig. 5.3-2 shows transient responses on total longitudinal force F_x (per tyre width unit) to step inputs in V_S, with constant V_C=30 m/s. The unusual shapes of the transient responses are understandable if the time histories of longitudinal force distributions along the footprint shown in Fig. 5.3-3 are analyzed. Two opposite phenomena happen whose balance depends on the intensity of the braking input: increases in F_x values are due to the growth of bristle deformation in the adhering part of the contact patch, while reductions in F_x values depend upon the increase in the extension of the sliding zone. For small steps of s_x (Δs_x = 0.0303) F_x increases gradually to its steady state value because the sliding zone is negligible. For greater steps, the F_x time history shows an overshoot which becomes stronger as the steady state extension of the adhering part of the contact patch decreases.

From the steady state values of the time histories in

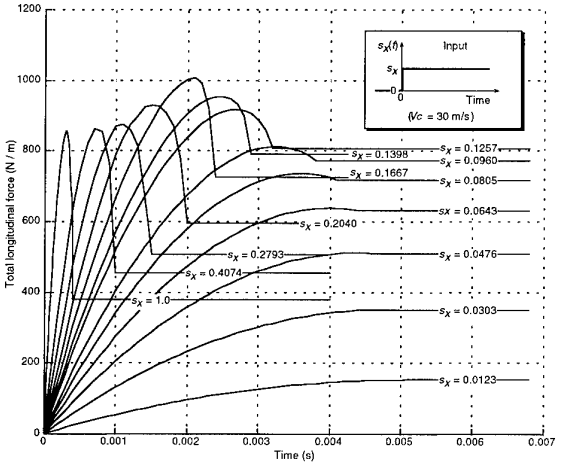

Fig. 5.3-2 Transient response in longitudinal force to a braking step input

Fig. 5.3-2, $\mu(\sigma)$, $\mu(s_x)$ and $\mu(V_S)$ curves were built for V_C=30 m/s and are shown in Fig. 5.3-4. The shape of these curves is fully understandable on the basis of steady state longitudinal force distributions along the footprint shown in Fig. 5.3-5. The integral value of such distributions depends upon the extent of the sliding portion of the contact patch (where long. stress has a parabolic shape) with respect to the non sliding one (where long. stress has a linear shape). A maximum occurs when the sliding zone is about 60% of the footprint length with $s_x \cong 0.15$. The integral values of the graphs in Fig. 5.3-5 were analytically calculated, too, by the means of the relationships [PACE2]:

$$F_x = \int_0^{\bar{x}_{tr}} K\sigma x\,\mathrm{d}x + \int_{\bar{x}_{tr}}^{2a} \mu(V_s) P_N(x)\mathrm{d}x \qquad (1)$$

with

$$\bar{x}_{tr}=2a(1-\eta\sigma);\ \eta=\frac{2Ka^2}{3\mu_o F_N} \qquad (2)$$

solving Eq. (1), the following function $F_x = F_x(\sigma)$ was obtained:

$$F_x=F_N\left\{3\mu_0\eta\sigma(1-\eta\sigma)^2+\mu\left[3(\eta\sigma)^2-2(\eta\sigma)^3\right]\right\}. \qquad (3)$$

In Fig. 5.3-4 the results of the analytical calculation for V_C = 5, 10, 15, 20, 25, 30 m/s are shown. The 30 m/s curves coincide with the ones obtained by numerical simulation. It is interesting that, when plotting μ as a function of slip velocity V_S, at high slip values μ depends only upon V_S.

• *Transient response analysis.* Fig. 5.3-6 shows the F_x responses for small steps of s_x starting from different steady state braking conditions; tests have been carried out at constant V_C=30 m/s. These tests aim at deepening system behaviour for small perturbations about steady state conditions, both at free rolling and in any braking stationary condition whatever.

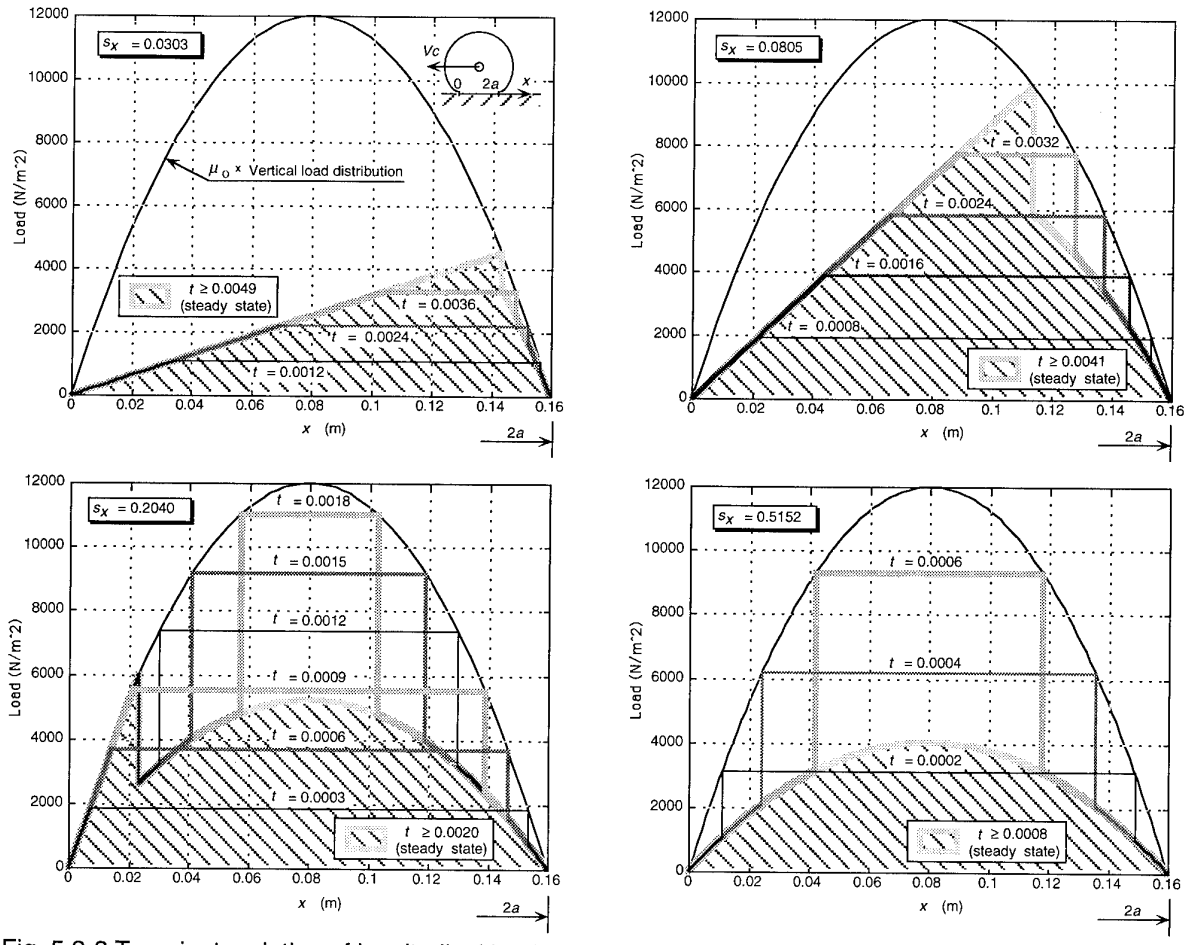

Fig. 5.3-3 Transient variation of longitudinal load distribution over the contact patch for a braking step input

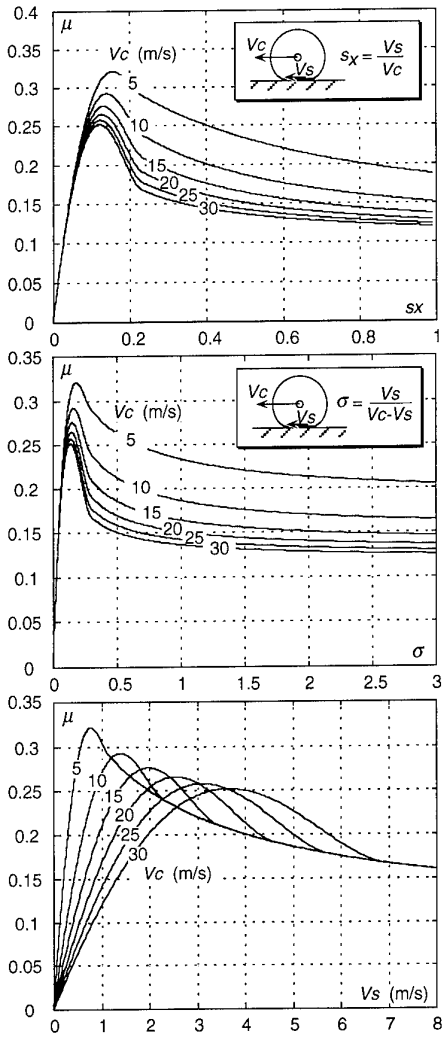

Fig. 5.3-4 Friction coeff. versus slip coeff.s and slip vel. in steady state cond.

The steady state values of F_x variations are of course different according to the local shape of the $\mu(s_x)$ curve at the point corresponding to the initial steady state condition. The shape of the transient responses on F_x are obviously linked to the time histories of load distribution along the contact patch. In order to obtain a deeper understanding of this influence, tests for higher s_x step inputs were carried out and both the transient responses and the time histories of the load distribution obtained are shown in Fig. 5.3-7. The initial down step is clearly due to the sudden variation in local friction forces on sliding bristles $\mu(V_{SL})$, caused by the sudden change of V_{SL} from its initial value to the final one (jump from condition 1 to 2 in fig. 5.3-7). The increase and decrease in the F_x value (passing from condition 2 to 3, 4, etc. in fig. 5.3-7) is essentially due to the balance between the rise in the number of sliding bristles (due to the advance of the transition point) and the rise in the deformation of the adhering ones.

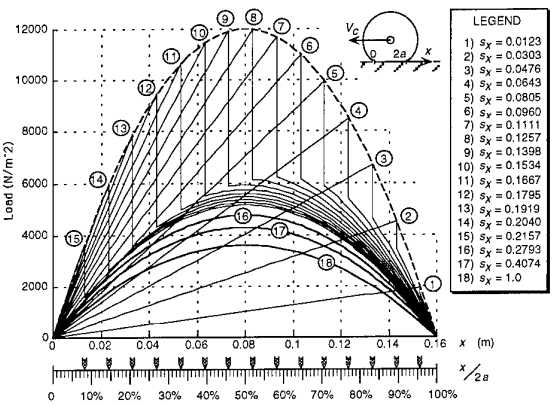

Fig. 5.3-5 Long. load distribution over the contact patch in steady state cond.

The investigation carried out also shows that the F_x response reaches its steady state values at a time which depends on the non sliding percentage of the contact patch. Such a time is equal to the "replacement time" necessary to replace all the bristles that are not sliding at the initial stationary state, given by:

$$t_r = \bar{x}_{tr}/(V_C - V_S). \tag{4}$$

The variation of t_r versus s_x is shown in Fig. 5.3-8.

Finally, to complete the analysis of the system dynamics, F_x responses for little steps of s_x, with constant V_S, were evaluated, starting from the same steady state braking conditions considered above. The results are given in Fig. 5.3-9. The response starting from s_x=0.3333 is not given because, at such high slip values, F_x does not depend on V_C if V_S=constant (see Fig. 5.3-4).

• *Conclusions*

The brush model presented, based on the bristle K Model, is not able to adequately represent sliding velocity V_{SL} which, at the transition point, suddenly changes from zero to the value of slip velocity V_S. This "unphysical" behaviour does not fit in with experiments that show (at least for small s_x) a linear shape variation of V_{SL} along the sliding zone [CLARK]. However all the above does not seem to affect too much the system response on the total longitudinal force which fits experimental measurements quite well [ZANT1].

This may be due to the fact that for small s_x values, the sliding zone is very small, while, for larger slip coefficients, the sliding zone is larger but the badly modelled one is confined to a restricted region after the transition point. In conclusion, the model seems to be able to represent contact dynamics in a numerical simulation of wheel behaviour.

Besides, the bristle K Model is simple enough to permit the development of analytical models of contact dynamics (see section 6).

5.4 Brush CK and MCK Models

Brush models based on the bristle MCK and CK Model, have not been investigated in detail yet. Judging from preliminary results, the CK Model seems to be interesting when a constant F_N distribution is used, while, with parabolic F_N distribution, it produces large sliding zones at the beginning of the contact patch that do not exist in experimental observations. The MCK

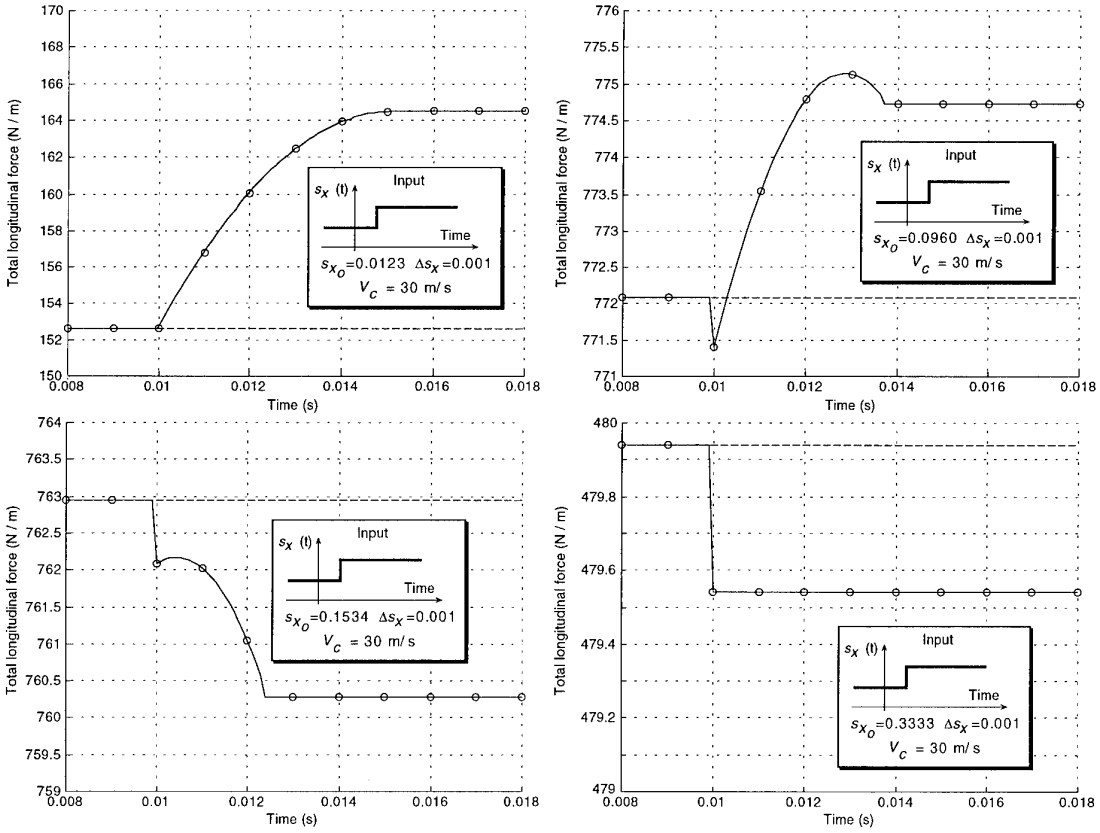

Fig. 5.3-6 Transient variation of the longitudinal force for small braking steps

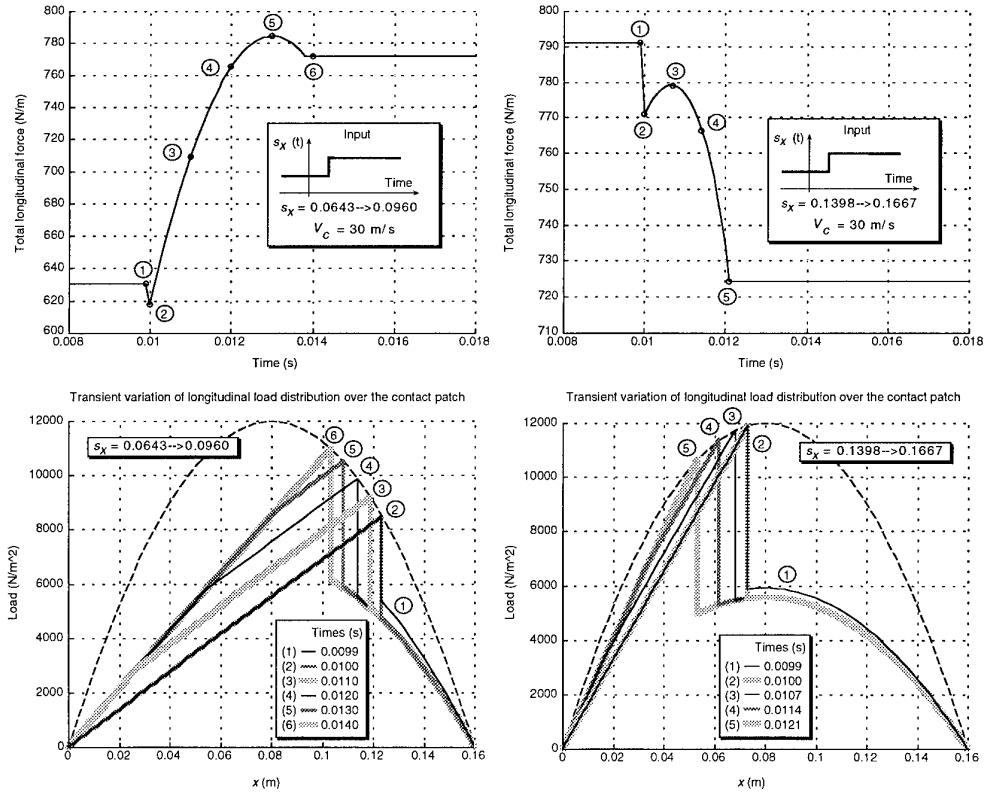

Fig. 5.3-7 Transient responses to "non small" braking steps

Model seems to give satisfactory V_{SL} distributions over the sliding zone even if it is very difficult to calibrate.

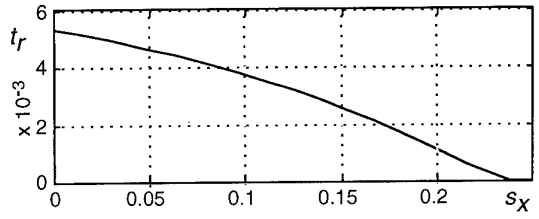

Fig. 5.3-8 "Replacement time" vs. slip coefficient

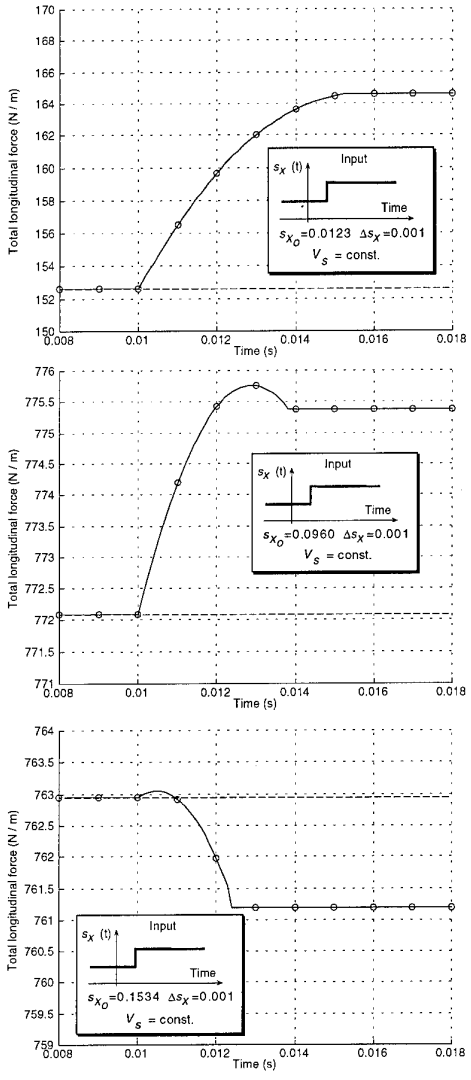

Fig. 5.3-9 Transient variation of the long. force for small steps in wheel speed

6. AN ANALYTICAL MODEL OF CONTACT DYNAMICS

6.1 μ(σ) model

If F_x is expressed as a function of V_C and V_S by means of μ curves, a linear model can be obtained as shown in the sketch in Fig. 6.1-1. In this case F_x variations are simply proportional to V_C and Vs variations; therefore to simulate the transient behaviour of F_x a more refined model is needed.

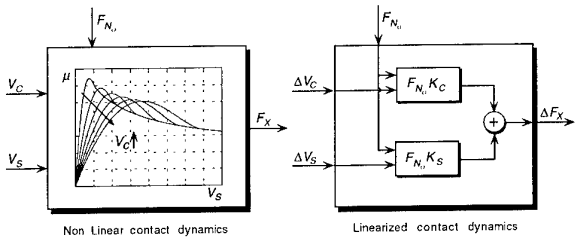

Fig. 6.1-1 Contact dynamics μ(σ) model

6.2 Brush model

In this section the dynamics of the braking force, for small disturbances from steady state conditions, is analytically investigated.

If we approach the tread as a continuum, adhering tread motion is governed by the following equation [CLARK]:

$$\frac{\partial \xi}{\partial t} = V_C - \Omega R_e - \Omega R_e \frac{\partial \xi}{\partial x} \tag{5}$$

where $\xi(x,t)$ is the longitudinal deformation of the tread, (O; x, z) is a frame of reference moving with the footprint (see Fig. 4-2) and the initial and boundary conditions are:

$$\xi(x,0) = \xi_o(x,0); \quad \xi(0,t) = 0. \tag{6}$$

Linearization of Eq. (5) with conditions (6) (with the assumption that R_e is constant) leads to the equations:

$$\frac{\partial e}{\partial t} = v_C - \omega R_e(1+\sigma_o) - \Omega_o R_e \frac{\partial e}{\partial x} \tag{7}$$

$$e(x,0) = 0; \qquad e(0,t) = 0 \tag{8}$$

where the symbols with subscript "o" indicate the reference steady state condition quantities and the lower case symbols indicate small variations around the reference condition, i.e.:

$$e(x,t) \equiv \Delta\xi(x,t); \quad v_C \equiv \Delta V_C; \quad \omega \equiv \Delta\Omega.$$

Close to the free rolling condition σ_o=0 and the tread sliding portion can be disregarded; so Eq. (7) is valid over the whole footprint and can be solved, using the Laplace transform technique, yielding the following result:

$$e(s,x) = v_S(s)\left\{1 - \exp\left[-(x\,s)/(R_e\,\Omega_o)\right]\right\}/s \tag{9}$$

where $e(x,s)$ is the Laplace-transform of $e(x,t)$ and $v_S(s) \equiv v_C(s) - R_e\,\omega(s)$ the Laplace-transform of the input. Now, with the same assumptions as in the K-Model, by integrating the product $K\,e(s,x)$ along the footprint, the following transfer function for the longitudinal force (f_x) can be obtained:

$$\frac{f_x(s)}{v_S(s)} = \frac{K}{s}\left\{2a + \frac{R_e\Omega_o}{s}\left[e^{(-\vartheta s)} - 1\right]\right\} \tag{10}$$

with $\vartheta \equiv 2a/R_e\Omega_o$. Fig. 6.2-1 shows the time response to a v_S step obtained from Eq. (10); it should be noted that this response is identical to that shown in Fig. 5.3-2, evaluated numerically for an s_x variation from zero to 0.0123.

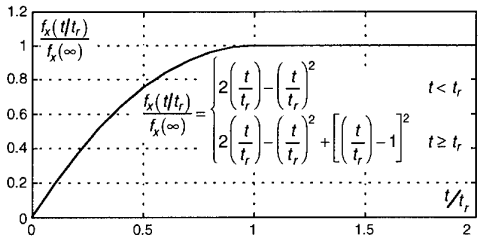

Fig. 6.2-1 Analytical response on the longitudinal force to a v_S step at free rolling

• *Linearized transfer function and system poles*

Linearizing Eq. (10) by means of a first order Padè technique, the following expression can be obtained:

$$\frac{f_x(s)}{v_S(s)} = \frac{K}{s}\left\{2a - \frac{R_e\Omega_o}{s}\left[\frac{s-2/\vartheta}{s+2/\vartheta}+1\right]\right\} \qquad (11)$$

which can be written in the form:

$$\frac{f_x(s)}{v_S(s)} = \frac{2Ka}{s+R_e\Omega_o/a} \qquad (12)$$

or, since $2Ka^2 = \left.\frac{\partial\mu}{\partial s_x}\right|_{s_x=0}$ (see Eq. (3)), in the form:

$$\frac{f_x(s)}{v_S(s)} = \frac{\tilde{K}\,p}{s+p} \qquad (13)$$

with: $$\tilde{K} = \frac{F_N}{R_e\Omega_o}\left.\frac{\partial\mu}{\partial s_x}\right|_{s_x=0}; \quad p = \frac{R_e\Omega_o}{a} = \frac{2}{\vartheta}\,. \qquad (14)$$

Eq.s (13) and (14) give the transfer function of the contact dynamics and its correlation with the rolling tyre stationary characteristics at free rolling. It is not difficult to demonstrate that these Eq.s are equivalent to the "relaxation system" proposed in [ZEGEL].

The transfer function in generic braking conditions ($\sigma_o \neq 0$) can be determined by extending the above mentioned procedure to the case of a non-negligible sliding zone, still with the same assumptions as in the K-Model. The dynamic displacement of the transition point $\Delta\bar{x}_{tr}(t)$ from the steady state reference position can be evaluated by linearizing the equation:

$$K\xi(\bar{x}_{tr},t) = \mu_o P_N(\bar{x}_{tr}) \qquad (15)$$

that represents the static friction threshold condition. The contribution of the adhering part to f_x can then be evaluated by applying Eq. (7) between 0 and $\bar{x}_{tr}(0)$, the contribution of the sliding part integrating the function $\mu(V_s)P_N(x)$ between $\bar{x}_{tr}(t)$ and $2a$.

This procedure leads to the linear model of the contact dynamics shown in the sketch in Fig. 6.2-1, where:

$$K_S = \left.\frac{\partial\mu}{\partial V_S}\right|_o \qquad K_C = \left.\frac{\partial\mu}{\partial V_C}\right|_o$$

$$p = \frac{R_e\Omega_o}{\left(\bar{x}_{tr_o}/2\right)} \qquad z = \frac{K_S p}{\beta}$$

$$\beta = \begin{cases} 0 & \sigma_0 = 0 \\ \dfrac{\sigma_0 K_S + (\sigma_0+1)K_C}{\sigma_0} & \sigma_0 \neq 0 \end{cases}$$

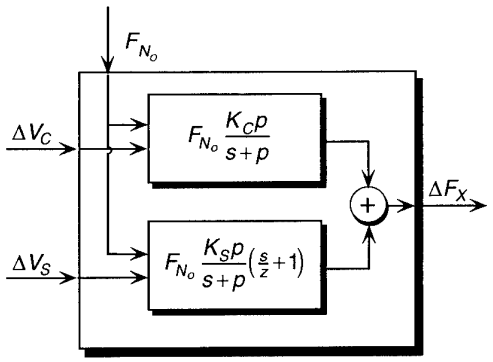

Fig. 6.2-2 Contact dynamics brush model

Note that in a free rolling condition $z \to \infty$. Furthermore, K_C=0 and V_S remain the only input of the system (see Eq. (13)); this does not mean that the system does not respond to V_C, as $V_S = V_C - \Omega R_e$.

7. LINEARIZED MODELS OF THE LANDING GEAR-WHEEL SYSTEM

In this section a preliminary analysis of the linear dynamics of the landing gear-wheel system shown in Fig. 7-1 is presented. Certain assumptions are made in order to simplify the analysis. Since the aim of this linearized model is to provide a tool for anti-lock system design, a constant aircraft speed V_A together with a constant vertical load on the gear leg is considered. Such hypotheses seem quite reasonable, since both vertical load and aircraft speed are slowly varying with respect to gear walk frequencies. Besides, the wheel model is simplified by disregarding both foundation and residual stiffness.

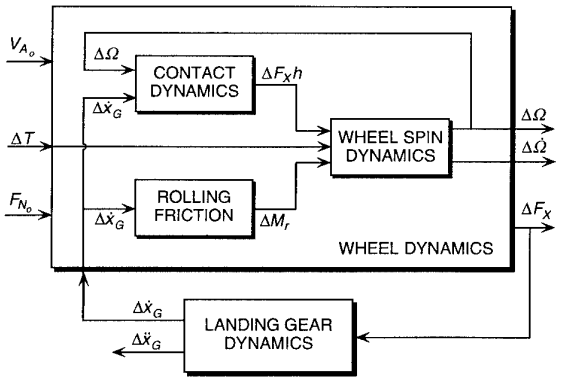

Fig. 7-1 Landing gear-wheel system

The transfer functions of the blocks in Fig. 7-1 are:

LANDING GEAR $$\frac{\Delta x_G}{\Delta F_x} = \frac{1}{M_G s^2 + C_G s + K_G}$$

WHEEL SPIN DYNAMICS $$\Delta\Omega = \frac{1}{sJ_w}\left(-\Delta T - F_{N_o}\Delta x_r + \Delta F_x h\right)$$

ROLLING FRICTION $$\Delta x_r = 2\hat{K}\frac{V_{A_o}}{F_{N_o}} h\,\Delta\dot{x}_G$$

For the box of the contact dynamics, both the $\mu(\sigma)$

model and the brush model (see sec. 6.1 and 6.2) may be used.
In generic braking conditions, poles and zeroes of the whole landing gear-wheel system, based on the brush model of the contact dynamics, have not been investigated in detail yet. When the $\mu(\sigma)$ model is used, the presence of the wheel augments the period and the dumping of the two complex poles of the landing gear; a third real and stable pole, due to the wheel spin dynamics, is also present and moves towards the origin as $(\partial\mu/\partial\sigma)|_o$ increases, becoming unstable when $(\partial\mu/\partial\sigma)|_o < 0$. When the brush model is used, at free rolling one more pole, real and stable, due to the contact dynamics, is present.
It is interesting to note that, with the simplifying hypotheses assumed, it is possible to analytically express the poles of the wheel system as functions of system parameters.

8. CONCLUSION

The review of the literature has shown that investigation into gear walk is difficult and few papers on specific problems of aircraft braking are available. Concerning tyre modelling, a rigid ring model with residual stiffness, for tyre structure, coupled with an unsteady brush model, seems to be a good choice for numerical investigation into gear walk.
In the present paper a numerical unsteady brush model, based on a Lagrangian approach, and an analytical model of the tyre in contact dynamics have been developed. The numerical model has been extensively tested providing a good qualitative understanding of contact phenomena. The analytical model is an extension of the ones in the literature, as it is able to take velocity variations of the wheel hub into account; this is essential when such a hub is connected to an elastic landing gear leg. Furthermore the poles of the brush subsystem in generic braking conditions are given.

REFERENCES

[BAKK1] **E.Bakker, L.Nyborg, H.B.Pacejka**, *Tyre Modelling for Use in Vehicle Dynamics Studies,* SAE Paper n° 870421, 1987, in SAE Transactions 1987.

[BAKK2] **E.Bakker, H.B.Pacejka, L.Linder**, *A New Tyre Model with an Application in Vehicle Dynamics Studies*, SAE Paper n° 890087, 1989, in SAE Transactions 1989.

[BOWMA] **J.E.Bowman, E.H.Law**, *A Feasibility Study of an Automotive Slip Control Braking System*, SAE Paper n° 930762, 1993, in SAE Transactions 1993.

[CLARK] **S.K.Clark**, *Mechanics of Pneumatic Tires*, National Bureau of Standards, Depart. of Commerce Washington D.C., 1971.

[CURRE] **N.S.Currey**, *Aircraft Landing Gear Design: Principles and Practices*, AIAA Educational Series, 1988.

[DENTI] **E.Denti, C.Brogi, L.De Francesco**, *Dynamic Simulation and Load Prediction for a Flexible Aircraft in Taxiing, Take-off and Landing,* AAAF - Proc. of the Int. Forum on Aeroelasticity and Struct. Dynamics, Strasbourg, v.2, pp. 839-856, 1993.

[DOYLE] **G.R.Doyle**, *A Review of Computer Simulations for Aircraft-Surface Dynamics*, AAIA Journal, v. 23, pp. 257-265, 1986

[DUGOF] **H.Dugoff, P.S.Fancher, L.Segel**, *An Analysis of Tire Traction Properties and Their Influence on Vehicle Dynamic Performance*, SAE Paper n° 700377, 1970, in SAE Transactions 1970.

[ENRIG] **J.J.Enright**, *Laboratory Simulation of Landing Gear Pitch-Plane Dynamics*, SAE Paper n° 851937, 1985, in Selected Paper SAE PT-37, Ed. by J. A. Tanner, 1989.

[FANCH] **P.S.Fancher, C.C.Macadam**, *Computer Analysis of Antilock System Performance in the Braking of Commercial Vehicles*, Braking of Road Vehicles, ImechE Conf. Publications, Published by Mechanical Engineering Pub. Ltd., 1976.

[GERDE] **J.C.Gerdes, D.B.Maciuca, E.Devlin, J.K.Hedrick**, *Brake System Modelling for IVHS Longitudinal Control*, Advances in Robust and Nonlinear Control Systems, ASME, Dynamic Syst. & Control Division DSC v. 53 pp. 119-126, 1993.

[GILES] **N.A.Giles**, *Integrated Braking Systems*, Aerospace Design Engineering, June 1993.

[HIRZE] **E.A.Hirzel**, *Antiskid and Modern Aircraft*, SAE Paper n° 720868,1972.

[HOHNO] **H.Ohno, T.Suzuki, K.Aoki, A. Takahasi, G.Sugimoto**, *Neural Network Control for Automatic Braking Control System*, Neural Networks, v. 7, n° 8, pp. 1303-1312, 1994.

[HUAN1] **S.Huang, C.Su**, *In-Plane Dynamics of Tyres on the Road Based on an Experimentally Verified Rolling Ring Model*, Vehicle System Dynamics, v. 21, pp. 247-267, 1992.

[HUAN2] **S.C.Huang**, *The Vibration of Rolling Tyres in Ground Contact*, Int. J. of Vehicle Design, v. 13, n° 1, pp. 78-95, 1992.

[LINDO] **W.C.Lin, D.J.Dobner, R.D.Fruechte**, *Design and Analysis of an Antilock Brake Control System with Electric Brake Actuator*, Int. J. of Vehicle Design, v. 14, n° 1, pp. 13-43, 1993.

[MAUER] **G.F.Mauer, G.F.Gissinger, Y. Chamaillard**, *Fuzzy Logic Continuous and Quantizing Control of an Abs Braking System*, SAE Paper n° 940830 in SAE Special Publication SP-1018.

[MIYAS] **N.Miyasaki, M.Fukumoto, Y.Sogo**

H.Tsukinoki, *Antilock Brake System (M-ABS) Based on the Friction Coefficient Between the Wheel and the Road Surface*, SAE Paper n° 912174, 1991.

[MOSEL] **D.D.Moseley**, **T.J.Carter**, *Performance Testing on an Electrically Actuated Aircraft Braking System*, SAE Paper n° 881399, 1988, in Selected Paper SAE PT-37, Ed. by J. A. Tanner, 1989.

[NEGRU] **D.Negrut**, **J.S.Freeman**, *Dynamic Tyre Modelling for Application with Vehicle Simulation Incorporating Terrain*, SAE Paper n° 940223 in SAE Special Pub. SP-1016.

[OOSTE] **J.J.M.van Oosten E.Bakker**, *Determination of Magic Tyre Model Parameters*, Tyre Models for Vehicle Dynamics Analysis, supplement to Vehicle System Dynamics v. 21, 1991.

[PACE1] **H.B.Pacejka**, **E.Bakker**, *The Magic Formula Tyre Model*, Tyre Models for Vehicle Dynamics Analysis, supplement to Vehicle System Dynamics. 21, 1991.

[PACE2] **H.B.Pacejka**, **R.S.Sharp**, *Shear Force Development by Pneumatic Tyres in Steady State Condition: A Review of Modelling Aspects*, Vehicle System Dynamics, v. 20, pp. 121-176, 1991.

[PERRO] **J.M.Perronne**, **M.Renner**, **G.Gissinger**, *On Line Measurement of Braking Torque Using a Strain Sensor*, SAE Paper n° 940333 in SAE Special Publication SP-1018.

[SAKA1] **H.Sakai**, *Theoretical and Experimental Study on the Dynamic Property of Tyres, Part 1: Review of Theories of Rubber Friction*, Int. J. of Vehicle Design, v. 2, n° 1, pp. 78-110, 1981.

[SAKA2] **H.Sakai**, *Theoretical and Experimental Study on the Dynamic Property of Tyres, Part 2: Experimental Investigation of Rubber Friction and Deformation of a Tyre*, Int. J. of Vehicle Design, v. 2, n° 2, pp. 182-226,1981.

[SAKA3] **H.Sakai**, *Theoretical and Experimental Study on the Dynamic Property Of Tyres, Part 3: Calculation of the Six Components of Force and Moment of a Tyre*, Int. J. of Vehicle Design, v. 2, n° 3, pp. 335-372, 1981

[SAKA4] **H.Sakai**, *Theoretical and Experimental Study on the Dynamic Property of Tyres, Part 4: Investigations of the Influences of Running Conditions By Calculation and Experiment*, Int. J. of Vehicle Design, v. 3, n° 3, pp. 333-375, 1982.

[SAVKO] **A.R.Savkoor**, *Boundary Conditions on Models for Predicting Tyre to Road Traction*, Tyre Models for Vehicle Dynamics Analysis, supplement to Vehicle System Dynamics, v. 21, 1991.

[SGONG] **S.Gong**, **A.R.Savkoor**, **H.B.Pacejka**, *The Influence of Boundary Conditions on the Vibration Transmission Properties of Tires*, SAE Paper n° 931280, 1993, in SAE Transactions 1993.

[SHURI] **D.J.Shuring**, **W.Pelz**, **M.G. Pottinger**, *The Bnps Model - An Automated Implementation of the "Magic Formula" Concept*, SAE Paper n° 931909 in SAE Special Publication SP-1016.

[SLAGM] **M.T.P.van Slagmaat**, *Tire Models in Aircraft Landing Gear Simulation*, Tyre Models for Vehicle Dynamics Analysis, supplement to Vehicle System Dynamics, v. 21, 1991.

[TANCH] **H.Tan**, **Y.Chin**, *Vehicle Antilock Braking and Traction Control: A Theoretical Study*, Int. J. of Systems Science, v. 23, n° 3, pp. 351-365, 1992.

[TANNE] **J.A.Tanner**, *Review of NASA Antiskid Braking Research*, SAE Paper n° 821393, 1982, in Selected Paper SAE PT-37, Ed. by J. A. Tanner, 1989.

[TARTE] **J.F.Tarter**, *Electric Brake System Modelling and Simulation*, SAE Paper n° 911200, 1991, in SAE Transactions 1991.

[WATAN] **M.Watanabe**, **N.Noguchi**, *A New Algorithm for Abs to Compensate for Road-Disturbance*, SAE Paper n° 900205, 1990, in SAE Transactions 1990.

[YEH_1] **E.C.Yeh**, **C.Kuo**, **P.Sun**, *Conjugate Boundary Method for Control Law Design of Antiskid Brake Systems*, Int. J. of Vehicle Design, v. 11, n° 1, pp. 40-62, 1990.

[YEH_2] **E.C.Yeh**, **G.C.Day**, A *Parametric Study of Antiskid Brake Systems Using Poincaré Map Concept*, Int. J. of Vehicle Design, v. 13, n° 3, pp. 210-232, 1992.

[ZANT1] **A.van Zanten**, **R.Erhardt**, **A.Lutz**, *Measurement and Simulation of Transient Tire Forces*, SAE Paper n° 890640, 1989.

[ZANT2] **A.van Zanten**, **R.Erhardt**, **A.Lutz**, *Measurement and Simulation of Transients in Longitudinal and Lateral Tire Forces*, SAE Paper n° 900210, 1990, in SAE Transactions 1990.

[ZEGEL] **P.W.A.Zegelaar**, **S.Gong**, **H.B. Pacejka**, *Tyre Models for the Study of In-Plane Dynamics*, Tyre Models for Vehicle Dynamics Analysis, supplement to Vehicle System Dynamics, v. 23, 1993.

Fuselage Vibration Control Using Semi-Active Front Gear

H. Wentscher, W. Kortüm, W.R. Krüger

DLR - Deutsche Forschungsanstalt für Luft- und Raumfahrt
Institut für Robotik und Systemdynamik, Postfach 11 16
D - 82234 Wessling, Germany

Summary:

This paper presents results of research performed in the field of semi-active suspensions for advanced landing gears and optimization of their associated design parameters to achieve minimum weight, maximum comfort under strict requirements with respect to safety and even increase lifetime by reducing the loads during landing impact and taxiing.

A detailed mechanical model is derived for an existing aircraft (AIRBUS A300) which will be used for simulating the standard design as well as the active optimized landing gear. The simulation is performed with SIMPACK, DLR's prime multibody computer code.

Results will be presented on using the multi-objective parameter optimization software ANDECS. The design case study will concentrate on taxiing of a flexible aircraft. Reduction of the so-called "beaming effect" (e.g. dynamic coupling of runway excitation with elastic fuselage eigenmodes) is the major design goal.

1. Introduction

1.1 Landing Gear Requirements

Among the numerous complex components that make up an aircraft the landing gear is often regarded only as a bothersome, but necessary attachment. It must not be forgotten that, while the predominant task of an aircraft is without doubt to fly with the best performance achievable, it will also spend a good part of its life on the ground. Typical cases are taxiing as well as take-off and landing. According to today's airlines' specifications an aircraft should reach up to 90 000 take-offs and landings as well as 500 000 km of ground roll during its life time. Statistics also show that accidents prior to or directly after take-off and touchdown relate their fair share (more than 50%) to the overall numbers. Hence, the importance of aircraft ground handling and therefore of landing gear design should not be underestimated.

Tests on life-size aircraft are obviously expensive and risky, and tests on test-rigs (namely drop-test facilities) allow only limited deduction of information about the landing gear's dynamics; especially the interaction between aircraft and landing gear is difficult to assess. On the contrary, simulation offers a means to examine the behavior of the airplane as a complex system in its environment at a reasonable cost. With a modern computer mechanical systems with a large number of degrees of freedom, both for rigid and elastic body motion, can be modelled.

The conventional landing gear type for large aircraft, consisting of a set of tires, sometimes a bogie, and almost always an oleo pneumatic shock absorber (often abbreviated as "oleo") today is a highly sophisticated device that leaves only limited room for improvement. With the advent of microelectronics both in digital computers and in controller development the idea of a controlled landing gear gained new momentum. Both systems controlling strut stiffness and damping coefficient (fully active) and controlling only the damping parameters (semi-active) are subjects of current research.

As stated above, aircraft landing gears are crucial for safety, comfort (both for passengers and pilots) and for weight considerations. As the device responsible for safely moving the aircraft on ground, the landing gear has to fulfill several, sometimes conflicting, needs. Jenkins, [1] and Young, [2] have given a detailed presentation of those requirements. In short, the landing gear must on one hand absorb vertical and horizontal energy during landing impact, and on the other hand keep the aircraft in a stable position during ground manoeuvres. Commercial aircraft should also provide a smooth ground ride during taxiing both for passenger comfort and safety reasons.

1.2 Landing Gear Simulation

The design of a new aircraft takes a long time span which can last up to a decade from the first proposals to customer delivery. The development process includes different manufacturers and suppliers who provide many components to the aircraft. Simulation has long been a necessary step in the development process. In addition to mechanical simulation (e.g. test rigs) numerical computer simulation gains more and more importance and acceptance.

The simulation used in the work presented in this paper was based on the Multi-Body-System (MBS) simulation tool SIMPACK. SIMPACK is *the* central MBS-tool of DLR and it is being applied there for aircraft (landing gears), robots, spacecraft structures, railway and road vehicles.

SIMPACK offers fast numerical analysis capabilities due to an extended *O(N)*-algorithm for tree-configured rigid body MBS. Dealing with closed loop systems the equations of motion are accompanied by a minimal set of algebraic constraint equations, resulting in a differential-algebraic description of the system.

For the examination of elastic vibration control it is of course necessary to use elastic instead of rigid bodies in the model setup. In SIMPACK the kinematics of elastic bodies as well as stress stiffening effects of elastic deformations are taken into account.

Extensive libraries of coupling elements like joints and force elements as well as excitations aid the engineer in setting up a model. This includes the kinematics of different suspension systems or other complex joints, force models for hydraulic components, various tire models etc.; subsystem modelling techniques enable the user to establish complex non-standard kinematic and force laws. User written subroutines extend the modelling options.

Paper presented at the 81st Meeting of the AGARD SMP Panel on "The Design, Qualification and Maintenance of Vibration-Free Landing Gear", held in Banff, Canada from 4-5 October 1995, and published in R-800.

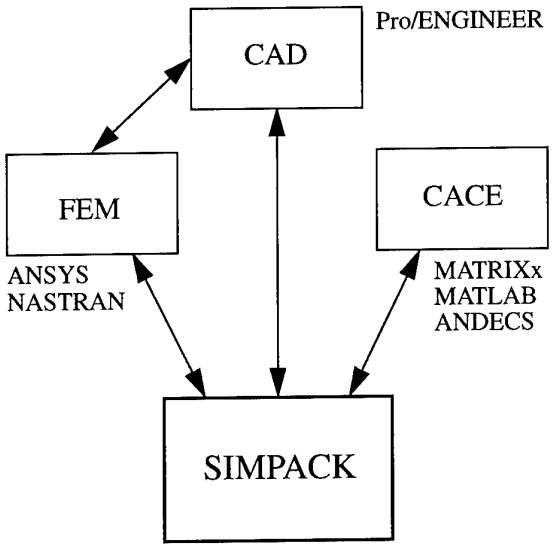

Figure 1: SIMPACK and its Interfaces

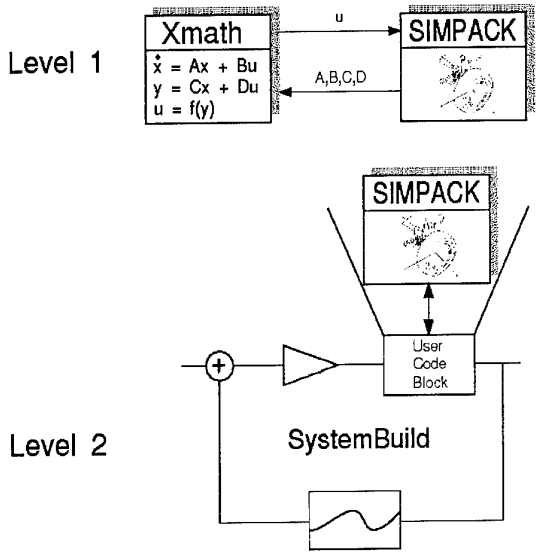

Figure 2: SIMPACK - MATRIXx Interface

SIMPACK Interfaces:

One of the most important features of SIMPACK is the fact that SIMPACK is an *open* system which possesses various interfaces to external standard software products (see figure 1) from the domain of finite element (FEM), computer aided design (CAD) and control system analysis (CACE) programs.

FEM:
To read in arbitrary flexible geometry a file interface to FEM-programs was developed. This gives access to mass, stiffness and damping matrices and to the above mentioned terms of second order. Vice versa, loads computed by SIMPACK can be transferred to the FEM-code.

CAD:
For the purpose of incorporating physical and graphical CAD-data, SIMPACK can be linked by a function call interface to CAD-packages. This means an addition to the interactive SIMPACK model setup tool. The link enables data consistency between MBS- and CAD-data at each step of the model establishing process. In general this feature is not guaranteed by just using file interfaces.

Control System Design and Analysis:
Due to its ability to numerically linearize the system equations, SIMPACK can be used as a simulation block within linear control design tools. SIMPACK may also be linked as a fully nonlinear block into nonlinear optimization and control tools like MATRIXx, MATLAB, ANDECS, etc. (figure 2 shows these links for the connection of SIMPACK to MATRIXx).
This gives the user the possibility to use SIMPACK and its parameter variation capability in a closed optimization loop to efficiently design dynamical systems.

1.3 Landing Gear Control

Active control of vehicle suspensions is not only an issue in the aircraft landing gear development. Cars, trucks and railway vehicles are the major applications to profit from active suspensions, and great efforts are made among the respective manufacturers to develop reliable and affordable systems.
The principles are largely independent of the specific vehicle employment. Although passive suspensions, mostly consisting of a spring and a damping device, today have a high standard, they suffer from a disadvantage that lies in their principle. Optimized to isolate the vehicle body from the ground best at a certain frequency range, their performance often diminishes at other frequencies. Additionally, the need to retain tire ground contact at all times poses a design conflict with comfort requirements.
For an aircraft the implications of the phenomena mentioned above is noteworthy: designed to absorb the energy of a hard landing impact, aircraft suspensions perform quite poorly in reduction of ground-induced loads during taxi and take-off. Not surprisingly, supersonic aircraft and a new generation of stretched civil transport aircraft suffer the most under ground-induced structural vibration because of their increased structural flexibility inherent in their design with slender bodies and, at supersonic aircraft, their relatively thin wings.
Active and semi-active suspensions promise a solution to this problem. An active suspension can be defined as a suspension layout which controls the forces acting in the shock absorber by control of energy dissipation, or, if required by the control law, by generating additional force. The usual means of control is a closed-loop control with a control law acting with respect to measured states (often velocities or accelerations) at certain points of reference. A suspension termed "semi-active" has the restriction that it cannot input energy into the system. Usually realized as damping control, it is therefore only able to control the amount of energy dissipation. Only forces of the same direction as that of the instantaneous relative damper velocity can be generated. Nevertheless, since fully active control sys-

tems usually require a heavy and costly force generation device (for aircraft landing gears mostly pressurized oil reservoirs have been proposed) they are unlikely to be quickly introduced in production aircraft. Semi-active suspension systems offer considerable advantages of light weight and less complicated mechanical requirements without suffering a great loss in performance.

Summarizing, the main reasons for the introduction of semi-active landing gear control are:

1. Minimize the load on the airframe structure, minimize force peak values and vibrations that can result in fatigue and reduce the life of the airframe.
2. Minimize accelerations acting on pilot and passengers since the induced vertical and horizontal accelerations and vibrations can lead to passenger discomfort and crew disorientation.

1.3.1 Activities

There have been several preceding efforts to the improvement of aircraft of ground ride. A typical measure to adopt the landing gear force-deflection curve toward a lower slope is the use of a two-chamber-oleo. In 1977, Somm/Straub/Kilner [4] proposed an adaptive landing gear system for several military transport aircraft to improve taxi performance on rough runways. They worked with a secondary air chamber that could be pressurized shortly after touchdown in order to generate the desired softer pneumatic spring rate as a function of aircraft weight. Today, with reliable, inexpensive and powerful electronic signal processing available, research has moved toward computerized closed-loop control. In 1984 a feasibility study for a series-hydraulic active control landing gear intended for supersonic military aircraft was published by McGehee and Morris, [5]. Additionally to theoretical analysis a number of tests had been performed on a test-rig to permit experimental verification of the concept. The setup is typical for a fully active control system and has before and since been investigated several times. The gear force applied to the airframe is regulated by the hydraulic pressure in the piston of the oleo which is used as an actuator.
The results obtained led to the modification of a F106 nose landing gear which was also tested in test-rig setups, [6]. Another investigation that combined an analytical and an experimental approach was conducted by Freymann, [7]. Object of research was the simulation of a nose gear oleo. Again the force generation was realized by pressurized oil, even though the valve layout was different. A laboratory setup was used to experimentally verify the basic control concept. Even though the results obtained in both cases might be overly optimistic when it comes to application to a realistic aircraft, the investigations showed nevertheless that a fully active landing gear is feasible and can lead to significantly reduced airframe loads. Another somewhat more recent approach is the analysis of improvements gained with closed loop semi-active oleo control. Studies by Karnopp [8] for automotive applications show that the performance of a semi-active damper is only marginally smaller than that of a fully active system, provided that an adequate control law is used. Catt/Cowling/Shepherd [9] come to a similar result in a simulation study of aircraft suspensions. The semi-active damping device is usually proposed to be an oleo with a modulated damping orifice cross-section, completely omitting the metering pin.

A study of the properties of fully and semi-active oleos led to the decision to take the semi-active damper as the system of choice (see table 1) for the work presented here, see [10].

passive	semi-active	active
low weight	low weight	high weight
good performance only for design case	good performance over broad range	good performance over broad range
relative low complexity	medium complexity	high complexity
stable	stable	potentially unstable

Table 1: System Features Comparison

The semi-active damper seems to provide the best compromise between performance and additional weight handicap. The investigations of ground-load reduction are concentrated on the nose gear, since results show that this has the most potential for ride quality improvement.

1.3.2 Control Laws

Different control laws are investigated in the literature, mostly for cars and trucks. During aircraft operations, however, associated parameters change during a wide range. Take-off weight will always differ drastically from landing weight, aircraft ground velocities vary between very low speed at taxi and 60 to 80 m/s at take-off and landing. Oleo and tire properties may vary depending on age and maintenance. Finally, runway quality differs from airport to airport.
Suitable control laws have to be robust against these changes. Several solutions to the problem exist and have been discussed thoroughly, ranging from sky-hook damping to nonlinear and adaptive control laws (for a state-of-the-art review see [11]).
For many problems the algorithms have to go further than to solely observe center of gravity motion. Other points influencing the results are maximum applicable actuator force and suspension travel limitations.
For the problem discussed in this paper, the sky-hook damping approach has been chosen.

1.3.3 Hardware

Since the idea of active and semi-active landing gear is relatively new, and no system for aircraft is as yet in the production stage, the hardware is still in the phase of concept evaluation. In the field of fully active oleo control so far heavy laboratory setups have been used to validate simulation results.
For semi-active control systems, some manufacturers, especially in the domain of heavy-duty trucks, have proposed and built technically feasible layouts. Other suggestions include dry friction damping (which, for large aircraft, is likely to be unrealistic due to the large energy dissipation). A relatively new proposal is the use of electro-rheological fluids, i.e. fluids that change their viscosity in response to an electrical field.
Objectives for the final choice of a system will surely be led by a consideration of performance against penalty. Surely low weight is desirable, and high safety against failure is essential. A good performance also requires a high bandwidth, low reac-

tion time actuator. The possible achievable actuator peak force might also be a decisive criterion.

2. Motivation

2.1 The Problem

2.1.1 Ride Comfort Assessment

In chapter 1 it could be seen that the improvement of crew and passenger ride comfort will be of growing concern for manufacturers of large aircraft.

As base measurement for ride comfort assessment the vertical accelerations are widely used. Since the individual perception is additionally influenced by other factors of the biomechanical human system, scales have been developed to weight the fact that certain frequencies are perceived to be more uncomfortable than others for a given amplitude. In ISO 2631, [12] the frequencies between 4 and 8 Hertz are denoted as the most crucial for comfort (figure 3). Ride comfort improvement has

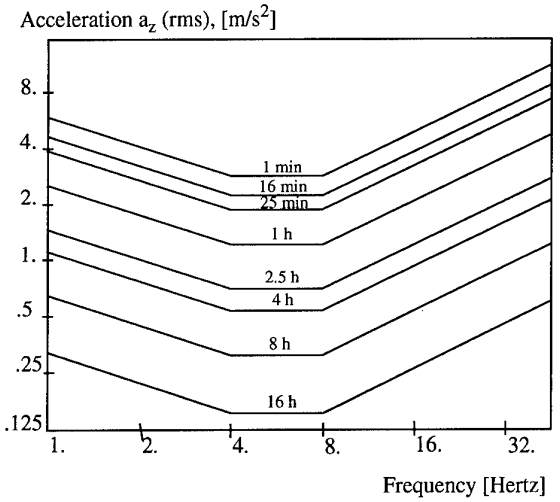

Figure 3: Fatigue-Decreased Proficiency Boundary (ISO 2631-1974(E))

therefore to concentrate on vertical accelerations in this frequency range, measured in the cockpit and passenger compartment.

2.1.2 Airframe Eigenfrequencies

Normal accelerations of the airframe originate in longitudinal rigid body modes as well as in elastic airframe eigenmodes.

Rigid body eigenmodes:

The important rigid body eigenmodes are found at frequencies where humans are less susceptible. The rigid airframe eigenmode of large aircraft in vertical direction is likely to be at a frequency below one Hertz, whereas the eigenfrequency of the unsprung mass (i.e. wheels, brakes, bogies), also denoted as wheel hop frequency, is found in the range above 50 Hertz.

Elastic airframe eigenmodes:

Five eigenmodes display frequencies where the human body is most sensitive, with an additional four eigenmodes in a two Hertz band above and below the critical range. A list of the rigid and flexible eigenmodes can be found in [10].

An active controlled landing gear introduced to improve the ride quality of a large aircraft would therefore have to concentrate on reduction of vertical accelerations due to elastic body oscillations in the 4 to 8 Hertz frequency range. The excitation of these oscillations is caused by runway roughness either due to wear and tear or to other unavoidable reasons. Typical excitations used in the simulations are presented in chapter 3.1.4.

2.2 A Proposed Solution

Recent research indicates (see chapter 1) that active gear technology may pose a possible solution to the problems of aircraft ground loads and that the semi-active controlled front landing gear promises to be the most likely solution to be incorporated in a production aircraft by the aircraft industry.

The proposal of this paper to solve the ride comfort problem is therefore: design the controller for a front landing gear, modify a conventional landing gear to incorporate controlled damping (thus creating a semi-active front landing gear), analyze it and compare it with the conventional gear.

2.2.1 Multi-Objective Parameter Optimization using MBS Models

The main part of the controller design, the optimization of the controller parameters, was performed using ANDECS, [13], developed also at the DLR. ANDECS is an open Computer Aided Engineering (CAE) software for the analysis and design of controlled systems. It offers interfaces with other CAE-tools, in particular with modelling environments such as SIMPACK, ACSL and DYMOLA. Besides these interfaces ANDECS provides as its core design environment MOPS (Multi-Objective Programming System).

Multi-objective parameter-optimization has become more and more a central design strategy for complex dynamical systems where "best" solutions are searched in the parameter space such that certain - sometimes conflicting - performance specifications have to be met, [14].

The design strategy for multi-objective parameter optimization is briefly sketched in figure 4. As usual the dynamic system is

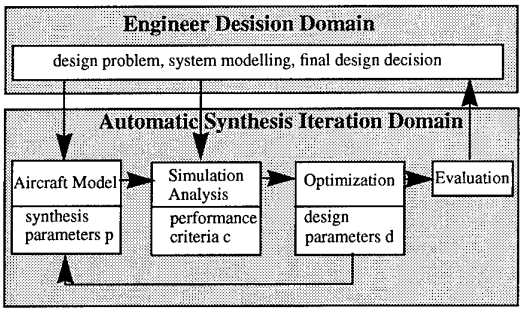

Figure 4: Synthesis Loop of Optimization

defined by the plant and the controller models; both are completely free and can be linear or nonlinear as appropriate.

A number of so-called synthesis-parameters, p, are set free within certain limits; they are "tuned" to yield an optimal design. It is indeed arbitrary whether these are some (or all)

control law parameters or some parameters characterizing the mechanical system, e.g. damping or stiffness parameters of passive suspension. The various performance criteria c_i, with respect to which the parameters should be optimized (minimized), are summarized in a criteria vector:

$$c = [c_1, c_2, \ldots, c_i]^T \qquad (2.1)$$

The complete strategy exists of two imbedded loops. The outer loop is initialized by the system definition and the criteria. The inner loop starts on the basis of simulation and analysis initialized by a provisionary parameter vector p^0 with a corresponding criteria value c^0.
The desired "design-direction" is defined by a design parameter vector ("design director"), d:

$$d = [d_1, d_2, \ldots, d_i]^T \qquad (2.2)$$

where d_i is a chosen design command level corresponding to criterion c_i; d_i are upper limits for the desired stepwise descent of the corresponding criteria:

$$c_i(p) \le d_i \qquad i = 1, \ldots, l \qquad (2.3)$$

As a design comparator for detecting "better" designs the max-function

$$\alpha = \max \frac{c_i}{d_i} \qquad i = 1, \ldots, l \qquad (2.4)$$

is chosen. The strategy is to find a minimum for this α in varying the synthesis parameters p:

$$\alpha^* = \min_p (\alpha(p)) \qquad (2.5)$$

The implemented strategy in MOPS does not only guarantee the monotonous descent of all criteria but also tries to solve efficiently the optimization goal for which $\alpha(p)$ is minimal. After a sufficient number of steps within the automatic synthesis iteration loop, an improved design is reached which is Pareto-optimal, i.e. no criterion can be further improved without deteriorating others.
At this stage certain decisions are possible, e.g. to change the design director in order to change the design direction. Thereby the designer gains experience which criteria can be easily improved and where the critical design conflicts (within the chosen structure) are located. Other decisions may be the change of the criteria or of the controller structure or the synthesis parameters. Within a number of such "experiments" the potentials of the chosen structure is accumulated.
The software modules and their interrelations as used for this paper are shown in figure 5.
The overall control of the computational process is done by MOPS; time-simulation of the nonlinear model is executed by DSSIM (Dynamic Simulation Module); the generation of the MBS and controller equations is performed by SIMPACK.
The end product of the optimizing process, the satisfactory compromise, is then used to visualize the final model behavior.

The following chapter will cover the model setup, the optimal controller design as result of the optimization process will be presented in chapter 4.

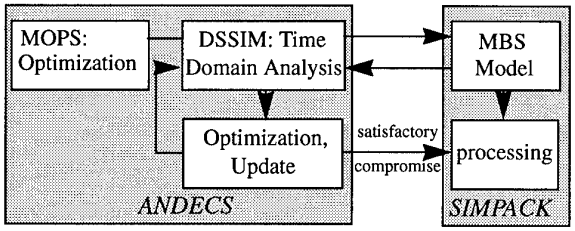

Figure 5: Software Interaction in the ANDECS/SIMPACK Design Environment

3. Modelling

3.1 Aircraft Model Built-Up

3.1.1 Modelling Approach

The AIRBUS A300, which was selected for the model buildup, represents a configuration widely used for commercial airliners: two wheel front gear, two four wheel bogie main gears, wide body fuselage, two engines and a maximum take off weight around 140 metric tons.
The literally central body of the AIRBUS model is the *wing spar frame*, the fuselage frame situated at the connection of the aft wing spars to the fuselage. It is modelled as a rigid body without mass or geometric extent. It serves as connection point between the elastic airframe bodies and the Inertial Reference Frame. The landing gears, built up by several smaller entities, are linked up to the airframe bodies on the one side. On the other side no joints, but tire force laws form the attachment to the runway surface.

3.1.2 The Elastic Airframe Bodies

For the incorporation of elastic bodies, the MBS package SIMPACK contains the possibilities to include FEM and beam-like structures. For the use of the BEAM preprocessor the body is divided up into several sections with piecewise constant stiffness, damping and distributed mass. This feature and the shape of the four airframe members modelled as elastic bodies (two wings, front and aft fuselage) made its usage feasible for the A300 model.

Fuselage:
The fuselage model consists of a front fuselage part with connection to the front landing gear and the aft fuselage part with the rigid elevator and horizontal stabilizer bodies. Both parts are linked to the wing spar frame with zero degrees of freedom joints. They are divided into five sections each. The characteristics of the fuselage were derived from design material provided by the airframe manufacturer.

Wings:
Like the fuselage, the wing is partitioned into five sections, connected to the wing spar frame on the inner side and left free on the outer. The engine is linked rigidly to the third node, the second node includes the attachment point for the main landing gear. Only bending in z is taken into account for the wing bodies.

Fed with this data, the BEAM preprocessor calculates the desired eigenmodes of the four airframe members. These eigenmodes are then used by SIMPACK to evaluate the aircraft eigenmodes implemented in the simulation. The selection of the number of eigenmodes plays an important role. High structural vibrations result in small integration stepsize and thus increase CPU work. On the other hand the SHANNON theorem determines the maximum eigenfrequency implemented in a certain model to be at least twice the maximum frequency under consideration ([15] and [16]). The eigenmodes for the taxi analysis were chosen in a way to guarantee a safe analysis up to 25Hz.

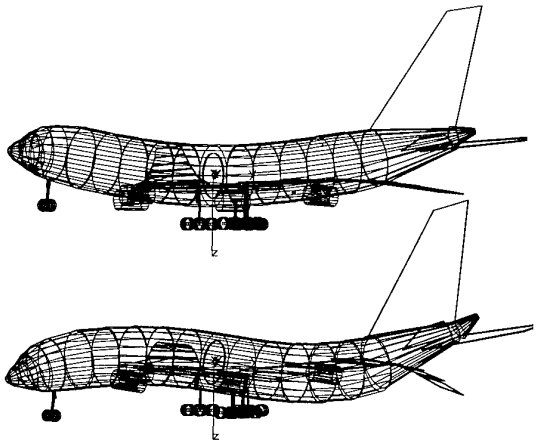

Figure 6: First and Second Fuselage Bending Eigenmode

In figure 6, the first two fuselage bending eigenmodes are shown.

3.1.3 Force Laws

To simulate the dynamical behavior of the A300 airplane, SIMPACK had to be given a set of force laws. With the aid of the relative displacements and velocities at the specified node points of the multi body system, the according forces were derived. The force laws are realized as user routines within SIMPACK and are explained in detail in [10].

Tire force law:

The tire force model has to yield the longitudinal and lateral forces and the torque moment acting between the road surface and the wheel and depending on the slip between tire and ground. Nevertheless, even with a relatively simple model, computational effort has proven to be substantial for an aircraft with ten or more wheels. Depending on the simulation case it proved to be helpful to linearize the tire behavior if possible. For an aircraft taxiing on ground without cornering or braking, a linear spring model was incorporated. The following suppositions apply:

* negligible slip (no braking),
* no side slip,
* no loss of ground contact for any tire,
* load variations small enough to allow linearization of deflection curve.

This tire model was used for most of the taxi simulations.

Oleo-Pneumatic Shock Absorber Force Law:

Conventional (Passive) System:

As primary force generating element each aircraft landing gear is equipped with one central oleo, acting on the principle of a one stage or single slope oleo like those used in the landing gears of the A300 aircraft. The passive oleo displays two separate force generating elements, the gas chamber that generates the spring force and the set of orifices responsible for the damping force. The total oleo force is composed of a gas spring part (calculated using the general gas law), a damping part and a friction part.

The damping force was calculated using the squared value of the relative velocity of the sliding oleo member and the main fitting attached to the fuselage. It is dependent on the direction of the relative motion because of different damping coefficients for compression and for extension. The values for theses coefficients, depending on the oleo orifice cross sections, were determined in tests by the landing gear manufacturer.

Friction forces are difficult to assess and depend on a multitude of parameters. Especially for the landing impact case, longitudinal forces increase the friction and can in fact block the gear and prevent spring deflection, leading to high structural loads and even structural failure. The gas chamber pressure influences the fitting pressure on the outer oleo wall, resulting also in higher friction forces. For the taxi condition the gas pressure variation and applied x-forces remain small, so a constant friction term supplied by the landing gear manufacturer was incorporated.

Semi-Active System:

The main difference between a semi-active and a conventional oleo is found in the oil orifices responsible for the damping force. To provide control over the damping force, the oil flow and thereby the damping coefficient is regulated. This can be achieved by variable diameter orifices or by implementation of a servo valve. Since the actual design may exhibit quite different oil flow regulators, but all of them control the damping coefficient, this coefficient was chosen as control variable. The control range, i.e. the maximum and minimum damping coefficient values achievable, was deliberately chosen to lie between 20 and 500% of the original value used in the conventional A300 oleo because this range was considered to be technically feasible.

Aerodynamics Force Law:

Stationary motion of an aircraft through the air results in an aerodynamic force acting on the aircraft. Taken into account the small influence of the aerodynamic forces and moments on the overall dynamics of the system, the aerodynamic force user routines were limited to the longitudinal motion. To account for non-stationary moments, the pitch damping coefficient was calculated.

3.1.4 Runway surface

To analyze the dynamic behavior of a general nonlinear MBS model, time histories have to be evaluated for a broad range of frequencies. The excitations used on the model should include a wide frequencies range. Additionally, single frequencies of special concern might be agitated separately.

The following existing runway disturbances have been taken into account in the present investigation:

- General roughness: Especially on older airports and on airports in the countries of the former Warsaw Pact, the run- and taxiways display undulations of all frequencies and with higher amplitudes than those measured on airports in western countries, [17]. These conditions have reportedly led to dangerous situations. Pilots of aircraft equipped with Cathode Ray Displays (so called "glass cockpits") experienced difficulties to read the instruments due to vertical accelerations during the take-off run.
- Concrete Plate Deforming: A widely used method to construct fortified runways is the casting of large plates using liquid concrete. These plates are separated from each other by gaps filled with rubber. Aging of concrete runways causes the plates to settle unevenly, leading to long wavelength bumps and steps at the gaps.
- Center Line Lights: All run- and taxiways are equipped with lights indicating the middle line during night time operation. These lamps extend a few centimeters from the ground (figure 7) and exert a shock when hit by a tire. They are spaced regularly and can induce oscillations.

a: Housing Height (2... 5 cm)
b: Length (15...30 cm)
c: Spacing (5... 15 m)

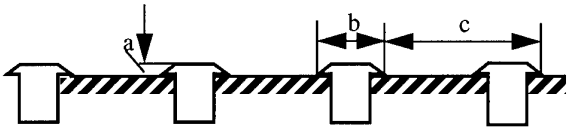

Figure 7: Center Line Light Housings in a Runway

To simulate these runway surface conditions, the following three distinct models have been programmed.

Quasi-stochastic Runway Model

Thompson [17] gave a list of a number of measured Power Spectral Densities (PSD) of runways in NATO countries. These were used to build up a deflection curve using a set of harmonic functions. The runway elevation curve resulting from this process is displayed in figure 8.

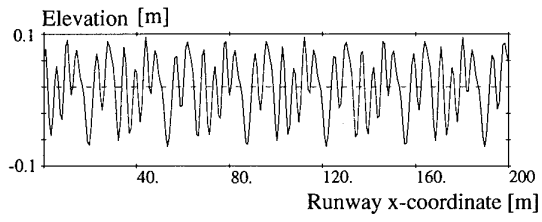

Figure 8: Quasi-stochastic Model Runway Surface

A comparison between four measured runway PSD's (thin lines) and the PSD of the implemented model runway (solid line) is shown in figure 9.

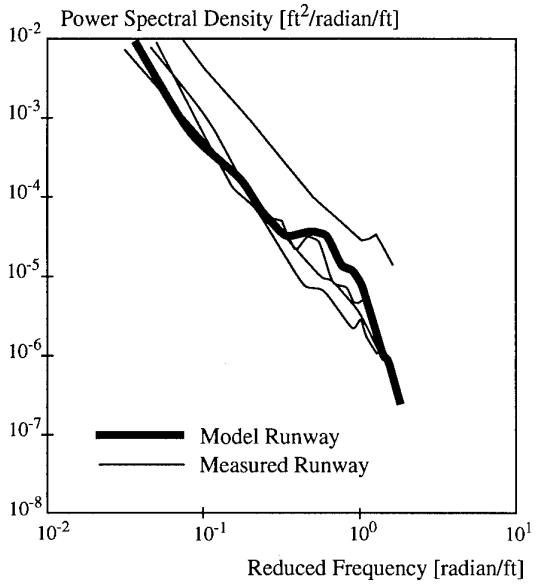

Figure 9: Power Spectral Density of Measured and Model Runway

Multiple Pulse Runway Model:

Step and pulse model inputs are especially suitable to induce a broad band of frequencies into a model. In practical ground operation, pulse inputs can result from concrete plate gaps or from center line light housings. In figure 7, a light housing built into the runway is sketched. In reality, the tire hitting the housing will deform, so that the impact of the heave motion of the bottom of the tire spring will be muffled. The multiple pulse runway model uses this kind of pulse shape. Housing dimensions and spacing are programmed as variables and are defined in the experiment model setup.

Harmonic Wave Runway Model:

The harmonic wave as excitation was included in the system analysis to perform a sort of "worst case" evaluation. With this runway model, a distinct frequency acts on the landing gear to induce potentially problematic oscillations like the main fuselage bending eigenfrequencies. A simple sinusoidal wave was used for the model. In figure 10, an example runway surface is

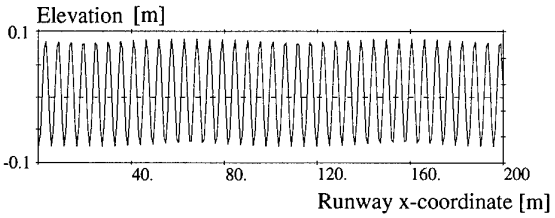

Figure 10: Harmonic Model Runway Surface

given used for the excitation of the 3.6 Hertz fuselage bending eigenmode of the A300 at a speed of 20 m/s.

4. Control Concept Analysis

4.1 Control System Lay-Out

During the selection process of a control law to be implemented, the rigorous safety requirements in aircraft design have to be taken into consideration. Thus, low system complexity is one of the design drivers for the control system. A single input single output (SISO) control system requires the minimum of one sensor signal and one actuator element and was therefore chosen.
Aircraft currently in commercial operation are in part already equipped with acceleration sensors. To keep additional system requirements low, a single acceleration sensor at the cockpit position was assumed and used for the feedback signal. Figure 11 shows the resulting system layout.

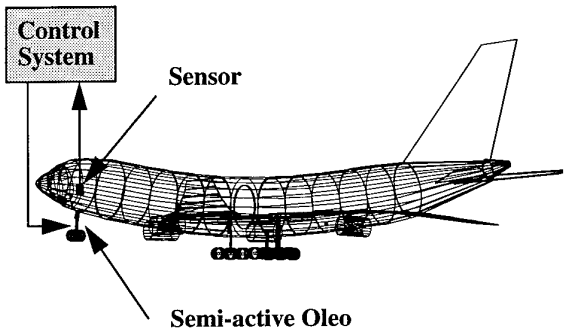

Figure 11: Control System Sensor and Actuator Location

The block diagram in figure 12 shows the general principle of the feedback system. The *Oleo Closure Rate* remains the main

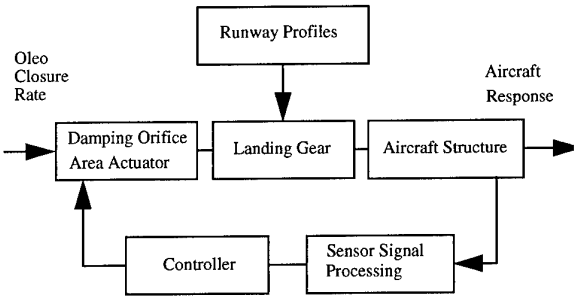

Figure 12: Control System Block Diagram

input for the *Landing Gear Oleo*. It determines the forces applied on the *Aircraft Structure* depending on the *Runway Profile* inputs and the *Damping Orifice Area Actuator*. The *Aircraft Response* coming from the *Aircraft Structure* is fed back using the *Sensor Signal Processing* and the control algorithm implemented in the *Controller*.
The velocity feedback used as controller input makes the chosen control concept a variation of the sky-hook approach.

4.2 Optimization Process

4.2.1 Criteria Selection

The goal of the implementation of a controlled front gear is to increase passenger and pilot comfort by reduction of fuselage vibration. The criterion vector c must take into account the necessary states. The aircraft state vector Y

$$\underline{Y} = \begin{bmatrix} y_I \\ y_{II} \\ q \\ \dot{q} \end{bmatrix} \tag{4.1}$$

contains the states describing the aircraft motion. Here,

$$y_I = [y_I^i], \quad i = 1, \ldots, n_G \tag{4.2}$$

denotes the position states for each of the n_G joints,

$$y_{II} = [y_{II}^i], \quad i = 1, \ldots, n_G \tag{4.3}$$

stands for the velocity states of the joints,

$$q = [q^i], \quad i = 1, \ldots, n_K \tag{4.4}$$

describes the deformation position coordinates for each elastic body n_K and

$$\dot{q} = [\dot{q}^i], \quad i = 1, \ldots, n_K \tag{4.5}$$

expresses the deformation coordinates in the velocity domain. For calculation and analysis the states of several distinct locations on the elastic bodies are needed. Unlike on rigid bodies, where states of any location can easily be derived if the states of the reference system of the body are known, the states of arbitrary locations on the elastic body depend on the deformation position and velocity coordinates.
To observe all interesting eigenmode shapes it is necessary to introduce measurements of suitable locations on all elastic bodies (fuselage and wings). For example, the first fuselage bending mode can be observed by measurements in the far front or far rear end of the fuselage, whereas for the second eigenmode additional information is needed from stations between the front and the center of gravity of the aircraft. As a compromise between the resolution of high frequency eigenmodes and simulation time, 16 locations have been selected on the A300 airframe.
The semi-active landing gear influences primarily the vertical motion of the aircraft. Vertical acceleration was therefore picked as criterion state to be measured. The Root Mean Square (RMS) value is calculated using

$$c_{i,RMS} = \sqrt{\int_{t_0}^{t_e} (\ddot{x}_z - \ddot{x}_m)^2 \, dt} \qquad (4.6)$$

with

x_z = vertical acceleration at sensor i

x_m= reference value for acceleration evaluation, to be set by operator

$c_{i,RMS}$=RMS-criterion for sensor i

t_0 = start of time integration interval

t_e = end of time integration interval

Besides the Root Mean Square value (RMS value), which rates amplitudes and their duration time, peak values are includes as well:

$$c_{i,peak} = max\,(abs\,(\ddot{x}_z - \ddot{x}_m)) \qquad (4.7)$$

where $c_{i,peak}$ denotes the peak-criterion value.
With this double criterion strategy, a trade-in of low RMS values for very high but short peaks is avoided. RMS values and peak values of all sensors were weighted equally, with slight emphasis on the front fuselage part.

4.2.2 Optimization Method

The numerical procedure used to solve this nonlinear multi objective multi parameter optimization problem is based on the technique of Sequential Quadratic Programming (SQP) described in [18] and [19] in an implementation in the ANDECS Control Systems Design Environment ([20], [21]). The aim is to determine a set of parameters p in a way that minimizes a cost function $f(x)$ under consideration of different equality and inequality constraints $g(x)$. The general form of the cost function can be stated as

$$f(x) = min \;\; ; \;\; x \in \Re^n \qquad (4.8)$$

with the constraints

$$g_j(\underline{x}) = 0 \;\; ; \;\; j = 1, 2, \ldots, m_G \qquad (4.9)$$

$$g_j(\underline{x}) \geq 0 \;\; ; \;\; j = m_G + 1, 2, \ldots, m \qquad (4.10)$$

and the parameter domain boundaries

$$\underline{x}_o \geq \underline{x} \geq \underline{x}_u \qquad (4.11)$$

Cost function and constraints have to be continuous, but no specific structure is required. For the acceleration minimization, the cost function can now be stated as

$$\sum_{i=1}^{16} \sqrt{\int_{t_0}^{t_e} \left(\ddot{x}_z - \ddot{x}_{m_{RMS}}\right)^2 dt} + \sum_{i=1}^{16} max\left(abs\left(\ddot{x}_z - \ddot{x}_{m_{peak}}\right)\right) = min \qquad (4.12)$$

The acceleration itself is determined as

$$\ddot{x}_z = f(\dot{x}(t),\, x(t),\, u(t)) \qquad (4.13)$$

with

$$u(t) = f(p, t) \qquad (4.14)$$

where $u(t)$ stands for the model input, a function dependent on time t and the controller parameters p.
To derive the free system parameters, the optimization strategy shown in figure 13 was used. The system was subjected to the

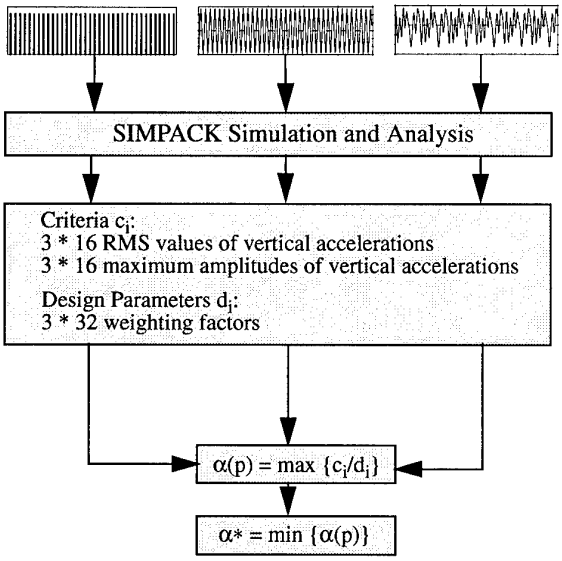

Figure 13: Multi Model Optimization Process

three different excitation cases which were described in chapter 3 earlier. In the following step, a complete and self-contained simulation run of the nonlinear model was performed for each excitation case. The criteria were evaluated using the steady state time response. After being weighted with the design parameters d, the optimization run was evaluated and the next optimization run initiated using changed parameters.

5. Results

5.1 Final Design Evaluation

The optimization process described above was used to derive a set of controller parameters best suited to minimize the design parameters d_i. On the following pages the system performance using those controller parameters is shown for the three excitation cases. The performance is subsequently compared with that of the original conventional type landing gear. A complete presentation and discussion of the results can be found in [10].

5.2 Quasistochastic Excitation Performance

In figure 14 the vertical cockpit acceleration response of both

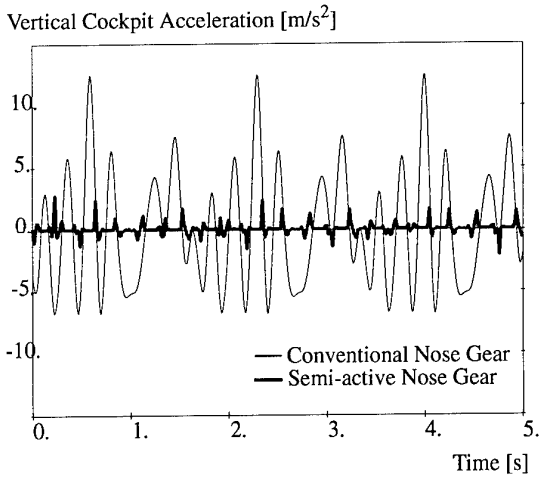

Figure 14: Time Domain Response for Quasistochastic Excitation

the conventional gear (thin line) and the semi-active gear (bold line) in the time domain are shown for a total simulation time of five seconds. The system state at the beginning of the simulation was determined by a pre-analysis time integration to guarantee a steady state response throughout the whole analysis period. It can be seen that no fading oscillations are present. The controlled gear performs well, the amplitudes of the acceleration are diminished by a factor of five.
The power spectral density (PSD) of the cockpit accelerations of this time history, shown in figure 15 for the frequency range

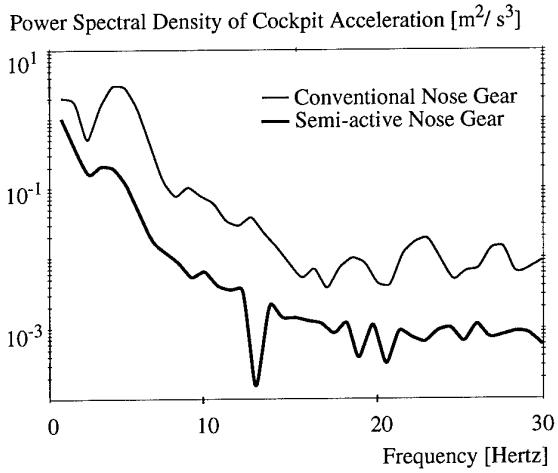

Figure 15: Power Spectral Density of Quasistochastic Excitation Response

from 0.1 to 30 Hertz, displays significant improvements over the whole frequency range. The influence of the semi-active gear can especially be seen for the first fuselage bending eigenmode at 3.6 Hertz and for the second symmetric and antimetric wing bending eigenmode at 5.6 and 5.7 Hertz, respectively.

5.3 Center Line Light Excitation

Figure 16 shows the system behavior for the repeated pulse excitation as exerted by center line light cases or concrete plate gaps.

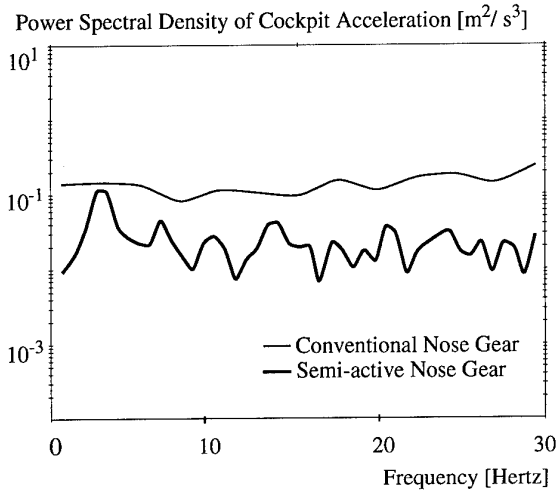

Figure 16: Power Spectral Density of Center Line Light Excitation Response

While the system response of the semi-active gear remains below the one of the passive gear over the whole frequency range, two distinct peaks can be seen below 10Hz for the aircraft structural eigenmodes. At those points the system performance of the semi-active oleo retains only a small advantage over the conventional system. This behavior differs from the one seen for quasistochastic excitation and may be amplified by the total absence of inputs between the bumps and on the main gears.

5.4 Harmonic Excitation

The frequency domain response for the harmonic excitation in figure 17 shows that a high level of accelerations at the frequency of the exciting undulations of the runway for the conventional gear has to be expected (thin line). Therefore the PSD in this frequency range exhibits high levels. The semi-active gear (bold line) transforms the response into small amplitudes over a wide frequency range, leading to higher PSD levels at higher frequencies than the conventional gear.
It must be taken into account, though, that the total absence of higher frequencies in the excitation was deliberately chosen to analyze this excitation form and will be accompanied by higher or lower levels of distributed runway inputs in each real runway excitation.
Nevertheless it can be stressed that the semi-active system performance displays an impressive lead in the low frequency range over the conventional gear. This result is even more important bearing in mind the susceptibility of the human body with its emphasis on the low frequency range.

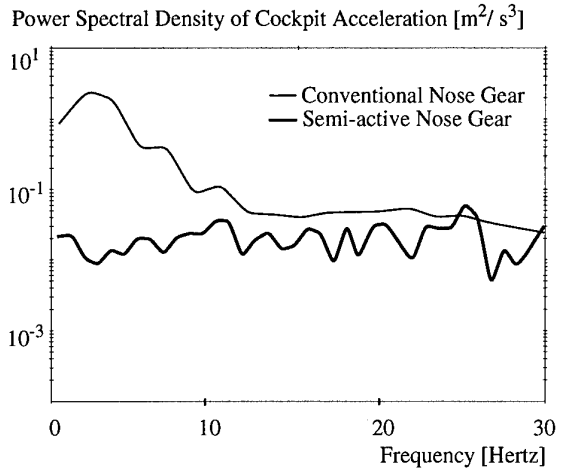

Figure 17: Power Spectral Density of Harmonic Excitation Response (3.6Hz)

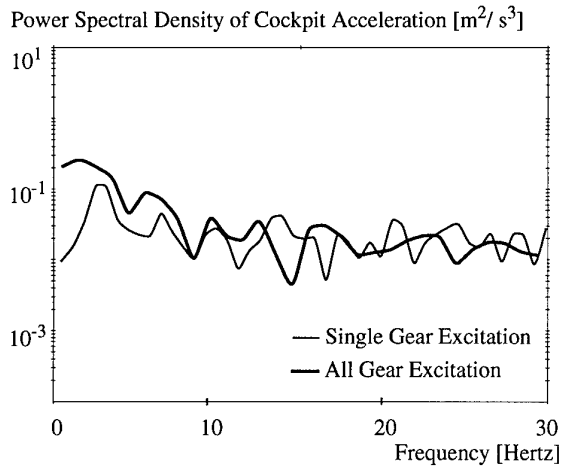

Figure 18: Comparison of Power Spectral Densities of Nose-Gear-Only and All-Gear Excitation Responses

To assess the impact of the excitation of the main gears, comparative simulations were performed. The results are presented in the next subchapter.

5.5 All-Gear Excitation

The general approach to the results obtained above was to excite the nose gear only. There are several reasons for this assumption. First, it is a contribution to the fact that the center line lights hit by the rolling aircraft would mostly be encountered by the nose landing gear only. The main landing gear is supposed to run on smooth surfaces. This argumentation is, with some restrictions, also valid for the harmonic excitation, due to the wide aircraft track of 9.6 m. Second, the excitation of all three landing gears adds considerably to the model size, translating into higher numerical simulation time. The time difference to the single gear simulations are substantial, since the main gears represent a highly nonlinear subsystem. Therefore it was decided that the system performance would be evaluated using the single gear excitation case for the optimization runs as well as for the subsequent evaluation simulations.

The following investigation was made to verify the justification of this assumption. It compares the A300 aircraft model with the conventional nose gear oleo with the model equipped with the semi-active nose gear oleo. For the main gears conventional oleos are implemented in both cases. The nose gear is subjected to the center line light excitation as described in chapter 3, the main gears are moved by the quasistochastic excitation described in the same chapter.

The maximum peak values for both simulations, caused by the center line light bumps, appear in both responses as nearly equivalent. The difference between the excitation cases lies at the interval between two bumps. Here the single excited case experiences almost no acceleration whereas the excitation of the main gears for the all gear excitation case causes long wavelength accelerations in the cockpit region. Thus, for low frequencies higher PSD levels can be expected.

Comparing the performance of the conventional gear with the semi-active gear (see figure 18), practically no difference is found for frequencies higher than 10 Hertz. In the range between 0.1 and 10 Hertz, the response to the all-gear excitation shows higher amplitudes than the response to the single-gear excitation.

Nevertheless, the relative improvements of the all-gear-excitation, semi-active gear against the all-gear-excitation, passive gear are at least as good as for the nose-gear-only excitation case (see [10]).

This gave rise to the decision to use the single gear excitation for optimization and evaluation, reducing the computation time to levels compatible with existing hardware without risking to produce overly optimistic results.

6. Summary

In the development of newer aircraft a tendency can be seen towards more flexible airframe structures and particularly towards smaller fuselage bending stiffness. During ground operations, this led to an increasing number of feedback problems between elastic structure eigenmodes and landing gear dynamics, induced by runway unevenness.

The aim of this work was therefore to analyze the performance potential of a semi-active nose landing gear oleo to reduce fuselage resonance motion. This oleo is derived from an existing oleo for the aircraft used for the analysis, an AIRBUS A300. It consists of the original gas spring and a modified oil orifice capable of changing the damping coefficient at a high frequency. A controller was derived and optimized which calculates the necessary damping following the "sky-hook" damping approach. Here the absolute fuselage vertical acceleration is measured and processed by the controller.

The analysis was performed using state-of-the-art simulation technology. A Multibody Simulation (MBS) model was derived, including the highly nonlinear kinematics and force laws of the landing gears and oleos and the airframe structure elasticities. The controller was optimized using multi criteria multi objective optimization software on three models with excitations representing different runway surfaces and excitation cases.

The performance of the semi-active system was assessed by time domain analysis with numerical integration as well as with frequency domain analysis using power spectral densities. The behavior of the proposed system showed significant improvements for all cases under consideration and for the

whole frequency range of interest. The results highlight the multi objective parameter optimization approach for finding a well performing parameter set. Since an indisputable dependency of the system fuselage acceleration in the frequency domain on any parameter cannot be established it seems to be difficult to come up with a satisfying controller layout by manually tuning its parameters.
Both optimization and performance evaluation simulations are based on the highly nonlinear and complex MBS model. It lines out a representation of the real aircraft in many aspects affecting the dynamical behavior. Nevertheless it has to be remembered that also this complex model uses assumptions that may or may not influence the dynamic behavior.

7. References

[1] S.F.N. Jenkins: *Landing gear design and development.* Proceedings of the Institution of Mechanical Engineers, Vol 203, 1989

[2] Donald W.S. Young: *Aircraft landing gears: the past, present, and future. Aircraft Landing Gear Systems,* Society of Automotive Engineers, page 179-196, 1986

[3] W. Kortüm and W. Rulka and A. Eichberger: Recent Enhancements of SIMPACK and Vehicle Applications. European Mechanics Colloquium, EUROMECH 320, Prague 1994

[4] P. T. Somm, H. H. Straub and J. R. Kilner: Adaptive landing gear for improved taxi performance. Boeing Aerospace Company,1977, AFFDL-TR-77-119

[5] John R. McGehee and D. L. Morris: Active control landing gear for ground load alleviation. Active Control Systems - Review, Evaluation and Projections (AGARD CP 384, NASA Langley R. C. ,1981

[6] W.E. Howell, J.R. McGehee, R.H. Daugherty, W.A. Vogler: F-106 airplane active control landing gear drop test performance. Landing Gear Design Loads (CP 484), AGARD,1990

[7] R. Freymann: An active control landing gear for the alleviation of aircraft taxi ground loads. Zeitschrift für Flugwissenschaft und Weltraumforschung, 1987

[8] D. Karnopp: Active Damping in Road Vehicle Suspension Systems. Vehicle System Dynamics, 12(6), Swets & Zeitlinger, Lisse, 1983

[9] Tyrone Catt, David Cowling and Alan Shepherd: Active landing gear control for improved ride quality during ground roll. Smart Structures for Aircraft and Spacecraft (AGARD CP 531), Stirling Dynamics Ltd, Bristol, 1993

[10] H. Wentscher: Design and Analysis of Semi- Active Landing Gears for Transport Aircraft. Ph.D. Thesis, TU München, 1995

[11] R.V. Dukkipati, S.S. Vallurupalli, M.O.M. Osman: Adaptive Control of Active Suspension - A State of the Art Review. The Archives of Transport, Vol. IV, 1992

[12] International Organization for Standardization: Guide for the Evaluation of Human Exposure to Whole Body Vibration. ISO 2631-1974(E), July 1974

[13] H.-D. Joos: ANDECS ANalysis and DEsign of Controlled Systems (ANDECS 1.0). Technical Report, DLR IB 515-94/17, 1994

[14] Kortüm W., Lugner P.: *Systemdynamik und Regelung von Fahrzeugen.* Springer Verlag Berlin, Heidelberg, New-York 1994

[15] H. Unbehauen: *Regelungstechnik I.* Vieweg Verlag, Braunschweig, Wiesbaden 1989

[16] H. Unbehauen: *Regelungstechnik II.* Vieweg Verlag, Braunschweig, Wiesbaden 1989

[17] W. E. Thompson: Measurements and Power Spectra of Runway Roughness at Airports in Countries of the North Atlantic Treaty Organization. NACA Technical Note 4303, Washington July 1958

[18] Fletcher R.: *Practical Methods of Optimization.* Vol. 2. John Wiley and Sons, USA, 1981

[19] Kraft D.: *A Software Package for Sequential Quadratic Programming.* DFVLR-FB 88-28, Oberpfaffenhofen, Juli 1988

[20] G. Grübel, H.-D. Joos, M. Otter: *The ANDECS Design Environment for Control Engineering.* In IFAC World Congress, Sidney, 18-23 July 1993

[21] H.-D. Joos: *Informationstechnische Behandlung des mehrzieligen optimierungsgestützten regelungstechnischen Entwurfs,* Ph.D. thesis, Universität Stuttgart, Prof. R. Rühle, 1992

[22] H. Wentscher and W. Kortüm: Multibody model-based multi-objective parameter optimization of aircraft landing gears. Proceedings of IUTAM-Symposium of Optimization of Mechanical Systems, Stuttgart 1995

[23] W. Kortüm and R. S. Sharp (Eds): Multibody Computer Codes in Vehicle System Dynamics. Vehicle System Dynamics, Supplement to Vol. 22. Swets & Zeitlinger, 1993

Dynamic Behaviour of Motorbikes

F. Böhm and H. P. Willumeit

Department of Traffic Engineering and Applied Mechanics
Technical University Berlin, Institut für Fahrweugtechnik
Sekr. TIB 13, Gustav-Meyer-Allee 25
13355 Berlin, Germany

Abstract

Dynamic behaviour of motorcycles front wheel are not different to similar wheel suspension motion of airplanes and road vehicles. In every case self excited oscillations caused by the tire occur. Only the different design of wheel suspension produces some different coupling. The deviation of a moving wheel on a horizontal plane from straight rolling is caused by unstable lateral contact forces. The kinematical generation of such forces can be imaginated looking on the elastic tire. A first order time-depending behaviour together with inertia mass and damping of the wheel using the HURWITZ stability criterion gives important insight into the main parameters of the problem.
Nevertheless the nonlinearities of the system overshadow this clear insight. Cornering force and cornering moment are nonlinear functions of cornering angle, so the use of the well known "Magic Formula" together with the black box method of control theory is a logical extension. The problem of instability arises again when thè wheel is excited from wavy surface or similar from mass unbalances of the tire. A direct time depending of the lateral tire forces can be used to show parametric instability of the system (MATHIEU equation). The rolling of the wheel on a non-smooth surface needs then to introduce methods of discrete system approach. The paper presents an overview of the problem of shimmy.

1 Introduction

The pneumatic tire as a rolling suspension is intended, on the one hand, to ensure that track unevennesses are traversed with as little vibration as possible, and, on the other, to guarantee the driving direction and stability of the vehicle. In sharp bends, the pneumatic tire should also withstand the centrifugal forces, and it should generate the appropriate longitudinal forces during braking and acceleration. These manifold requirements, however, can only be met by means of a constructive compromise, wherein an unavoidable coupling arises, by virtue of the elasticity of the tire in all three dimensions, between the longitudinal, lateral and vertical forces and between their associated dynamic deformations. These couplings lead to non-linearities, which complicate mathematical treatment.
A first attempt to solve the problem starts out from the premise that the track is even and the tire ideally round, and also assumes, with regard to the contact time of a tire particle with the ground, that the associated slippage between tire and ground occurs in linear fashion, from the entry point of the contact surface to the exit point thereof. If one additionally takes into consideration an average deformation $\bar{y}$ of the contact surface, due to the effective lateral force S, then a linear elastic deformation equation can in principle be written down for the lateral deformation as a function of lateral force:

$$S = c_S \, \bar{y}. \tag{1}$$

Paper presented at the 81st Meeting of the AGARD SMP Panel on "The Design, Qualification and Maintenance of Vibration-Free Landing Gear", held in Banff, Canada from 4-5 October 1995, and published in R-800.

The associated lateral spring coefficient c_S can be determined experimentally. The linearly increasing deformation from the entry point to the exit point, by contrast, is assigned to the travelling surface (shear deformation) and is superposed onto the deformation $\bar{y}$. This enables one to write down a kinematic equation for the slip angle of the tire to which the lateral force S is assigned, of the form

$$S = S(\delta_{eff}) \doteq P_0\, c'\, \delta_{eff} = P_0\, c' \left(\delta_{Rim} - \frac{\dot{\bar{y}}}{v} \right). \tag{2}$$

This effective slip angle δ_{eff}, which is a function of the elastic lateral deformation of the tire carcase, is equal to the stationary slip angle for the case $S = constant$. The function S is non-linear, since it describes the partial sliding of the tire, and even progressively decreases overall once it has passed beyond the sticking state. If one only takes into consideration small slip angles in the region of zero (driving straight ahead, equation (2)), then the increase $P_0\, c'$ in the cornering force function at the zero point yields the following linear differential equation of first order, whose eigenvalue is negative and therefore exhibits damping behaviour. Any disturbance of the stationary rolling state is therefore damped along the direction of rolling, wherein the damping distance is approximately equal to the tire radius. Since, however, the stationary slip angle characteristic curve is largely a function of the length of the contact area, which in turn is a function of the possibly dynamic wheel load, there is automatically a coupling between the horizontal and vertical dynamics of the tire.

2 Analytical investigation of the stability of shimmy

Let us now consider a wheel elastically mounted on a large mass in accordance with the examples of figure 1, and investigate the stability of small vibrations of a wheel that can be rotated around a vertical axis. In actual technical realisations the pivot point of the steering axle is always in front of the contact patch, see figure 2. Let the wheel be elastic mounted to the straight-ahead position by means of an elastic attachment (torsion spring coefficient c_L). There is a principal moment of inertia I about the vertical axis. For the pneumatic tracking we designate $n_P = \frac{M}{S}$. In the case of damping proportional to velocity (steering damping), a coefficient k_L is used. The characteristic curves for the tire are displayed in figure 3. Analytically, the use of n_P has the advantage of a simpler mathematical description. The equations of motion are as follows:

1. Angular momentum about the steering axle:

$$\left(I + m\, a^2\right)\, \ddot{\varphi} = -c_L\, \varphi - k_L\, \dot{\varphi} - S\, (a + n_P). \tag{3}$$

2. Lateral guiding force S for small slip angles

$$S = S(\delta_{eff}) = P_0\, c'\, \delta_{eff} = \bar{y}\, c_S. \tag{4}$$

3. The effective slip angle:

$$\delta_{eff} = \delta_{Rim} - \frac{\dot{\bar{y}}}{v} = \varphi + \frac{a\,\dot{\varphi}}{v} - \frac{\dot{\bar{y}}}{v} \quad \text{mit} \quad \delta_{Rim} = \varphi + \frac{a\,\dot{\varphi}}{v}. \tag{5}$$

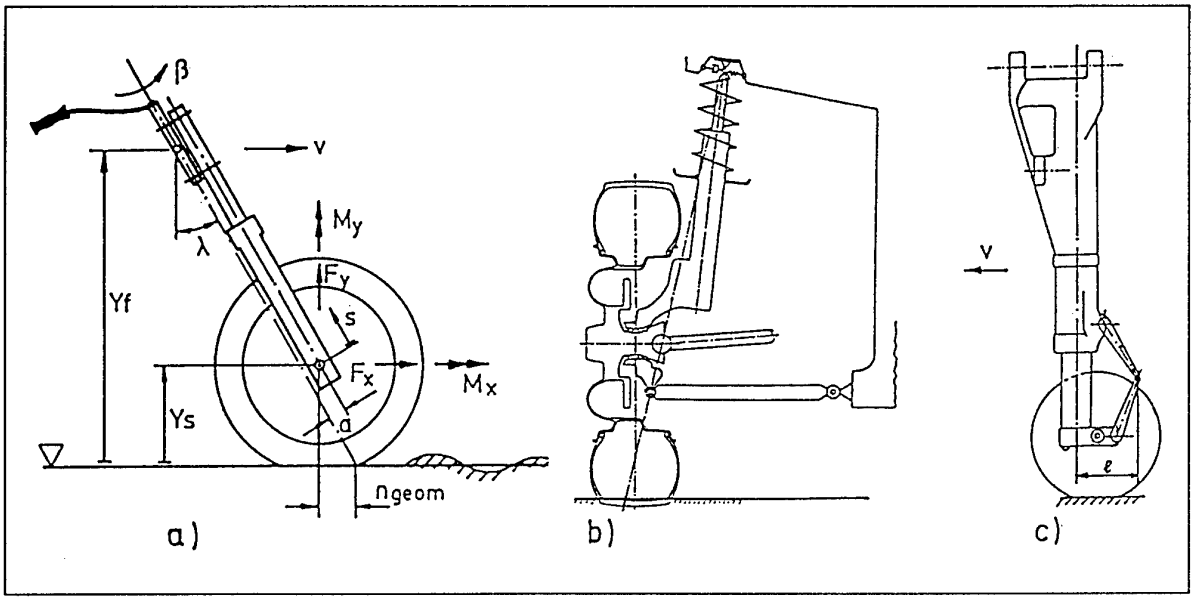

Figure 1: *Examples of wheel suspension: a) motorcycle, b) motor car and c) aeroplane (after [Volk93])*

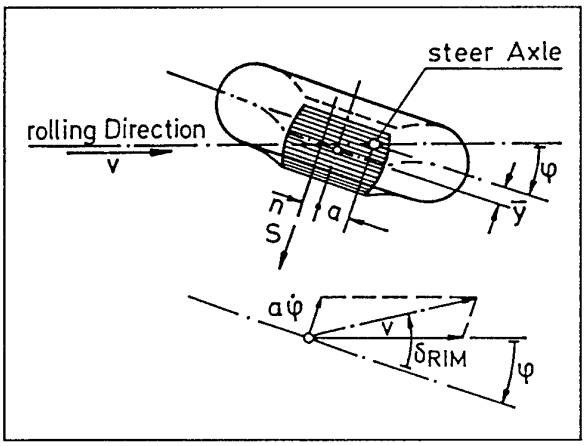

Figure 2: *kinetic and dynamic quantities of the steered wheel*

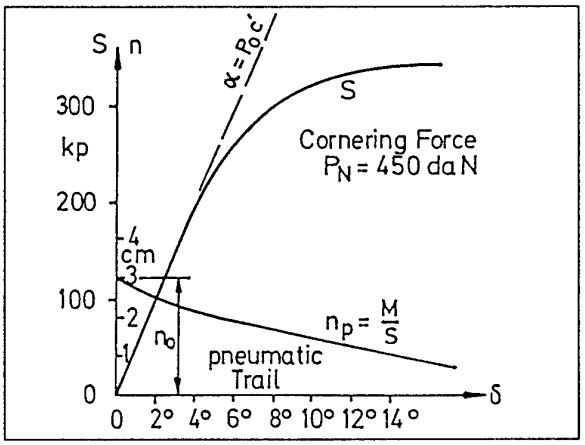

Figure 3: *Lateral guiding force and pneumatic trackinglength*

After linearisation ($n_P \approx n_0$ — see figure 3), it follows that:

$$\left(I + m\,a^2\right)\,\ddot{\varphi} + k_L\,\dot{\varphi} + c_L\,\varphi + (a + n_0)\;P_0\,c'\left(\varphi + \frac{a\,\dot{\varphi}}{v} - \frac{\dot{\bar{y}}}{v}\right) \;=\; 0, \tag{6}$$

$$P_0\,c'\left(\varphi + \frac{a\,\dot{\varphi}}{v} - \frac{\dot{\bar{y}}}{v}\right) - c_S\,\bar{y} \;=\; 0. \tag{7}$$

With $\bar{y} \sim e^{\lambda\,t}$, that leads to the characteristic determinant solutions ($I_a = I + m\,a^2$):

$$\begin{vmatrix} I_a\,\lambda^2 + \left[k_L + \frac{a}{v}\,(a + n_0)\,P_0\,c'\right]\,\lambda + c_L + (a + n_0)\,P_0\,c' & -(a + n_0)\,\frac{P_0\,c'}{v}\,\lambda \\ P_0\,c'\,\left(1 + \frac{a}{v}\,\lambda\right) & -c_S - P_0\,c'\frac{\lambda}{v} \end{vmatrix} = 0. \tag{8}$$

The expansion of this gives:

$$I_a \frac{P_0\, c'}{v}\, \lambda^3 + \left(I_a\, c_S + \frac{k_L\, P_0\, c'}{v}\right)\, \lambda^2 + \left[(a+n_0)\, c_S\, \frac{a}{v}\, P_0\, c' + \ldots \right.$$
$$\left. \ldots + c_L\, \frac{P_0\, c'}{v} + c_S\, k_L\right]\, \lambda + (a+n_0)\, c_S\, P_0\, c' + c_L\, c_S = 0. \tag{9}$$

2.1 The unconstrained wheel

If, for example, one sets $c_L = k_L = 0$, the characteristic equation obtained is:

$$\lambda^3 + \frac{v\, c_S}{P_0\, c'}\, \lambda^2 + (a+n_0)\, \frac{a\, c_S}{I_a}\, \lambda + (a+n_0)\, \frac{v\, c_S}{I_a} = 0. \tag{10}$$

In the case of a wheel free to rotate around the steering axle $c_L = 0$, $k_L = 0$, the ROUTH-HURWITZ stability conditions for the bow wheel of an aeroplane or for the steering of a motorcycle give

$$a\, c_S - P_0\, c' > 0. \tag{11}$$

2.2 Elastic mounted wheel with steering tolerance

If, by contrast, one considers a steered wheel, tolerance can arise in the steering, which can be represented in a simple equivalent linearisation by a steering stiffness c_L^* as a function of the torsional vibration amplitude. The steering tolerance is represented by an angle of rotation $\pm\varphi_0$ (see figure 4). For the equivalent linearisation of the function $\varphi = A\, \cos(\nu\, t)$

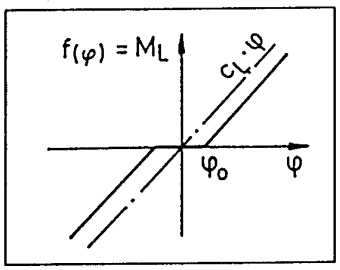

Figure 4: *Dependence of the steering tolerance*

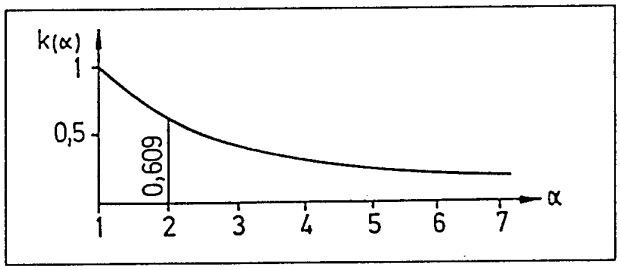

Figure 5: *Shape function of rotational oscillation amplitude dependend steering stiffness*

holds:

$$\frac{\nu}{\pi} \int_0^{2\pi} f(A\cos(\nu\, t))\, \cos(\nu\, t)\, dt = c_L^*(A)\, \cos(\nu\, t). \tag{12}$$

In both of the partial domains $A < \varphi_0$ and $A \geq \varphi_0$, or for $\alpha = \left|\frac{A}{\varphi_0}\right|$ with $\alpha < 1$ and $\alpha \geq 1$, the following equivalent torsion spring coefficients shall be taken into account

$$\begin{aligned} \alpha < 1: &\qquad c_L^* = 0 \\ \alpha \geq 1: &\qquad c_L^* = c_L\, (1 - k(\alpha)) \end{aligned} \tag{13}$$

The shape of the function $k(\alpha)$ is given in figure 5. From the polynomial of third degree for the characteristic value λ

$$\lambda^3 + \frac{v\, c_S}{P_0\, c'}\, \lambda^2 + \left[(a+n_0)\, \frac{a\, c_S}{I_a} + \frac{c_L^*}{I_a}\right]\, \lambda + (a+n_0)\, \frac{v\, c_S}{I_a} + \frac{v\, c_L^*\, c_S}{P_0\, c'\, I_a} = 0 \tag{14}$$

for $c_L^* \neq 0$ but $k_L = 0$, we obtain the HURWITZ determinant

$$\Delta_{20} = (a + n_0)\,\frac{c_S\,v}{I_a}\,\left[\frac{a\,c_S}{P_0\,c'} - 1\right]. \tag{15}$$

The determinant vanishes for $\alpha = \frac{P_0\,c'}{c_S}$, the relaxation length.
For $k_L \neq 0$ (and $c_L^* \neq 0$), the HURWITZ determinant is

$$\Delta_2 = \Delta_{20} + \frac{c_L^*\,k_L}{I_a^2} + k_L\,\left[\frac{(a + n_0)\,c_S\,a}{I_a^2} + \left(\frac{v\,c_S}{P_0\,c'}\right)^2\,\frac{1}{I_a}\right] + k_L^2\,\frac{v\,c_S}{P_0\,c'\,I_a^2} \tag{16}$$

from which it can be gathered that there is an additional term proportional to the factor c_L^*.
From these formulae it can be seen that

1. without steering damping there can be no stabilisation and
2. if there is steering damping, sufficient stabilisation can also be provided with a diminished steering stiffness c_L^*.
3. Since in general the geometric tracking length is significantly smaller than the relaxation distance, the additional terms in equation (9) must compensate for the negative effects of the stability condition (equation (15)).

Thus steering tolerance is frequently not immediately recognised, since the graph of the function $k(\alpha)$ only slightly diminishes the effect of the steering damping. Thus a maintenance problem arises from the fact that, even with a very small amount of steering tolerance, vibrations are amplified.

2.3 Taking friction into consideration

In order to avoid the effect of steering tolerance, therefore, friction is introduced into the steering by means of constructive measures. If one considers the effect of friction (figure 6),

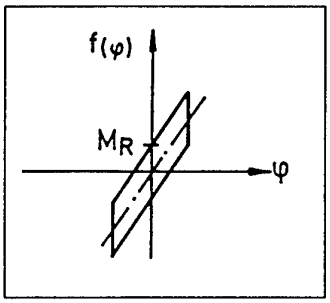

Figure 6: *Dependency of steering restistance on friction*

this can be represented by an eqivalent linear term of the form

$$k_L^* = \frac{4\,M_R}{\pi\,A\,\Omega} \tag{17}$$

where M_R represents the frictional moment in the steering. For the case where $c_L = 0$, but $k_L^* \neq 0$, the characteristic polynomial is now:

$$\lambda^3 + \left(\frac{v\, c_S}{P_0\, c'} + \frac{k_L^*}{I_a}\right)\lambda^2 + \left[(a+n_0)\,\frac{a\, c_S}{I_a} + \frac{v\, c_S\, k_L^*}{P_0\, c'\, I_a}\right]\lambda + (a+n_0)\,\frac{v\, c_S}{I_a} = 0. \qquad (18)$$

The HURWITZ determinant is given by:

$$\Delta_2 = \Delta_{20} + k_L^* \left[\frac{(a+n_0)\, a\, c_S}{I_a^2} + \left(\frac{v\, c_S}{P_0\, c'}\right)^2 \frac{1}{I_a}\right] + k_L^{*\,2}\,\frac{v\, c_S}{P_0\, c'\, I_a^2} \qquad (19)$$

Here one can also see that irrespective of whether Δ_{20}, i.e. the HURWITZ determinant for the case $c_L = k_L = 0$, is positive or not, a suitably dimensioned frictional moment or k_L^* compels stability.

This simple analytic investigation makes it clear that every rotating but elastically mounted wheel is capable of exhibiting self-excited rotational vibrations about the axis of steering. Even if wheel load variations are not taken into consideration, and thus an even ground is assumed, there is a tendency towards so-called wobble vibrations in case of a motorcycle. The effect of the non-linearity of the system on the amplitudes of vibration alone is also exhibited, wherein more exhaustive efforts with the aid of harmonic balances also take into consideration the non-linearity of the cornering curve. Unfortunately this effect is in principle non-linear, also with respect to the vertical dynamics of the wheel, leading to states of motion at several frequencies. The method of harmonic balances is thereby rendered useless for dealing with the problem. Notably the tire width and curvature of the contact area have a stabilising effect [Boe77].

3 Steer–Shimmy of Motorcycles

Instabilities of the steering system are known for several types of vehicles, e. g. the tail- or mainwheel of airplanes and the (steer-)shimmy of automobiles. This instability also accurs at single-track vehicles as bicycles, scooter, and motorcycle. It describes the resonance movements of the steering-system around the steering axis.

Several authors examined this phenomenon of motorcycles (e. g. [Pac66], [Sha71], [Sha77], and [Koch80]).

The modelling of the motorcycle by means of a linear differential equation system of 20. order provides the main (eigen) figures of the driver - single-track vehicle system. [Sha71] indicated the terms for three eigen-values:

- capsize mode, as vibration-free movement of tilting (tipping) of the whole motorcycle to one side, which is stable in the lower velocity range, and constantly instable in the medium and higher velocity range.
- wobble mode, which is called "shimmy" at other vehicles, and is steer motion which occurs at motorcycles as a frequency between 7 and 10 Hz almost independent from the vehicle velocity, and is good damped in the lower and medium velocity range.
- weave mode, as vibration of the whole motorcycle around the yaw axis with an increasing frequency at lower driving speed and in the medium and higher velocity range movement tending towards a limit value between 2 and 3 Hz.

The linear theory, however, does in comparison with measurements on the motorcycle not come up with real-world condition results for the wobble mode, since the whole calculation model for the medium velocity range calculates a well damped vibration then, the measurements show that especially here just very low, respectively no damping exists. Other mechanical couplings are, therefore, effective as they are enclosed in the linear vehicle model. From the observation of a real vehicle showing that shimmy movements are very much coupled with the balancing condition of the wheel, [Koch80] developed a model, which contains the steering system of the motorcycle alone, without the rear frame. As a fundamental addition compared to previous modelling, he encludes the periodic wheel load oscillation, which comprise a force component around the steering axis, supplying the energy for exciting the wobble mode. These wheel load oscillations occur through pitching and vertical motions of the vehicle and front wheel which are connected with the radial deformation of the tire. These oscillations are produced by road irregularities, as well as by the periodic forces of a poor balanced wheel.
[Koch80], herewith, got a mechanical backup system, which encludes the radial deformation of the tire in the wobble mode. Result of this modelling is a non-linear differential equation system, which can be transformed to a MATHIEU differential equation, so that the kinetic ranges of instability of the wobble mode can be demonstrated.

1. Solution of the vertical motion
   Fig. 7 may be used as model. The following differential equation gives the force-balance

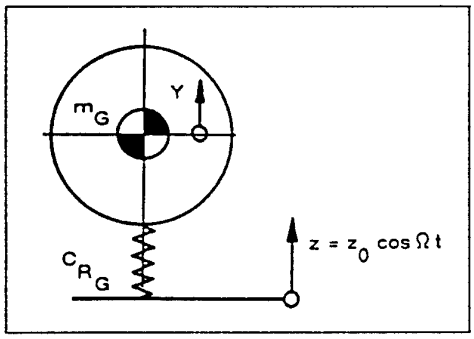

Figure 7: *model of the vertical motion*

in the vertical direction:

$$m_G\,\ddot{y} + c_R\,y = c_R\,z, \tag{20}$$

$$\ddot{y} + \omega_R^2\,y = \omega_R^2\,z, \tag{21}$$

$$\ddot{y} + \omega_R^2\,y = \omega_R^2\,z_0\,\cos(\Omega\,t) \tag{22}$$

(m_G: Mass of wheel, c_R: Tire radial stiffness, y: vertical motion of wheel axis, z: vertical motion of road surface). With $y = y_0\,\cos(\Omega\,t)$ one gets:

$$y_0 = \frac{\omega_R^2}{\omega_R^2 - \Omega^2}\,z_0, \tag{23}$$

$$y = y_0\,\cos(\Omega\,t) = \frac{\omega_R^2}{\omega_R^2 - \Omega^2}\,z_0\,\cos(\Omega\,t). \tag{24}$$

The reaction force coming from the road excitation results as radial force to

$$F_R = c_R\,(y - z) \tag{25}$$

at the center of the tire contact.

2. Solution of the pitching motion
A road irregularity at the front wheel produces a pitching motion of the vehicle. Fig. 8 may be used as model. The following differential equation for the center of gravity

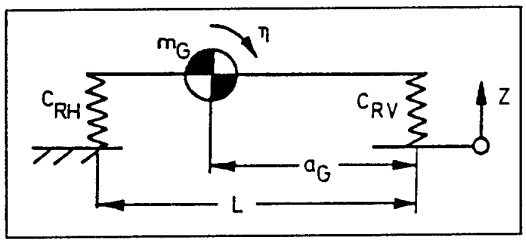

Figure 8: *Model of the pitching motion*

of vehicle results from the torque balance

$$\theta_\eta\,\ddot{\eta} - F_{CV}\,a_G + F_{CH}\,(L - a_G) = c_{RV}\,a_G\,z, \tag{26}$$

$$F_{CV} = -c_{RV}\,a_G\,\eta, \tag{27}$$

$$F_{CH} = c_{RH}\,(L - a_G)\,\eta, \tag{28}$$

$$z(t) = z_0\,\cos(\Omega\,t), \tag{29}$$

$$\theta_\eta\,\ddot{\eta} + c_{RV}\,a_G^2\,\eta + c_{RH}\,(L - a_G)^2\,\eta = c_{RV}\,a_G\,z_0\,\cos(\Omega\,t), \tag{30}$$

$$\ddot{\eta} + \underbrace{\frac{c_{RV}\,a_G^2 + c_{RH}\,(L - a_G)^2}{\theta_\eta}}_{\omega_\eta^2}\,\eta = c_{RV}\,a_G\,z_0\,\cos(\Omega\,t), \tag{31}$$

(η: pitch angle, $c_{RV/R}$: front/rear wheel stiffness, z: vertical motion of road surface, ω_η: Eigenfrequency of pitch motion) so finally the solution is

$$\eta = \eta_0\,\cos(\Omega\,t) = \frac{c_{RV}\,a_G}{\theta_\eta\,(\omega_\eta^2 - \Omega^2)}\,z_0\,\cos(\Omega\,t). \tag{32}$$

The following superposed movement results from the pitching and vertical motion of the whole vehicle for the front wheel

$$y_V = \left[\frac{\omega_R^2}{\omega_R^2 - \Omega^2} - \frac{c_{RV}\,a_G^2}{\theta_\eta\,(\omega_\eta^2 - \Omega^2)}\right]\,z_0\,\cos(\Omega\,t), \tag{33}$$

out of which the radial force can be calculated:

$$F_R = c_R\,(y_V - z) \tag{34}$$

3. Equation of motion around the steering axis
This torque balance around the steering axis gives the following differential equation, the model is shown in fig. 9

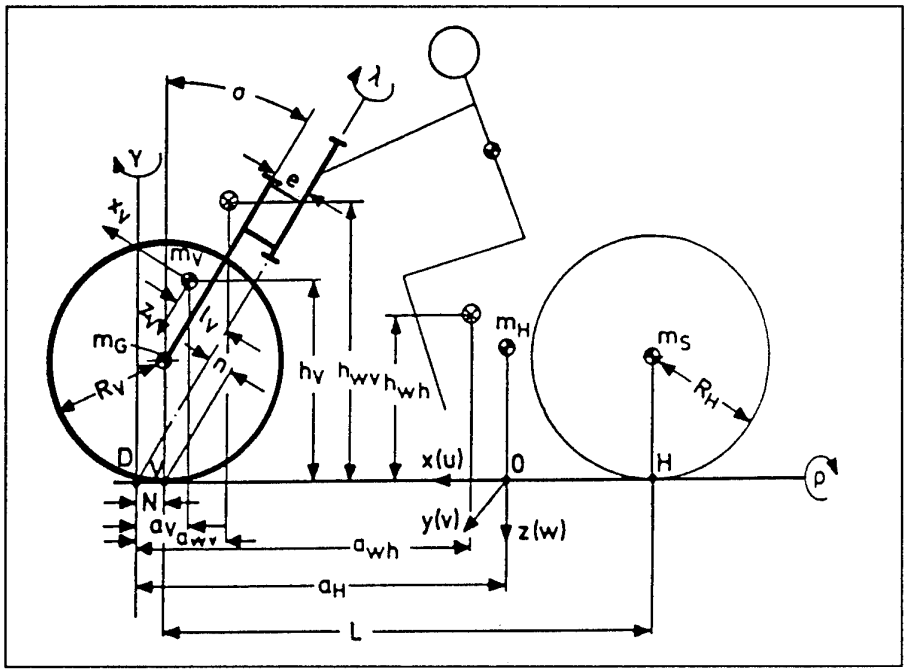

Figure 9: *Model for the motion around the steering axis*

$$\theta\,\ddot{\lambda} + r_l\,\dot{\lambda} + (F_N\,n - m_V\,l_V\,g - m_G\,e\,g)\,\sin\sigma\,\sin\lambda + \cdots \\ \cdots + n\,F_{SV} + M_{ZV}\,\cos\sigma + F_R\,n\,\sin\lambda = 0, \tag{35}$$

$$\theta = I_{VZ} + m_V\,l_V^2 + I_{GZ} + m_G\,e^2. \tag{36}$$

Linearization for small steering angles and with

$$c_\lambda = (F_N\,n - m_V\,l_V\,g - m_G\,e\,g)\sin\sigma + n\,c_{V\alpha} + c_{MZV\alpha}\,\cos\sigma \tag{37}$$

$$\omega_\lambda^2 = \frac{c_\lambda}{\theta}, \tag{38}$$

results in

$$\ddot{\lambda} + 2\,\omega_\lambda\,D\,\dot{\lambda} + \omega_\lambda^2\left(1 + \frac{F_R}{c_\lambda}\,n\right)\,\lambda = 0. \tag{39}$$

If the radial force from the pitching and vertical motion are introduced into the quations of motion around the steering axis the following nonlinear equation results out of it:

$$\ddot{\lambda} + 2\,\omega_\lambda\,D\,\dot{\lambda} + \omega_\lambda^2\,\lambda\left\{1 + \underbrace{\frac{c_{RV}}{c_\lambda}\,z_0\,n\left[\frac{-\Omega^2}{\Omega^2 - \omega_R^2} + \frac{c_{RV}\,a_G^2}{\theta_\eta\,\left(\Omega^2 - \omega_\eta^2\right)}\right]}_{2\,\mu}\,\cos(\Omega\,t)\right\} = 0, \tag{40}$$

$$\ddot{\lambda} + 2\,\omega_\lambda\,D\,\dot{\lambda} + \omega_\lambda^2\,\lambda\,(1 + 2\,\mu\,\cos(\Omega\,t)) = 0, \tag{41}$$

the MATHIEU differential equation.
The interesting part of this equation is that unlimited expanding solutions for particular values of its coefficients are given These values produce ranges of instability.

Although the solution of the MATHIEU differential equation demonstrates especially at double excitation frequency its main range of instability, the chape of the non-linear function, however, dictates what happens.
The shape of this function is shown in fig. 10 using the data of a motorcycle as function of the driving speed v, respectively wheel frequency Ω. The shape of the front axle amplitude

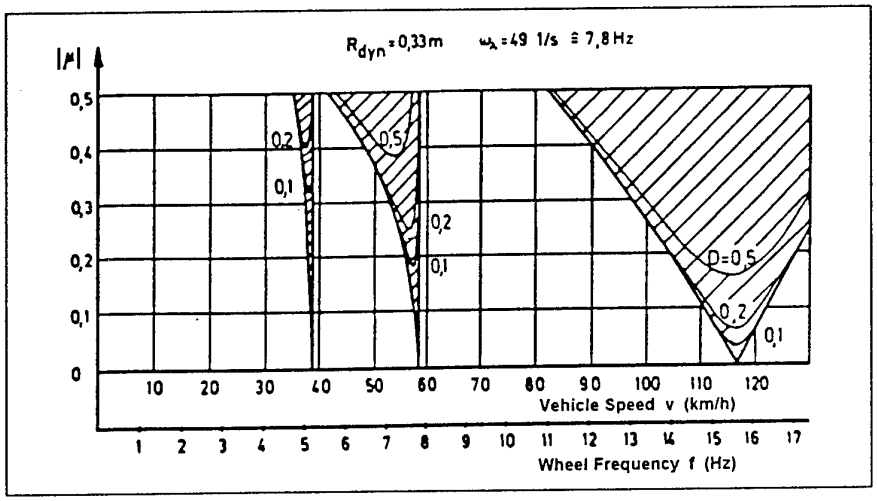

Figure 10: *Kinetic ranges of instability of the steering system vs vehicle speed (after [Koch80])*

as function of the driving speed, respectively wheel frequency is shown in fig. 11 showing two resonances of the vertical and pitching eigenfrequency. Since the resonance of the pitching-

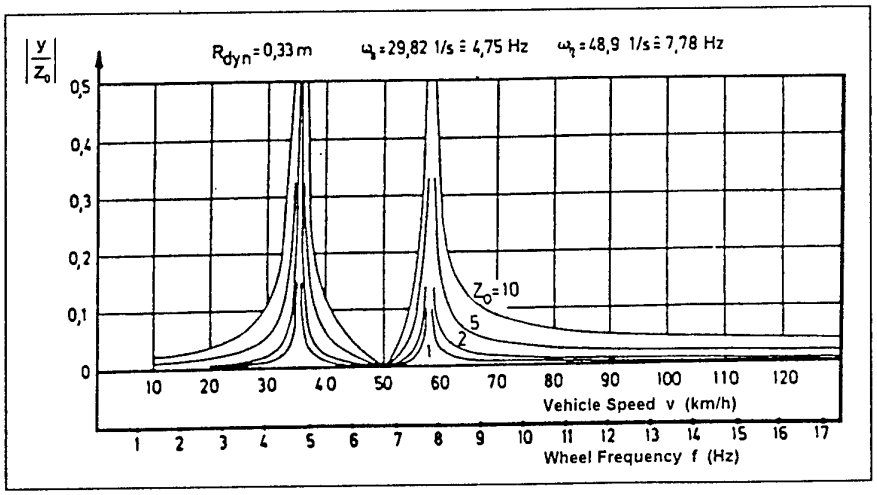

Figure 11: *Amplitude rate of the vertical front-axle track (after [Koch80])*

eigenfrequency ($\omega_\eta = 7,78$ Hz) approximately coincides with the medium range of instability, also instable wobble motion is to be expected within this velocity range.
The measured frequency and velocity during the wobbling of this vehicle agrees with theoretically gained values of the nonlinear stability analysis. These results show beautifully that the wobble mode can also be determined as a characteristic value with the help of the linear theory, though it does not agree with measurements at the motorcycle, with respect to either frequency or damping. Only by including in the modelling the vertical dynamics

of the wheel together with the lateral dynamic characteristics, which leads to a non-linear differential equation, results in regions of instability that can be confirmed by measurements. A first- or higher-order theory of tires for the lateral characteristics and a radial tire stiffness dependent on the tire speed may further refine the results.
Even if [Koch80] only used the balanced masses in its model as an excitation, the broad spectrum of road unevennesses also provides excitations. This is also confirmed by measurements wherein greater instability arises with an unbalanced front wheel.
Also G. Nybakken is engaged in work in his dissertation [Nyb73] on investigating the stability of rheolinear aeroplane landing gear.

4 Tire Magic Formulas

Simulation of systems in general but also of tires can be done for two goals:

1. Description of the physical happening in a system by using physical laws:
2. Imitating the physical behaviour — in the meaning of a black-box view — by approximating the behaviour.

Engineers use both methods for simulation, whereby the imitation of the physical behaviour must be done by system identification on the basis of estimated and anticipated describing rules; e.g. by theoretical control assessments.
Both methods deliver also different statements. Using physical laws, precise predictions about non existing systems, and their influence by physical parameters are possible. On the other hand the computation effort is generally very high. The advantage, and very often, also the goal of the second method is the real time ability for a complex dynamic system combined with the disadvantage not to entirely comprehend the influences of physical parameters of that system.
The method to imitate the physical behaviour by its approximation on the basis of behaviour equivalent formulas is called in the last time "magic formula".
On one hand in the area of vehicle development but also for driving simulators a real time ability or at least a very quick statement about the system behaviour of the total vehicle is necessary without for instance to accomplish a physically exact description of a shock absorber.
In the following two of these approximating formulas are described, one could be used for calculation of the tires static and the other for the calculation of the tires dynamic behaviour.

4.1 Static behaviour of tires

Since the static behaviour with respeckt to side force, self aligning torque, camberforce etc. for braking and tracking forces of all tires are similar the effort to build up a physical modell and the effort to estimate all necessary physical parameters is enormous, so the idea of using only some mathematical functions which fits the measured results by changing only some of function parameters came up.
[Bak87] and [Bak89] presented a paper in which they proposed a formula with coefficients which describe some of the typifying quantities of a tire, such as slip stiffness at zero slip and force and torque values. The formula is capable of describing the characteristic of side force,

brake force and self aligning torque with great accuracy. That mathematical representation is limited to steady-state conditions.
Figure 12 shows the basic form of each characteristic of the tire. Bakker et al. took over the

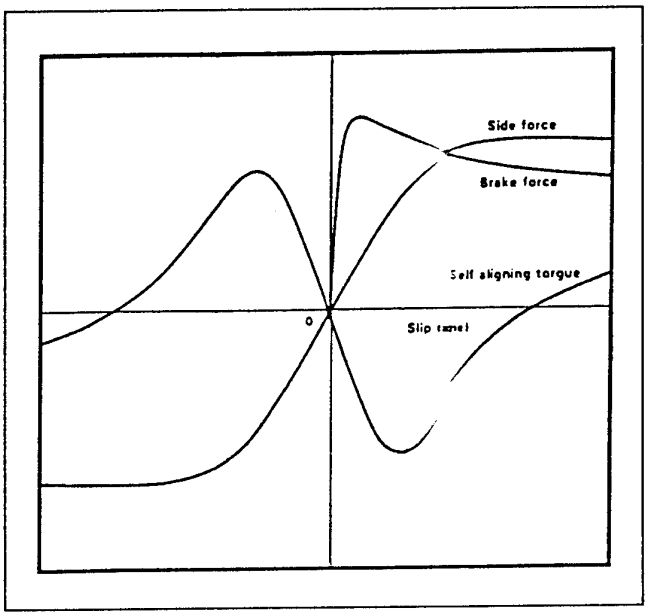

Figure 12: *Steady-state tire characteristics (after [Bak87])*

idea by Ruf [Ruf83] to approximate these tire behaviour by special angular functions.
The demands for that formula was expressed

- to be able to describe all steady-state tire characteristics,
- being easily obtainable from measured dates,
- being physically meaningful; its parameters should characterize in some way the typifying quantities of the tire,
- being compact and easy to use,
- contributing to a better understanding of tire behaviour, and
- being accurate.

These demands were found for all tire characteristics in the expression

$$y(x) = D \sin\{C \arctan[B\,x - E\,(B\,x - \arctan(B\,x))]\}, \quad (42)$$

$$Y(X) = y(x) + S_v, \quad (43)$$

$$x = X + S_h \quad (44)$$

with $Y(X)$ standing for either side force, self aligning torque or brake force and X denoting slip angle (α) or longitudinal slip (κ).
D in equation (42) is the peak value and the product $D\ C\ B$ equals the slip stiffness at zero slip. The coefficient C governs the shape of the curve and the coefficient E makes it

possible to accomplish a local extra stretch or compression while stiffness and peak value remain uneffected.
Due to ply steer, conicity, rolling resistance and camber, the characteristics will be shifted in horizontal and/or vertical directions. These shifts are represented by S_h and S_v respectively. By these approximating functions Bakker et al. got in parts excellent fitting results of measured and calculated tire behaviour as shown in Fig. 13 and 14.

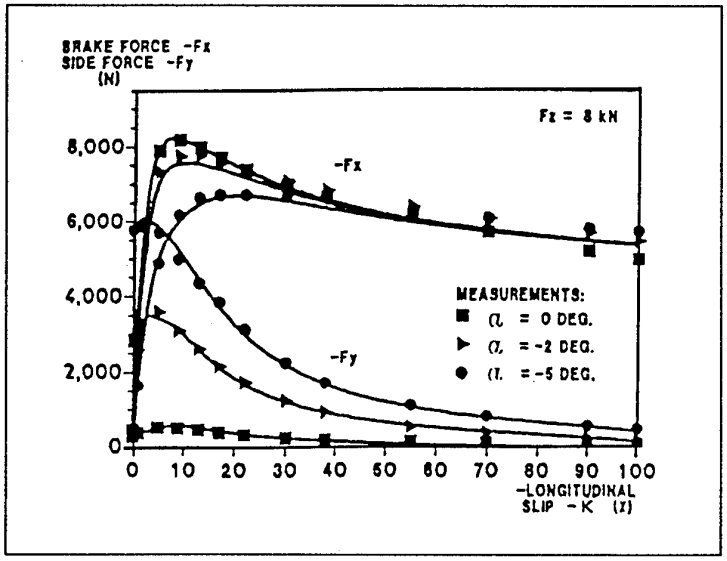

Figure 13: *Brake and side force vs slip (after [Bak87])*

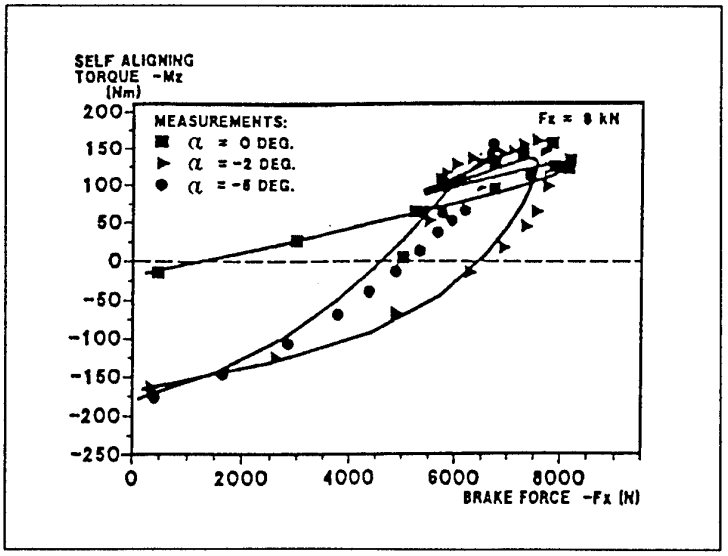

Figure 14: *self aligning torque vs break force (after [Bak87])*

4.2 Measured Transfer Properties of the Tire at time varying side slip angle and its approximation by control theory transformations.

[Will89], [Nast91] and [Will95] reported about the dynamic behaviour of tires due to dynamic changes of side slip angle and wheel load.

For simulation respectively pre-calculation of the dynamic driving behaviour of single and double track vehicles, the knowledge of the dynamic behaviour of the tire is necessary, without time consuming sub-routines for a tire model. [Schu87] reports in detail on the latter.
Easier and without time consuming appliance the transfer properties on a test stand with time varying exitation signals can be evaluated. This leads to no explanation, and realization on the physical processes inside the tire respectively in the contact area though, but enables the vehicle engineer to easily integrate the tire dynamic into a model of vehicle dynamic or driving dynamic. When measuring the tire with time varying exitation, the simultaneously occurring inertia forces and gyroscopic torques, which do not occur at static measurements, have to be corrected carefully. On this procedure, and the following description of the transfer function by means of control equations reported [Will87], and [Nast91] applied to 4 different tires, two motorcycle, and two passenger car tires. The time varying side slip angle $\alpha(t)$ was described with a frequency limited white noise up to approximately 17 Hz with a variance of $0,21°$ (see fig. 15).

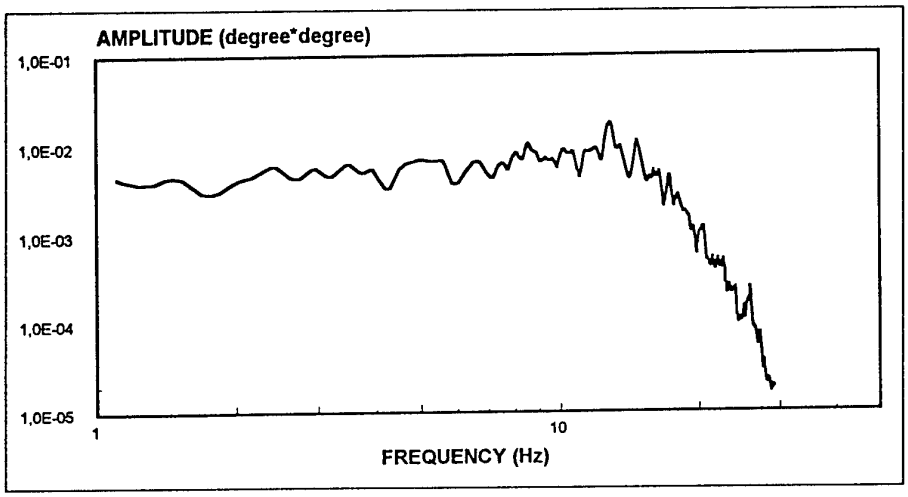

Figure 15: *Power spectral density of side slip angle (after [Nast91])*

If one applies the corrected dynamic self aligning torque, and the corrected dynamic side force to the stationary values, that are these values, which occur at side slip angles ($f = 0$ Hz) constant with time, so one will come to non-dimensional self aligning torques and side forces. By computing the power spectral densities, one finally gets the transfer function M_α/α of the self aligning torque, and F_α/α of the side force. The fig. 16, and 17 show this exemplarily as Bodeplot.

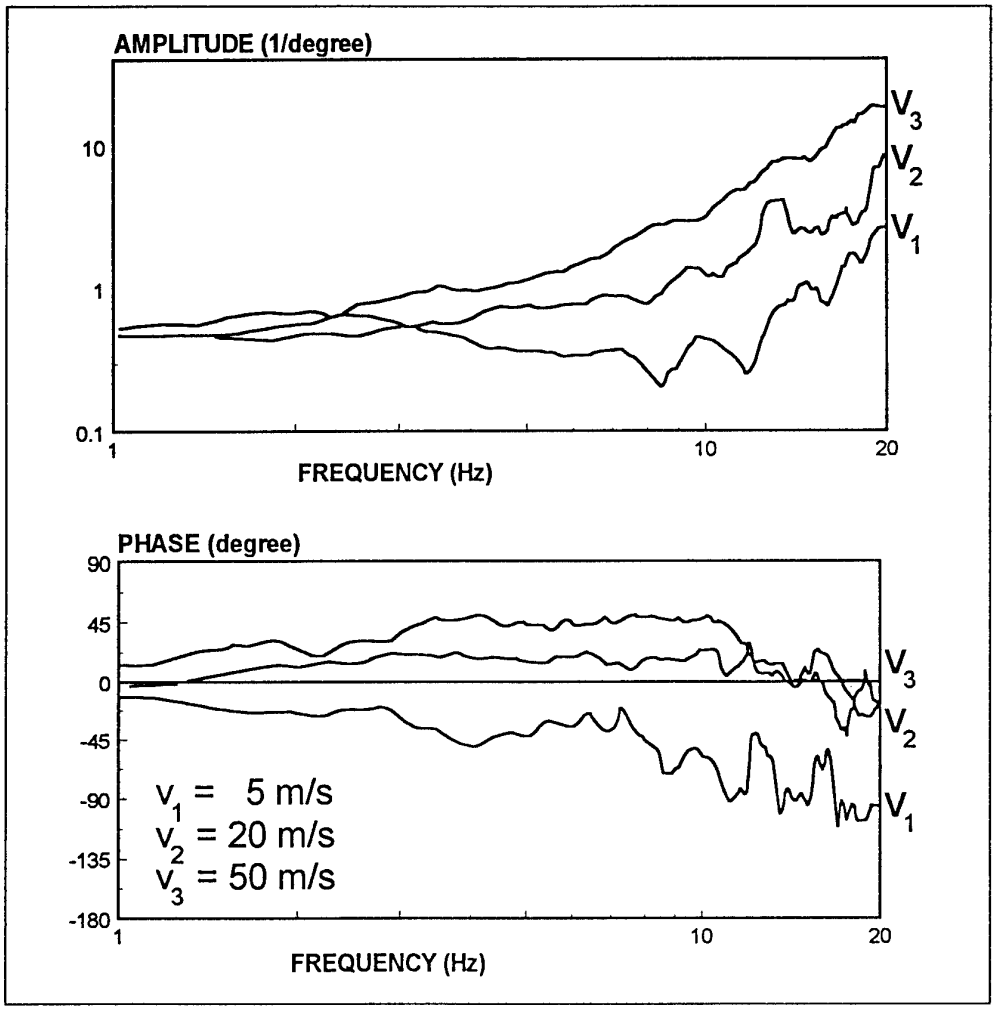

Figure 16: *Measured transfer function of self aligning torque relative to side slip angle (after [Nast91])*

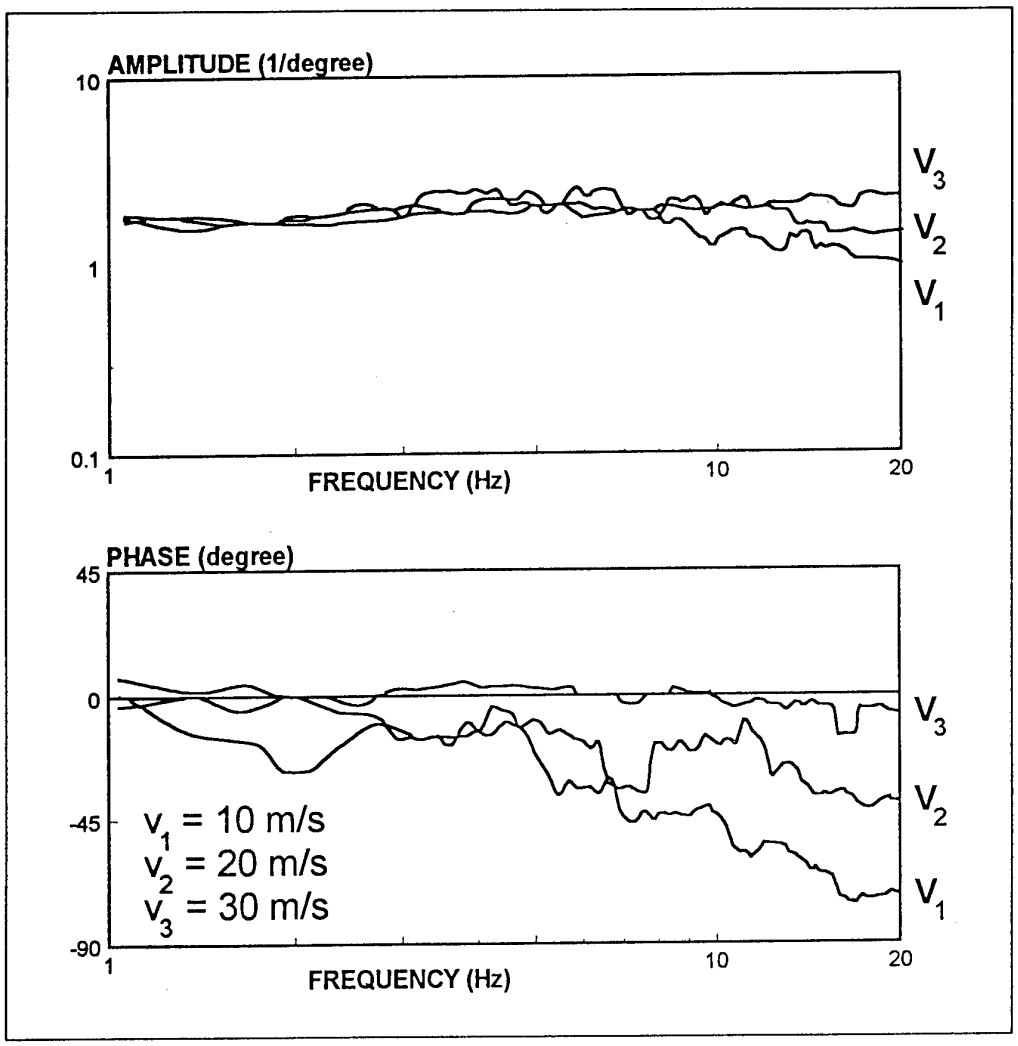

Figure 17: *Measured transfer function of side slip force relative to side slip angle (after [Nast91])*

A PD_2-behaviour (proportional plus double derivative action controller) is assumed as approximation equation for the transfer function, which reproduces both amplitude channels appropriately. Merely the phase has to be adapted by another approximation term — a dead time term. That means that the dynamic behaviour of self aligning torque, and side force has to be adapted by higher terms as 2nd order.
The approximation equation in the time domain for the self aligning torque are

$$M_R \frac{d^2\alpha\,(t-T_R)}{dt^2} + D_R \frac{d\alpha\,(t-T_R)}{dt} + C_R\,\alpha\,(t-T_R) = M_\alpha(t) \tag{45}$$

and for the side force

$$M_S \frac{d^2\alpha\,(t-T_S)}{dt^2} + D_S \frac{d\alpha\,(t-T_S)}{dt} + C_S\,\alpha\,(t-T_S) = F_\alpha(t) \tag{46}$$

Fig. 18 to 20 show each time the mass factors M_R and M_S, damping factors D_R and D_S, stiffness factors C_R and C_S for the 4 measured tires depending on the wheel load, and wheel speed. The index R refers to the self aligning torque, the index S to the side force. The types were:

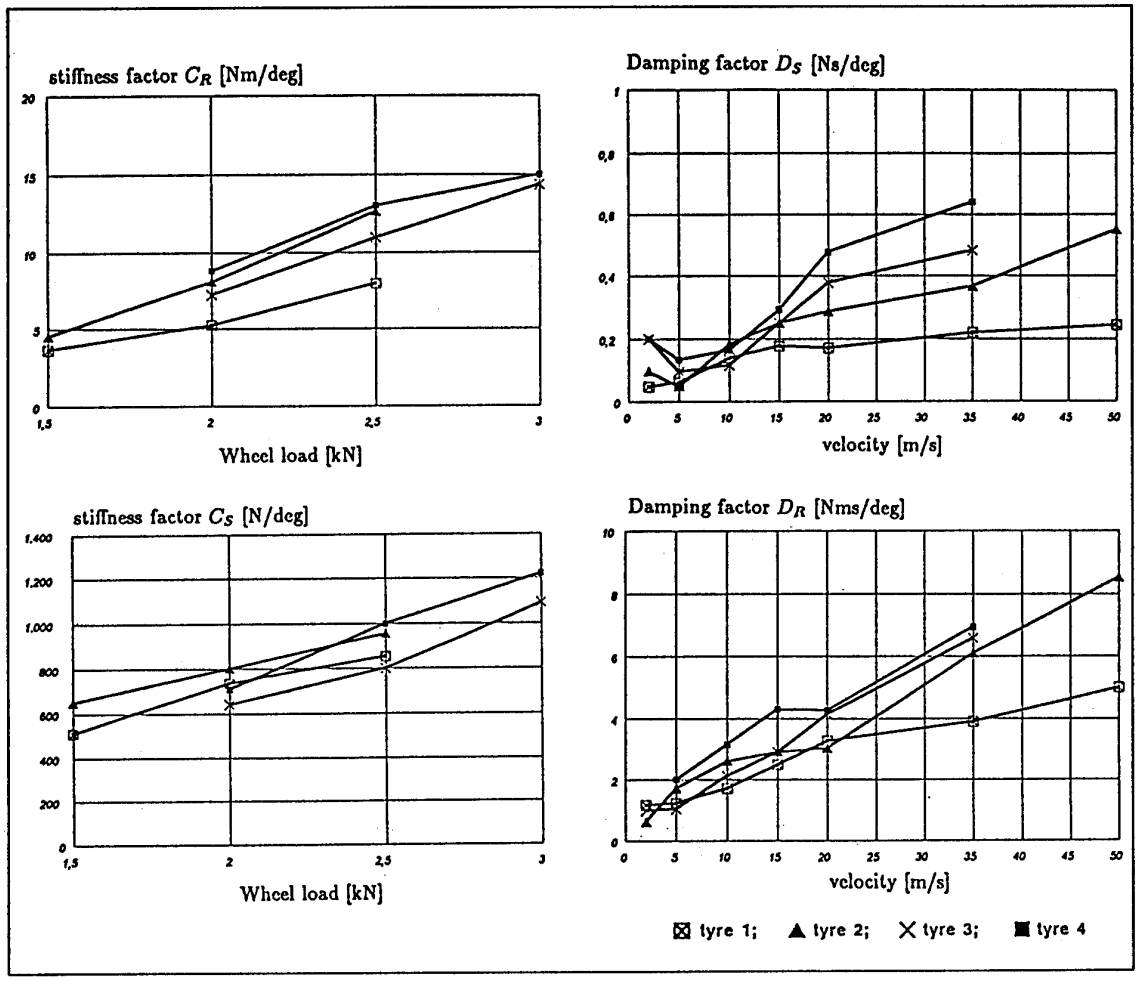

Figure 18: *Stiffness factors C_R and C_S as function of wheel load; damping factors D_R and D_S as function of wheel speed: 1. Bridgestone 120/80 V 16 (motorcycle); 2. Bridgestone 150/80 V 16 (motorcycle); 3. Conti Contact 155 R 13 (automobile); 4. Conti Contact 175/70 R 13 (automobile) (after [Nast91])*

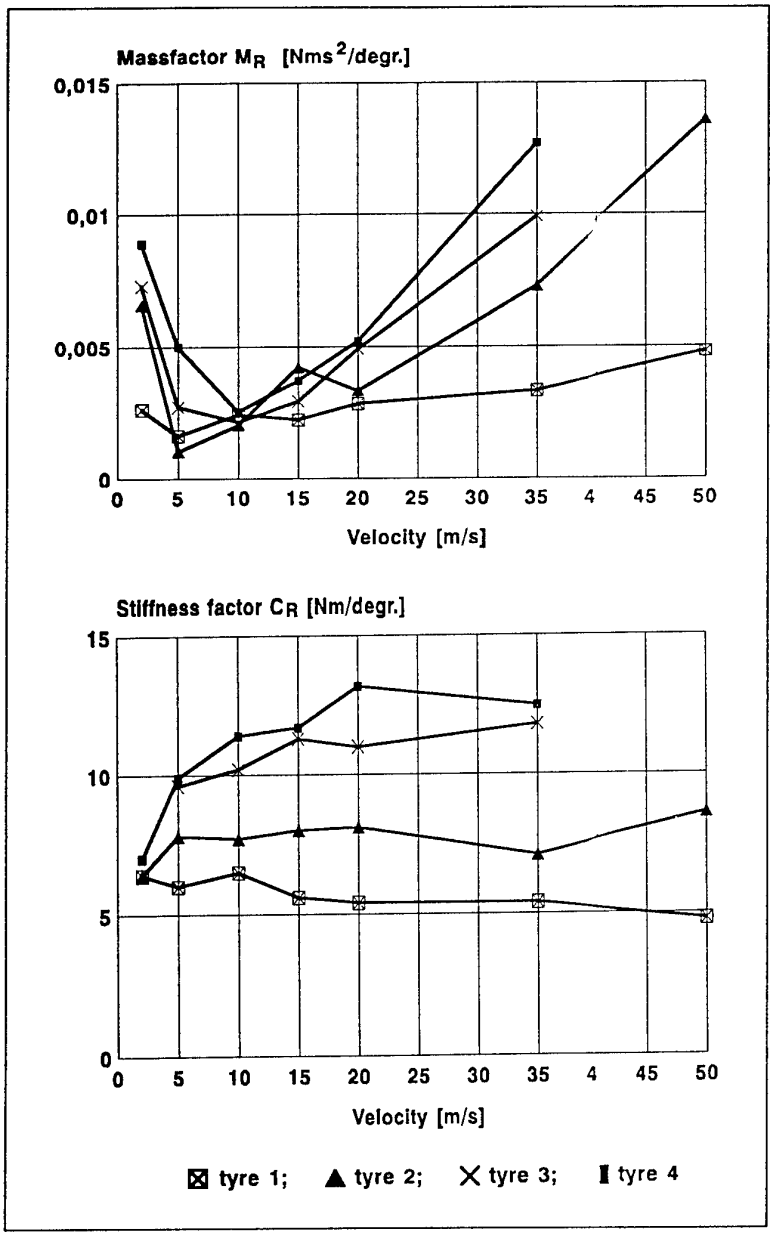

Figure 19: *Mass factor M_R and stiffness factor C_R as function of wheel speed (after [Nast91])*

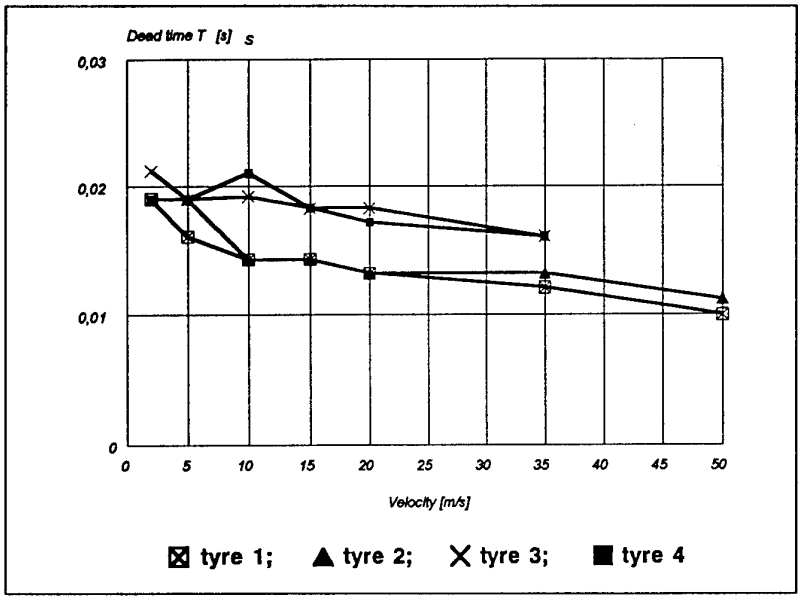

Figure 20: *Dead time as function of wheel speed (after [Nast91])*

As result there can be concluded:

- the stiffness factor increases on increasing wheel load for the side force as well as for the self aligning torque.
- the damping factors D_R and D_S increase on increasing speed.
- the dead time of the side force reduces on increasing speed.
- C_R is constant for motorcycle tires (cross bias type) over the speed, for passenger car tires (radial tires) the stiffness factor and C_R increases degressively on increasing speed.
- M_R increases progressively over the speed.
- an influence of the inflation pressure of the tire on the factors could not be measured.

On further measurements at time varying wheel load F. Sun [Sun90] also reports in his Ph.D. thesis, and reached similar results, in which he additionally determined the dynamic transfer characteristics for time varying wheel load.
Since the whole transfer behaviour is still very much depending on the wheel velocity, except the stiffness factor C_R for the self aligning torque of the motorcycle tire (cross bias type), one can assume that non linear effects, i.e. because of gyroscopic effects can not fully be recorded by means of the linear approximation formulation.
Assuming black-box-formulas are available as break-, sideforces and torques are described in their dynamic behaviour a straight forward integration procedure is possible which will be shown here.

5 Numerical method of investigating wobble

For every non-linear function $S(\delta_{eff}, P)$, an implicit differential equation of first order can be given for the non-stationary process:

$$S\left(\delta_{Rim} - \frac{\dot{\bar{y}}}{v}, P\right) = c_S\, \bar{y}. \tag{47}$$

A stabilisation of the numerical or piecewise linear integration in the case $\frac{\partial S}{\partial \delta} > 0$ can be achieved through an extension of the equation by a damping term

$$S\left(\delta_{Rim} - \frac{\dot{\bar{y}}}{v}, P\right) = c_S\, \bar{y} + d_S\, \dot{\bar{y}} + m_S\, \ddot{\bar{y}} \tag{48}$$

and possibly a mass compensation term. These, however, does not render impossible the correct assessment of short-wave surface unevennesses, with regard to their effect on $P(t)$ and on $S(t)$. As a result, the high-frequency rolling process cannot be treated further by means of analytical mechanics.

Since further investigations of an analytic kind are not possible, one is compelled to resort to numerical methods. In these, the contact surface is modelled as discrete, and the sequence of contact points is investigated in discrete calculating steps. A unilateral contact condition enables the numerical representation of partial lifting and traversing of track unevennesses. In the process, the tire structure is resolved into many degrees of freedom, taking into consideration the tire mass and damping. Such a structure is geometrically non-linear in principle and has a relatively high frequency. It is guided by means of a rigid body system of low frequency, consisting of a rim and shock absorber. If, as is customary for motorcycles, one introduces a head lug angle λ, then one obtains the following system of equations of motion for the steering angle β and the spring deformation s of the wheel axle (see figure 1).

$$J_L\, \ddot{\beta} + k_L\, \dot{\beta} + c_L\, \beta = M_y\, \cos\lambda - M_x\, \sin\lambda + a\, F_z \tag{49}$$

$$m_F\, \ddot{s} + k_F\, \dot{s} + c_F\, s = F_y\, \cos\lambda - F_x\, \sin\lambda \tag{50}$$

$$Y_s = Y_f + (s - l_0)\, \cos\lambda \tag{51}$$

In addition, there are also the lateral motion and longitudinal motion of the motor vehicle mass itself. The contact forces generated while traversing the ground unevennesses follow from the equations of motion for the tire structure, which are not given here [Boe93]. The sample calculation given in figure 21 shows the dynamic effect of wheel load variations on a stable steering system that is nevertheless capable of damped wobble. The non-linearities taken into account in the numerical integration are the deformations of finite magnitude, the unilateral contact, i.e. local lifting and settling of the running surface on rough obstacles, and the effects of traction and sliding friction. The model does not take into account the effects of tire width or of cross-sectional bending. Wobble damping, however, is markedly influenced by enlarging the tire width and increasing the length of the contact surfaces. The resultant moment of pivoting has the effect of diminishing wobble. Thus, not surprisingly, for small contact surfaces, which arise under low wheel loads, have an especially critical effect on wobble. A surface-oriented theory of non-stationary rolling contact has been analytically developed for perfect roadholding, taking into account the bending of the trajectories of the

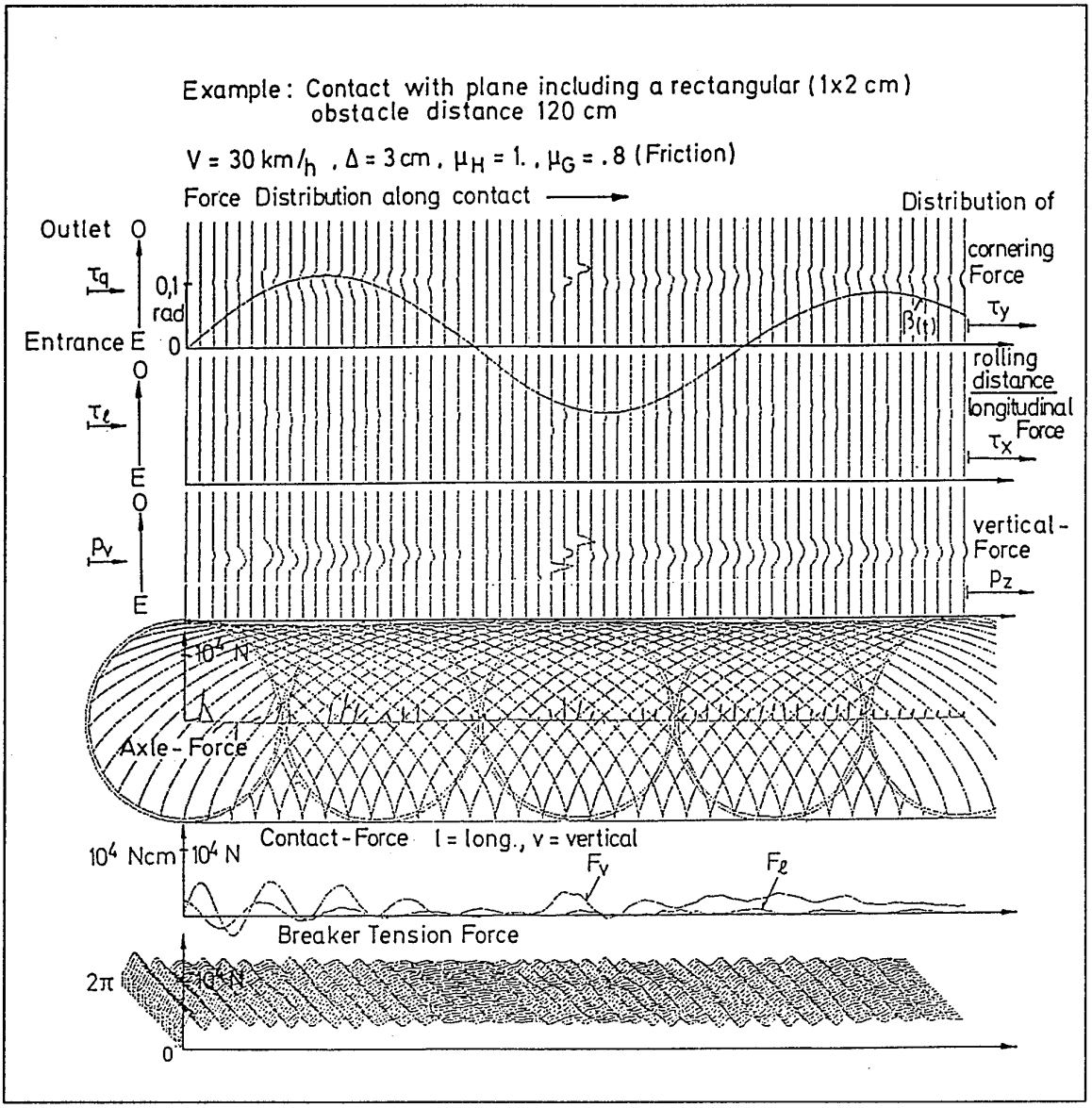

Figure 21: *Sample calculation for the steering system of the front wheel of a motorcycle*

contact particles of a flattened tire. Wobble vibrations produced on the testing stand show that the phase angle between the amplitude of wobble and the restoring torque of the tire can certainly pass beyond 90°, which cannot be represented by tire behaviour of the first order. The tendency of the system to auto-excitation is thereby markedly reduced when there is a sufficient area of contact between the tire and the ground. If the ground is uneven, however, so that the contact surface is at times considerably reduced, one speaks of a transition to hard auto-excitation, since the stabilisation is now only produced by the kinematic terms of first order. At high speeds, therefore, the reduction of load on the front wheel due to the air resistance of the vehicle necessarily leads to critical states of wobble, while the axial load is sufficiently large in the normal driving state. The non-linear coupling between the horizontal and vertical dynamics of the wheel also calls for numerical treatment here, since an analytic procedure only permits calculation in the case of perfect roadholding. Such a

numerical procedure, however, is very costly in terms of computing time, and has only been carried out until now with coarse substitute models with few degrees of freedom. If, however, one starts out with an analytically based strategy, then the destabilisation effect can also be demonstrated here by means of numerical examples for integrating the rolling action on rough ground.

6 Conclusion

Starting from that given overview furture theoretical investigation should include. It is possible to stabilise the system even in case of small contact area using the main influencing parameters found by linear theory. If the parameters are near stability border the nonlinear effects may suddenly disturb the rolling wheel and self-excitation occurs due to vanishing of vertical spin effects in contact area. In any case also for nonlinear computation the linear theory can be used as a guideline. All possible non-smooth surfaces could be taken into account using discret system modeling for the tire.

Literatur

[Bak87] E. Bakker, L. Nyborg, and H. B. Pacejka:
Tyre Modelling for use in vehicle dynamics studies.
SAE-P 87 04 21, Society of Automotive Studies, Inc., 1987.

[Bak89] E. Bakker, H. B. Pacejka:
A new tire model wih an application in vehicle dynamics studies.
SAE-P 89 00 87, Society of Automotive Studies, Inc., 1989.

[Boe77] F. Böhm:
Computing and measurements of the handling qualities of the belted Tyre.
Proc. 5th VSD 2nd INTAM Symposium, Vienna, pp 85–103, Swets and Zeitlingen, Amsterdam and Lisse, 1978.

[Boe93] F. Böhm:
Reifenmodell für hochfrequente Rollvorgänge auf kurzwelligen Fahrbahnen.
(Tire model for high-frequency rolling processes on short-wave tracks.)
(Bericht Sonderforschungsbereich 181, Teilprojekt B1)
VDI-Berichte Nr. 1088, pp 65–81, VDI-Verlag, Düsseldorf/Germany 1991

[Koch80] J. Koch:
Experimentelle und analytische Untersuchungen des Motorrad-Fahrer-Systems
(Experimental and analytical assessment of the Motorcycle-Driver-System; PhD-Thesis 1978).
Fortschr.-Ber. VDI-Z., Reihe 12, Nr. 40, 1980.

[Nast91] R. Nast, Chr. Teubert and H.-P. Willumeit:
Messungen der Übertragungseigenschaften von Luftreifen bei zeitlich veränderten Schräglaufwinkeln und anschließende Nachbildung dieser Größen durch Approximationsgleichungen
(Measurement of transfer properties of pneumatic tires under time varying side slip angle and followed by modelling using approximation equations.)
VDI-Berichte Nr. 916, pp 321–344, VDI-Verlag, Düsseldorf/Germany, 1991.

[Nyb73] G. Nybakken:
Investigation of Tire Parameter Variations in Wheel Shimmy.
PhD-Thesis, The University of Michigan, 1973.

[Pac66] H. B. Pacejka:
The wheel-Shimmy phenomenon.
PhD-Thesis, Technische Hogeschool, Delft, 1966

[Ruf83] E. Ruf:
Theoretische Untersuchungen des Federungsverhaltens von Vierrad–Straßenfahrzeugen.
(Theoretical investigations into the suspension behaviour of four-wheel road vehicles.)
Fortschr.-Ber. VDI-Z., Reihe 12, Nr. 44, S. 104–105, Düsseldorf, 1983.

[Schu87] D. H. Schulze:
Instationäre Modelle des Luftreifens als Bindungselement in Mehrkörpersystemen für fahrdynamische Untersuchungen.
(Non-stationary models of the pneumatic tire as a linkage element in many-body systems for investigations into the dynamics of driving.)
VDI-Fortschritt-Berichte, Reihe 12, Nr. 88, VDI-Verlag, Düsseldorf, 1987.

[Sha71] R. S. Sharp:
The Stability and Control of Motorcycles.
J. Mech. Engin. Sci., **13** No. 5, pp 316 - 329, 1971.

[Sha77] R. S. Sharp and C. J. Jones:
The straight running stability of single track vehicles.
Proc. 5th VSD 2nd INTAM Symposium, Vienna, pp 334–342, Swets and Zeitlingen, Amsterdam and Lisse, 1978.

[Sun90] F. Sun:
Dynamic Properties of Motorcycle Tires.
Dissertation, Beijing Institute of Technology, 1990.

[Valk93] R. van der Valk, H. B. Pacejka:
An analysis of a civil aircraft main gear shimmy failure.
Vehicle System Dynamics, **22**, Swets and Zeitlingen, BV Lisse, Netherlands, 1993.

[Will87] H.-P. Willumeit und Ch. Teubert:
Dynamische Eigenschaften von Motorradreifen bei zeitlich veränderlichem Schräglaufwinkel.
(Dynamic properties of motorcycle tires at slip angles varying with time.)
VDI-Berichte Nr. 657, pp 127–136, VDI-Verlag, Düsseldorf, 1987.

[Will89] H.-P. Willumeit and F. Sun:
Dynamische Eigenschaften von Motorradreifen bei zeitlich veränderlicher Radlast
(Dynamic properties of motorcycle tires under time varying, wheel-load).
VDI Berichte Nr. 779, pp 389–401. VDI-Verlag, Düsseldorf/Germany, 1989.

[Will95] H.-P. Willumeit and F. Böhm:
Wheel Vibrations and Transient Tire Forces.
Vehicle System Dynamics, **24**, Swets and Zeitlingen, BV Lisse, Netherlands, 1995.

LANDING GEAR SHIMMY — DE HAVILLAND'S EXPERIENCE

John Glaser and George Hrycko
Structural Dynamics Group
de Havilland Inc.
123 Garratt Blvd.
Downsview, Ontario, M3K 1Y5
Canada

1. SUMMARY

Landing gear shimmy is an unacceptable situation which, at the very least, leads to increased maintenance costs and at the worst could result in catastrophic failure of the gear and/or the attaching structure. Two landing gear shimmy problems experienced by de Havilland are presented, one in service and the other predicted during design. While these problems occurred over 10 years ago, it is the authors' contention that little progress has been made in this design discipline in the intervening years. It is recommended that advisory material is needed in this important but often neglected subject.

2. LIST OF SYMBOLS

C_{Ty} tire lateral damping coefficient
$C_{T\alpha}$ tire torsional damping coefficient
C_ψ tire cornering power
$\mathbf{D}$ damping matrix
F_c tire cornering force
F_t tire side force
F_y side force
F_z landing gear vertical force (static)
F_z^L vertical force on left tire
F_z^R vertical force on right tire
$\mathbf{G}$ gyroscopic matrix
h half footprint length
$\mathbf{I}$ inertia matrix
I_ω polar moment of inertia of wheel assembly
$\mathbf{K}$ stiffness matrix
K_{Ty} tire lateral spring constant
$K_{T\alpha}$ tire torsional spring constant
K_z tire vertical stiffness
$k_{\psi\psi}$ structural torsion stiffness
L mechanical trail
L_G geometric trail
L_R half axle length
M_t moment due to tire torsional stiffness
M_ϕ roll moment
M_ψ yaw moment
R tire (deflected) rolling radius
R_T undeflected tire radius
t time
$\mathbf{U}$ displacement vector $[\, y,\ \phi,\ \psi \,]^T$
V ground speed
y lateral displacement
Y tire equator coordinate at forward end of contact patch
$\hat{Y}$ tire equator coordinate at aft end of contact patch
Z tire lateral defection at forward end of contact patch
$\hat{Z}$ tire lateral deflection at aft end of contact patch
Δ tire lateral deflection (elastic)
ΔM_ϕ incremental roll moment
ΔM_ψ incremental yaw moment
ε_p pneumatic trail parallel to ground
θ_g gear tilt angle
λ_G yawed-rolling relaxation length
μ friction coefficient
ξ critical damping ratio
ξ_s structural damping ratio
τ_υ (Moreland) tire time constant
τ_υ^* equals τ_υ at 100 kts (Reference 3)
ϕ roll displacement
ψ yaw displacement
ψ_t tire elastic twist deflection in yaw
ω circular frequency

3. INTRODUCTION

Landing gears that shimmy are unacceptable, causing considerable discomfort and annoyance to passengers and crew. In fact, a severe occurrence of shimmy can damage the landing gear and its attaching structure, resulting in significant repair costs and airplane down time. The prevention of shimmy on an airplane with a shimmy-prone gear increases maintenance costs and may burden the pilot with self-established shimmy avoidance procedures. Some assurance is therefore needed that landing gear designs will be free from shimmy under all operating conditions taking into account normal wear and tear experienced in service.

Two examples of landing gear shimmy are presented in this report; the first involving the DASH 7 nose landing gear and the second the DASH 8 main landing gear. The DASH 7 airplane is a 4-engined turboprop, seating 54 passengers, that is no longer in production but is still in service. Nose landing gear shimmy appeared early in the flight development phase of this aircraft and re-appeared again after its introduction into service.

The DASH 8 airplane is a twin turboprop that seats 36 passengers in its earliest version, the series 100. Landing gear shimmy did not occur physically in this case, but was predicted to occur during the design phase. What is troubling about this example is that it took an inordinate amount of time for de Havilland and the landing gear vendor to settle on a design considered to be shimmy free. Obviously, the design process was costly and, despite the time spent, the structural efficiency of the design remains an open question: ie., the landing gear may be heavier than necessary.

Paper presented at the 81st Meeting of the AGARD SMP Panel on "The Design, Qualification and Maintenance of Vibration-Free Landing Gear", held in Banff, Canada from 4-5 October 1995, and published in R-800.

These examples occurred over 10 years ago. While this may be considered ancient history by some standards – the computer industry, for example – it is the authors' opinion that there has been little progress in the state of the art of shimmy design in the intervening years.

The authors have reason to believe that the shimmy "problem" is perceived by many to be a "black art" with no basis in sound engineering methods. The authors disagree and are concerned that this "black art" perception has hindered progress in shimmy design unnecessarily. The shimmy "problem" is no more mysterious than, say, aircraft flutter with which the authors have experience. What is lacking is the accumulation, integration and dissemination of currently available analytical and experimental experience to support the development of practical design processes. These, in turn, would yield structurally efficient, shimmy-free designs. The authors are optimistic that practical design processes are feasible and believe that the aerospace industry would benefit if those processes were formulated and made generally available.

Presented in this report are reviews of the DASH 7 and DASH 8 shimmy problems experienced by de Havilland. The report outlines the analysis models and methods used and presents the stability results obtained from those methods. The report concludes with a recommendation for the development of advisory material on shimmy design.

4. DASH 7 NOSE LANDING GEAR SHIMMY EXPERIENCE

4.1 The Occurrence of Shimmy

The nose landing gear on the DASH 7 airplane (see Figure 1) has two modes of operation, a castering mode with high angular damping – sometimes referred to as the "high damped mode" – and a steering mode with relatively low angular damping. Set for castering at touchdown, the nose gear automatically transitions to the steering mode by a weight-on-wheels switch.

In 1976, during the flight development trials, nose landing gear shimmy was experienced in the lower-damped steering mode. This resulted in two modifications to the design:

(1) the introduction of a 0.75 second time delay between the nose wheel weight switch closure and power steering activation to allow the spin-up transient to subside before switching into the lower damped steering mode.

(2) the introduction of a 0.01 inch diameter cross bleed damper in the steering mode to increase the angular damping in that mode. Further additional damping was prohibited by steering torque requirements.

The shimmy problem was thought to have been solved by these modifications as there were no further occurrences during the flight trials. However, by the Fall of 1980, reports of nose wheel shimmy were accumulating from aircraft in service. These problems took two forms, one involving feedback from the steering actuator and the second, the more classical process addressed during airplane development.

In the first case, shimmy occurred at relatively low speed and produced alarmingly large lateral oscillations of the airplane nose. One report tells of tire marks on the runway indicating angular deflections of up to 40° from centre in one direction and up to 35° degrees in the other. This rather violent form of shimmy was caused by backlash at the tiller input potentiometer to the steering actuator and a modification was introduced to eliminated the backlash. This type of 'system induced' shimmy problem will not be discussed further.

The second type of shimmy, unlike the first, occurred at relatively high speed and with fairly modest amplitude oscillations of the gear assembly at a relatively high frequency (approximately 20 Hz). It usually occurred with the steering system ON (ie., the mode with lower damping), but there were reports of shimmy with the steering system OFF as well.

This latter shimmy problem stimulated a broad range of immediate and longer term actions, all intended to achieve an expedient and lasting solution. The actions taken were:

(1) Introduce (large) "unpaved runway" tires across the fleet because there were fewer reported incidents of shimmy involving these tires.

(2) Recommend operational procedures for curtailing shimmy onset until a solution was found; specifically, that steering be left off during landing and that steering engagement be avoided at high speed.

(3) Undertake inspections of the nose landing gear to ensure that its modification status is current and its maintenance condition is to specification (e.g., wheels within balance, tires in good condition, etc.).

(4) Institute a questionnaire style reporting procedure to accumulate information on shimmy occurrences in service.

(5) Undertake taxi trials using a typically worn landing gear to obtain quantitative information on nose gear shimmy.

(6) Measure the frequency response characteristics of the steering actuator in an isolated test rig to establish its (dynamic) stiffness and damping properties as a function of frequency.

(7) Develop an in-house analytical methodology calibrated to the results obtained from the above tests. This analytical capability could then be used to evaluate the benefit of design treatments; such as, a torque link damper, torsionally coupled nose wheels (live axle), changes in trail, "mass balance", etc.

It is not the purpose of this report to review each and every action taken to resolve the DASH 7 nose gear shimmy problem; rather,

the purpose for presenting the above list is to indicate the effort required to resolve a shimmy problem when it is experienced in service. Following are some experimental and analytical results which were important in helping us develop a physical understanding of our nose gear shimmy process and in establishing our analysis methods.

4.2 Shimmy Test Results

The test results presented in Figures 2, 3 and 4 are instructive. In all cases, the ground speed is about 55 knots. Figures 2 and 3 apply to a "tight" gear for which free play in the scissors – the only significant source of free play – was removed using shims. In the case of Figure 2, the weight-on-wheels switch was deactivated to allow excitation by the spin-up transient and steering was ON at the outset. The result clearly shows the landing gear is fundamentally unstable at 55 kts in this low-damped configuration.

In Figure 3, the landing was made with the time delay circuitry operating in order to eliminate excitation by the spin-up transient. With steering OFF at touchdown, the large transient oscillations due to spin-up are observed to attenuate quickly, due to the relatively high damping in the castering mode. While small random vibrations persist, there is no evidence of shimmy after the time delay period when steering is ON, showing that the time delay was effective in circumventing the excitation of shimmy by the wheel spin-up transient.

Figure 4a shows results for which the shims in the torque scissors were removed to produce approximately 1/8 inch of free play in the scissor apex. Again, steering was OFF at touchdown and the transient oscillations are observed to decay to limit cycle oscillations within the free play range wherein, steering actuator damping has negligible effect. With steering ON – activated after the 0.75 second time delay – and with torsion damping thus decreased, the oscillations within the free-play band cause the gear to go unstable, that is, to shimmy (Figure 4b).

4.3 Analysis Model

The analysis model used to investigate shimmy follows the approach used by Lockheed in Reference 1. It consists of a torsion model defined relative to the inclined leg axis and a side displacement model (Figure 5). The torsion model is made up of 4 concentrated inertias to give the freedoms required to represent free play (backlash), bearing friction (coulomb damping) and torque scissor stiffness and free play (both functions of stroke). Fuselage torsion stiffness and trunnion attachment free play are also included in this model. Initially, the steering actuator stiffness was defined solely by the value of bulk modulus for hydraulic fluid which was assumed to have a value of approximately 100,000 psi (with typical air entrainment). This value was subsequently reduced to about 34,000 psi to account for the flexibility of the steering actuator structure determined from an isolated shake test of that unit.

The side displacement model used eliminates the y independent degree of freedom by assuming an infinitely stiff leg free to roll (ϕ) about an effective rotation point as illustrated in Figure 5b. As indicated in that figure, effective values for rotation arm length, inertia, damping and frequency are dependent on the length of the shock strut. Coulomb damping or free play is not included in the side displacement model.

The equations of motion for shimmy analysis, including the von Schlippe and Moreland tire models, are presented in Appendix A. The tire coefficients used in the equations derive directly from Reference 2, except for Moreland's tire time constant, τ_v, which was selected to conform with test results. The structural damping ratio, ξ_s, was assumed to lie in the range zero to 0.03.

4.4 Results

Stability analysis results for both the von Schlippe and Moreland tire models are presented in Figure 6 for the case of steering system ON and no free play. As noted, all curves except one apply for a single point model of the nose gear. Also plotted in Figure 6 is the damping result obtained from the test data given in Figure 2, a single point at 55 knots ground speed with a damping value of 0.007.

The predicted frequencies are not shown but lie in the 26 Hz range. This is about 20% higher than the value measured and is attributed to mass and stiffness modelling inaccuracies. The effect of this higher torsion frequency was determined by analysis to increase the predicted stability by 0.01; i.e., to lower the curves in Figure 6 by that amount.

With respect to damping, three curves are indicated to give reasonably good agreement to the test result in the 55 knot speed range: the von Schlippe single point result for $\xi_s = 0$, the von Schlippe distributed mass model result for $\xi_s = 0.03$ and the Moreland single point result for $\xi_s = 0.03$ and $\tau_v^* = 0.002$. Clearly, much better agreement with this single test point could have been obtained both in frequency and damping by applying arbitrary adjustments to the parameter values initially chosen. However, this was not pursued because the problem remained that no conclusion could be drawn as to which structural and tire models would give the most reliable result due to the lack of test data.

The analysis was extended to investigate the effect of free play using the distributed mass model (Figure 5a) and the von Schlippe tire model. These results demonstrate why free play must be avoided in landing gear design. Its presence can result in limit cycle vibrations at speeds lower than the classical shimmy speed – the speed obtained from the solution for a tight gear.

The addition of "mass balance" to the shock strut, was investigated as a means for improving nose gear stability. The results presented in Figure 8 show that the forward placement of weight has a stabilizing effect and that the most effective arm length, at least for this landing gear, is equal to the tire radius. This approach ultimately led to a modification – using a 25 pound bob weight – which was made available to operators as an option. While the increase in stability is predicted to be only 0.01, it is the authors' opinion, based on reported performance, that the mass balance modification is more effective than predicted.

5. DASH 8 MAIN LANDING GEAR SHIMMY EXPERIENCE

5.1 The Occurrence of Shimmy

Early in the design phase, the vendor for the main landing gear, using analysis methods which they considered reliable, reported that shimmy would occur within the operating speed range of the airplane and that torsion and side bending stiffnesses would have to be increased to achieve stability. Because of the weight increase involved, many months of intense analysis effort and debate were required before de Havilland and the landing gear vendor agreed on final design values.

5.2 Analysis Models

The main landing gear for the DASH 8 airplane is shown in Figure 9. The DASH 8 is a high wing aircraft with the main landing gear supported from within the nacelle. As a result, the landing gear is relatively long and flexible and therefore may be more prone to shimmy.

During the course of the shimmy investigation, a variety of gear structural models were developed ranging from simple "stick" (Figure 10), to full finite element. In all cases, except for the modal analysis discussed below, these structural models were used to define a 3x3 stiffness (or flexibility) matrix defined at the axle centreline in the single point analysis method.

In the modal analysis method, the finite element model for the landing gear and nacelle structure was extended to include a stick model for the wing with distributed mass and stiffness properties. The mode shapes and frequencies for this system were calculated and the shimmy equations were then set up and solved in modal form.

The single point analysis method was extended to include free play. Its effect was simulated (in a global sense) by replacing the linear stiffness matrix defined at the wheel axle centreline with a non-linear stiffness matrix having low angular stiffness, $k_{\psi\psi}$, within the free play range and full predicted stiffness outside that range. These equations were solved in the time domain.

Both Moreland and von Schlippe tire models were used to represent tire dynamic properties. However, the Moreland model was considered less reliable for absolute stability results because there was no empirical method for defining the tire time constant, τ_υ (see comments in Appendix A).

For structural damping, a typical value of $\xi_s = 0.03$ was assumed in the computations. However, no allowance for this damping was given in defining stability; that is, stability curves had to have a margin of 0.03 to be considered shimmy free.

5.3 Analysis Results

In January 1981, using the simpler "stick" models shown in Figure 10, de havilland confirmed that the landing gear would be unstable within the operating speed range and that the most effective way to increase the shimmy speed was to increase the torsion stiffness of the gear (at the time 1.13×10^6 lb-in/rad). Increasing the side bending stiffness was also determined to be important but not as important as increasing the torsion stiffness. It was also determined that shimmy stability could be improved by increasing the mechanical trail so the design was changed to increase the mechanical trail to the maximum extent possible.

The results from more elaborate analysis models indicated that a torsion stiffness of 2.2×10^6 lb-in/rad and a side bending stiffness in the range of 6,000 to 8,000 lb/in would be required to preclude shimmy. By mid 1981, these stiffness requirements grew to a high of 2.4×10^6 lb-in/rad and 14,000 lb/in. As noted above, it was only after a long, protracted period that the final design values of approximately 1.8×10^6 lb-in/rad and 7,600 lb/in, with nacelle flexibility included, were agreed to by both the vendor and de Havilland.

Final analysis results are presented in Figures 11 and 12. Stability in the side bending mode is of little interest because the damping values in this mode are high and increasing at speeds above the no-slip speed. Regarding torsion stability, Figure 11 shows the rigid wing giving generally conservative results compared to the full finite element analysis. Figure 12 shows stability in the torsion mode increases with stroke. The results indicate the landing gear to be stable for the complete operating speed range of interest with a damping margin of 0.03.

Summarized in Figure 13 are the results of a non-linear analysis to establish the influence of bearing friction and free play on shimmy. These results contributed to the specification of free play limits in the main landing gear design.

6. DISCUSSION

In the case of the DASH 7, it appears that the nose landing gear problem has been "contained" provided the tires are matched and in good condition, the wheels are kept in good dynamic balance, free play is limited and nose gear touchdown and taxi speeds are kept low. Nose gear mass balance is generally considered to be beneficial by those operators who elected to have that option. Obviously, the containment of nose gear shimmy has increased the maintenance cost, pilot workload and in some instances, the airplane weight.

In the case of the DASH 8, with over 400 airplanes in service, all shimmy free, it is safe to say that the main landing gear design has now been proven. However, the main concerns in this case are the time and effort required to establish the final design requirements and the degree of over-design (weight penalty) that may have been included in the final product.

7. RECOMMENDATIONS

At the time the DASH 8 was being designed, there was no well established consensus on what constituted a reliable shimmy design methodology. This still appears to be the case today. For this reason, it is recommended that some guidance information be provided - similar to an advisory circular issued by aircraft airworthiness authorities. This advisory material should:

- Establish standardized terminology
- Give guidelines on structural modeling
- Define tire models, including the assumptions and limitations
- Review and update tire properties and ranges of parameter variation
- Provide expressions for the tire terms appearing in the equations of motion for a variety of wheel configurations
- Recommend design analysis guidelines taking into account free play, recommended stability margins, structural and tire parameter variability, etc. (Table 1 suggests variances for some parameters appearing in the equations of motion and indicates whether they have a stabilizing or destabilizing effect on shimmy.)
- Provide guidelines on component and vehicle test procedures:
  - tire properties
  - structural properties (static and dynamic)
  - complete installed system
- Provide practical design information on anti-shimmy tires, live axle, etc.
- Provide standardized analysis cases for a variety of landing gear configurations
- Provide information on related vibration processes and problems - sometimes confused with shimmy - such as wheel unbalance, tire out-of-round, judder, anti-skid processes, steering feedback processes, gear walk, etc. Some of these processes may warrant separate advisory material of their own.
- Provide landing gear maintenance guidelines, based on analytical and experimental data, for minimizing landing gear vibrations
- Provide a bibliography

8. CONCLUDING REMARKS

As a consequence of the DASH 7 and DASH 8 shimmy problems experienced at de Havilland, the authors were required to develop analytical tools for problem solving and design. This work was accomplished successfully despite the lack of a 'standardized' industry accepted methodology at the time. It is the authors' contention that reliable shimmy design procedures are required and that it is feasible to do so. Had advisory material been available during the design of the DASH 7 and DASH 8 landing gears, de Havilland may not have had the problems outlined herein. At the very least, their resolution would have been more expeditious.

REFERENCES

(1) "Active Shimmy Control System", *AFFDL-TR-75-136*, Lockheed-California Company, Burbank California, December, 1975.

(2) Smiley, R. F., Horne, W. B. "Mechanical Properties of Pneumatic Tires with Special Reference to Modern Aircraft Tires", *NASA TR-R-64*, 1960

(3) Leve, H. L., "Designing Stable Dual Wheel Gears", *AIAA 69-769*, July 1969

(4) Moreland, W.J., "The Story of Shimmy", *Journal of the Aeronautical Sciences*, pp. 793 - 808 (1954).

(5) Collins, R. L., "Frequency Response of Tires using the Point Contact Theory", *J. Aircraft*, June 1972.

(6) Clark, S. K., "Dynamic Properties of Aircraft Tires", *J. Aircraft*, March 1974.

(7) Collins, R. L. and Black, R. J., "Tire Parameters for Landing-Gear Shimmy Studies", *J. Aircraft*, May-June 1969

(8) Grossman, "F-15 Nose Landing Gear Shimmy, Taxi Test and correlative Analyses", *SAE Paper*, No. 801239.

(9) "Shimmy Analysis Addendum to QTR No. ATR 923, 13.5 x 6.00 – 4, DR17922T 14 PR Outrigger Tire", Dunlop Manufacturing, England, September 1981.

(10) von Schlippe, B., "Shimmy of a Pneumatic Wheel", *NACA TM-1365*, August 1954

APPENDIX A. SHIMMY ANALYSIS MODELS

This Appendix describes the shimmy analysis methods developed at de Havilland.

A.1 Equations of Motion

A much simplified model for a single or dual wheel landing gear is illustrated in Figure A1 which shows an inclined shock strut with mechanical trail, L, measured parallel to the torsion axis and geometric trail, $L_G = R \times \sin\theta_g$, where θ_g is the inclination angle and R is the deflected tire radius.

Also shown in Figure A1 are two equally valid coordinate analysis systems, one located at the apex of the shock strut and the mechanical trail arm and aligned with the strut, and the other located at the wheel axle with axes orthogonal to the ground plane. The former system simplifies the mechanical terms in the equations of motion while the latter simplifies the tire force and moment terms. In order to expose more clearly the less familiar tire terms, the latter coordinate system is used in this report to

develop the equations of motion. These equations are written in terms of the lateral (y), roll (ϕ) and yaw (ψ) degrees of freedom defined at the wheel axle;

$$\mathbf{I}\ddot{U} + \mathbf{D}\dot{U} + \mathbf{G}\dot{U} + \mathbf{K}U = \begin{bmatrix} F_y \\ M\phi \\ M\psi \end{bmatrix} \quad \text{(A1)}$$

$$\mathbf{I}\ddot{U} + \mathbf{D}\dot{U} + \mathbf{G}\dot{U} + \mathbf{K}U = 0 \quad \text{(A2)}$$

where $$U = \begin{bmatrix} y \\ \phi \\ \psi \end{bmatrix}$$

and where **I** = inertia matrix
D = damping matrix
G = gyroscopic matrix
K = stiffness matrix

A.2 Structural Terms

Formulations for the left hand side terms are not given in this report but they can be found in References 1 and 3. It is imperative that utmost care be taken in defining and verifying the assumptions made in establishing the analysis model and in developing the data used. For instance, if a landing gear is assumed to be a uniform structure, its mass and inertia effects can be 'lumped' at the wheel axle and a 'single point' model analyzed. In this case the mass and inertias of the wheel rolling assembly should be supplemented with appropriate effective masses and inertias of the supporting gear structure. The 3x3 mass matrix, **M**, will contain (off-diagonal) terms that couple the three degrees of freedom, y, ϕ and ψ. If it is important to include detailed representations of bearing friction or free play (backlash), then a distributed mass model will be required to provide the additional degrees of freedom needed to represent these characteristics.

The damping matrix, **D**, should include both structural and bearing friction damping terms, if appropriate. As indicated above, this may require the development of a more complex gear dynamic model than can be expressed by a single point formulation with 3x3 matrices.

The gyroscopic matrix contains roll-yaw coupling terms with coefficients $I_\omega \times (V/R_T)$ where I_ω is the polar moment of inertia of the wheel rolling assembly, V is the ground speed and R_T is the tire undeflected radius.

As in the case of the mass matrix, if the gear structure is assumed to be uniform, its stiffness properties can be represented by a 3x3 stiffness matrix, **K**, defined at the wheel axle. Once again, if it is important to include detailed representation of bearing friction or free play, then additional degrees of freedom and stiffness terms will be required.

Finally, the mass, stiffness and damping effects of the landing gear's supporting structure should be included in the equations of motion because they can have a strong effect on the stability results.

A.3 Tire Terms

During shimmy, the motions of the gear axle are coupled not only through the gear structure as expressed by the terms on the left hand side of equation (A1) but also through the interaction between the tire and ground, as represented by the tire forces and moments appearing on the right hand side of that equation.

Two tire models were considered, the Moreland "Point Contact" model and the von Schlippe "Stretched String" model. Both models are presented below in a coordinate system orthogonal to the ground plane. This was done in order to develop the simplest possible expressions for the tire forces and moments. Formulations for single and dual wheel assemblies are included.

A.4 The Moreland Point Contact Model (Single Wheel)

The Moreland point contact model (Reference 4) expresses the tire contact forces and moments in terms of the tire cornering force, F_c , and pneumatic trail, ε_p , as follows (Figure A2):

$$\begin{bmatrix} F_y \\ M\phi \\ M\psi \end{bmatrix} = \begin{bmatrix} F_c \\ RF_c \\ -\varepsilon_p F_c \end{bmatrix} \quad \text{(A3)}$$

where

$$F_c = K_{Ty}\Delta + C_{Ty}\dot{\Delta} \quad \text{(A4)}$$

and where K_{Ty} = tire lateral spring constant
C_{Ty} = tire lateral damping coefficient
ε_p = pneumatic trail parallel to ground
Δ = tire lateral deflection (elastic)
R = tire (deflected) rolling radius

To enable a solution of the shimmy equations, Moreland postulates an alternate expression for the tire cornering force in terms of a tire cornering power, C_ψ , and time constant, τ_υ , as follows:

$$F_c = C_\psi \Psi_t + C_\psi \tau_\upsilon \dot{\Psi}_t \quad \text{(A5)}$$

where Ψ_t = the tire elastic twist deflection

Finally, Moreland assumes the absence of slipping or scrubbing between the tire and ground by imposing the kinematic relationship;

$$\dot{y} + \dot{\Delta} + V(\Psi + \Psi_t) = 0 \quad \text{(A6)}$$

Embodied in the above kinematic relation is the assumption of no slipping or scrubbing. According to the empirical data presented in References 5 and 6, this assumption is invalid and therefore, "classical" shimmy is not likely to occur at ground speeds

$$V < \frac{\omega h}{0.8} \quad \text{(A7)}$$

where ω is the shimmy frequency and h is half the tire footprint length. (The von Schlippe model described below also assumes that no slipping or scrubbing occurs between tire and ground and therefore it too is subject to the same speed limitation.)

Empirical values for the tire parameters appearing in the above equations can be obtained from Reference 2 with one notable

exception - the tire time constant, τ_υ. Choosing a reliable value for τ_υ is generally a problem because no consistency can be found in the literature for this parameter as illustrated by the compiled data of Figure A3. Since τ_υ has a strong influence on the results, it is recommended that the value used should be validated in some way if the results are to be accepted in absolute terms.

Also, while empirical values for the pneumatic trail, ε_p, are available, some analysts prefer to base the tire torsion moment, M_t, directly on the tire torsional stiffness $K_{T\alpha}$, viz;

$$M_t = K_{T\alpha}\psi_t \tag{A8}$$

instead of using the expression proposed by Moreland. This variation has not been used in the present report.

A.5 The von Schlippe Stretched String Model (Single Wheel)

The von Schlippe tire model (References 10 and 1) assumes that the tire equator is represented by a "stretched string" that takes on the deflected shape shown in Figure A4 due to out-of-plane motions. In this model the tire forces and moments are:

$$\begin{bmatrix} F_y \\ M_\phi \\ M_\psi \end{bmatrix} = \begin{bmatrix} F_t \\ RF_t \\ -M_t \end{bmatrix} \tag{A9}$$

where

$$\begin{aligned} F_t &= K_{Ty}\Delta + C_{Ty}\dot{\Delta} \\ M_t &= K_{T\alpha}\psi_t \end{aligned} \tag{A10}$$

and where the tire elastic lateral and torsional deflections are given by:

$$\begin{aligned} \Delta &= \frac{Z+\hat{Z}}{2} \\ \psi_t &= \frac{Z-\hat{Z}}{2h} \end{aligned} \tag{A11}$$

As before, h equals half the footprint length.

Z and $\hat{Z}$ are defined in Figure A4 from which the following geometric relationships can be deduced.

$$\begin{aligned} Z &= Y - y - R\phi - h\psi \\ \hat{Z} &= \hat{Y} - y - R\phi + h\psi \\ \hat{Y}(t) &= Y\left(t - \frac{2h}{V}\right) \end{aligned} \tag{A12}$$

Finally, the kinematic relationship that assumes no slippage between the tire and ground is given by the following expression in terms of the yawed-rolling relaxation length, λ_G. This geometric relationship can also be deduced from Figure A4.

$$\frac{\lambda_G}{V}\dot{Y} + Y = y + R\phi + (\lambda_G + h)\psi \tag{A13}$$
(A14)

Empirical values for all of the parameters required by the von Schlippe tire model can be obtained from Reference 2. It might be noted that some analysts also extend the expression for M_t by including the tire torsion damping term, $C_{T\alpha}$, viz;

$$M_t = K_{T\alpha}\psi_t + C_{T\alpha}\dot{\psi}_t \tag{A15}$$

This variation has not been used in the present report.

A.6 Dual Wheel Gears

The Moreland and von Schlippe tire models given above apply for a landing gear with a single wheel. The following steps extend those formulations to dual wheel landing gears:

(1) Factor the force and moment expressions by 2

(2) Add the following rolling moment term to account for the vertical ground reaction forces. Assuming the total static force, F_z, is shared equally, the ground reaction force on each tire is comprised of a static force and a dynamic force due to roll displacement ϕ. Thus,

$$\Delta M_\phi = L_R\left(F_z^L - F_z^R\right) \tag{A16}$$

where the (upward acting) ground reaction forces on the right and left tires are, respectively;

$$\begin{aligned} F_z^R &= \frac{F_z}{2} + L_R\phi K_z \\ F_z^L &= \frac{F_z}{2} - L_R\phi K_z \end{aligned} \tag{A17}$$

and where L_R = half axle length
K_z = the tire vertical stiffness

(3) Add the following yawing moment term to account for the ground friction force;

$$\Delta M_\psi = L_R\mu\left(F_z^L - F_z^R\right) \tag{A18}$$

where μ = tire rolling friction coefficient.

TABLE 1 SIGNIFICANT FACTORS AFFECTING SHIMMY

PARAMETER	ACCURACY OF VALUE ± %	DIRECTION FOR STABILITY
GEAR LATERAL BENDING STIFFNESS	50	+
GEAR TORSION STIFFNESS	50	+
GEAR YAW INERTIA	20	-
TIRE RELAXATION LENGTH *	50	+
TIRE FOOTPRINT LENGTH *	20	+
TIRE TORSION STIFFNESS *	40	-
TIRE TORSION DAMPING *	15	+

* NOMINAL TIRE DATA FROM REFERENCE 2 FOR TYPE VII TIRE

FIGURE 1 DASH 7 NOSE LANDING GEAR

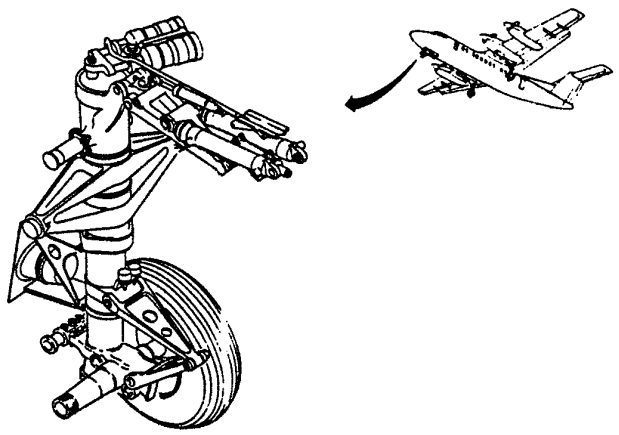

FIGURE 2 DASH 7 NOSE LANDING GEAR TESTS
STEERING "ON", TIME DELAY "OFF", NO FREE PLAY

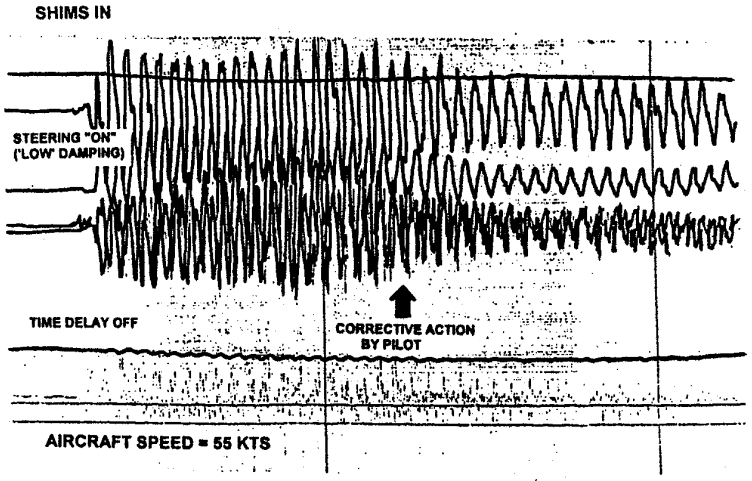

FIGURE 3 DASH 7 NOSE LANDING GEAR TESTS
STEERING "OFF", TIME DELAY "ON", NO FREE PLAY

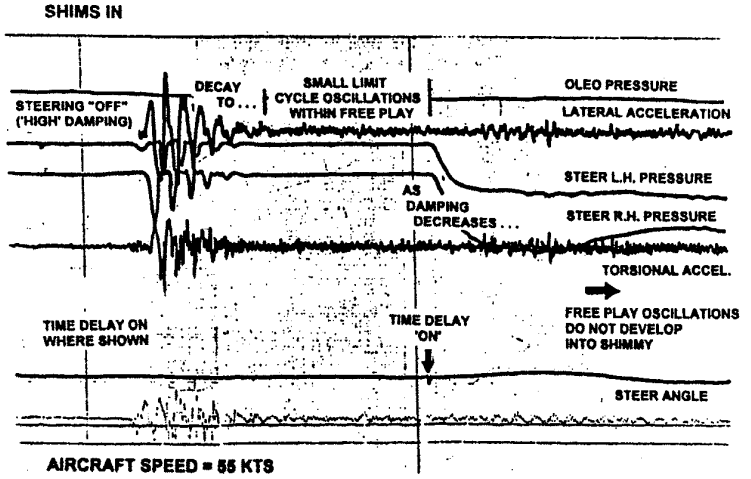

FIGURE 4a DASH 7 NOSE LANDING GEAR TESTS
STEERING "OFF", TIME DELAY "ON", FREE PLAY

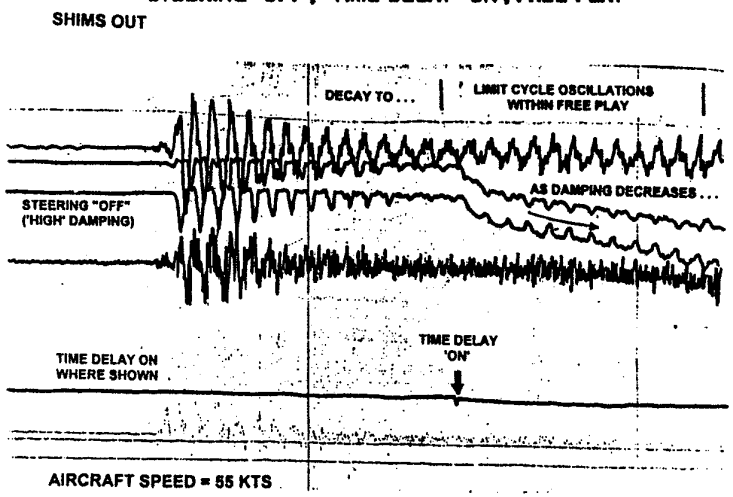

FIGURE 4b DASH 7 NOSE LANDING GEAR TESTS
STEERING "OFF", TIME DELAY "ON", FREE PLAY

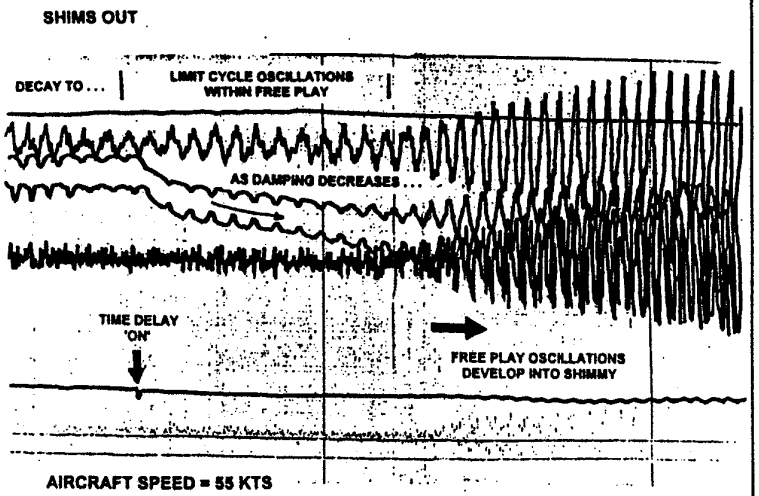

FIGURE 5 DHC-7 NOSE GEAR ANALYSIS MODEL

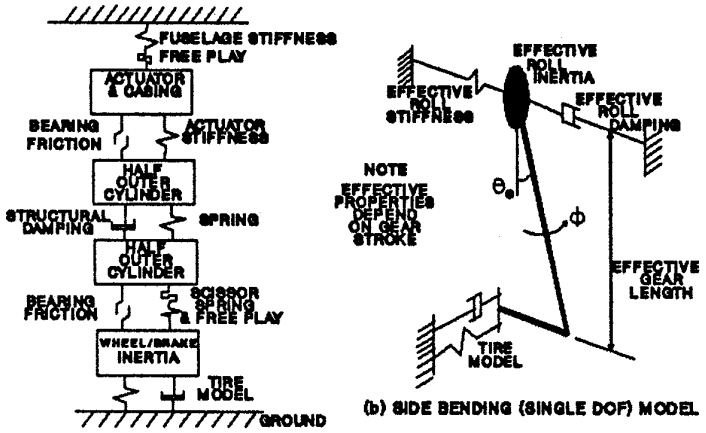

FIGURE 6 DASH 7 NOSE GEAR SHIMMY
CORRELATION WITH TEST (FIGURE 2)

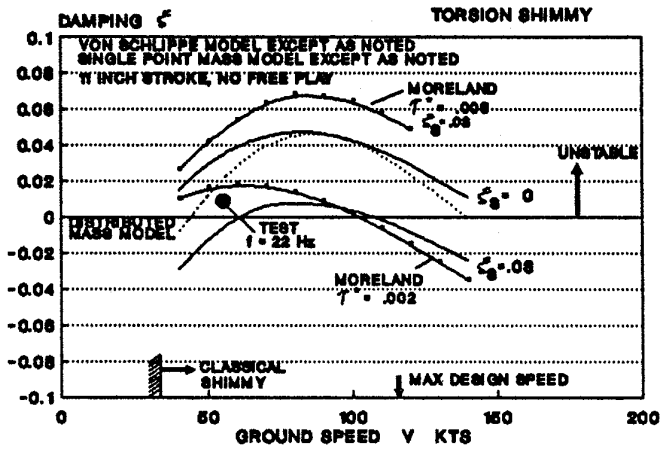

FIGURE 7 DASH 7 NOSE GEAR SHIMMY
EFFECT OF FREE PLAY - STEERING ON

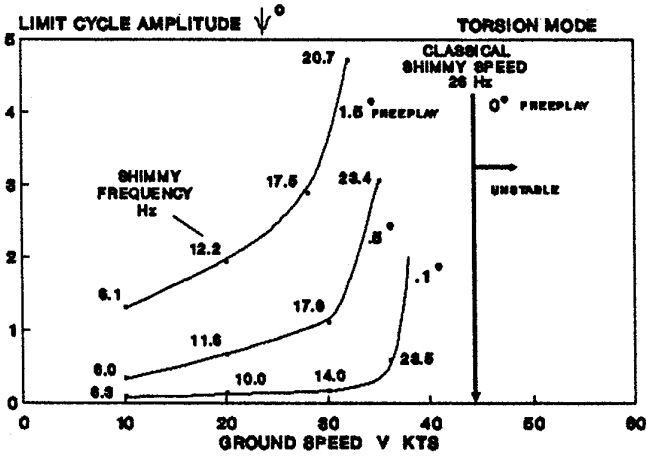

FIGURE 8 DASH 7 NOSE GEAR SHIMMY
EFFECT OF MASS BALANCE - STEERING ON

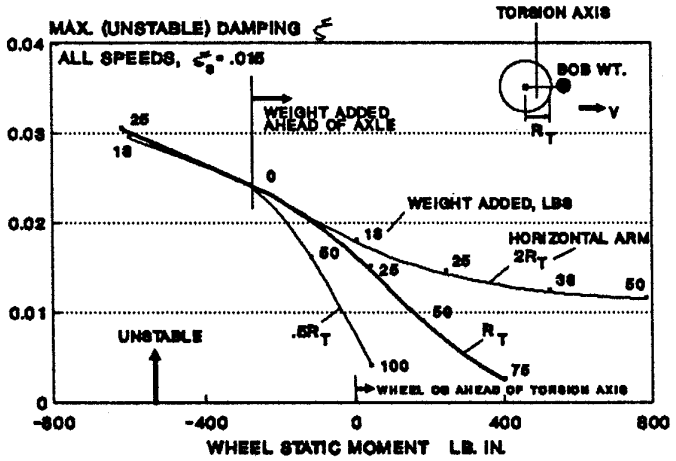

FIGURE 9 DASH 8 MAIN LANDING GEAR

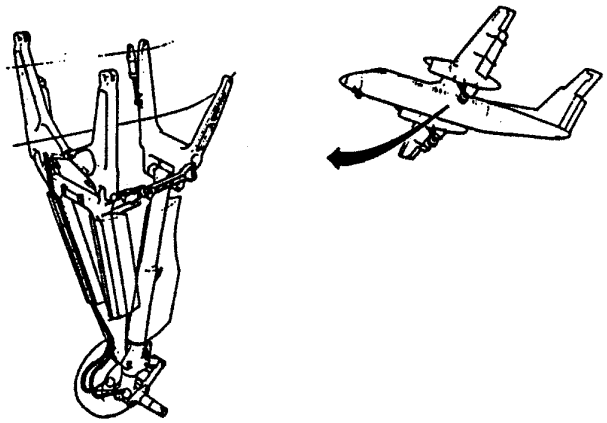

FIGURE 10 DASH 8 MAIN LANDING GEAR
SIMPLE "STICK" ANALYSIS MODELS

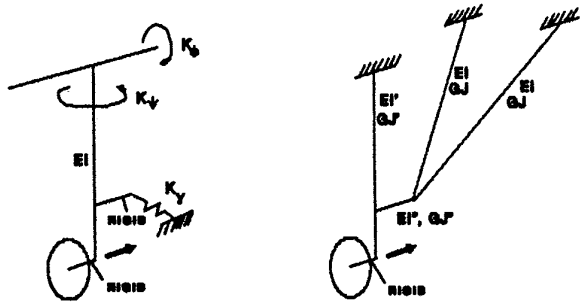

NOTE: FULL FINITE ELEMENT MODELS ALSO USED

FIGURE 11 DASH 8 MAIN GEAR SHIMMY
EFFECT OF WING FLEXIBILITY

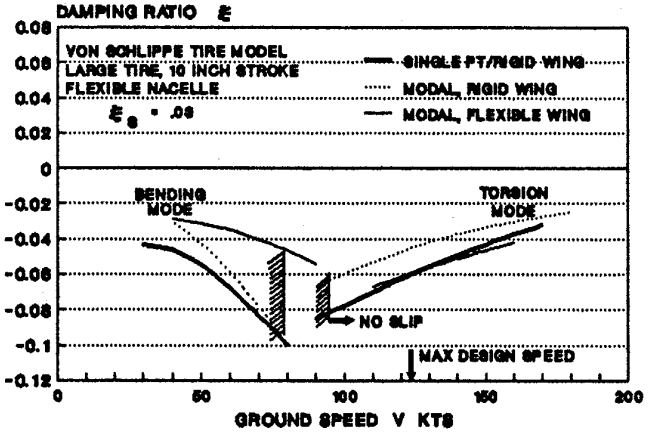

FIGURE 12 DASH 8 MAIN GEAR SHIMMY
EFFECT OF TIRE SIZE AND GEAR STROKE

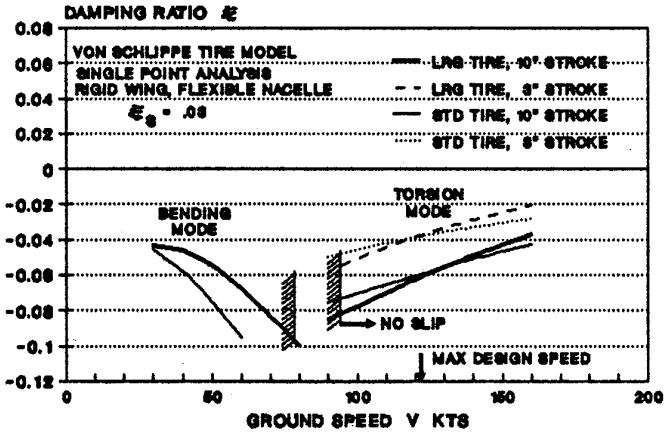

FIGURE 13 DASH 8 MAIN GEAR SHIMMY
EFFECT OF FREE PLAY AND BEARING FRICTION

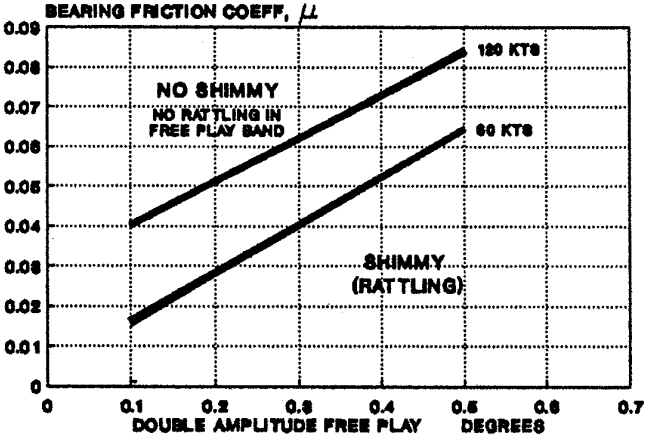

FIGURE A1 LANDING GEAR COORDINATE SYSTEMS

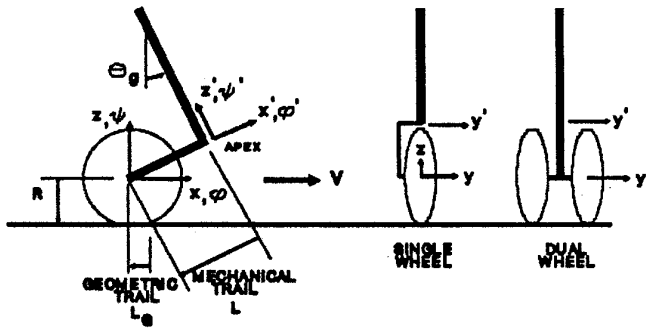

FIGURE A2 MORELAND TIRE MODEL GEOMETRY

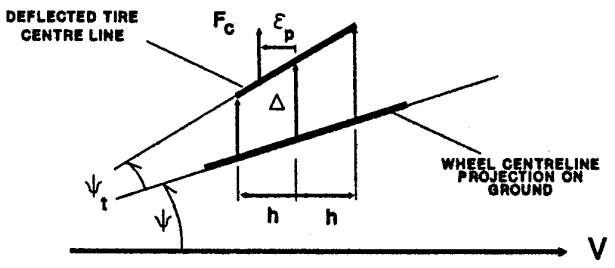

VIEW LOOKING DOWN

FIGURE A3 MORELAND'S TIME CONSTANT MEASURED AND SUGGESTED

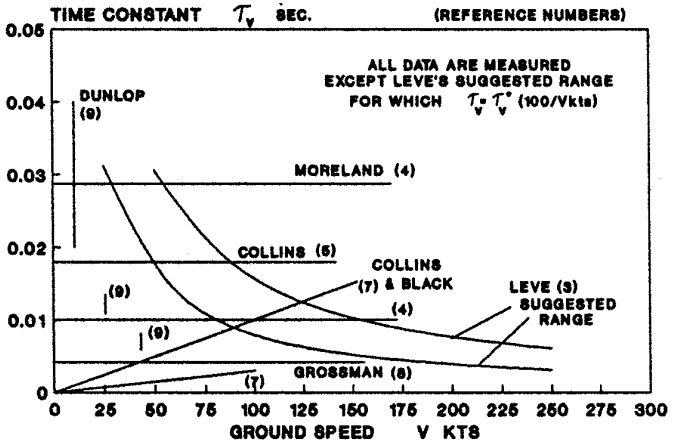

FIGURE A4 VON SCHLIPPE TIRE MODEL GEOMETRY

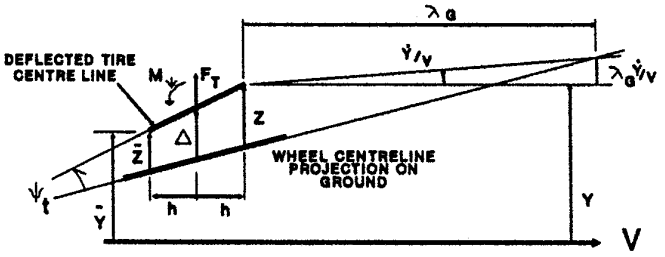

VIEW LOOKING DOWN

FIGURE A5 DUAL WHEEL GEARS ADDITIONAL TIRE TERMS

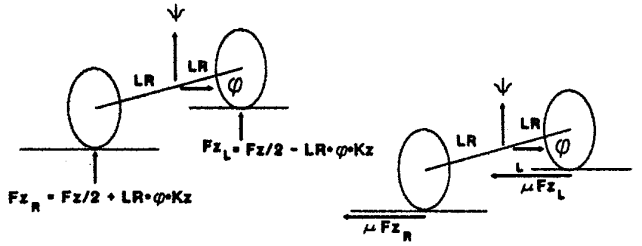

VERTICAL DRAG

Unsteady Tire Dynamics and the Application Thereof to Shimmy and Landing Load Computations

Klaus Koenig
Daimler-Benz Aerospace Airbus GmbH
Hünefeldstraße 1-5
28199 Bremen, Germany

SUMMARY

A complete set of nonlinear equations of unsteady tire dynamics for all the 6 degrees of freedom of the wheel movement is presented. The coefficients of these equations are based on available publications and may need some improvements.
The influence of some of the coefficients which are new or controversely discussed is shown revealing areas of caution and stressing the necessity of adequate tire tests.
Nevertheless it could be demonstrated that reasonable shimmy analyses are possible with these equations and that the computation of realistic unsymmetric landing impacts require their inclusion as a must.

1. INTRODUCTION

The wheel – without example in nature – is one of the most efficient inventions of human spirit and a fundamental element of technical constructions. The inflated tire is a relatively new additive to the wheel but most probably its best improvement.
Modern civilization is inconceiveable without wheels and tires. Millions of them are rolling on the streets every day and every minute . But in spite of the huge application of tires no comprehensive mathematical description of their characteristics is available.
It is nearly unbelievable but it seems that all the progress of modern transportation technique was possible without a qualified theory of tire dynamics. There are early publications with rather good results already 50 years ago but there is no reliable up–to–date theory available (s. ref. 8).
What are the reasons? Is there really no need for a better theory? Was it too expensive to establish one? Was it just not published or available or was it too difficult for the engineers?

Tire dynamics is characterized as the dynamics of any ordinary vibrator by the interaction of elasticities and masses. But superimposed in this special case is the creeping process within the contact area between tire and ground – the so called relaxation mechanism.
One of the earliest studies of tire behavior was performed by Fromm at the German university of Danzig. The first real shimmy theory was published by von Schlippe and Dietrich (s. ref. 1). The last fundamental collection of applicable data was presented by Smiley and Horne (s. ref. 2) in 1960.
So what is available in 1995 can only be called a substitute or "stopgap" but not an applicable theory of modern tires for reliable dynamic studies of dynamic structures.
Therefore in the following first some thoughts are spent on how to get qualified tire data. After that published shimmy theories are compared. Based on this and together with some amendments from other sources a complete set of equations for tire dynamics is given. Eventually, its application to shimmy and landing loads computation is studied.

2. GENERAL TIRE DYNAMICS

The most simple way to establish reliable tire dynamics at least applicable to shimmy or linear stability studies would be to put a rolling wheel with tire on a drum to excite the wheel at its centre by frequency sweeps of deflections and to measure the load response. If this is done at a well defined working point of the tire and subsequently for all the 6 components of the deflection applicable at the wheel centre 36 transfer functions (frequency response functions) for all the 6 possible perturbations of the steady state movement of the wheel centre will be available. Each transfer function can be linearly approximated by a fraction of polynominals of the imaginary Fourier frequency.

If one uses as a first approximation the same denominator polynomial for the same load component and accepts that for linear systems superposition is possible, then Fourier transformation allows to establish with the polynomial coefficients the simple matrix equation*:

$$\sum_{n} Bn \cdot \overset{(n)}{p}_{tR} = \sum_{m} Wm \cdot \overset{(m)}{r}_{tA}$$

where $p_{tR} = \lfloor px_{tR}, py_{tR}, pz_{tR}, p\phi_{tR}, p\theta_{tR}, p\psi_{tR} \rfloor'$
is the perturbation vector of loads and $\overset{(n)}{p}_{tR}$ its derivative to the time

$r_{tA} = \lfloor x_{tA}, y_{tA}, z_{tA}, \phi_{am}, \theta_{rr}, \psi_{mt} \rfloor'$
is the perturbation vector of wheel centre deflections

Bn,Wm are coefficient matrices.The diagonal Bn contains the denominator and the complete Wm the nominator coefficients of the n'th or m'th order polynomials

That is all, at least for the small perturbations of shimmy.

**The more general solution would result in 36 scalar differential equations which must be solved first to allow a summation of the 6 load portions of each load component caused by the 6 different excitations.*
By the way, for second order polynomials one would get 2 times 36 eigenvalues. That would allow 36 possible tire load oscillations without wheel movement perturbations and 36 wheel movement oscillations without tire load perturbations.

Paper presented at the 81st Meeting of the AGARD SMP Panel on "The Design, Qualification and Maintenance of Vibration-Free Landing Gear", held in Banff, Canada from 4-5 October 1995, and published in R-800.

For larger deformations as they occur at landing impact further investigations with larger amplitudes and with and without rolling velocity are necessary.
But this should be a second step to be defined in detail after successful execution of the first one with small perturbations.
Partially such studies have already been performed (s. ref. 5) but no complete test result is known to the author.
Nevertheless, since no principle obstacle to such an approach to establish reliable equations of tire dynamic is evident, it can be hoped that perhaps in another 50 years such data will be available for the benefit of future engineers and of technical progress – if further progress is ever wanted at that time.

3. COMPARISON OF SOME PUBLISHED TIRE EQUATIONS

The following publications will be compared:
- von Schlippe, and Dietrich, (s. ref. 1)
- Smiley, (s. ref. 3)
- Pacejka, (s. ref. 4)
- Rogers, and Brewer, (s. ref. 5) with the Moreland theory.

If the equations of movement as given in these publications are transformed to the coordinate system of Fig. 3–1 and linearized by series developments up to elements of second order coefficients for matrices B and W as defined in chapter 2 can be derived as given in table 3–1.
These equations are given in their original symbols without further explanation of the symbols.
Nevertheless some basic conclusions can be drawn:
- There are really only diagonal elements in the B matrices.
- $B_{\cdot yy} = B_{\cdot\phi\phi} = B_{\cdot\psi\psi}$ are equal for all theories . This may mean that the tire can vibrate in itself with a single mode, showing at least 3 different load components
- The different theories don't place coefficients at the same places.
- A larger portion of the matrices is non–symmetric.
- Von Schlippe and Dietrich do not study the tilt. Pacejka does not give tilt moments .
- Remarkable are the missing coefficients $W1_{y\psi}$, $W2_{y\psi}$, in the theories of Smiley and Pacejka, the missing coefficient $W2_{\psi\psi}$, $W0_{y\phi}$, $Wo_{\phi\phi}$, $W0_{\psi\phi}$ in Moreland's theory and the missing coefficient $W2_{\psi y}$ in Pacejka's theory.
- The absence of the elements $W0_{yy}$, $W0_{\phi y}$, $W0_{\psi y}$ is caused by the relaxation mechanism. Loadings caused by sideward deflections will disappear with time.
- The theories of von Schlippe and Dietrich, Smiley and Pacejka look rather similar, they are based on equal basic thougths. The Moreland theory is fundamentally different
- Moreland introduces a time constant C_1 [sec] for description of the relaxation mechanism while the other theories use a relaxation length [m]. This leads to the fact that e.g. $B2_{\cdot\cdot}$ depend only on the rolling velocity v in the Mooreland theory but on v^2 in the other theories.
- Moreland originally only studied ψ. The extension by y was introduced by Rogers and Brewer, and the extension by ϕ by Edman (9).

4. A COMPLETE SET OF TIRE EQUATIONS

For the following, Smiley's equations as given in chapter 3 will be used as a basis. They are modified by neglection of minor unknown elements (ξ=0) inclusion of information from ref. 2 ($W0_{y\phi}$, $W0_{\phi\phi}$, $W0_{\psi\phi}$), assumption of symmetry ($W1_{\phi y}$, $W2_{\phi y}$) and some other simplifications ($W0_{\phi\psi}$: analog to $W1_{\psi y}$ and $W1_{\phi\phi}$, $W2_{\phi\phi}$: reduction to the main element). But this is not sufficient. Even for tire rolling in steady state one needs information for the x,z and ϑ components. They are taken from ref. 2 and 6 and mainly based on radial tire stiffness and respectively the assumption that x loads depend on a friction coefficient and that this coefficient itself depends on the slip ratio as shown in Fig. 4–1.

For the not free rolling tire in the spin up phase of landing the situation is more complicated. Nearly nothing is known. The only fact is, that for the pure sliding, all horizontal ground loads depend on the vertical load and a friction coefficient while their direction is opposite to the movement.

To have at least something in hand a very crude assumption was made. It defines that during the spin up phase both types of loads are acting but the one for pure rolling with a factor between 0 and 1 increasing with the slip ratio and the other one for pure sliding decreasing in the same way down from 1 to 0 until the slip ratio reaches its zero for the first time.
More details of the derivation should not be given here to avoid any boredom. But the final result is presented in table 4–1.
These are rather complicated non linear equations but they should be valid for the whole landing process of horizontal landings.

5. SHIMMY ANALYSES

5.1. Tire Equations

First linearized tire equations should be derived from the nonlinear set given in table 4–1.
Details are given in table 5.1–1. This leads to extended equations of unsteady tire loads for all the 6 degrees of wheel freedom.

5.2. Influence of Tires on Shimmy

To study this it is reasonable to look at a rigid undercarriage to avoid coupling of structure and tire elasticity. For the most simple rigid model of Fig. 5.2–1, after some rearrangements, one obtains the equations of motion

$$0 = 2 \cdot p - (d_R/z_0) \cdot I_p \cdot \ddot{\theta} - 2 \cdot Iw \cdot \ddot{\psi}_{st} - d_s \cdot \dot{\psi}_{st}$$

$$0 = z_0 \cdot W1_{xx} \cdot (2 \cdot d_R \cdot \psi_{st} + r_r \cdot \theta) - Ip \cdot \dot{\theta}$$

$$B2 \cdot \ddot{p} + B1 \cdot \dot{p} + p = \psi_{st} \cdot (W0_{\psi\psi} - L_R \cdot W0_{y\psi}) +$$

$$+ \dot{\psi}_{st} \cdot (W1_{\psi\psi} - L_R \cdot (W1_{\psi y} + W1_{y\psi}) + L_R^2 \cdot W1_{yy}) +$$

$$+ \ddot{\psi}_{st} \cdot (W2_{\psi\psi} - L_R \cdot (W2_{\psi y} + W2_{y\psi}) + L_R^2 \cdot W2_{yy})$$

with

$$2 \cdot p = p\psi(R1) + p\psi(R2) - L_R \cdot (py(R1) + py(R2))$$

$$\theta = \theta_{ra}(R2) - \theta_{ra}(R1)$$

$$I_W = I_R + m_W \cdot (d_R^2 + L_R^2)$$

I_R = radial moment of inertia of wheel including tire

I_p = polar moment of inertia of wheel including tire

d_s = swivel damper constant

An eigenvalue analysis of these equations delivers frequencies and modal dampings. Different cases were analyzed and compared.

Variant S :
$K_\lambda = 44145$ N/m
$K_\alpha = 298.224$ Nm/rad
$L_1 = 0.142222$ m
$L_2 = 5.1136 \cdot 10^{-3}$ m²
$I_R = 0.051993$ kg·m²
$m_w = 2.4525$ kg
$K_\tau = 0$
$W1_{xx} = 0$

These are the original data from ref. 3 case I approximation B. They are based on a test performed by v. Schlippe and Dietrich.
Fig. 5.2–2 shows eigenfrequencies and modal dampings over the rolling velocity for the single wheel case $d_R = 0$, $L_R = 0{,}08$m, $d_s = 0{,}06$ Nm/(rad/sec).The eigenvalues of the decoupled tire mode are included.
One can discern that the frequencies of the tire modes increase with velocity, while the frequencies of the shimmy mode remains about constant.
The dampings of the tire modes are rather large. The damping of the shimmy mode crosses zero at about 3,7 m/s. At larger velocities the system is instable.
Fig. 5.2–3 shows the stability areas and the shimmy frequencies on the stability boundary for different swivel damping values d_s together with the test results of v. Schlippe and Dietrich and theoretical results from Smiley ref. 3.
Smiley's results were computed without swivel damper. The agreement is rather good. With $d_s = 0{,}6$ Nm/(rad/see) the computation fits to the test results.

In Fig. 5.2–4 the influence of x and θ movement is studied. Unfortunately no measured tire data are available to do this.
So an estimation, Variant E was necessary which should approach to Variant S.
Used are (Variant E) :
Type III
$p_R(0) = 1765.8$ N
$z_p = 0.02$ m
$r_0 = 0.13$ m
$z_0 = 0.12$ m
$d_R = 0.085$ m
$p_i = 225630$ N/m²
$p_r = p_i$
$\mu_r = 0$
$\mu_k = 0.8$
$s_k = 0.2$
$m_w = 2.4525$ kg
$I_R = 0.051993$ kg m²
$I_p = 0.0981$ kg m²
$m_t = 0$

For the single wheel case the estimation did not lead to exactly the same stability areas as Variant S.
For the double wheel first only the wheel distance d_R was introduced to show the influence of the increased swivel inertia $2 \cdot mw \cdot d_R^2$. Then the polar inertia I_p of the wheel was introduced and the influence of the swivel damper shown. Finally the tire coefficients $W(x,\theta)$ are added.
As one can see there are some influences. The shimmy velocity of the double wheel is smaller than that of the single wheel. Both the swivel and polar inertia contribute to this effect.
For smaller trails there is no influence of the tire coefficients $W(x,\theta)$ while for larger trails the influence is strong and increases the shimmy velocity.

Fig. 5.2–5 shows the influence of some other coefficients. Basis is again Variant S.
First $W1_{y\psi}$ is studied since it was $W1_{y\psi} \neq 0$ in the Moreland theory. $W1_{y\psi} = W1_{\psi y}$ was tried (case a) but a completely different stability boundary occurred, absolutely not in agreement with the test results. Next by analogy with $W2_{yy} / W1_{yy}$ it was set $W1_{y\psi} = K_\lambda \cdot L_2 / v$ (case b) but with the same result. Even the inclusion of a swivel damper did not help.
Another critical element is $W2_{\psi\psi}$ which is not included in Moreland's theory. But with $W2_{\psi\psi} = 0$ the whole stability area for smaller trails disappears.
Eventually a different influence of v in $W2_{yy}$ and $W2_{\psi\psi}$ was studied (case c) to allow better comparison with the Moreland theory. It was assumed that $W2_{yy}$ and $W2_{\psi\psi}$ were measured at 3 m/s and that these coefficients depend only on 1/v but not on $1/v^2$.
The result was not very different as one can see in Fig.5.2–5.
So the final conclusion is that detailed tests are necessary to check $W1_{y\psi}$ and $W2_{\psi\psi}$.
Caution is necessary and if nothing better is known the coefficients given by Smiley should be chosen.

6. COMPUTATION OF THE LANDING IMPACT-

For the landing impact often just the vertical stiffness of the tire and a friction coefficient are considered. But that is not adequate in our times. With modern computers equations as given in table 4–1 can be handled without problems.
Of course the inclusion of such tires is only reasonable if also the elasticity of the undercarriage structure is adequately modelled.
At least 6 degrees of freedom for each wheel centre should be available and the variation with shock absorber deflection should be included. Ref. 7 gives some indications how to do this.
Fig. 6–1 gives an example of a computation. Loads at the right and left main undercarriage together with shock absorber deflection (u) and parameters of the aircraft movement are shown. The results belong to a smaller aircraft with one wheel per undercarriage. The landing conditions are 2.44 m/s sink speed ($\dot{z}_{tS}$), 69.5 m/s horizontal speed ($\dot{x}_{tS}$), 9 degrees pitch (ϑ_{ft}) and 8 degrees yaw (ψ_{ft}) angle. ϕ_{ft} is the bank angle and $\dot{y}_{tS}$ the lateral velocity of the aircraft centre of gravity. p_L is the total lift. The tire loads are px_{tR}, py_{tR}, pz_{tR} and the undercarriage loads at the wheel centre are px_{uU}, py_{uU}, pz_{uU}. The $p\cdot_{tR}$ are measured parallel to the ground, the $p\cdot_{uU}$ are measured in a coordinate system of the undercarriage. The undercarriage loads include the tire loads and the wheel inertia loads.

In Fig. 6–1 one can see first of all how different the loads of the two undercarriages are.
Further, one can clearly discern that the loads oscillate and that this oscillation was obviously induced by the wheel spin up / spring back effect.
The large sideloads are remarkable. They reach their maximum after spin up – on the rolling tire. They are nearly doubled on the undercarriage if compared with the loads on the tire and they don't always decay with the vertical loads. They are mainly caused by the tire dynamics and can not be predicted without such a complete set of equations as presented above in table 4–1. Since the whole movement of the aircraft in this unsymmetric landing case is determined by the sideloads one can conclude that no prediction of the unsymmetric impact loads which is in the least reliable can be computed without inclusion of the complete tire dynamics of the rolling tire under varying vertical deflections.
A measurement on the flying aircraft instead comes comparatively late and is tremendously more expensive.

Finally it should be said that also a shimmy analysis together with the landing impact may be more realistic and would cover a larger area of possible instabilities including nonlinear effects.

REFERENCES

1. Von Schlippe, B. and Dietrich, R.
"Zur Mechanik des Luftreifens"
ZWB Verlag Oldenbourg, München, 1942

2. Smiley, R.F. and Horne, W.B.
"MECHANICAL PROPERTIES OF PNEUMATIC TIRES WITH SPECIAL REFERENCE TO MODERN TIRES"
NASA TR–64, 1960

3. Smiley, R.F.
"CORRELATION, EVALUATION AND EXTENSION OF LINEARIZED THEORIES FOR TIRE MOTION AND WHEEL SHIMMY"
NACA–TN–3632, 1956

4. Pacejka, H.B.
"THE WHEEL SHIMMY PHENOMENON"
Dissertation TH Delft, 1966

5. Rogers, L.C. and Brewer, H.K.
"Synthesis of Tire Equations for Use in Shimmy and Other Dynamic Studies"
Journal of Aircraft Vol.8 No.9, Sept.1971, p.689–697

6. Horne, W.B. and Leyland, T.J.W.
"INFLUENCE OF TIRE TREAD PATTERN AND RUNWAY SURFACE CONDITION ON BRAKING FRICTION AND ROLLING RESISTANCE OF MODERN AIRCRAFT TIRE"
NASA–TN–D 1376

7. Koenig, K.
"Die Lasten des Landesstoßes"
ZFW 3 (1979) H6, p.344–360

8. Krabacher, W.E.
"Aircraft Landing Gear Dynamics Present and Future"
SAE–paper 931400 (1993, Dayton Conference)

9. Edman,J.L.
"Experimental Study of Moreland's Theory of Shimmy"
WADC Techn. Rep. 56–197 (July 1958)

	v. Schlippe+Dietrich	Smiley	Pacejka	Rogers + Brewer
B0	1	1	1	1
B1	$(C+K) / v$	l_1 / v	$(\sigma+a) / V$	$(1+V_x \cdot C_y \cdot C_l) / (V_x \cdot C_y \cdot k_l)$
B2	$C \cdot K / v^2$	l_2 / v^2	$\sigma \cdot a / V^2$	$C_1 / (V_x \cdot C_y \cdot k_l)$
$W1_{yy}$	$-2 \cdot U_1 \cdot (h+C) / v$	$-K_\lambda \cdot l_1 / v$	$-C / V$	$-1 / (V_x \cdot C_y)$
$W2_{yy}$	$-2 \cdot U_1 \cdot (h^2 - h \cdot K - C \cdot K) / v^2$	$-K_\lambda \cdot l_2 / v^2$	$-a \cdot \sigma \cdot C / (v^2 \cdot (a+\sigma))$	$-(k_l \cdot C_1 + C_l) / (V_x \cdot C_y \cdot k_l)$
$W0_{y\varphi}$		$K_\gamma + K_\lambda \cdot \xi \cdot L \cdot h / r$	N	
$W1_{y\varphi}$		$(K_\gamma + r_3 \cdot K_\lambda) \cdot l_1 / v$	$(N \cdot (a+\sigma) + R \cdot C) / V$	$r / (V_x \cdot C_y)$
$W2_{y\varphi}$		$(K_\gamma + r_3 \cdot K_\lambda) \cdot l_2 / v^2$	$(N \cdot (a+\sigma) + R \cdot C) \cdot a \cdot \sigma / (V^2 \cdot (a+\sigma))$	$(k_l \cdot C_1 + C_l) \cdot r / (V_x \cdot C_y \cdot k_l)$
$W0_{y\Psi}$	$2 \cdot U_1 \cdot (h+C)$	$K_\lambda \cdot l_1$	C	$1 / C_y$
$W1_{y\Psi}$	$2 \cdot U_1 \cdot (h+C) \cdot (K-h) / v$			$(k_l \cdot C_1 + C_l) / (C_y \cdot k_l)$
$W2_{y\Psi}$				$C_1 \cdot C_l / (C_y \cdot k_l)$
$W1_{\varphi y}$		$(F_z \cdot c_\lambda + r_3 \cdot K_\lambda) \cdot l_1 / v$		$r / (V_x \cdot C_y)$
$W2_{\varphi y}$		$(F_z \cdot c_\lambda + r_3 \cdot K_\lambda) \cdot l_2 / v^2$		$(k_l \cdot C_1 + C_l) \cdot r / (V_x \cdot C_y \cdot k_l)$
$W0_{\varphi\varphi}$		$F_z \cdot (r_3 - c_\gamma) - K_\gamma \cdot r_3 - \xi \cdot L \cdot h \cdot (F_z \cdot c_\lambda + K_\lambda \cdot r_3) / r$		
$W1_{\varphi\varphi}$		$(F_z \cdot r_3 \cdot (1-c_\lambda) - F_z \cdot (\gamma - K_\lambda \cdot r_3^2 - K_\gamma \cdot r_3) \cdot l_1 / v$		$-r^2 / (V_x \cdot C_y)$
$W2_{\varphi\varphi}$		$(F_z \cdot r_3 \cdot (1-c_\lambda) - F_z \cdot (\gamma - K_\lambda \cdot r_3^2 - K_\gamma \cdot r_3) \cdot l_2 / v^2$		$-(k_l \cdot C_1 + C_l) \cdot r^2 / (V_x \cdot C_y \cdot k_l)$
$W0_{\varphi\Psi}$		$-(F_z \cdot c_\lambda + r_3 \cdot K_\lambda) \cdot l_1$		
$W1_{\varphi\Psi}$				
$W2_{\varphi\Psi}$				
$W1_{\Psi y}$	$2 \cdot U_2 \cdot h / v$	K_α / v	C_M / V	k_t / V_x
$W2_{\Psi y}$	$2 \cdot (U_2 \cdot h \cdot (K-h) - U_3 \cdot (K+h)) \cdot v^2$	$\tau \cdot l_1$		$C_l \cdot k_t / (V_x \cdot k_l)$
$W0_{\Psi\varphi}$				
$W1_{\Psi\varphi}$		$-K_\alpha \cdot (r_3 - \xi \cdot L \cdot h / r) / v - \tau \cdot v \cdot \xi \cdot L \cdot h / r$	$-C_M \cdot R / V$	$-k_t \cdot r / V_x$
$W2_{\Psi\varphi}$		$-\tau \cdot r_3 \cdot l_1$		$-C_l \cdot k_t \cdot r / (V_x \cdot k_l)$
$W0_{\Psi\Psi}$	$-2 \cdot U_2 \cdot h$	$-K_\alpha$	$-C_M$	$-k_t$
$W1_{\Psi\Psi}$	$-2 \cdot U_2 \cdot h \cdot (K-h)$	$-\tau \cdot v \cdot l_1$	$-\varkappa / V$	$-k_t \cdot C_l / k_l$
$W2_{\Psi\Psi}$		$-K_\alpha \cdot l_2 / v^2$	$-(\varkappa \cdot (a+\sigma) + C_M \cdot a \cdot \sigma) / V^2$	
Remark	**non linear**	**$l_1 = L+h$**	**non linear**	**3. order**

Table 3 – 1 COMPARISON OF PUBLISHED THEORIES

total tire loads at the centre of the wheel

$$px_{tR} = \mu \cdot pz_{tR}$$
$$py_{tR} = py \cdot (1 - |s| \cdot a) + \mu \cdot pz_{tR} \cdot (\dot{y}_{tA} - r_0 \cdot \dot{\phi}_{am}) \cdot \cdot |s| \cdot a/\dot{x}_{tA}$$
$$pz_{tR} = -p_R - 0.1 \cdot \sqrt{K_{z1} \cdot m_w} \cdot \dot{z}_{tA} \leq 0$$
$$p\phi_{tR} = p\phi \cdot (1 - |s| \cdot a) + z_{tA} \cdot \mu \cdot pz_{tR} \cdot \cdot (\dot{y}_{tA} - r_0 \cdot \dot{\phi}_{am}) \cdot |s| \cdot a/\dot{x}_{tA}$$
$$p\theta_{tR} = \mu \cdot pz_{tR} \cdot (-z_{tA} - 0.25 \cdot pz_{tR}/K_x)$$
$$p\psi_{tR} = p\psi \cdot (1 - |s| \cdot a)$$
if $z_p > 0$; but all $p._{tR} = 0$ if $z_p \leq 0$

radial deflection load

$$p_R = 0 \quad ; \text{ if } z_{pe} \leq 0$$
$$= K_{z1} \cdot d_0 \cdot \left(\frac{z_{pe}}{d_0} - b_z \cdot (1 - e^{-\frac{0.6 \cdot z_{pe}}{d_0 \cdot b_z}})\right) \quad \text{if } 0 > z_{pe} \leq z_{pk}$$
$$= p_{RK} + K_{z2} \cdot (z_{pe} - z_{pk}) \quad ; \text{ if } z_{pe} > z_{pk}$$
where $p_{RK} = p_R(z_{pe} = z_{pk})$

load portions of the rolling tire

$$B2 \cdot \ddot{py} + B1 \cdot \dot{py} + py = W1_{yy} \cdot \dot{y}_{tA} + W2_{yy} \cdot \cdot \ddot{y}_{tA} + W0_{y\phi} \cdot \phi_{am} + W1_{y\phi} \cdot \dot{\phi}_{am} + W2_{y\phi} \cdot \ddot{\phi}_{am} + + W0_{y\psi} \cdot \psi_{mt} + W1_{y\psi} \cdot \dot{\psi}_{mt} + W2_{y\psi} \cdot \ddot{\psi}_{mt}$$

$$B2 \cdot \ddot{p\phi} + B1 \cdot \dot{p\phi} + p\phi = W1_{\phi y} \cdot \dot{y}_{tA} + W2_{\phi y} \cdot \cdot \ddot{y}_{tA} + W0_{\phi\phi} \cdot \phi_{am} + W1_{\phi\phi} \cdot \dot{\phi}_{am} + W2_{\phi\phi} \cdot \ddot{\phi}_{am} + + W0_{\phi\psi} \cdot \psi_{mt} + W1_{\phi\psi} \cdot \dot{\psi}_{mt} + W2_{\phi\psi} \cdot \ddot{\psi}_{mt}$$

$$B2 \cdot \ddot{p\psi} + B1 \cdot \dot{p\psi} + p\psi = W1_{\psi y} \cdot \dot{y}_{tA} + W2_{\psi y} \cdot \cdot \ddot{y}_{tA} + W0_{\psi\phi} \cdot \phi_{am} + W1_{\psi\phi} \cdot \dot{\phi}_{am} + W2_{\psi\phi} \cdot \ddot{\phi}_{am} + + W0_{\psi\psi} \cdot \psi_{mt} + W1_{\psi\psi} \cdot \dot{\psi}_{mt} + W2_{\psi\psi} \cdot \ddot{\psi}_{mt}$$

but always

$$|py| \leq |\mu_k \cdot pz_{tR}|$$
$$|p\phi| \leq |z_{tA} \cdot \mu k \cdot pz_{tR}|$$
$$|p\psi| \leq |\mu_k \cdot 0.44 \cdot r_0 \cdot pz_{tR}/6|$$

so that for a new start :

$$p. = |p.| \cdot \operatorname{sgn}(p.(t - \Delta t))$$
$$\dot{p}. = 0 \; ; \text{ if } \operatorname{sgn}(p.) = \operatorname{sgn}(\ddot{p}.)$$
$$\dot{p}. = \int_t^{t+\Delta t} -\ddot{p}. \cdot dt \; ; \text{ if } \operatorname{sgn}(p.) \neq \operatorname{sgn}(\ddot{p}.)$$

coefficients of rolling tire

$$B2 = L_2/\dot{x}_{tA}^2$$
$$B1 = L_1/\dot{x}_{tA}$$
$$W1_{yy} = -K_\lambda \cdot L_1/\dot{x}_{tA}$$
$$W2_{yy} = -K_\lambda \cdot L_2/\dot{x}^2_{tA}$$
$$W0_{y\phi} = p_R$$
$$W1_{y\phi} = W1_{\phi y} = (K_\gamma - K_\lambda \cdot z_{tA}) \cdot L_1/\dot{x}_{tA}$$
$$W2_{y\phi} = W2_{\phi y} = (K_\gamma - K_\lambda \cdot z_{tA}) \cdot L_2/\dot{x}^2_{tA}$$
$$W0_{y\psi} = K_\lambda \cdot L_1$$
$$W1_{y\psi} = W2_{y\psi} = W1_{\phi\psi} = W2_{\phi\psi} = 0$$
$$W0_{\phi\phi} = -p_R \cdot b_\gamma$$
$$W1_{\phi\phi} = -K_\lambda \cdot z_{tA}^2 \cdot L_1/\dot{x}_{tA}$$
$$W2_{\phi\phi} = -K_\lambda \cdot z_{tA}^2 \cdot L_2/\dot{x}^2_{tA}$$
$$W0_{\phi\psi} = -(K_\gamma - K_\lambda \cdot z_{tA}) \cdot L_1$$
$$W1_{\psi y} = K_\alpha/\dot{x}_{tA}$$
$$W2_{\psi y} = K_\tau \cdot L_1$$
$$W0_{\psi\phi} = 0.01 \cdot d_0^2 \cdot K_x$$
$$W1_{\psi\phi} = K_\alpha \cdot z_{tA}/\dot{x}_{tA}$$
$$W2_{\psi\phi} = K_\tau \cdot L_1 \cdot z_{tA}$$
$$W0_{\psi\psi} = -K_\alpha$$
$$W1_{\psi\psi} = -K_\tau \cdot L_1 \cdot \dot{x}_{tA}$$
$$W2_{\psi\psi} = -K_\alpha \cdot L_2/\dot{x}_{tA}^2$$

Stiffnesses

$$K_x = 0.8 \cdot 2 \cdot r_0 \cdot (p_i + 4 \cdot p_r) \cdot \sqrt[3]{z_{pe}/(2 \cdot r_0)} + + K_{x\min} \quad \text{(fore/aft)}$$
$$K_{z1} = 2.4 \cdot (p_i + 0.08 \cdot p_r) \cdot \sqrt{d_0 \cdot 2 \cdot r_0} \quad \text{(radial)}$$
$$K_\alpha = (p_i + 0.8 \cdot p_r) \cdot d_0^3 \cdot b_t \cdot b_m + K_{\alpha\min} \quad \text{(torsion)}$$
$$K_\gamma = 0,57 \cdot p_R$$
$$K_\tau = 2 \cdot m_t \cdot r_0 \cdot (L_h + L_r \cdot \sqrt{1 - L_h^2/r_0^2}/ /(3 \cdot \pi \cdot (L_r^2 + r_0^2)) \quad \text{(gyroscopic)}$$
$$K_\lambda = b_\lambda \cdot d_0 \cdot (p_i + 0.24 \cdot p_r) \cdot (1 - 0.7 \cdot z_{pe}/d_0) \cdot \cdot b_m \quad \text{(lateral)}$$

lengths

$$L_1 = L_r + L_h \quad \text{(damping length)}$$
$$L_2 = ((2 \cdot L_r + L_h) \cdot L_h / 2) \quad \text{(inertia length)}$$
$$L_r = (2.8 - 0.5 \cdot p_i/p_r) \cdot (1 - 4.5 \cdot z_{pe}/(2 \cdot r_0)) \cdot d_0 \quad \text{relaxation}$$
$$L_h = 0.85 \cdot 2 \cdot r_0 \cdot \sqrt{z_{pe}/(2 \cdot r_0) - z_{pe}^2/(2 \cdot r_0)^2} \quad \text{(1/2 foot print)}$$

general tire factors

$$b_m = 1 + m_t \cdot \dot{x}_{tA}^2/(4 \cdot \pi \cdot r_0^2 \cdot d_0 \cdot pi) \quad \text{centrifugal}$$
$$b_t = 250 \cdot z_{pe}^2/(2 \cdot r_0)^2 \quad \text{(Type III and VII) torsion if } z_{pe}/(2 \cdot r_0) \leq 0.03$$
$$= 15 \cdot (z_{pe}/(2 \cdot r_0) - 0.015) \quad \text{if } z_{pe}/(2 \cdot r_0) > 0.03$$
$$= 475 \cdot z_{pe}^2/(2 \cdot r_0)^2 \quad \text{(Type I) if } z_{pe}/(2 \cdot r_0) \leq 0.02$$
$$= 19 \cdot (z_{pe}/(2 \cdot r_0) - 0.01) \quad \text{if } z_{pe}/(2 \cdot r_0) > 0.02$$
$$b_y = 0.21 \cdot \text{(Type I)}; = 0.15 \text{ (Type III and VII)} \quad \text{side}$$
$$b_z = 0.02 \cdot \text{(Type I)}; = 0.03 \text{ (Type III and VII)} \quad \text{vertical}$$
$$b_\gamma = 0.48 \cdot d_0 \quad \text{tilt}$$
$$b_\lambda = 3 \text{ (Type I); } = 2 \text{ (Type III and VII)} \quad \text{side}$$

deflections

$$z_{pe} = z_p - z_{px} - z_{py} - z_{p\psi} \geq 0 \quad \text{effective}$$
$$z_p = r_0 + r_\theta + z_{tA} \geq 0 \quad \text{visible}$$
$$r_\theta = 0.01 \cdot m_t \cdot \dot{\theta}_{ra}^2/pi \quad \text{centrifugal}$$
$$z_{px} = 0.1 \cdot |px_{tA}/K_x| \quad \text{x loading}$$
$$z_{py} = b_y \cdot |py_{tA} \cdot b_m/K_\lambda| \quad \text{y loading}$$
$$z_{p\psi} = 0.1 \cdot |p\psi_{tA} \cdot b_m \cdot L_h/K_\alpha| \quad \psi \text{ loading}$$

friction coefficient

$$\mu = \mu_r + (\mu_k - \mu_r) \cdot s_k \quad ; \quad \text{if } -s_k \leq s \leq s_k$$
$$= \mu_k + (\mu_s - \mu_k) \cdot (s - s_k)/(1 - s_k) \quad \text{if not}$$

slip ratio

$$s = 1 + \dot{\theta}_{ra} \cdot (r_0 - z_p/3)/\dot{x}_{tA} \quad \text{but always } |s| \leq 1$$

indicator of spin up period

a = 1 at the beginning of a horizontal landing
= 0 all time after s passed first time s = 0

Table 4 – 1 Complete Tire Equations

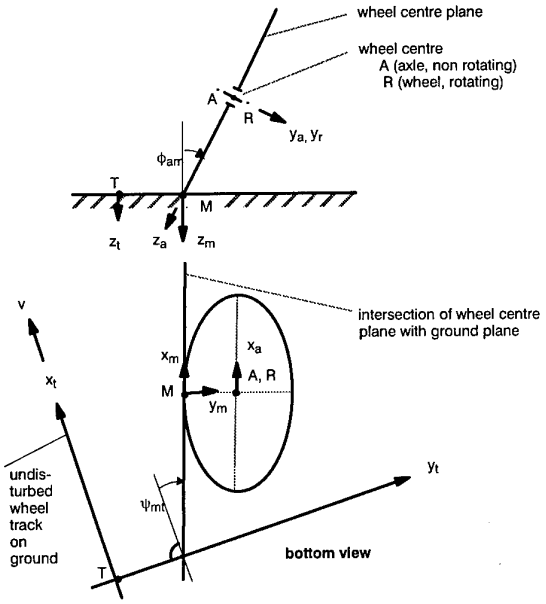

Fig. 3–1 WHEEL COORDINATES

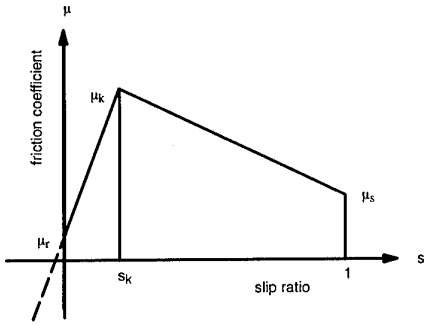

Fig. 4–1 FRICTION COEFFICIENT DEPENDING ON SLIP RATIO

Constants (input data)

TYP	tire type
d_0	tire width nominal (undeflected)
K_{z2}	radial tire stiffness after bottoming
m_t	tire mass
m_w	wheel mass including tire
pi	tire pressure
pr	rated pressure
r_0	tire radius nominal (undeflected)
s_k	slip ratio with maximal friction
z_{pk}	bottoming deflection
μ_k	maximal friction coefficient
μ_s	full gliding friction coefficient
μ_r	full rolling friction coefficient

$K_{x\min} \neq 0$ minimal fore/aft stiffness

$K_{\alpha\min} \neq 0$ minimal torsional stiffness

Table 4 – 1 Complete Tire Equations (continued)

definition of working point:

$\mu_r = 0$ (free rolling)

$a = 0$ (free rolling)

$s(0) = 0$ (free rolling)

$\dot{y}_{tA}(0) = \dot{z}_{tA}(0) = \dot{\phi}_{am}(0) = \dot{\psi}_{mt}(0) = 0$ (straight on)

conditions of linearization:

$0 < z_{pe} < z_{pk}$ (no bottoming)

$r_\theta = z_{px} = z_{py} = z_{p\psi} = 0$ (simplification)

$b_c = 0$ (linear vertical stiffness)

W.... = W....(0) (as would be measured)

B.... = B....(0) (as would be measured)

$1/\dot{x}_{tA} \approx (1 - \Delta\dot{x}_{tA}/v)/v$

abbreviations:

$\dot{x}_{tA}(0) = v$

$z_{tA}(0) - 0,25 \cdot p_R(0)/K_x(0) = z_o$

$r_r = r_o - z_p(0)/3$

additional tire coefficients for the extended unsteady tire loads

$W1_{xx} = -\mu_k \cdot p_R(0)/(s_k \cdot v)$

$W0_{xz} = -\mu_k \cdot p_R(0)/(3 \cdot s_k \cdot r_r)$

$W1_{x\theta} = -\mu_k \cdot p_R(0) \cdot r_r/(s_k \cdot v)$

$W0_{zz} = -K_{z1}(0)$

$W1_{zz} = -0,1 \cdot \sqrt{K_{z1}(0) \cdot m_w}$

$W1_{\theta x} = -\mu_k \cdot p_R(0) \cdot z(0)/(s_k \cdot v)$

$W0_{\theta z} = -\mu_k \cdot p_R(0) \cdot z(0)/(3 \cdot s_k \cdot r_r)$

$W1_{\theta\theta} = -\mu_k \cdot p_R(0) \cdot r_r \cdot z_o/(s_k \cdot v)$

$B1(x, z, \theta) = B2(x, z, \theta) = 0$

Table 5.1–1 Definitions and Coefficients for Linearized Shimmy Analyses

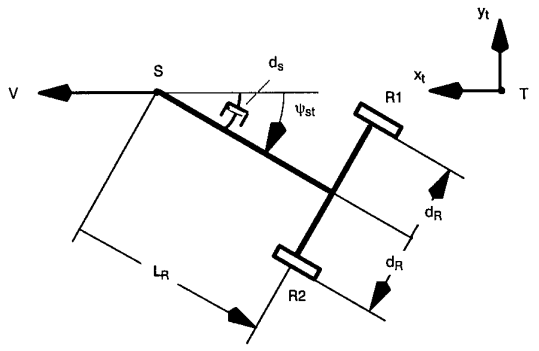

Fig. 5.2–1 SIMPLIFIED SHIMMY MODEL

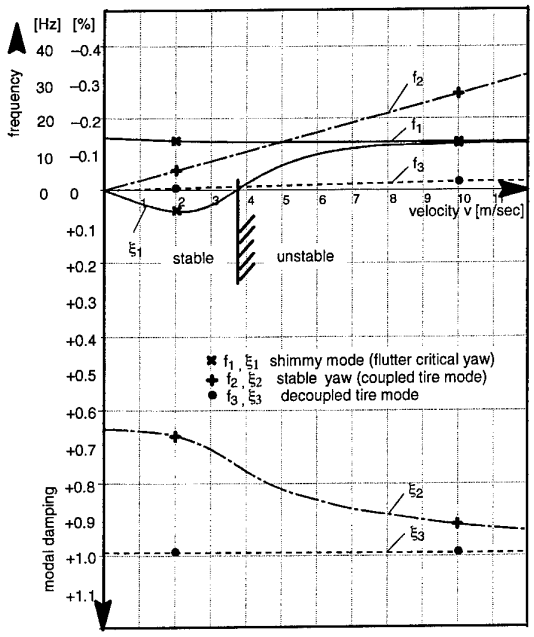

Fig. 5.2–2
EIGENFREQUENCIES AND MODAL DAMPINGS
single wheel ; rigid u/c
Smiley case I approx. B
d_s = 0.06Nm/(rad/sec) ; L_R = 0.08 m

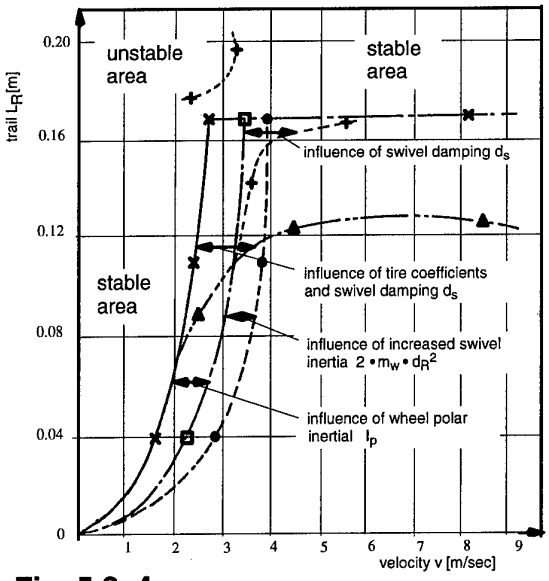

Fig. 5.2–4
INFLUENCE OF x AND ϑ MOVEMENT

variations :
- ● single wheel $W(x,\vartheta) = d_R = d_s = 0$
- ◘ double wheel $W(x,\vartheta) = I_p = d_s = 0$
- ✖ " " $W(x,\vartheta) = d_s = 0$
- ✚ " " $W(x,\vartheta) = I_p = 0$; $d_s = 0.06$
- ▲ " " variant E ; $d_s = 0.06$

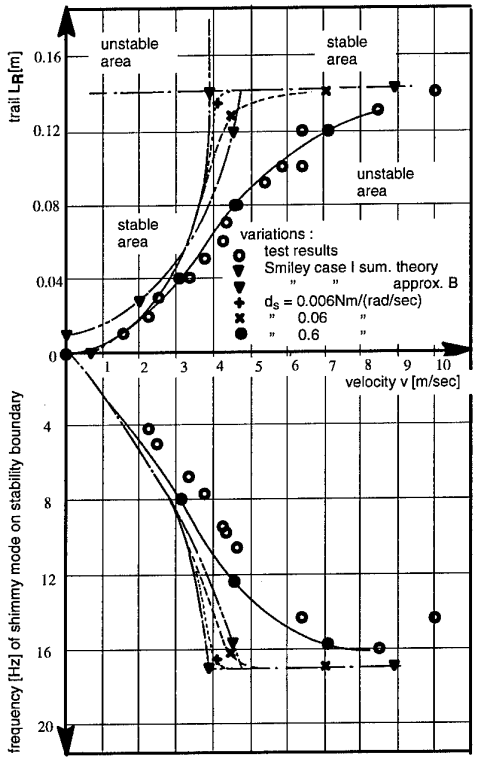

Fig. 5.2–3 STABILITY DIAGRAM
single wheel

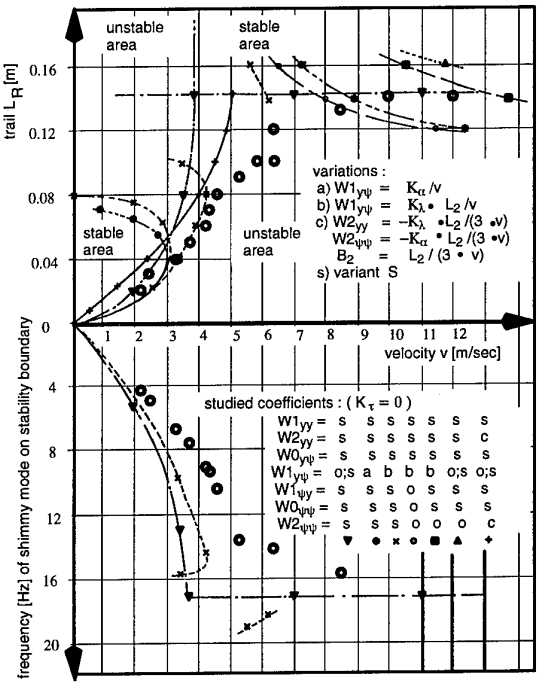

Fig. 5.2–5
INFLUENCE OF y AND ψ COEFFICIENTS
single wheel o **test results**
– × – d_s = 0.6 Nm/(rad/sec)

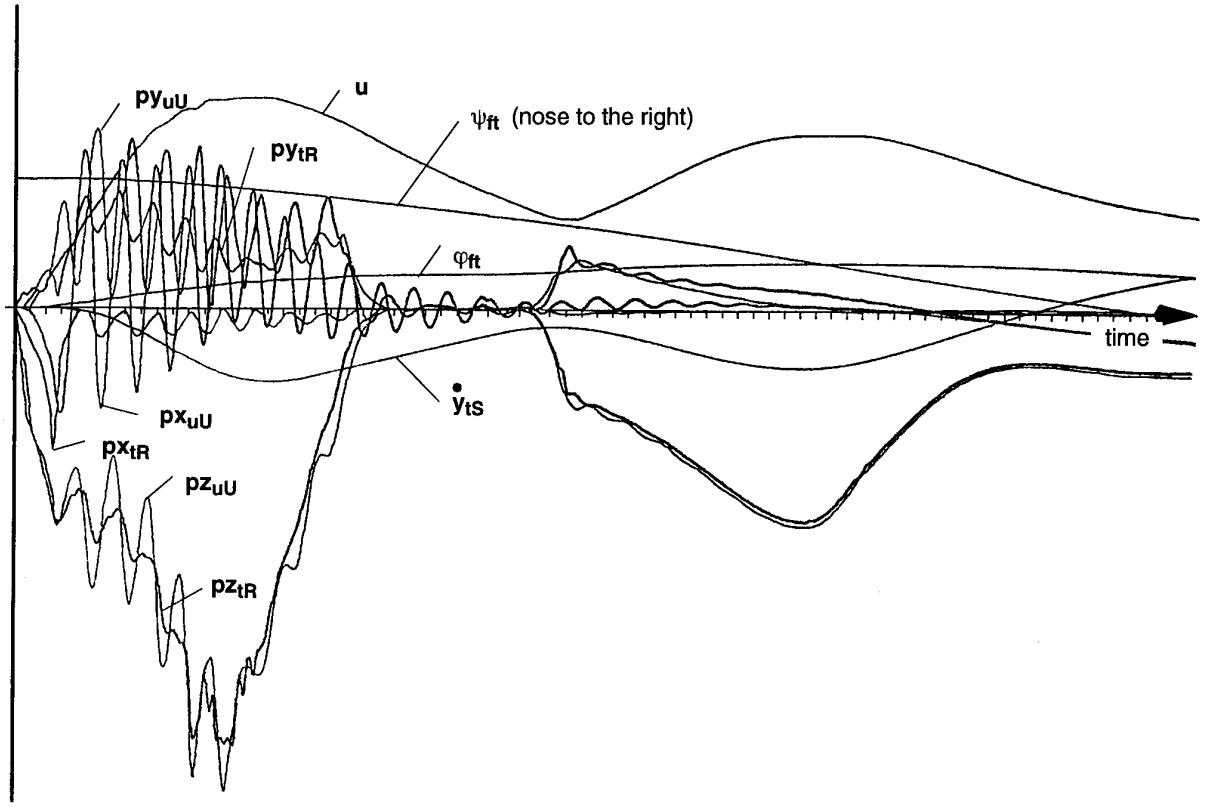

Fig. 6–1a LANDING IMPACT, LEFT MAIN UNDERCARRIAGE

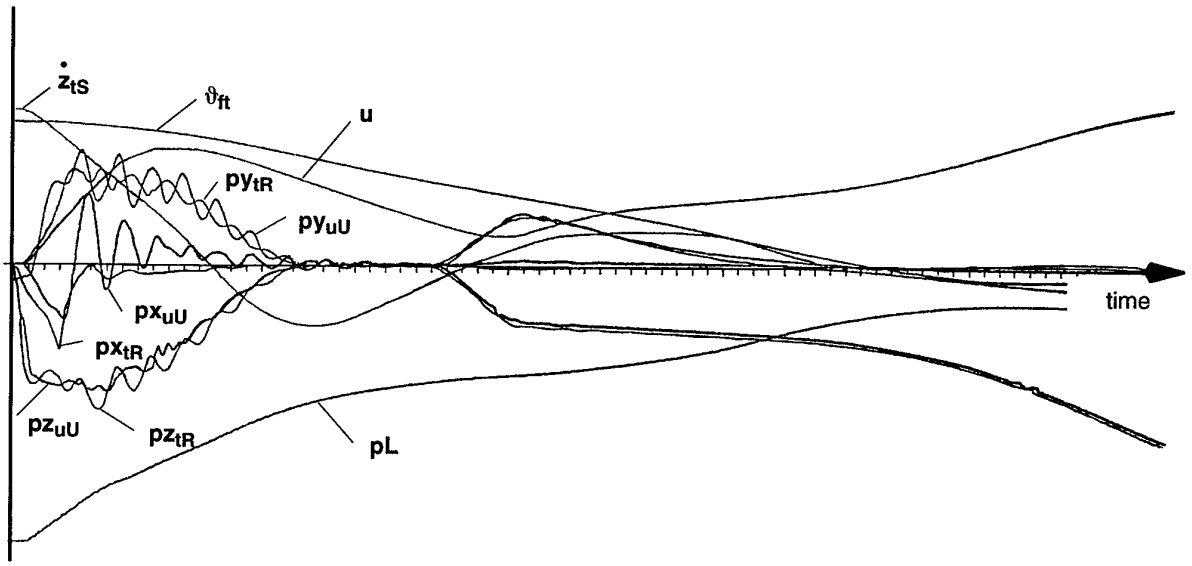

Fig. 6–1b LANDING IMPACT, RIGHT MAIN UNDERCARRIAGE

INFLUENCE OF NONLINEARITY ON THE SHIMMY BEHAVIOUR OF LANDING GEAR

P. WOERNER, O. NOEL
Messier-Dowty S.A.
Zone Aéronautique Louis Breguet
BP 10, 78142 Vélizy Cedex
France

ABSTRACT

One of the most critical vibratory phenomena which may occur on a landing gear is called "shimmy". It is typically unstable oscillations that could reach such a level of instability that major landing gear structural components may be damaged or destroyed.

For many years, Messier–Dowty S.A. has studied this phenomenon in order to perform more accurate predictions of the dynamic behaviour of landing gear. Several models have been developed taking into account many parameters, and especially the non–linear ones, in agreement with test measurements. Simulations have been performed, which show the sensitivity of shimmy stability to variations of these parameters, and therefore the importance of taking account non–linearities in shimmy landing gear models.

1. INTRODUCTION

Airplane landing gear shimmy can be defined as a self–excited instability during take–off, landing or taxiing, involving up to three vibration motions : angular wheel motion about a vertical axis (yaw), angular motion about a fore and aft axis (roll), and lateral displacement of the wheel.

The basic cause of shimmy is an energy transfer from the contact force between the tires and the ground to the vibratory modes of the landing gear system. The vibration stability depends on the dynamic characteristics of the gear, tires and fuselage, as well as the degree of coupling that exists between the modes of these components. At certain speeds, small motions may be unstable, and in most severe cases, the pilot can not take corrective action, and failure of the gear structure may occur.

One of the difficulties of a shimmy analysis is that real landing gear systems exhibit many non–linear characteristics : swivel friction from the action of the upper and lower bearings of the shock strut, steering collar friction, non–linear viscous damping from the steer–damp unit, mechanical deadband associated with the strut lateral motion, and slippage of the tires : some non–linear characteristics are dependent on landing gear wear. Nonlinear behaviour of landing gear makes the shimmy phenomenon less predictable : if a test is performed to reproduce conditions of a severe landing gear vibration, nothing out of the ordinary may occur.

It is therefore necessary to evaluate and model landing gear non–linearities in order to improve the predictability of the shimmy phenomenon; an accurate shimmy analysis must take into account a range of non–linearities values as wide as necessary, in order to reveal the most unstable configurations.

Messier–Dowty S.A. has performed many analyses on a landing gear which showed some instabilities under certain conditions, due to the appearance of coupling between torsion and lateral flexion. These analyses have permitted the identification of parameters that influence the phenomenon, in particular aircraft speeds and loads, and have validated the improvement achieved by increasing the stiffness of this landing gear's torque link, to increase torsion frequency and move it away from lateral flexion frequency, thus reducing coupling tendancy.

These analyses are still in progress in *Messier–Dowty S.A.*, in order to take more precisely into account the non–linearities of the landing gear and to improve the knowledge of their effects, which will permit to anticipate early in the design the landing gear's shimmy stability.

This paper describes the methods developed in order to build such a model, namely an analytical way to describe these nonlinear effects, as well as an experimental determination of its numeric coefficients, and simulations results and conclusions.

2. GENERALITIES ABOUT MODAL ANALYSIS AND TESTS

2.1 Concept of eigenmode for linear models

In theory, the notion of mode of a linear structure is introduced from the equation of motion :

$$MX'' + CX' + KX = F \quad (1)$$

– X , X', X'' : vectors of displacements, velocities, accelerations
– M , C , K : matrices of mass, damping and stiffness of the structure
– F : vector of excitation forces

Eigenmodes of the structure are defined as the roots of equation (1) without righthand term, which caracterizes the free structure :

$$MX'' + CX' + KX = 0 \quad (2)$$

The determination of these modes constitutes an intermediate calculation to solve equation (1), whose general solution is the sum of general solution (2) and of a particular solution dependent on F.

Physical interpretation of modes is not obvious, because the solutions of (2) correspond to complex motions such as damped vibratory : because of damping influence, an imaginary quantity appears, from which the denomination of "complex modes". This damping term can be suppressed in equation (2) to obtain the equation of the conservating system associated :

$$MX'' + KX = 0 \quad (3)$$

Paper presented at the 81st Meeting of the AGARD SMP Panel on "The Design, Qualification and Maintenance of Vibration-Free Landing Gear", held in Banff, Canada from 4-5 October 1995, and published in R-800.

Solutions of (3) correspond to pure sinusoidal motions, and are denominated "real modes" : all the nodes of the structure are in phase or opposite phase, whereas, for a complex mode, vibration nodes move independently from each other, and make the observation of motion more difficult.

Equation (3), which governs real modes, has a solution of the form : $X = \overline{X}\, e^{j\omega t}$, which leads to find eigenvalues of : $(-\omega^2 M + K)\,\overline{X} = 0$

- eigenvalues ω_i^2 are the squares of mode pulsations ω_i
- eigenvectors ϕ_i represent eigenshapes or mode deform

With the variable change : $X = \phi\, q$ **(4)**

- ϕ matrice of eigenshapes ϕ_i
- q generalized coordinates in modal basis

we obtain, after pre–multiplication by ϕ^T :

$$\phi^T M \phi \quad q'' + \phi^T C \phi \quad q' + \phi^T K \phi \quad q = \phi^T F$$

M and K are symetric matrices, and modes are orthogonal relating to them ; we obtain :

$$m\, q'' + c\, q' + k\, q = \phi^T F \quad \textbf{(5)}$$

- m : diagonal matrix of generalised masses m_i
- k : diagonal matrix of generalised stiffnesses k_i with $k_i = \omega_i^2\, m_i$
- c : damping matrix , symetric, non diagonal in general

We can assume c to be diagonal (terms c_i) if the structure is weakly damped (*Basile* hypothesis) ; we can define a reduced damping ξ_i , without dimension, as:

$$\xi_i = c_i \,/\, 2\, m_i\, \omega_i$$

Equation (5) clearly shows the parameters to determine during a modal test :

- eigen pulsations ω_i
- eigenshapes ϕ_i
- generalised masses m_i and generalised stiffnesses k_i
- damping coefficients of matrix c, assumed to be symetric

When those terms are known, equation (5) allows to calculate q as a function of F, then equation (4) allows to calculate motion of structure X sollicitated by forces F: X is obtained by taking all modes into account.

Equation (5) is matricial, but can be expressed as N scalar equations upon each eigenmode ; for the i–th mode : $m_i\, q_i'' + c_i\, q_i' + k_i\, q_i = f_i$, with the notation : $f = \phi^T F$

Generalised masses m_i can be normalised, and be chosen to equal 1 : generalised stiffnesses k_i are therefore equal to ω_i^2

After substituting c_i by $2\, \xi_i\, m_i\, \omega_i$ and k_i by $m_i\, \omega_i^2$, and with $m_i = 1$:

$$q_i'' + 2\, \xi_i\, \omega_i\, q_i' + \omega_i^2\, q_i = f_i$$

It can be expressed as Laplacian variables :

$$(s^2 + 2\, \xi_i\, \omega_i\, s + \omega_i^2)\, q_i = f_i$$

After substituting s by $j\omega$ (for frequency response) :

$$(\omega_i^2 - \omega^2 + j\, 2\, \xi_i\, \omega_i\, \omega)\, q_i = f_i$$

We can return to a matricial expression between q and f:

$$q = diag\,(\,[\omega_i^2 - \omega^2 + j\, 2\, \xi_i\, \omega_i\, \omega\,]^{-1}) f = A f$$

We can express X as a function of excitation F :

$$X = \phi\, q = \phi\ A f = \phi\ A \phi^T F = H F$$

H matrix has the signification of a transfer matrix between input F and output X, whose expression is :

$$H(\omega) = \phi\ A \phi^T$$

$$H(\omega) = \phi\ diag\,(\,[\omega_i^2 - \omega^2 + j\, 2\, \xi_i\, \omega_i\, \omega\,]^{-1})\, \phi^T$$

If H_{ij} and ϕ_{ij} are the ij–th term of matrices H and ϕ , the product of above matrices, taking into account the presence of a diagonal matrix, leads to :

$$H_{ij}\ (\omega) = \sum_{r=1}^{N} \frac{\phi_{ri}\ \phi_{rj}}{\omega_r^2 - \omega^2 + j\ 2\xi_r\ \omega\ \omega_r}$$

If the modes of the system are well spaced, this expression evaluated at a natural frequency ω_r will be dominated by the term corresponding to that frequency, with an amplitude depending on its modal damping :

$$|H_{ij}\ (\omega_r)| = \frac{|\ \phi_{ri}\ \phi_{rj}\ |}{2\ \xi_r\ \omega_r^2}$$

This expression in modal basis (after variable change) leads to less voluminous calculations than a direct method, because of the limited number of parameters : we can choose the number of modes N to be retained, which is the dimension of matrices m , c and k.

2.2 Modal tests classification in linear configuration

We first assume that the structure is linear, or weakly non–linear.

There are two main categories of modal tests :

- tests with appropriation of the excitation, which allow the isolation of each mode and the direct measurement of their characteristics.
- tests with transfer functions measurements, to sollicite a group of modes which are determined by means of post–processing measurement results.

2.2.1 *Tests with appropriation of the excitation*

The structure is loaded by the means of a sinusoidal excitation sent to an excitator, whose level is tuned in order to isolate each mode. The domain of excitation frequencies is known by the means of a previous frequency sweep to locate the interesting modes.

The theoretical explanation of this method follows from solving equation (1) with a sinusoidal sollicitation :

$$MX'' + CX' + KX = F = f\, e^{j\omega t}$$

The solution is of the form : $X = x\, e^{j\omega t}$, which leads to :

$$(K - \omega^2 M + j\omega C)\, x = f$$

Isolating an eigenmode by the means of an appropriate excitation consists of realising $\omega = \omega_{0k}$, where ω_{0k} is the kth eigen pulsation, from the excitation amplitude f_k. This leads to : $(K - \omega_{0k}^2 M + j\omega_{0k} C)\, x_k = f_k$

ω_{0k} and x_k are roots of the associate conservative system, thus : $(K - \omega_{0k}^2 M)\, x_k = 0$

We deduce the expression of loading which excites the ω_{0k} mode : $f_k = j\omega_{0k} C\, x_k$

With an appropriate excitation, the loading force compensates internal dissipation forces, and has a 90°phase with the response : the criterion for appropriation is a phase criterion. For an isolated mode, all responses are in phase quadrature with excitation, which can be easily shown during testing by examination of Lissajous's curves.

The advantage of this method is the ease of exploitation of results, which are based on a physical approach; however, experimental procedure may be delicate : phase criteria for all measures may be difficult to adjust for some modes.

2.2.2 *Tests with transfer functions measurements*

The structure is loaded on one or many excitation nodes. The input signal is sinusoidal, transient, or random, and is multifrequency : all the modes can be simultaneously excited.

The modal analysis is performed by transfer function measurement and processing : the theoretical explanation of this method follows from solving equation **(4)** and **(5)** with whatever load form :

$$X = \phi\, q \quad \textbf{(4)}$$
$$m\, q'' + c\, q' + k\, q = f = \phi^T F \quad \textbf{(5)}$$

According to **2.1**, this can be explained as a transfer matrix between input F and output X, whose terms are of the form :

$$H_{ij}(\omega) = \sum_{r=1}^{N} \frac{\phi_{ri}\, \phi_{rj}}{\omega_r^2 - \omega^2 + j\, 2\xi_r\, \omega\, \omega_r}$$

The term $H_{ij}(\omega)$ links the dynamic response in the accelerometer localized in d.o.f. i , to the excitation applied in d.o.f. j .

When the transfer matrix between input and output is measured, we have to find an analytical expression such as mentioned above, which best fits the experimental result (identification process), then to deduce eigen pulsations ω_r and damping coefficients ξ_r . The determination of ϕ_{ri} terms can be made easier by measuring responses on the same points as excitation : we have $i=j$, thus :

$$H_{ii}(\omega) = \sum_{r=1}^{N} \frac{\phi_{ri}^2}{\omega_r^2 - \omega^2 + j\, 2\xi_r\, \omega\, \omega_r}$$

The advantage of this method, as opposed to the appropriation method, is the comparative simplicity of experimental proceedings, which imposes few restraints on choice of excitation; however, this method requires a more complex method to exploit measured results, which are based on a mathematical, rather than physical, approach; moreover, accelerometers must be located near mode antinodes, in order to achieve better measurement precision.

3. LANDING GEAR NON-LINEARITIES THEORETICAL DESCRIPTION

The shimmy analyses in progress in *Messier-Dowty S.A.* show that most important non-linearities are friction and freeplay along torque links, with non-linear effects in torsion motion. This chapter presents a theoretical description of those effects, and their experimental determination.

3.1 Theoretical description of friction

"Coulomb friction" or "stick-slip friction" is a nonlinear function of relative velocity between the two bodies in contact inside the landing gear. Such contact surfaces are never completely smooth : when two "peaks" come into contact, the corresponding force is similar to a rigid mass-spring system, a function of position but not of velocity; on the other hand, with no contact between such peaks, slipping occurs, and this force depends only on the velocity. A good model must take both aspects into account : cf reference [1].

Elementary representation of friction as a function of relative velocity alone is shown below.

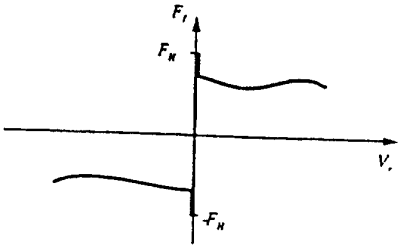

Standard stick-slip friction model

There is a strong nonlinearity around $V_r=0$, with a multiple evaluation of friction between $-F_h$ and F_h : this is unacceptable for numeric computations, which impose the linearization of such a zone.

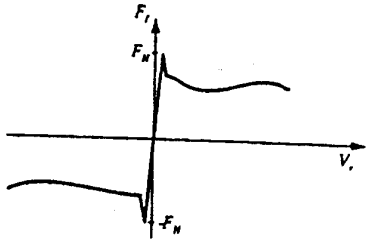

Approximation of stick-slip friction

3.2 Numerical simulation of friction

The friction nonlinear model must have a good physical interpretation of its parameters, as well as an easy implementation in numerical software : a satisfactory representation for friction is the *Dahl* model (1968), described in reference [2], in which friction force is the solution of following first order differential equation :

$$\frac{dF}{dt} = \frac{\dot{\theta}}{f_0^2} K_f (F - f_0\ sign(\dot{\theta}))^2 \text{ , equivalent to :}$$

$$\frac{dF}{d\theta} = \frac{K_f}{f_0^2} (F - f_0\ sign(\dot{\theta}))^2$$

Such a system is in fact a combination of a stiffness and a Coulomb friction, whose parameters are K_f and f_o :

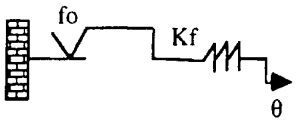

The significance of these parameters appears when solving the above differential equation : we obtain an hysteresis curve F as a function of Θ :

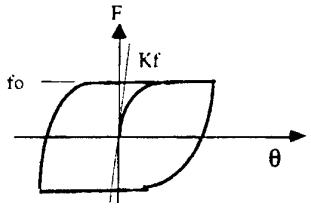

Such a system behaves as "stick–slip" friction, with 2 parameters K_f and f_o :

– K_f is the system's apparent stiffness, which occurs during friction initiation, which is a sticking phase (Θ is small) ; the friction equation becomes $\frac{dF}{d\theta} = K_f$ around $F=0$: K_f is the zero point slope of above curve.

– f_o is the level of sliding friction ; when $F = \pm f_0$, we obtain $\frac{dF}{d\theta} = 0$: friction force depends on Θ' only, not on Θ, during this slipping phase.

This model requires identification of parameter f_0 and K_f from test results.

3.3 Numerical simulation of landing gear torsion freeplay and friction

Freeplay nonlinearity is classically described as a variable stiffness, which poses no particular problem to model. According to above, we can model a nonlinear torsion link of a landing gear with a straightforward 1 d.o.f. model :

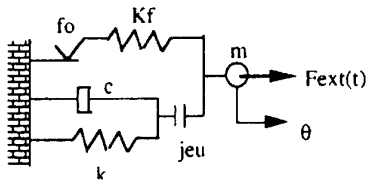

If m is the inertia moment relative to torsion, described by wheel masses with respect to vertical, we have a system of 2 equations with 2 unknown values F and θ, with 2 values f_o and K_f to identify :

$$\frac{dF}{dt} - \frac{\dot{\theta}}{f_0^2} K_f (F - f_0\ sign(\dot{\theta}))^2 = 0 \quad (6)$$

$$m\ddot{\theta} + c(\theta)\dot{\theta} + k(\theta)\theta + F - F_{ext}(t) = 0 \quad (7)$$

with initial conditions : $\theta'(0) = 0 \quad \theta(0) = 0 \quad F(0) = 0$

$c(\theta)$ and $k(\theta)$ depend on the angular limit of freeplay j.

Such behaviour can be described with a non–linear model with torsion freeplay and friction, whose parameters are in agreement with experience, taking into account that stiffness and damping depend on torsion angle θ.

As far as $|\theta| < j/2$, the system is in free motion, with $c(\theta)=k(\theta)=0$, so only friction force F occurs.

For greater amplitudes, freeplay limits are reached, with non–zero stiffness k and damping c, coming principally from torque link flexion characteristics.

3.4 Numerical simulation of non–linearities with sweeping frequency.

To characterize non–linear parameters, tests were performed by *Messier–Dowty S.A.* with sinusoidal excitations. Before describing these test proceedings, we show a few theoretical results from the numerical resolution of equations (6) and (7) with $F_{ext}(t) = F \sin \omega t$, which shows a physical interpretation of such tests when ω varies.

To make it easier, we solve separately two straightforward 1 d.o.f. models, with friction only and with freeplay only.

3.4.1 *Nonlinear friction model*

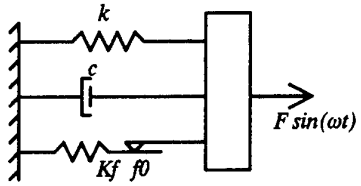

$$\frac{dF}{dt} = \frac{\dot{\theta}}{f_0^2} K_f (F - f_0\ sign(\dot{\theta}))^2$$

$$m\ddot{\theta} + c\dot{\theta} + k\theta + F = F \sin \omega t$$

$$m = 0.1\ ;\ c = 0.1\ ;\ k = 3\ ;\ F_0 = 2\ ;\ K_f = 10$$

We obtain the following result with this model :

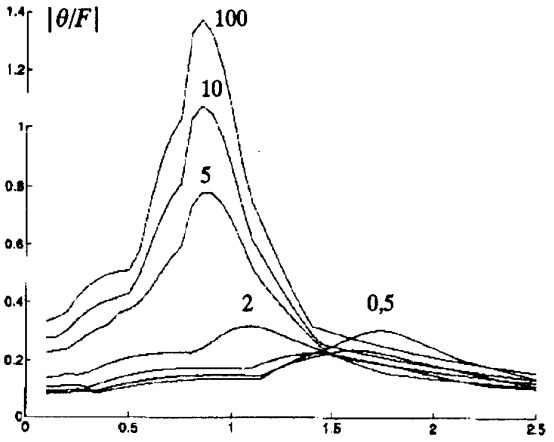

Frequency responses of friction model for different excitation levels (between 0,5 and 100 Nm)

This system has two characteristic frequencies :

– the first one, associated with lower excitation levels (cf curve with 0,5 Nm), when the threshold force before sliding is not reached: the friction model is in fact a stiffness model, with value K_f., which is the zero point slope of the above curve. (cf **3.2**). This frequency is: $f_1 = \frac{1}{2\pi}\sqrt{\frac{K_f + k}{m}}$, therefore : $f_1 = 1.81\ Hz$

– the second one, associated with higher excitation levels (cf curve with 100 Nm), when sliding can appear ; the stiffness K_f does not occur any more. This frequency is : $f_2 = \frac{1}{2\pi}\sqrt{\frac{k}{m}}$, therefore : $f_2 = 0.87\ Hz$

The system gets less stiff when excitation level grows: it progressively slides between f_1 and f_2 when excitation level grows ($f_2 < f_1$) .

3.4.2 *Nonlinear freeplay model*

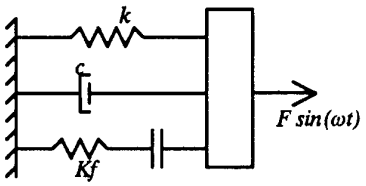

$$m\ddot{\theta} + c\dot{\theta} + k(\theta)\theta = F\sin(\omega t)$$

$$m = 0.1\ ;\ c = 0.1\ ;\ k = 3\ ;\ K_f = 10$$

We obtain the following result with this model :

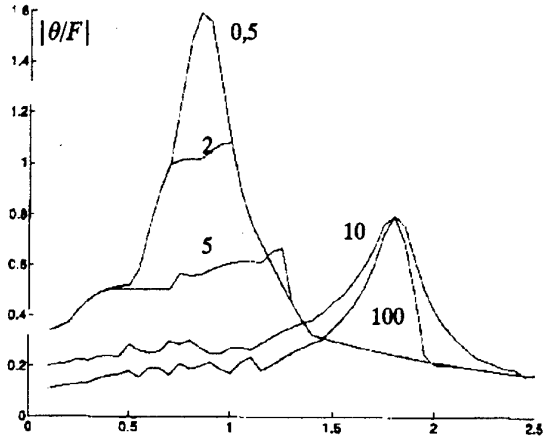

Frequency response of freeplay model for different excitation levels (between 0,5 and 100 Nm)

This system also has two characteristic frequencies :

– the first one, associated with lower excitation levels, when the threshold freeplay is not reached . This frequency is : $f_1 = \frac{1}{2\pi}\sqrt{\frac{k}{m}}$, therefore : $f_1 = 0.87\ Hz$

– the second one, associated with higher excitation levels, when the threshold freeplay is reached. This frequency is : $f_2 = \frac{1}{2\pi}\sqrt{\frac{K_f + k}{m}}$, therefore : $f_2 = 1.81\ Hz$

The system gets more stiff when excitation level grows; the frequency suddenly moves from f_1 to f_2 when the excitation level grows ($f_2 > f_1$) , which is often called the "*jump*" phenomenon.

This freeplay behaviour is not the same as friction behaviour, which helps to characterize these two kinds of non–linearity during sweeping frequencies tests.

4. MEASUREMENTS AND IDENTIFICATION OF LANDING GEAR NON–LINEARITIES

4.1 Landing gear test description

The shimmy analysis, mentioned in the introduction, has required several tests to measure dynamic characteristics of this main landing gear, in linear and non–linear domains.

A preliminary test campaign was performed to verify the closeness of the two frequencies set in evidence with the initial configuration, and their spreading out with the new one (cf introduction); insofar as the order of size of such frequencies was known, tests with appropriation were suitable.

A second test campaign was performed to obtain a more complete dynamic characterization of the landing gear, in order to validate the numerical model on many modes and to make it more accurate. Tests with transfer function measurements were well–suited, to measure many frequencies initially unknown.

4.2 Identification of non linearities with respect to tests with appropriation

4.2.1 *Experimental characterization of landing gear with appropriation*

Messier–Dowty S.A. has performed a modal analysis on a clamped main landing gear with no contact between wheels and ground, by means of appropriation of the excitation on a wheel center, with 10 levels of excitation force. Landing gear experimental curves show a non–linear behaviour in torsion, with dependance of frequencies and displacement on excitation amplitude : in particular, for low values of excitation, frequency decreases, but reaches an asymptote for higher values of excitation, for which the phenomenon becomes quasi–linear.

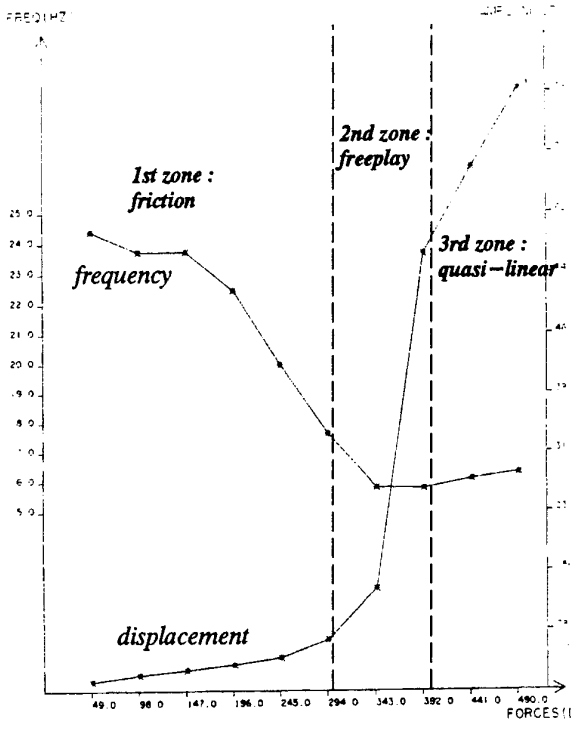

Appropriation test : torsion amplitudes and frequencies

Such a curve shows 3 zones, successively reached for increasing excitation values, whose physical interpretation is :

– the first zone is governed by friction : low excitation levels do not allow the system to reach freeplay thresholds : it behaves like a 1 d.o.f. oscillator with friction, which produces a frequency drop when the excitation level increases (cf nonlinear friction model : $f_1 > f_2$)

– the second zone is governed by freeplay : displacement increases a lot, which shows a strong non–linearity ; friction influence is less sensitive : frequency drop noted in first zone fades.

– the third zone approaches linear behaviour : displacement increases lineary, and frequency reaches an asymptotic value.

These tests with appropriation have shown that, when the studied landing gear has this linear behaviour, torsional frequency is about 16 Hz and lateral flexion frequency about 14 Hz, which are close values. This result will be recalled further in non–linear simulation analyses (cf **5.3**)

Furthermore, this test permits the deduction of damping C in linear behaviour from force and displacement measurements, according to relation shown in **2.2.1** when the ω_{0k} mode is excited : $f_k = j\,\omega_{0k}\,C\,x_k$

4.2.2 *Friction parameter identification*

In addition to linear characterization of landing gear, this kind of test permits the identification of non–linear parameters to be introduced in a numeric model to fit the three zones previously identified.

In particular, we have to determine f_o and K_f values so that the solution of above equations (**6**) and (**7**) (cf **3.3**) fits tests measurements with frequency sollicitation : one possibility is to solve this equation analytically from f_o and K_f values , and looping on those 2 values to minimize the gap between numerical solution and test result : this leads to relatively long computations.

A better way consists of finding a straightforward approximated solution of these equations, insofar as the external loading is sinusoidal : the assumption is that response will be harmonic too, with the same pulsation : this is the *"harmonic linearization method"*, or *"Ritz averaging criterion"* : cf references [3] and [8].

If $F_{ext}(t) = F_{ext}\,\sin\omega t$, we have F and θ in the form :

$$F = Fc\,\cos\omega t + Fs\,\sin\omega t$$

$$\theta = Uc\,\cos\omega t + Us\,\sin\omega t$$

$$\frac{dF}{dt} - \frac{\dot\theta}{f_0^{\,2}}\,K_f\,(F - f_0\,sign(\dot\theta))^2 = 0 \quad (6)$$

$$m\ddot\theta + c(\theta)\dot\theta + k(\theta)\theta + F - F_{ext}\sin\omega t = 0 \quad (7)$$

These expressions of F and θ are only approximate solutions, so their substitution in equations (**6**) and (**7**) leads to non–zero values. However, according to *Ritz* criterion, weighting factors U_c, U_s, F_c and F_s can be determined in such a manner that, over the period $2\pi/\omega$, the weighted averages of those non–zero values vanish, with the same weight functions $\cos\omega t$ and $\sin\omega t$ as defined in F and θ expressions; if $\gamma = K_f / f_0^{\,2}$, and with the above expression of F and θ, we have the conditions:

$$\varepsilon_1 = \int_0^{\frac{2\pi}{\omega}} (m\theta'' + c(\theta)\theta' + k(\theta)\theta + F - F_{ext}\,\sin\omega t)\,\cos\omega t\,dt = 0$$

$$\varepsilon_2 = \int_0^{\frac{2\pi}{\omega}} (m\theta'' + c(\theta)\theta' + k(\theta)\theta + F - F_{ext}\,\sin\omega t)\,\sin\omega t\,dt = 0$$

$$\varepsilon_3 = \int_0^{\frac{2\pi}{\omega}} (F' - \gamma\,\theta'(F - f_0\,sign(\theta'))^2)\ cos\ \omega t\ dt = 0$$

$$\varepsilon_4 = \int_0^{\frac{2\pi}{\omega}} (F' - \gamma\,\theta'\ (F - f_0\,sign(\theta'))^2)\ sin\ \omega t\ dt = 0$$

These 4 integrations can be computed numerically by substituing F and θ by their approximate expressions : they cancel out for optimised values of weighting factors U_c, U_s, F_c and F_s, which define F and θ solutions.

4.2.3 *Example of experimental fitting of nonlinear landing gear model*

The experimental landing gear torsion frequency response curve is shown as a solid line: this frequency varies between 16 Hz (in the linear zone) and 24 Hz.

For each excitation level, friction parameters were adjusted to fit the experimental curve : stars indicate the frequency level reached from these values.

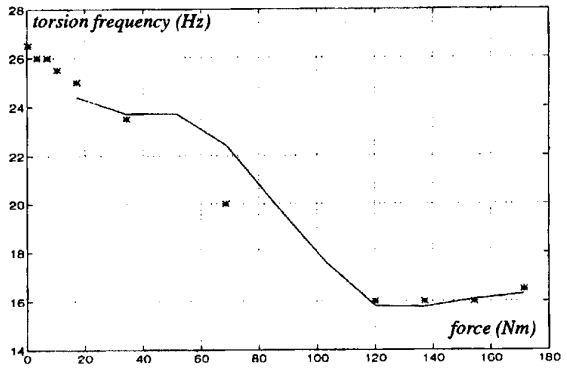

Identification of the experimental torsion frequency response

Experimental frequency evolution is well respected, especially around the asymptotic frequency for higher force levels; the most important gap between the experimental curve and computed points is around the median zone, seen above as the most nonlinear zone of the system, which makes it more difficult to model precisely.

It is possible to improve the non–linear behaviour of this model, for example by defining force f_0 as an exponential function of angular velocity : its maximum absolute value is greater than slipping value f_∞ , which represents maximum sticking before sliding.

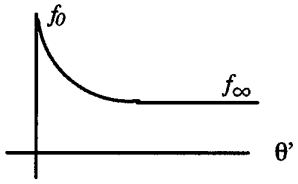

Such an improvement will be tested in future shimmy analysis.

4.2.4 *Limitations of tests with appropriation*

Despite the relative easiness of these test procedure, many limitations exist :

– in order to reach asymptotic values for frequency and damping, the excitation level must be sufficiently high, all the more as the landing gear has a more non–linear behaviour : as long as frequencies depend on excitation level, linear behaviour is not reached.

– if excitation level is not sufficient, identification of friction parameters becomes less accurate.

– during this test campaign, some modes were difficult to appropriate : their measured frequencies and damping were not accurate enough.

Besides, the identification of friction parameters shown above may not be accurate enough when coupling appears between modes if corresponding friction is not negligeable, insofar as its hypothesis is the behaviour like a single 1 d.o.f. model, uncoupled with other d.o.f.

4.3 Identification of non linearities with respect to tests with transfer function measurements

4.3.1 *Experimental characterization of non–linearities with transfer function measurements*

To reduce the limitations mentioned above, *Messier–Dowty S.A.* performed a second modal test campaign on the same landing gear with transfer function measurements, in order to obtain more eigenfrequencies (around 10) in free–free boundary conditions. The landing gear was instrumented with 19 accelerometers, whose localization allowed the measurement of modes beyond the first one.

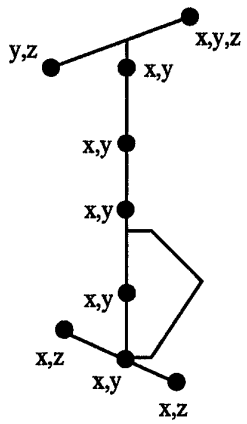

Accelerometers for transfer functions measurements.

Several frequency responses were tested with different excitation levels, in order to detect non–linearities : each frequency response is obtained from a constant excitation level. We show below experimental results.

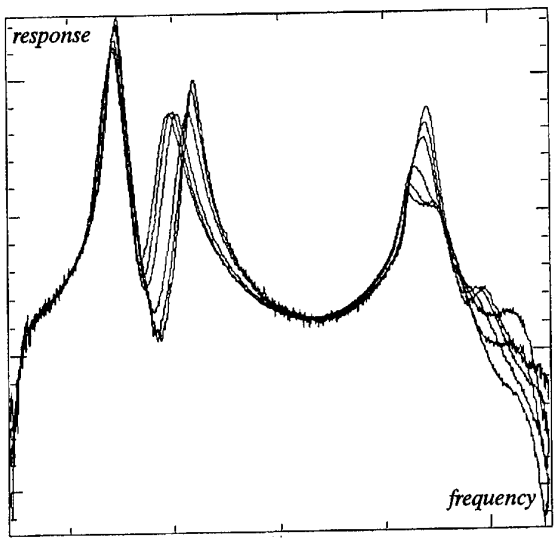

Frequency responses for different excitation levels

The following elements can be noticed from this experimental result :

– the first frequency peak is independent of excitation level, but its amplitude value, which characterizes damping value (cf $H_{ij}(\omega_r)$ expression in **2.1**), depends on this excitation level, which shows a nonlinear behaviour.

– the second frequency peak depends on the excitation level, with a "jump" between two frequencies, which also shows a nonlinear behaviour, identical to the freeplay 1 d.o.f. model seen in **3.4.2.**

Other tests on this system showed nonlinear behaviour:

– when exciting the system with a single frequency equal to this first peak, the response showed harmonic components of that frequency, which should not appear in a linear system.
– when exciting the system with a swept sine, some peak frequencies depend on the direction of sweeping (increasing or decreasing sine), which shows freeplay nonlinear behaviour, with a "jump" phenomenon between these frequency values.

4.3.2 *Identification of non–linearities from transfer function measurements*

The identification of non–linearities consists of finding a model whose FRF (Frequency Response Functions) agree with all the experimental FRF for each accelerometer : this identification is obtained with specific software, integrated into the measurement chain.

There are several ways to examine the measured frequency response function to extract these data, which are described in reference [4]. The numerical method used here is called "Polyreference Time Domain Technique " (cf reference [5]), and allows the extraction of modal parameters, namely modal damping and frequencies, from experimental data.

Instead of using a frequency response function, like many frequency domain algorithms, this method is formulated from the impulse function (due to Dirac impulse), which may be obtained from the inverse Fourier transform of the frequency response function; the theoretical identification process is the same as shown in **2.2.2** , but expressed in the time domain. One of the advantages of this method is the possibility to take many excitation sources more easily into account.

Transfer function measurements are today in progress, so we have not yet obtained all these characteristics. We show below an example of such identification, in agreement with the first 3 modes of an experimental FRF :

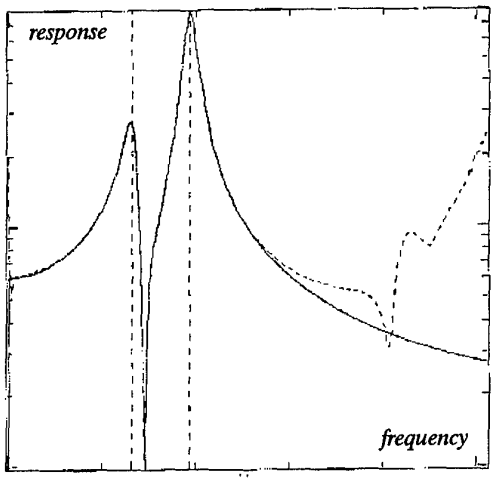

Experimental and identified FRF with 3 first modes

As shown in **4.3.1**, such identification must be made from tests with different excitation levels and different sine sweeping directions, necessary for detecting non–linearities.

5. SHIMMY NUMERICAL MODEL

5.1 Shimmy model hypothesis

5.1.1 *Degrees of freedom of shimmy model*

A complete shimmy numerical model has been developed from previous structural characteristics, including linear and non–linear behaviour of the main landing gear, in agreement with test measurements mentioned above.

This model takes into account 3 d.o.f. of the landing gear, located on the center of wheel axle : lateral displacement U_y, rotation M_x about ox longitudinal axis, which represent both lateral flexion, and rotation M_z about oz vertical axis, which represents torsion.

This model must take into account the following elements:

– structural description of landing gear
– gyroscopic effects
– dynamic tire
– landing gear non–linearities
– applied excitation

5.1.2 *Structural description of landing gear*

Landing gear structure is taken into account with :

– 2 matrices 3x3 *[M]* and *[K]* obtained from a dynamic condensation (*Guyan* method) on the center of wheel axle of the landing gear finite element model, whose calculated modes agree with modal tests with appropriation when linear behaviour is reached (cf **4.2.1**)

– a damping matrix 3x3 *[C]* , directly built from measured damping coefficients with the same modal tests (cf **4.2.1**)

5.1.3 *Description of gyroscopic effects*

We must take into account gyroscopic effects due to rolling wheels of the gear, in the form of a 3x3 matrix *[G]* which contains a term $J*V / R$: J is the moment of inertia for the system "wheel + tyre", R is the tire radius, V is the longitudinal airplane velocity .

5.1.4 *Description of dynamic tire*

A dynamic tire frequencial model was conveyed by its manufacturer, in the form :

$$F_{pneu}(s) = P(s)\ U(s) = P(s)\ [U_y(s)\ M_x(s)\ M_z(s)]^T$$

$P(s)$ is a 3x3 transfer matrix (s is Laplace variable), made up with 9 elementary transfer functions, whose terms agree with manufacturer dynamic tire tests, and depend explicitly on airplane velocity.

5.1.5 *Landing gear non–linearities*

Experimental results show more frequency variations in torsion tests than in flexion : consequently landing gear non–linearities, which are principally friction and freeplay, are only localized in torsional d.o.f. M_z, with the expression described in **3.3** : cf equations **(6)** and **(7)** .

5.1.6 *Applied excitation*

An excitation in moment along the *oz* axis is introduced in the model, to load the landing gear in torsion : this load will be applied in future shimmy tests.

5.2 Shimmy model numerical resolution

This non–linear shimmy model must be solved with a temporal analysis. Insofar as frequential analysis with a Laplace variable is limited to linear models, we must express the tire model in temporal variable, which requires the inverse Laplace transformation of each of the nine transfer functions of the above transfer matrix $P(s)$: this leads to a temporal expression $F_{pneu}(t)$.

The general form of the 3 d.o.f. shimmy model is :

$$M_{(\theta z)}\ U'' + (C+G)\ U' + K_{(\theta z)}\ U + F_{pneu}(t) + [0\ 0\ F_{frot}]^T = F_{ext}\text{ , with } U = [U_y\ M_x\ M_z]^T$$

$M_{(\theta z)}$ and $K_{(\theta z)}$ depend on θ_z because of torsional freeplay.

The scalar form of F_{frot} comes from equation **(6)** :

$$\frac{dF_{frot}}{dt} - \frac{\dot{\theta}}{{f_0}^2}\ K_f\ (F_{frot} - f_0\ sign(\dot{\theta}))^2 \ = \ 0$$

This non–linear system is solved iteratively, with a discretisation of the derived temporal terms (*Newmark* schema) and friction forces (*Crank–Nicholson* schema).

The solution depends on aircraft velocity, which appears in the gyroscopic matrix G and in the frequential tire model $P(s)$.

5.3 Results of model computation

From the previous temporal equation, we can obtain torsion responses of landing gear, for different non–linear parameter values and airplane velocities :

– torsional freeplay values : correspond to a translation freeplay measured of a standard point of measure, whose values are *0 , 0.5 , 1, 1.5* mm.

– torsional friction values : maximum force f_0 values are *0, 25 , 50* Nm, with a constant friction slope K_f in agreement with modal tests (cf *4.2.2*) .

– airplane velocity values : *45, 55 , 65, 75, 85* m/s.

The torsional damping can be deduced from logarithmic decrement of temporal torsion response.

The results can be summarized in diagrams showing torsional damping versus airplane velocity : each diagram corresponds to one freeplay value, with the 3 friction values : × : 0 Nm ; ▲ : 25 Nm ; + : 50 Nm

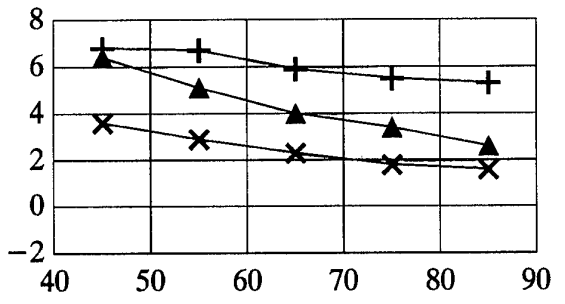

Freeplay 0 mm

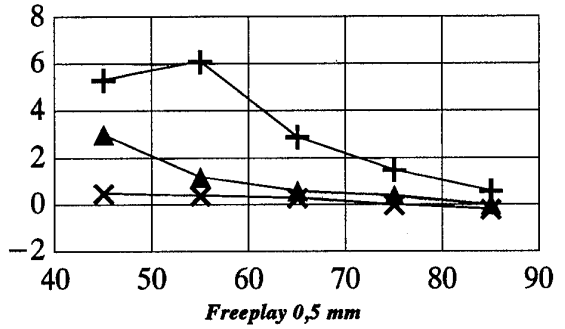

Freeplay 0,5 mm

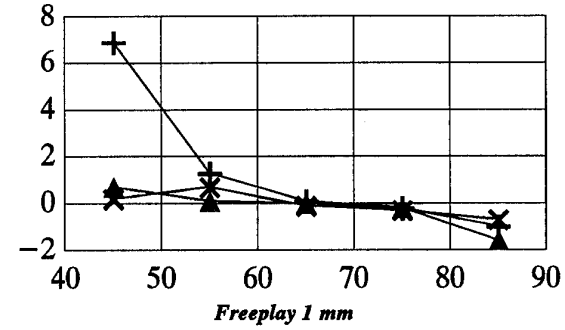

Freeplay 1 mm

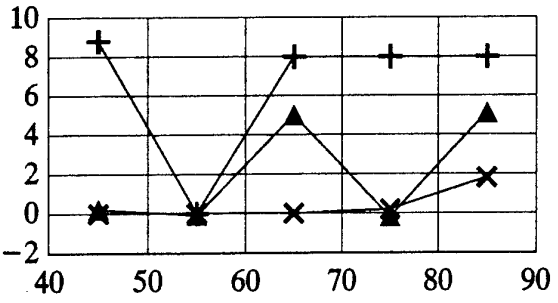

Freeplay 1,5 mm

The results can be also summarized in diagrams showing torsional damping versus airplane velocity : each diagram corresponds to one friction value 0 or 25 Nm, with the 3 freeplay values :

× : freeplay value 0 mm ▲ : freeplay value 0,5 mm.
\+ : freeplay value 1 mm ◆ : freeplay value 1,5 mm.

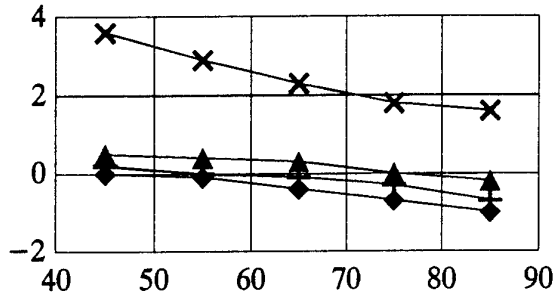

Friction 0

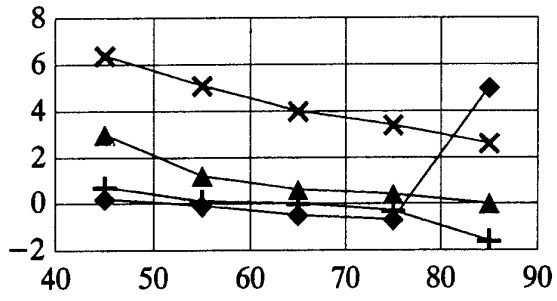

Friction 25

5.4 Influence of non–linearities on stability

These diagrams show that the linearized landing gear (freeplay and friction equal to zero) appears to be stable, but non–linearities lead to zero damping, which corresponds to limit cycles, and even to negative damping, which corresponds to divergence in torsion, hence the importance of taking non–linearities into account in shimmy models.

In general, this landing gear gets more stable when friction increases, and when freeplay decreases: this can be explained from the general results of the 1 d.o.f. non–linear model shown in **3.4.1** and **3.4.2** , and from flexion and torsion frequency values :

– when friction increases, the excitation level becomes insufficient to reach the limit force f_0 before sliding: friction behaves like an additional stiffness K_f, so the torsional frequency increases comparatively to its quasi–linear value.
– when freeplay increases, the excitation level becomes insufficient to reach the freeplay thresholds: this system gets less stiff, so the torsional frequency decreases comparatively to its quasi–linear value.

As shown in **4.2.1**, the studied landing gear, when behaving in a quasi–linear manner, has close frequencies in torsion (16 Hz) and in lateral flexion (14 Hz), which may occur coupling between these 2 modes. When non–linear friction increases, the torsional frequency increases too, so the 2 frequencies move aside : the coupling decreases and this landing gear gets more stable. Inversely, when non–linear freeplay increases, the torsional frequency decreases, and becomes closer to the lateral flexion frequency, which renders this landing gear more unstable : so this landing gear gets more stable when non–linear freeplay decreases.

This qualitative influence of non–linearities gets less clear when both freeplay and friction become important, as shown in the diagram for freeplay *1,5 mm* : in particular, for a friction value of *25 Nm*, the system becomes alternatively stable or unstable when aircraft velocity increases. This result is also shown in the following temporal curves for velocities values of 65, 75 and 85 m/s

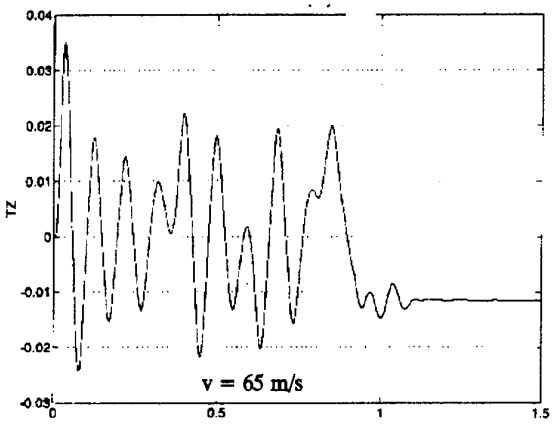

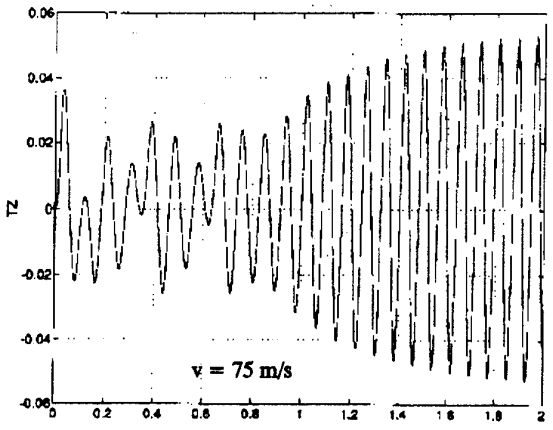

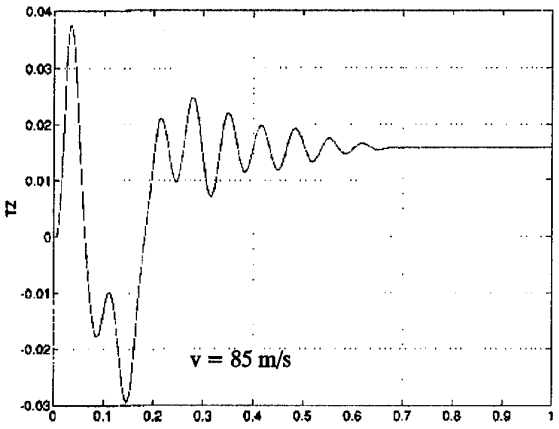

Such unpredictability caused by non–linearities can also be found in theoretical examples, such as the *"Duffing spring"*, whose behaviour is highly sensitive to initial conditions, so far as to become chaotic, in spite of a comparatively simple behavioural expression :

$$X'' + 0.05\,X'' + X^4 = 7.5\cos t$$

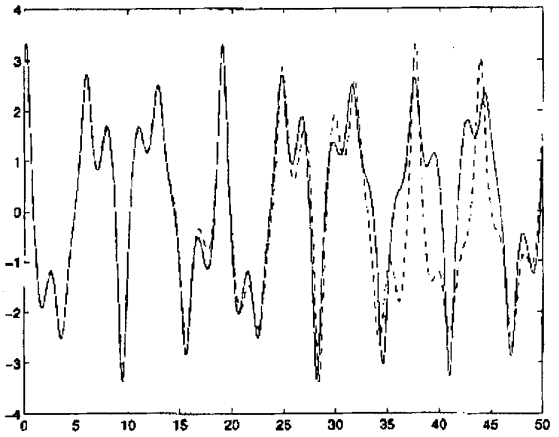

Duffing spring sensitivity to initial conditions
solid line : X(0) = 3 X'(0) = 4
dashed line : X(0) = 3.01 X'(0) = 4.01

Moreover, such chaotic behaviour has been expressed in previous landing gear nonlinear studies, in particular in reference [6] paragraph 4.

However, it is important to notice that this qualitative influence of non–linearities cannot apply to all landing gears, insofar as torsion and lateral flexion frequencies can be more or less close to each other; for instance, if frequencies in linear behaviour are 10 Hz in torsion and 15 Hz in lateral flexion, increasing friction increases torsion frequency, which gets closer to lateral frequency: the system may become more unstable, in opposition to this studied landing gear.

6. CONCLUSIONS

Calculation results shown above prove the importance of non–linearities in shimmy phenomena, and their influence on landing gear stability.

Some numerical procedures, such as shown in this text, enable one to obtain, from tests results, non–linearity values to be introduced into a shimmy model : however, these values are not intrinsic to the landing gear, insofar as they are highly dependant on its wear.

For this reason, it is important to continue shimmy studies by exploring non–linear parameters inside their possible range of variations, in order to define the most unfavourable configurations in terms of shimmy stability.

This is currently in progress at *Messier–Dowty S.A.*, with a more accurate non–linear characterization of the studied main landing gear from tests with transfer function measurements, and with the development of a complete shimmy numerical model, in agreement with modal test results.

Future shimmy tests on a flywheel will enable the validation of this non–linear numeric model, and the tests of configurations able to improve landing gear stability.

This improved modelization of the landing gear will allow to analyse its dynamic behaviour in its development. At this stage, it will be therefore convenient to define and qualify possible improvement of the design if necessary to achieve the requested dynamic stability of the landing gear in its range of operation conditions.

7. REFERENCES

[1] Computer Simulation of stick–slip friction in Mechanical Dynamic Systems – D. Karnopp – Journal of Dynamic Systems, Measurements and Control – March 1985, Vol. 107

[2] On the modelling and simulation of friction – D.A. Haessing, Jr. B. Friedland – Journal of Dynamic Systems, Measurements and Control – Transactions of the ASME – September 1991, Vol. 113

[3] Engineering Vibrations – Jacobsen, Ayre

[4] Modal testing : theory and practise – D.J. Ewins – John Wiley, 1984

[5] The polyreference time domain technique – F. Deblauwe, D.L. Brown, R.J. Allemang – IMAC 1987 p. 832,845

[6] Modeling and Analysis of a Dual–Wheel Nosegear : Shimmy Instability and Impact Motions – G. Li

[7] F15 Nose Landing Gear Shimmy Taxi Test and Correlative Analyses – D. Grossmann

[8] The behaviour of Non–linear Vibration Systems – W. Szemplinska–Stupnica – Kluwer Academic Publisher

[9] Engineering Vibrations – D. Inman – Prentice Hall

[10] L'essai de vibration des structures imparfaitement linéaires – R. Dat – Revue Française de Mécanique no 1987–3

A Nonlinear Model for Landing Gear Shimmy with Applications to the McDonnell Douglas F/A-18A

Jeff Baumann
Senior Engineer, Structural Dynamics and Loads
McDonnell Douglas Aerospace
P.O. Box 516
St. Louis, MO 63166-0516
USA

SUMMARY

This paper discusses a nonlinear shimmy model that includes components and features typically found in the nose landing gear of fighter aircraft. The gear structural model includes inertia, coulomb and viscous damping, stiffness, and torsional freeplay. Single and dual non-corotating wheels are considered. The tires are represented with the Moreland point-contact tire model.

Qualitative analytical results from modeling the nose landing gear of the McDonnell Douglas F/A-18A are presented. This landing gear, in the normal US Navy carrier-based configuration, is stable. When the launch bar and its power unit are removed for land-based versions of the aircraft, the nose gear may, under certain adverse conditions, experience shimmy. This condition can be aggravated by rotating forces due to tire unbalance or other irregularities. A number of corrective modification have been attempted with varying degrees of success. These range from relatively simple measures, such as increasing attention to tire maintenance, to more complicated schemes, such as adding a friction collar, adding mass dampers or even adding a dummy launch bar. For the most severe cases, the dummy launch bar seems to be required, however, the friction collar with mass dampers does show a significant improvement.

NOMENCLATURE

$\overline{A}$ = acceleration, $in / \sec^2$
C = tire coefficient of yaw, $1 / lb$
C_1 = tire yaw time constant, sec
C_D = tire lateral damping, lb sec/ in
CPC = Cleveland Pneumatic Company
C_{SD} = exponential steering damper coefficient, $in\ lb\ \sec^{MSD}$
C_{TL} = torque link structural damping, $in\ lb$ sec
D = distance between piston bearings, in
$DEAD$ = deadband function
$\overline{F_O}$ = force the strut must transmit to the wheel at point 0 for dynamic equilibrium, lb
$\overline{F_A}$ = force of the strut on the effective rigid body at point A, lb
F_L = resultant force in the lower piston bearing, lb
FMS = foreign military sales
FP = freeplay, rad(deg)
F_U = resultant force in the upper piston bearing, lb
H = overall length of the strut, in
$\overline{H}$ = angular momentum, $in\ lb$ sec
$[I]_{body}$ = effective inertia tensor for the rotating lower strut, $in\ lb\ \sec^2$
I_D = diametral moment of inertia of the wheel, $in\ lb\ \sec^2$
I_P = polar moment of inertia of the wheel, $in\ lb\ \sec^2$
J_{COLLAR} = collar/launch bar moment of inertia, $in\ lb\ \sec^2$
K_D = tire lateral stiffness, lb / in
K_{SD} = steering damper torsional stiffness, $in\ lb$
K_{TL} =torque link torsional stiffness, $in\ lb$
K_W = tire radial stiffness, lb / in
L = trailing arm length, in
L_P = length of the piston, in
$\overline{M_O}$ = moment the strut must transmit to the wheel at point 0 for dynamic equilibrium, $in\ lb$
$\overline{M_A}$ = moment of the strut on the effective rigid body point A, $in\ lb$
MDA = McDonnell Douglas Aerospace
m_e = effective mass of the strut, $lb\ \sec^2 / in$
MR = rotating unbalance, $lb\ \sec^2$

Paper presented at the 81st Meeting of the AGARD SMP Panel on "The Design, Qualification and Maintenance of Vibration-Free Landing Gear", held in Banff, Canada from 4-5 October 1995, and published in R-800.

MSD = steering damper exponent

m_W = mass of the wheel, $lb\ \sec^2/in$

R = wheel radius, in

R_{ST} = static wheel radius, in

$\overline{R}$ = position vector, in

R_L = lower piston bearing radius, in

R_{ROLL} = tire rolling radius, in

R_U = upper piston bearing radius, in

S = position(s) of the wheel(s) on the axle, in

sgn = signum function

t = time, sec

T_1 = spring torque on steering damper, $in\ lb$

T_2 = required torque in exponential damper, $in\ lb$

T_A = torque of torque linkage/steering damper at point A, $in\ lb$

T_{CP} = total Coulomb friction torque at piston, $in\ lb$

T_{PCON} = Coulomb friction torque at piston (constant), $in\ lb$

T_{SD} = steering damper Coulomb friction torque, $in\ lb$

T_{SF} = Coulomb seal friction, $in\ lb$

$\hat{u}$ = unit vector aligned with the axle

U_G = position of the CG, $\hat{i}_3$ component, in

USN = United States Navy

$\overline{V}$ = velocity, in / sec

V_G = position of the CG, $\hat{j}_3$ component, in

V_{TAXI} = taxi speed, in / sec $(knots)$

W = aircraft weight on the strut, lb

W_G = position of the CG, $\hat{k}_3$ component, in

x = lateral strut tip deflection, in

α = strut tip bending angle, rad (deg)

$\overline{\alpha}$ = angular acceleration, $rad / \sec^2$

β = position of rotating unbalance, rad (deg)

γ = constant strut caster angle, rad (deg)

Δ = lateral tire deflection, in

θ = steering angle, rad (deg)

θ_C = collar angle, rad (deg)

θ_D = damper angle, rad (deg)

λ = tire camber angle, rad (deg)

μ = coefficient of friction at piston bearings

μ_R = coefficient of rolling resistance

μ_T = tire moment coefficient, $in\ lb$

σ = angle between the coordinate system at the strut tip and the one at the tire, measured about the axle, rad

ϕ = tire yaw angle, rad (deg)

ψ = tire drift angle, rad (deg)

Ω = wheel spin rate, rad / sec

$\overline{\omega}$ = angular velocity, rad / sec

1. INTRODUCTION

As efforts are made to increase the performance and to decrease the weight of modern aircraft landing gears, shimmy problems often result. Much effort has gone into predicting the shimmy stability of landing gear designs and in studying ways to stabilize shimmy prone gears.

One of the most important factors in the shimmy model is the modeling of the tires. Two main theories have been used to describe the interaction between the tire and the ground. The 'stretched string' tire model, proposed by vonSchlippe and Dietrich [1] analyzes the tire as if it were a taut string on an elastic foundation. The point-contact tire model was proposed by Moreland [2] In this model, the effects of the ground on the tire are assumed to act at a single idealized contact point. The lateral displacement of the contact point and the tire drift angle are related by the model to the lateral restoring force and the vertical restoring moment. Many researchers have since examined and compared these models. Collins [3], for example, finds that the point contact tire model is adequate for qualitative and, in most cases, quantitative studies. Also, Black [4] has shown that the point contact tire model can be derived from the stretched-string tire model. Since the point-contact tire model is much easier to implement and the required parameters are better understood, it is used for this work.

Since some of the original analysis and verification of the analysis program was related to the nose landing gear of the McDonnell Douglas F-15 it is worth special mention at this time.

The original nonlinear analysis of the F-15 nose gear was performed by Cleveland Pneumatic Company (CPC), the gear's manufacturer. Southerland [5] describes the original analysis and computer simulation of the gear.

Both this early analysis and subsequent dynamometer testing suggested that no problems existed with the design. As aircraft were put into service and began to wear, however, shimmy problems developed. These instabilities were traced to the presence of larger than anticipated values for the torsional freeplay. When shims were added to reduce this freeplay, the shimmy disappeared.

Grossman [6] describes experimental and analytical shimmy tests performed as part of the modification to the design of the F-15. In the first phase of the study, a series of taxi tests were performed with a specially instrumented aircraft. Vibrations were measured as the aircraft was taxied at a variety of speeds and conditions.

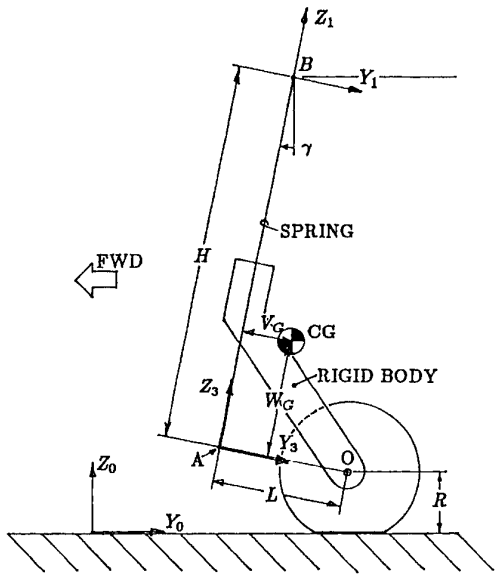

Fig. 1a. Model Geometry for Cantilevered Landing Gear

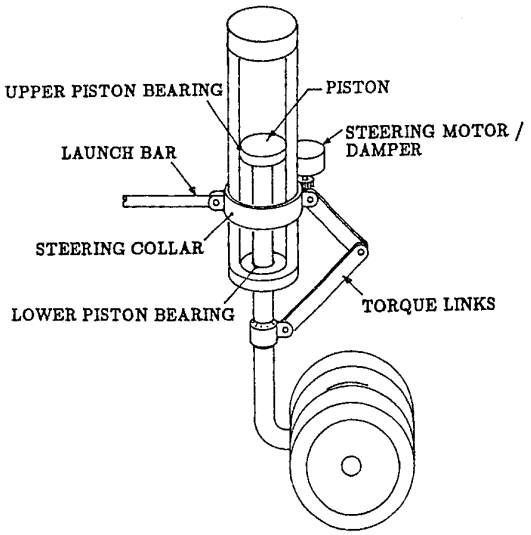

Fig. 1b. Cantilevered Landing Gear

The second phase of Grossman's study involved repeating the CPC analysis with more realistic values for the parameters. An attempt was also made to linearize the nonlinear terms in the equations.

The analysis correlated well with the shimmy speed - freeplay relations found in the taxi tests. Absolute stability was obtained for torsional freeplay less than 0.75 degrees. Also, the linearized models were shown to agree with the nonlinear model for the range of parameters tested.

2. NONLINEAR LANDING GEAR MODEL

The objective of this work was to develop software that would aid landing gear engineers in assessing the shimmy stability of a more general class of landing gear designs. With this analysis capability, potential problems could be identified early in the design process. It was also desired to be able to predict how changes to existing design would affect the shimmy stability.

Special care was taken to realistically model the torsional components that are typically found in fighter aircraft nose landing gears. Three different landing gear geometries were studied: cantilevered, fully-levered and semilevered. Only the cantilevered type, as pictured in Fig. 1, will be discussed here.

The strategy employed was to analyze the landing gear structure and the tire separately from each other. The structural model and tire model were programmed as separate computer subroutines that would share information as the simulation ran. This made the simulation modular in that new tire or structural models could be added later.

Since the details of this analytical model have been presented elsewhere (Baumann, Barker and Koval [7] and Baumann [8], a more general description will follow. Table 1 lists the degrees of freedom/state variables used for this model.

2.1. Kinematics

2.1.1. Coordinate systems

The inertial coordinate system $X_O Y_O Z_O$ is attached to the runway (see Fig. 1a). The Z_O axis point upwards, the Y_O axis is aligned with the runway axis and points aft, the X_O axis completes the right-handed triad and points to the port side of the aircraft.

A moving $X_1 Y_1 Z_1$ is fixed to the top of the aircraft strut. It is rotated away from the $X_O Y_O Z_O$ about the negative X_O axis by the constant caster angle γ.

The $X_2 Y_2 Z_2$ system is fixed to the bottom of the strut and accounts for bending of the strut. It is rotated away from the $X_1 Y_1 Z_1$ about the Y_1 axis by the variable strut bending angle α.

The $X_3 Y_3 Z_3$ system is fixed to the bottom of the strut and accounts for rotations of the strut. It is rotated away from the $X_2 Y_2 Z_2$ about the Z_2 axis by the variable steering angle θ.

TABLE 1 - Degrees of Freedom

Strut Model

x	= lateral strut tip deflection, *in*
$\dot{x}$	$= \frac{dx}{dt}$
α	= strut tip bending angle, *rad* (deg)
$\dot{\alpha}$	$= \frac{d\alpha}{dt}$
θ	= steering angle, *rad* (deg)
$\dot{\theta}$	$= \frac{d\theta}{dt}$
θ_C	= collar angle, *rad* (deg)
$\dot{\theta}_C$	$= \frac{d\theta_C}{dt}$
θ_D	= damper angle, *rad* (deg)

Tire Model

β	= position of rotating unbalance, *rad* (deg)
Δ	= lateral tire deflection, *in*
ψ	= tire drift angle, *rad* (deg)

away from the $X_2Y_2Z_2$ about the Z_2 axis by the variable steering angle θ .

2.1.2. Rotational Kinematics

The angular velocity of the bottom of the strut is equal to the angular velocity of the $X_3Y_3Z_3$ coordinate system. This angular velocity accounts for the strut bending rotation α plus changes in the steering angle θ and is given by

$$\overline{\omega}_3 = (\dot{\alpha}\sin\theta)\hat{i}_3 + (\dot{\alpha}\cos\theta)\hat{j}_3 + \dot{\theta}\hat{k}_3 .$$

The corresponding angular acceleration is

$$\overline{\alpha}_3 = (\ddot{\alpha}\sin\theta + \dot{\alpha}\dot{\theta}\cos\theta)\hat{i}_3 + (\ddot{\alpha}\cos\theta + \dot{\alpha}\dot{\theta}\sin\theta)\hat{j}_3 + \ddot{\theta}\hat{k}_3$$

2.1.3. Translational Kinematics

The position, velocity and acceleration of four key points on the strut are needed for this analysis. Reference is made to Fig. 1a.

Point B is at the intersection of the strut axis and the trunnion axis. This point is assumed to remain a constant height above the runway and have a constant taxi speed V_{TAXI} .

Point A, the reference point at the bottom of the strut is separated from point B by the strut of length H which is held constant over the simulation. Also, the strut may bend laterally, with the tip (Point A) deflecting a variable distance x .

Point O, at the intersection of the strut and the axle, is separated from Point A by the trailing arm length L .

The motion of this point will also be subject to the variable strut bending angle, α ,and steering angle, θ .

The center of mass of the effective rigid body, Point CG, of the effective rigid body which represents the swiveling mass of the landing gear is located with respect to point A by the arbitrary vector

$$\overline{R}_{CG/A} = U_G\hat{i}_3 + V_G\hat{j}_3 + W_G\hat{k}_3 .$$

Thus, motion of this point will also be subjected to the three flexible degrees of freedom described above.

2.2. Tire Effects

Based on a complete kinematic description of the axle, a separate tire model is used to determine the force and moment that the strut must exert on the tire(s) to maintain dynamic equilibrium. This force may include suspension, traction, rotating unbalance, and inertia effects. One such tire model is described in detail in Section **3**.

For convenience, it is assumed that the force and moment act at point O, no matter where the tire is mounted on the axle. Any transformations that are required are included in the tire model.

The force and the moment will generally be of the form

$$\overline{F}_O = \overline{F}_O(\overline{A}_O, \overline{\alpha}_3)$$

$$\overline{M}_O = \overline{M}_O(\overline{A}_O, \overline{\alpha}_3)$$

which requires that previously defined expressions for $\overline{A}_O$ and $\overline{\alpha}_3$ be substituted into the moment expressions.

2.3 Strut Forces

2.3.1. Elastic Restoring Forces and Moments.

The restoring force (F_S) and moment (M_S) due to the bending (x, α) of spring element AB is given by a 2x2 stiffness matrix and a 2x2 structural damping matrix. This force acts at point A in the ($\hat{i}_3$) direction. The moment also acts at point A about the (- j_3) axis.

2.3.2. Shock Strut Bearing Forces

Considering the forces and moments acting on the piston/spring at Point A (due to bending and the weight of the aircraft on the nose gear) statics can be used to determine the forces in the upper and lower piston bearings (F_U and F_L , respectively). The resulting torque exerted on the piston (and hence on

the lower strut) is

$$T_{CP} = \left\{T_{PCON} + \mu\left[R_U F_U + R_L F_L\right]\right\}\mathrm{sgn}(\dot{\theta})$$

where T_{PCON} is an additional friction torque arising from Coulomb friction between the piston and cylinder walls (independent of loading at point A).

2.4 Dynamic Analysis

At point A, the force $\overline{F}_A$ and the moment $\overline{M}_A$ represent the force and moment of the strut on the rigid body. At point O, the force $\overline{F}_O$ and the moment $\overline{M}_O$ represent the force and moment required by the wheels for static equilibrium.

2.4.1. Translational Dynamics

From Newton's second law applied to the strut rigid body,

$$\overline{F}_A = \overline{F}_O + m_e\,\overline{A}_{CG}$$

where m_e is the effective translational mass of the strut.

2.4.2. Rotational Dynamics

From Newton's second law for rigid body rotations about the mass center of the strut rigid body,

$$\begin{aligned}\dot{\overline{H}}_G &= \sum \overline{M}_G \\ &= \overline{M}_A + (-\overline{M}_O) + (-\overline{R}_{CG/A}) \times \overline{F}_A \\ &\quad + \overline{R}_{O/A} \times (-\overline{F}_O) + (-\overline{R}_{CG/A}) \times (-\overline{F}_O).\end{aligned}$$

Solving for $\overline{M}_A$,

$$\begin{aligned}\overline{M}_A &= \dot{\overline{H}}_G + \overline{M}_O + \overline{R}_{CG/A} \times \overline{F}_A + \overline{R}_{O/A} \times \overline{F}_O \\ &\quad - \overline{R}_{CG/A} \times \overline{F}_O \\ &= [I]_{BODY}\overline{\alpha}_3 + \overline{\omega}_3 \times \overline{H}_G + \overline{M}_O + \overline{R}_{CG/A} \times \overline{F}_A \\ &\quad + \overline{R}_{O/A} \times \overline{F}_O - \overline{R}_{CG/A} \times \overline{F}_O.\end{aligned}$$

2.4.3. Torque Models

Since shimmy involves rotations about the strut axis and since most corrective measures involve torsional components (often torsional dampers), a good torsional model is very important. Figure 2 shows how the system of Fig. 1b is modeled.

Starting at the bottom of Fig. 1b, the interaction between the tire and the ground plays a large role in any torsional model. The modeling of the tire is discussed in Section 3.

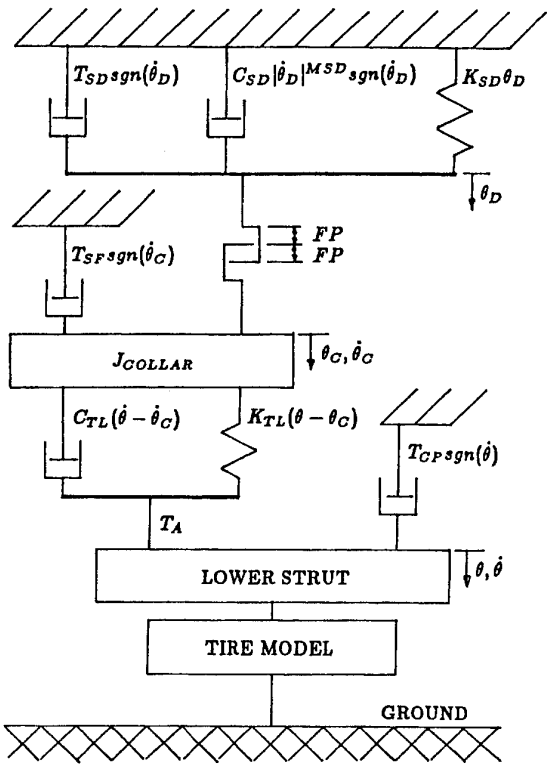

Fig. 2. Model for Torques

The lower shock strut can translate along the strut axis with motion restricted by oleo-pneumatic forces within the strut. Coulomb friction will be present in the upper and lower piston bearings. This friction will oppose translation as well as rotation of the lower shock strut. Gross rotations of the lower shock strut is prevented with internal splines or with an external torque linkage, as shown in Fig. 1b.

The upper arm of the torque linkage is connected to the steering collar. For carrier based aircraft, such as the F/A-18A described below, a launch bar would also be attached to this steering collar and its effects would have to be included in the torque model.

The steering collar is driven by a steering motor. When not actively steering, this motor will serve as a shimmy damper. This damper is modeled with a spring, a Coulomb damper and an exponential damper. The exponential damper will generate a damping torque proportional to the relative angular velocity across the damper raised to some exponent. If this exponent were 1.0, the damper would be a linear viscous damper. If this exponent were 2.0, the damper would be a "velocity-squared" damper.

The connection between the steering collar and the damper will often have some freeplay. This freeplay, caused by gear backlash and clearance between mating parts, will allow some relative motion across the connection between the collar and the damper.

A total of three degrees of freedom are required to describe the full torsional model described above. These degrees of freedom are the collar angle θ_C, its derivative $\dot{\theta}_C$, and the damper angle θ_D. The torque model will contain the derivatives of these three quantities as well as the torque T_A which the above components will apply to the lower strut rigid body.

Since some of these components may not be present or may have only minimal effect, provisions are made to remove one or more of the degrees of freedom from the model. Six separate cases involving various combinations of degrees of freedom were analyzed. Each of these special cases are treated separately in numerical computations. Only the first of these cases, the full model as pictured in Figs. 1b and 2, is discussed here.

It is first necessary to determine if the steering damper is engaged to the collar. This depends on the absolute difference between the collar angular position, θ_C and the damper angle, θ_D.

a)Steering damper disengaged: $|q_C - q_D| < FP.$

The torque of the strut on the wheel, T_A, is transmitted through the torque links, so that

$$T_A = K_{TL}(\theta - \theta_C) + C_{TL}(\dot{\theta} - \dot{\theta}_C)$$

If no structural damping is present in the torque links, C_{TL} can be set to zero.

Summing torques in the disengaged steering damper requires

$$K_{SD}\theta_D + C_{SD}|\dot{\theta}_D|^{MSD}\,\mathrm{sgn}(\dot{\theta}_D) + T_{SD}\,\mathrm{sgn}(\dot{\theta}_D) = 0$$

This can be solved for $\dot{\theta}_D$ by first defining

$$T_1 = -K_{SD}\theta_D$$

and

$$T_2 = |T_1| - T_{SD}.$$

If T_2 is greater than zero, then the spring torque (T_1) will overcome the Coulomb friction and need to be reacted by the exponential damper. If T_2 is less than zero, the Coulomb friction alone will be sufficient to react the spring torque. Summarizing:

$$\dot{\theta}_D = \frac{d}{dt}(\theta_D) = \begin{cases} 0 & \text{for } T_2 \le 0 \\ \mathrm{sgn}(T_1)\left(\dfrac{T_2}{C_{SD}}\right)^{\frac{1}{MSD}} & \text{for } T_2 > 0 \end{cases}$$

Note that the latter expression requires a nonzero steering damper coefficient, C_{SD}. If this coefficient is set to zero, θ_D is no longer considered to be a degree of freedom and one of the other torque models would be used.

Applying Newton's second law of motion for rotations to the collar yields

$$\ddot{\theta}_C = \frac{d}{dt}(\dot{\theta}_C) = \frac{\left[K_{TL}(\theta - \theta_C) + C_{TL}(\dot{\theta} - \dot{\theta}_C) - T_{SF}\,\mathrm{sgn}(\dot{\theta}_C)\right]}{J_{COLLAR}}$$

Note that this equation requires that collar rotary inertia be present ($J_{COLLAR} \neq 0$). If the rotary inertia is zero, θ_C is not considered to be a degree of freedom and again one of the torque models would be used.

The final state variable derivative

$$\dot{\theta}_C = \frac{d}{dt}(\theta_C)$$

is already defined since it is also a state variable.

b) Steering damper engaged: $|\theta_C - \theta_D| \ge FP.$

As before, the torque of the strut on the wheel, T_A, is transmitted through the torque links and is given by

$$T_A = K_{TL}(\theta - \theta_C) + C_{TL}(\dot{\theta} - \dot{\theta}_C)$$

If no structural damping is present in the torque links, C_{TL} can be set to zero.

Because the steering damper is connected to the collar,

$$\dot{\theta}_D = \frac{d}{dt}(\theta_D) = \dot{\theta}_C$$

Since $\dot{\theta}_C$ is a state variable, this is already defined.

Applying Newton's second law of motion for rotations to the collar,

$$\ddot{\theta}_C = \frac{d}{dt}(\dot{\theta}_C) = \Big[K_{TL}(\theta - \theta_C) + C_{TL}(\dot{\theta} - \dot{\theta}_C) - T_{SF}\,\mathrm{sgn}(\dot{\theta}_C) - K_{SD}DEAD(\theta_C, FP) - T_{SD}\,\mathrm{sgn}(\dot{\theta}_C) - C_{SD}|\dot{\theta}_C|^{MSD}\,\mathrm{sgn}(\dot{\theta}_C)\Big] / J_{COLLAR}$$

Again notice that J_{COLLAR} must be nonzero for this model to apply. This expression uses the deadband function to account for freeplay. This function is given by

$$DEAD(X, FP) = \begin{cases} X + FP & \text{for } X < (-FP) \\ 0 & \text{for } |X| < FP \\ X - FP & \text{for } X > FP \end{cases}$$

3. MORELAND POINT-CONTACT TIRE MODEL

This model computes the effects of a single non-corotating wheel on the strut. Moreland's point-contact theory [2] is used to describe the cornering and drift of the tire.

It is assumed that the torque about the axis of rotation is negligible. This means that no bearing friction or braking of the wheel is permitted. A rotating unbalance in the center plane of the tire is considered.

3.1 Kinematic Analysis

The following information regarding the strut axle is required by the tire model: $\overline{R}_O, \overline{V}_O, \hat{u}, \overline{\omega}_{STRUT}, S$.

The acceleration of point O and the angular velocity of the lower strut will generally not be known to the tire model. They are assumed to be of the form:

$$\overline{A}_O = A_O^X \hat{i}_O + A_O^Y \hat{j}_O + A_O^Z \hat{k}_O,$$

$$\overline{\alpha}_{STRUT} = \alpha_X \hat{i}_O + \alpha_y \hat{j}_O + \alpha_z \hat{k}_O.$$

3.1.1. Coordinate Systems

Three coordinate systems are employed in this tire model. The first $X_O Y_O Z_O$ is an inertial system aligned with the ground. The Y_O axis points to the left side of the runway, the X_O axis is aligned with the runway axis and points to the rear of the aircraft and the Z_O axis points up. This corresponds to the $X_O Y_O Z_O$ axis of the landing gear strut model.

The second coordinate system $X_1 Y_1 Z_1$ is rotated from the $X_O Y_O Z_O$ about the Z_O axis by the yaw angle ϕ (Fig. 3).

The third coordinate system $X_2 Y_2 Z_2$ is rotated from the $X_1 Y_1 Z_1$ about the Y_1 axis by the camber angle λ (Fig. 4).

Note that $\hat{i}_2 = \hat{u}$ is the unit vector aligned with the axle. Since $\hat{u}$ is specified in the strut model, it is possible to solve for the angles ϕ and λ :

$$\tan\phi = u_Y / u_X$$

$$\tan\lambda = -u_Z \sin\phi / u_Y.$$

3.1.2. Rotational Kinematics

The angular velocity of the axle used in this tire model accounts for changes in the yaw angle $\dot{\phi}$ and changes in the camber angle $\dot{\lambda}$ and is

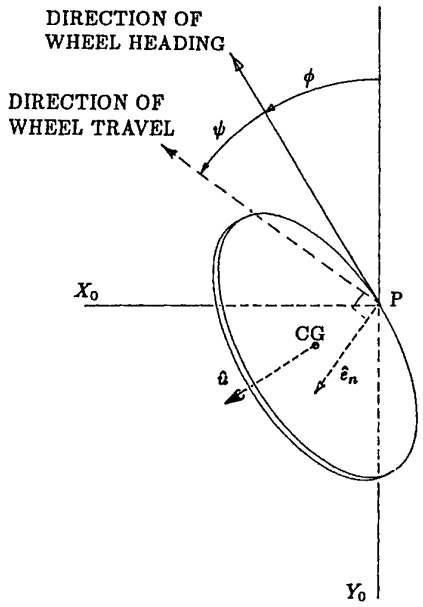

Fig. 3. Top of Wheel

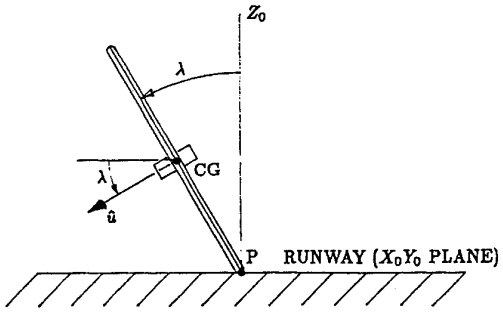

Fig. 4. End View of Wheel

$$\overline{\omega}_2 = -\dot{\phi}\sin\lambda \hat{i}_2 + \dot{\lambda}\hat{j}_2 + \dot{\phi}\cos\lambda \hat{k}_2$$

The angular velocity of the axle is specified by the strut model as

$$\overline{\omega}_{STRUT} = \omega_X \hat{i}_O + \omega_Y \hat{j}_O + \omega_Z \hat{k}_O.$$

Generally, it will not be possible to find values for $\dot{\phi}$ and $\dot{\lambda}$ that will satisfy $\overline{\omega}_2 = \overline{\omega}_{STRUT}$ for all three components (there are three equations but only two unknowns). The difference between the two angular velocities is a relative rotation about the $\hat{u}$ axis. This rate $\dot{\sigma}$, and acceleration $\ddot{\sigma}$ can be solved and used to account for the discrepancies between the strut and wheel system.

3.1.3. Translational Kinematics

Point CG, the wheel center of mass is separated from point O by a distance S along the axis. Thus,

$$\overline{R}_{CG/O} = S\hat{u} = S\hat{i}_2 .$$

The general position, velocity and acceleration equations can be used to determine the motion of CG.

3.2. Kinematic Constraints

Three kinematic constraints must be satisfied. They are the following:

3.2.1. Tire Rolls Without Slipping

This can be used to define Ω, the spin rate of the wheel. This condition is

$$-\overline{V}_{CG} \cdot \hat{j}_1 = R_{ROLL}\Omega ,$$

where R_{ROLL} is the rolling radius of the tire. The left side of the equation gives the component of the wheel CG velocity in the direction of the wheel heading.

Differentiating with respect to time,

$$-\overline{A}_{CG} \cdot \hat{j}_1 = R_{ROLL}\dot{\Omega} ,$$

where $\dot{\Omega}$ is the time rate of change of the wheel spin rate.

3.2.2. Vertical Constraint

This constraint sets the geometric radius, R, of the tire by requiring that the tire always maintains contact with the ground at the contact point. The appropriate equation is

$$\overline{R}_{CG} \cdot \hat{k}_O = R\hat{k}_2 \cdot \hat{k}_O .$$

Differentiating,

$$\overline{V}_{CG} \cdot \hat{k}_O - R\dot{\hat{k}}_2 \cdot \hat{k}_O = \dot{R}\hat{k}_2 \cdot \hat{k}_O .$$

These two equations can be solved for R and $\dot{R}$.

3.2.3. No Side Slip

A tire under the action of a side force will drift or yaw (as it rolls) from the direction in which it is pointed (see Fig. 3). This angle is called the side-slip angle or the drift angle and is denoted by ψ. A standard condition is to require that as the wheel rolls and side slips, the component of the velocity normal to the path of travel becomes zero, i.e.,

$$\overline{V}_P \cdot \hat{e}_n = 0$$

where $\hat{e}_n$ is the unit vector indicated in Fig. 3, and P is the contact point. The unit normal vector, $\hat{e}_n$ can be written as

$$\hat{e}_n = \cos(\phi + \psi)\hat{i}_O + \sin(\phi + \psi)\hat{j}_O .$$

The position of point P, the contact point, is given by

$$\overline{R}_P = \overline{R}_O + S\hat{i}_2 - R\hat{k}_2 + \Delta\hat{i}_1 .$$

The velocity of P is found by differentiating. This constraint is used to solve for the unknown $\dot{\Delta}$.

3.3. Forces and Moments Acting on the Wheel

3.3.1. Ground Forces and Moments

The moment exerted by the tire on the ground, by virtue of side slip and the twist is given by Moreland [2] as

$$\overline{M}_T = \mu_T \psi \hat{k}_O .$$

There are also forces applied to the tire:

$$\overline{F}_{GROUND} = F_{RAD}\hat{k}_O + F_N\hat{i}_1 + F_D\hat{j}_1$$

where

$F_{RAD} = W - K_W(R - R_{ST})$ = tire radial force,

$F_N = K_D\Delta + C_D\dot{\Delta}$ = Moreland tire side force

and

$F_D = \mu_R(F_{RAD}\cos\lambda)$ = tire drag force.

The final element of Moreland's model relates yaw to side force:

$$\dot{\psi} = -\frac{1}{C_1}(CF_N + \psi) .$$

3.3.2. Tire Unbalance

Tire unbalance forces are due to centrifugal effects of a rotating unbalance. If the product of the unbalance mass and radius is MR and the wheel spins at a rate Ω, then the unbalance force is

$$\overline{F}_{UNBAL} = MR\Omega^2(-\sin\beta\hat{j}_2 + \cos\beta\hat{k}_2)$$

where β is the rotation of the unbalance mass and is equal to $(\Omega t + \beta_O)$; β_O is the initial wheel position.

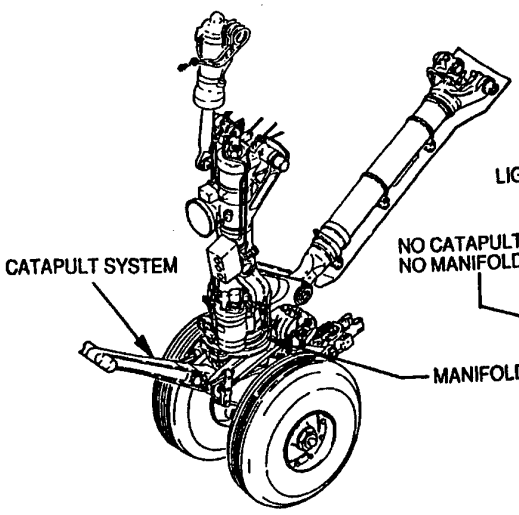

Fig. 5. F/A-18 NLG (USN)

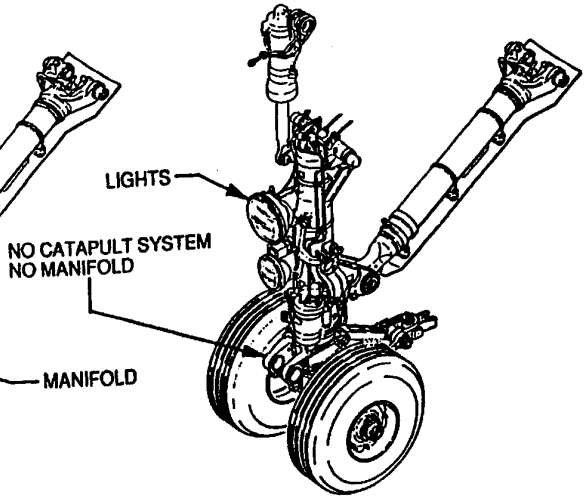

Fig. 6. F/A-18 NLG (FMS)

3.4. Tire Dynamics

Summing forces by Newton's second law, the force exerted by the strut on the wheel is

$$\overline{F}_O = m_W \overline{A}_{CG} - \overline{F}_{GROUND} - \overline{F}_{UNBAL} .$$

Summing Moments about the wheel's mass center and applying Newton's second law for rotations yields the moment of the strut on the wheel

$$\overline{M}_O = \dot{\overline{H}}_G - \overline{M}_T + \overline{R}_{CG/O} \times \overline{F}_O - \overline{R}_{P/CG} \times \overline{F}_{GROUND}$$

The condition of no wheel bearing friction is imposed by requiring that

$$\overline{M}_O \cdot \hat{u} = 0 .$$

4. THE F/A-18A

4.1. Description of the F/A-18A

The F/A-18A is a single place carrier-based fighter attack aircraft built by McDonnell Douglas, originally for the US Navy. First flight occurred in November 1978. Since then, the F/A-18A and its two-seat variant the F/A-18B have also been sold to Canada (with the landing gear in the original USN configuration) and to Australia and Spain (in a land-based foreign military sales, or FMS, configuration).

The landing gear is in the tricycle configuration with a dual wheel cantilevered nose landing gear (Fig. 5) and fully levered single wheel main landing gears.

A nose wheel steering (NWS) unit has three modes of operation: high gain steering (for low speed taxiing), low gain steering, and off/passive damping. The low gain mode is automatically active for landing and rollout but can be deselected by the pilot using a switch on the control stick.

4.2 Configuration Differences (USN vs. FMS)

The launch bar is used to connect the aircraft to the shuttle of a catapult and launch the aircraft off the deck of an aircraft carrier. When the aircraft is intended to be solely land-based, weight savings and reduced maintenance expense could be realized by deleting the launch bar (about 35 pounds) and associated systems (Fig. 6). The launch bar power unit manifold, Fig. 7, is a collar that rotates with the torque links and wheels. This manifold provides the hydraulic power necessary to raise and lower the launch bar. Seals which contain this hydraulic pressure provide a stabilizing friction torque.

FMS versions may also include taxi lights and other minor differences not relevant to the present work.

Numerical analysis of the FMS landing gear by the landing gear vendor prior to fabrication suggested no problems would result from removing the launch bar alone or in combination with the manifold collar.

4.3 General Observations

Most reports of shimmy in the F/A-18 have been described as pilot annoyance and decreased comfort. In the most severe conditions, however, safety-of-flight concerns have been raised, primarily due to vibration levels sufficient to make cockpit instrumentation (excluding the head-up-display) difficult to read.

Wide variations are found in the ages of the aircraft and the tires where shimmy is reported.

4.4. Tires

The condition of the tires appears to play a large role in shimmy. One common, apparently effective, short term maintenance correction is to change the tires

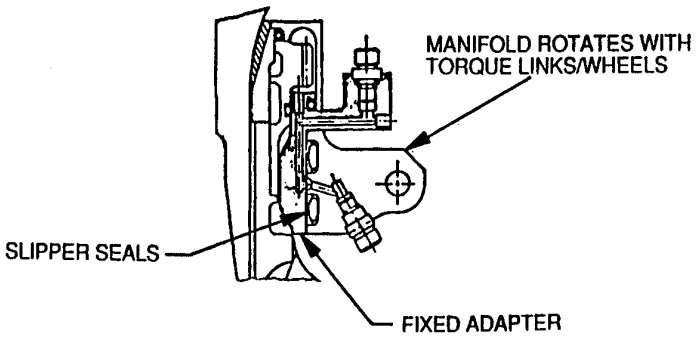

Fig. 7. Steering Manifold

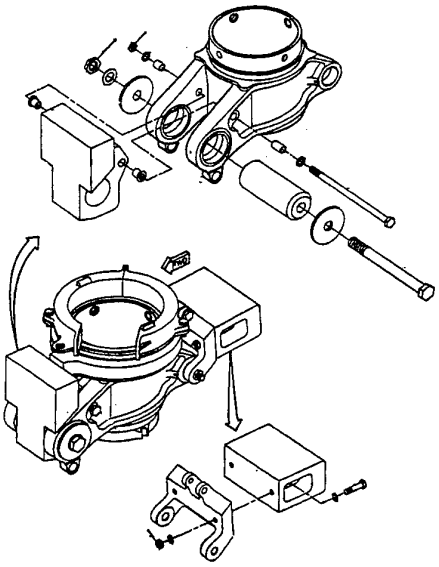

Fig. 8. Mass Damper

when shimmy is reported. As this reduces the tire life, this makes the aircraft more costly to operate.

Two specific factors have been observed to be important. These factors lead to cyclic forcing of the nose gear and, while this is not shimmy, it can drive similar vibrations. The first effect is rotating unbalance. The wheels and tires are checked to insure specification compliance but the combined assembly is not. A production tire-wheel assembly was tested by MDA on a commercial automotive wheel balancing machine and the unbalance was measured at 12 inch-ounces. While this is a severe unbalance, it is roughly the sum of the two unbalances allowed by the specifications. Since the tires wear quickly with use, it would seem impractical to balance the assembly on a routine basis.

The second factor is cold set of the rubber resulting in flat spots. This can result from loading the tire before the rubber is fully stretched by the inflation pressure, or by leaving the aircraft parked on the tires for several days. This was observed during a winter flight test in St. Louis. The tires were inadvertently allowed to cold set and shimmy resulted.

4.5. Corrections

Several modifications to the FMS landing gear configuration have been proposed and/or attempted to correct shimmy. These will be discussed in order of increasing cost and complexity.

4.5.1. Increased Attention to Tire Maintenance

As earlier discussed, the condition of the tires has a big effect on shimmy and increased emphasis on maintenance can do a lot to mitigate shimmy.

While the wheels are not balanced, the tires are marked by the manufacturer with a balance mark that can be aligned with the valve stem on the wheel to minimize static unbalance. Additionally, the tires should be inflated with dry air or nitrogen (to minimize internal moisture) and be allowed to grow for at least 12 hours before loading. This ensures an even stretch of the rubber. An effort should also be made to match tire diameters and pressures for the two nose gear tires. The tire pressure should be regularly checked.

To prevent formation of flat spots, the aircraft should be moved every 48 hours or jacked if unused for long periods of time.

4.5.2. Addition of a Friction Collar to Replace the Launch Bar Power Unit Manifold

The seals of the launch bar power unit manifold represent about 20% of the breakout torque and about 10% of the running torque required to swivel the wheels. This damping (along with some stabilizing mass) can be regained by adding a collar where the manifold is usually situated.

4.5.3. Addition of Simple Masses in Conjunction with the Collar Assembly

Additional weights can be added to the above collar, as shown in Fig. 8, to replace some or all of the mass removed with the launch bar. Since this mass has no mechanical function it can be placed where it will not interfere with gear stowage. Due to the smaller radius of gyration, this mass adds up to about 30% of the original rotational inertia. The weights can be

modular in design and be added incrementally to correct the problem with a minimum of increased weight.

4.5.4. Reduce Freeplay

As discussed above, freeplay has previously been shown to be a significant factor in causing shimmy. Closing the tolerances in the torque links by adding special bushings has been suggested. Another possible source of freeplay is gear backlash between the steering motor/damping unit and the ring gear on the strut.

4.5.5. Addition of a Dummy Launch Bar

This solution is more complicated than the simple masses since it must be moved for the gear to retract. As the USN configuration is quite stable, this will solve shimmy problems.

The Spanish F/A-18 problem was corrected by incorporating a collar with a simple mass damper as described in item three, above. A flight test program was undertaken to evaluate this correction. Qualitative pilot comments were used as a basis for comparing different arrangements and to select a final design.

The Australians have had a more chronic problem. This is believed to be due, at least in part, to operating the aircraft from rougher runways. A flight test program was flown from May through October 1991 and examined the five corrective actions described above (Ranson, et al., [9]). The flight test instrumentation included triaxial accelerometers attached near the bottom of the nose gear strut and on the fuselage near the nose gear trunnion. Also, high-speed motion picture cameras were mounted on the aircraft keel and at the wing tips. Nearly 300 touch-and-go landings were performed over almost 60 flights as part of this test.

In the flight test program flown by the Royal Australian Air Force, they identified a shimmy mode as well as a speed-dependent vibration mode of the gear, with a frequency equal to the wheel rotation rate. At typical landing speeds, this speed-dependent vibration mode is very close to the second harmonic of the shimmy mode, explaining why the wheel unbalance and flat spots seem to aggravate shimmy.

The NWS was deselected for about half of the landings performed. This decreased the severity of shimmy only slightly. Of the above solutions, only the addition of the dummy launch bar was found to be acceptable. The Australians are currently considering this retrofit.

4.6. Qualitative Analytical Comparison

To demonstrate the analytical model presented in sections **2** and **3**, simulations of the USN and FMS F/A-18 landing gear configurations were run under identical conditions. A limited amount of correlated input data was available (much of it came from the gear vendor's original analysis).

For this comparison, the aircraft is taxiing at 110 knots and the gear is disturbed with an initial 40 in/sec lateral deflection rate. Figure 9 shows the lateral deflection of the axle as a function of time. As shown in Fig. 9a, the USN configuration with a launch bar is stable and the oscillations decay. When the launch bar inertia and collar damping friction are removed, as for the Spanish FMS gear (Fig. 9b), the model predicts a limit cycle oscillation will result for this condition.

5. CONCLUSIONS

Based on experiences described here with the FMS F/A-18A, the current FMS version of the F/A-18C/D retains the launch bar to ensure dynamic stability of the nose gear.

The analytical model described was developed partially in response to the problems encountered with the F/A-18A. The model has demonstrated good qualitative agreement with the F-15 and F/A-18A nose landing gears and stands ready to aid designers and dynamicists in assessing the shimmy properties of future MDA landing gear designs.

Future analytical work may center on correlating the model with quantitative test data and in developing guidelines for assigning values to the parameters. The large amount of data required by this model is regarded as a drawback. Sensitivity analysis could be used to determine the relative importance of each parameter to the final result.

ACKNOWLEDGMENTS

The author wishes to thank Prof. C. R. Barker and Prof. L. R. Koval of the University of Missouri-Rolla, who were the principal investigators in developing the analytical model described here; and Jeff Pew and Suresh Patel who were involved with the design and analysis of shimmy corrections for the FMS F/A-18 gear.

Thanks also to Craig Beebe, Pauline Bowermaster, Tom Burkhart, Matt Jansen, and Bill Macy of MDA who have been involved in the analysis and correction effort and who offered comments and suggestions for this paper. The encouragement of Terry Rodewald and John Coyle, both also of MDA, is acknowledged.

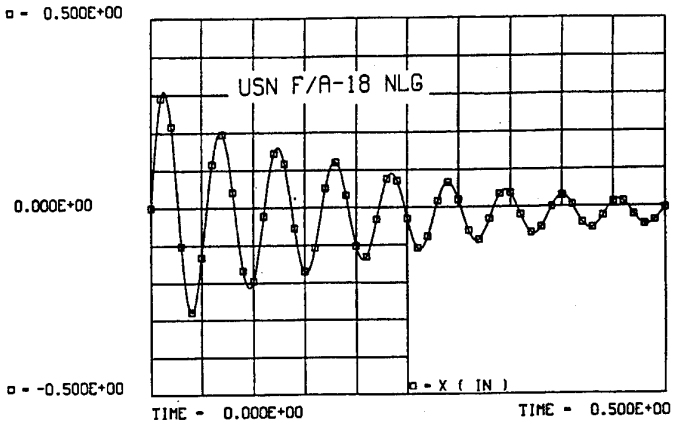

Fig. 9a. Simulation of F/A-18A (USN)

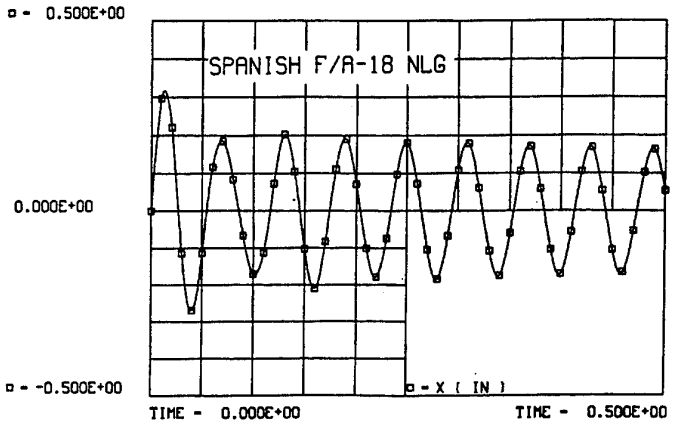

Fig. 9b. Simulation of F/A-18A (FMS)

REFERENCES

[1] vonSchlippe, B., and Dietrich, R., "Shimmying of a Pneumatic Wheel," Papers on Shimmy and Rolling Behavior of Landing Gears presented at the Stuttgart Conference, October 16-17, 1941. NACA TM 1365, August 1954.

[2] Moreland, W. J., "The Story of Shimmy," Journal of the Aeronautical Sciences, December 1954, pp. 793-808.

[3] Collins, R. L., Theories on the Mechanics of Tires and their Applications to Shimmy Analysis," AIAA Journal of Aircraft, Vol. 8, No. 4, April 1971, pp. 271-277.

[4] Black, R. J., "Application of Tire Dynamics to Aircraft Landing Gear Design Analysis," NASA CP-2264, Workshop on "Tire Modeling," at Langley Research Center, September 7 - 9, 1982, pp. 71-93.

[5] Southerland, K. F., "Shimmy Analysis for the F-15 Nose Landing Gear Report," McDonnell Aircraft Company Report MDC A0932, March 1971.

[6] Grossman, D. T., "F-15 Nose Landing Gear Shimmy, Taxi Test and Correlative Analysis," SAE Paper 801239, October 1980.

[7] Baumann, J., Barker, C. R., Koval, L. R., "A Nonlinear Model for Landing Gear Shimmy," presented at the ASME Winter Annual Meeting in Atlanta, GA, December 1-6, 1991. ASME 91-WA-DSC-14

[8] Baumann, J., "Aircraft Landing Gear Shimmy," Ph.D. Dissertation, University of Missouri-Rolla, 1992.

[9] Ranson, S. M., Jurd, K. W., and Ford, N. J., "Hornet Nose Wheel Shimmy Evaluation," July 1992, Royal Australian Air Force Report AR-006-562.

REPORT DOCUMENTATION PAGE

1. Recipient's Reference	2. Originator's Reference	3. Further Reference	4. Security Classification of Document
	AGARD-R-800	ISBN 92-836-1032-6	UNCLASSIFIED/ UNLIMITED

5. Originator Advisory Group for Aerospace Research and Development
North Atlantic Treaty Organization
7 rue Ancelle, 92200 Neuilly-sur-Seine, France

6. Title

The Design, Qualification and Maintenance of Vibration-Free Landing Gear

7. Presented at/sponsored by

The 81st Meeting of the AGARD Structures and Materials Panel,
held in Banff, Canada 4-5 October 1995.

8. Author(s)/Editor(s)	9. Date
Multiple	March 1996
10. Author's/Editor's Address	**11. Pages**
Multiple	156

12. Distribution Statement There are no restrictions on the distribution of this document. Information about the availability of this and other AGARD unclassified publications is given on the back cover.

13. Keywords/Descriptors

Landing gear	Stability
Aircraft landing	Landing simulation
Aircraft	Design
Vibration	Maintenance
Damage	Vibration analysis

14. Abstract

The Structures and Materials Panel of AGARD sponsored a Workshop focusing on the various vibrational and stability problems (e.g. shimmy, antiskid induced vibrations) that must be considered in the early design phase of landing gear systems, especially problems which are related to vibrations of the combined structural system formed by the landing gear, its tyres and the flexible aircraft structure. The intention was to indicate the impact of (combined) landing gear/aircraft vibration problems on aircraft design and to discuss the state-of-the-art technology in this area and to define possible future steps of development.

AGARD

NATO OTAN

7 RUE ANCELLE • 92200 NEUILLY-SUR-SEINE

FRANCE

Télécopie (1)47.38.57.99 • Télex 610 176

DIFFUSION DES PUBLICATIONS

AGARD NON CLASSIFIEES

Aucun stock de publications n'a existé à AGARD. A partir de 1993, AGARD détiendra un stock limité des publications associées aux cycles de conférences et cours spéciaux ainsi que les AGARDographies et les rapports des groupes de travail, organisés et publiés à partir de 1993 inclus. Les demandes de renseignements doivent être adressées à AGARD par lettre ou par fax à l'adresse indiquée ci-dessus. *Veuillez ne pas téléphoner.* La diffusion initiale de toutes les publications de l'AGARD est effectuée auprès des pays membres de l'OTAN par l'intermédiaire des centres de distribution nationaux indiqués ci-dessous. Des exemplaires supplémentaires peuvent parfois être obtenus auprès de ces centres (à l'exception des Etats-Unis). Si vous souhaitez recevoir toutes les publications de l'AGARD, ou simplement celles qui concernent certains Panels, vous pouvez demander à être inclu sur la liste d'envoi de l'un de ces centres. Les publications de l'AGARD sont en vente auprès des agences indiquées ci-dessous, sous forme de photocopie ou de microfiche.

CENTRES DE DIFFUSION NATIONAUX

ALLEMAGNE
Fachinformationszentrum Karlsruhe
D-76344 Eggenstein-Leopoldshafen 2

BELGIQUE
Coordonnateur AGARD-VSL
Etat-major de la Force aérienne
Quartier Reine Elisabeth
Rue d'Evere, 1140 Bruxelles

CANADA
Directeur, Services d'information scientifique
Ministère de la Défense nationale
Ottawa, Ontario K1A 0K2

DANEMARK
Danish Defence Research Establishment
Ryvangs Allé 1
P.O. Box 2715
DK-2100 Copenhagen Ø

ESPAGNE
INTA (AGARD Publications)
Pintor Rosales 34
28008 Madrid

ETATS-UNIS
NASA Headquarters
Code JOB-1
Washington, D.C. 20546

FRANCE
O.N.E.R.A. (Direction)
29, Avenue de la Division Leclerc
92322 Châtillon Cedex

GRECE
Hellenic Air Force
Air War College
Scientific and Technical Library
Dekelia Air Force Base
Dekelia, Athens TGA 1010

ISLANDE
Director of Aviation
c/o Flugrad
Reykjavik

ITALIE
Aeronautica Militare
Ufficio del Delegato Nazionale all'AGARD
Aeroporto Pratica di Mare
00040 Pomezia (Roma)

LUXEMBOURG
Voir Belgique

NORVEGE
Norwegian Defence Research Establishment
Attn: Biblioteket
P.O. Box 25
N-2007 Kjeller

PAYS-BAS
Netherlands Delegation to AGARD
National Aerospace Laboratory NLR
P.O. Box 90502
1006 BM Amsterdam

PORTUGAL
Estado Maior da Força Aérea
SDFA - Centro de Documentação
Alfragide
2700 Amadora

ROYAUME-UNI
Defence Research Information Centre
Kentigern House
65 Brown Street
Glasgow G2 8EX

TURQUIE
Millî Savunma Başkanliği (MSB)
ARGE Dairesi Başkanliği (MSB)
06650 Bakanliklar-Ankara

Le centre de distribution national des Etats-Unis ne détient PAS de stocks des publications de l'AGARD.
D'éventuelles demandes de photocopies doivent être formulées directement auprès du NASA Center for AeroSpace Information (CASI) à l'adresse ci-dessous. Toute notification de changement d'adresse doit être fait également auprès de CASI.

AGENCES DE VENTE

NASA Center for
AeroSpace Information (CASI)
800 Elkridge Landing Road
Linthicum Heights, MD 21090-2934
Etats-Unis

ESA/Information Retrieval Service
European Space Agency
10, rue Mario Nikis
75015 Paris
France

The British Library
Document Supply Division
Boston Spa, Wetherby
West Yorkshire LS23 7BQ
Royaume-Uni

Les demandes de microfiches ou de photocopies de documents AGARD (y compris les demandes faites auprès du CASI) doivent comporter la dénomination AGARD, ainsi que le numéro de série d'AGARD (par exemple AGARD-AG-315). Des informations analogues, telles que le titre et la date de publication sont souhaitables. Veuiller noter qu'il y a lieu de spécifier AGARD-R-nnn et AGARD-AR-nnn lors de la commande des rapports AGARD et des rapports consultatifs AGARD respectivement. Des références bibliographiques complètes ainsi que des résumés des publications AGARD figurent dans les journaux suivants:

Scientific and Technical Aerospace Reports (STAR)
publié par la NASA Scientific and Technical
Information Division
NASA Headquarters (JTT)
Washington D.C. 20546
Etats-Unis

Government Reports Announcements and Index (GRA&I)
publié par le National Technical Information Service
Springfield
Virginia 22161
Etats-Unis
(accessible également en mode interactif dans la base de
données bibliographiques en ligne du NTIS, et sur CD-ROM)

Imprimé par le Groupe Communication Canada
45, boul. Sacré-Cœur, Hull (Québec), Canada K1A 0S7

AGARD

NATO OTAN

7 RUE ANCELLE • 92200 NEUILLY-SUR-SEINE

FRANCE

Telefax (1)47.38.57.99 • Telex 610 176

DISTRIBUTION OF UNCLASSIFIED

AGARD PUBLICATIONS

AGARD holds limited quantities of the publications that accompanied Lecture Series and Special Courses held in 1993 or later, and of AGARDographs and Working Group reports published from 1993 onward. For details, write or send a telefax to the address given above. *Please do not telephone.*

AGARD does not hold stocks of publications that accompanied earlier Lecture Series or Courses or of any other publications. Initial distribution of all AGARD publications is made to NATO nations through the National Distribution Centres listed below. Further copies are sometimes available from these centres (except in the United States). If you have a need to receive all AGARD publications, or just those relating to one or more specific AGARD Panels, they may be willing to include you (or your organisation) on their distribution list. AGARD publications may be purchased from the Sales Agencies listed below, in photocopy or microfiche form.

NATIONAL DISTRIBUTION CENTRES

BELGIUM
Coordonnateur AGARD — VSL
Etat-major de la Force aérienne
Quartier Reine Elisabeth
Rue d'Evere, 1140 Bruxelles

CANADA
Director Scientific Information Services
Dept of National Defence
Ottawa, Ontario K1A 0K2

DENMARK
Danish Defence Research Establishment
Ryvangs Allé 1
P.O. Box 2715
DK-2100 Copenhagen Ø

FRANCE
O.N.E.R.A. (Direction)
29 Avenue de la Division Leclerc
92322 Châtillon Cedex

GERMANY
Fachinformationszentrum Karlsruhe
D-76344 Eggenstein-Leopoldshafen 2

GREECE
Hellenic Air Force
Air War College
Scientific and Technical Library
Dekelia Air Force Base
Dekelia, Athens TGA 1010

ICELAND
Director of Aviation
c/o Flugrad
Reykjavik

ITALY
Aeronautica Militare
Ufficio del Delegato Nazionale all'AGARD
Aeroporto Pratica di Mare
00040 Pomezia (Roma)

LUXEMBOURG
See Belgium

NETHERLANDS
Netherlands Delegation to AGARD
National Aerospace Laboratory, NLR
P.O. Box 90502
1006 BM Amsterdam

NORWAY
Norwegian Defence Research Establishment
Attn: Biblioteket
P.O. Box 25
N-2007 Kjeller

PORTUGAL
Estado Maior da Força Aérea
SDFA - Centro de Documentação
Alfragide
2700 Amadora

SPAIN
INTA (AGARD Publications)
Pintor Rosales 34
28008 Madrid

TURKEY
Millî Savunma Başkanliği (MSB)
ARGE Dairesi Başkanliği (MSB)
06650 Bakanliklar-Ankara

UNITED KINGDOM
Defence Research Information Centre
Kentigern House
65 Brown Street
Glasgow G2 8EX

UNITED STATES
NASA Headquarters
Code JOB-1
Washington, D.C. 20546

The United States National Distribution Centre does NOT hold stocks of AGARD publications.
Applications for copies should be made direct to the NASA Center for AeroSpace Information (CASI) at the address below. Change of address requests should also go to CASI.

SALES AGENCIES

NASA Center for
AeroSpace Information (CASI)
800 Elkridge Landing Road
Linthicum Heights, MD 21090-2934
United States

ESA/Information Retrieval Service
European Space Agency
10, rue Mario Nikis
75015 Paris
France

The British Library
Document Supply Centre
Boston Spa, Wetherby
West Yorkshire LS23 7BQ
United Kingdom

Requests for microfiches or photocopies of AGARD documents (including requests to CASI) should include the word 'AGARD' and the AGARD serial number (for example AGARD-AG-315). Collateral information such as title and publication date is desirable. Note that AGARD Reports and Advisory Reports should be specified as AGARD-R-nnn and AGARD-AR-nnn, respectively. Full bibliographical references and abstracts of AGARD publications are given in the following journals:

Scientific and Technical Aerospace Reports (STAR)
published by NASA Scientific and Technical
Information Division
NASA Headquarters (JTT)
Washington D.C. 20546
United States

Government Reports Announcements and Index (GRA&I)
published by the National Technical Information Service
Springfield
Virginia 22161
United States
(also available online in the NTIS Bibliographic
Database or on CD-ROM)

Printed by Canada Communication Group
45 Sacré-Cœur Blvd., Hull (Québec), Canada K1A 0S7

ISBN 92-836-1032-6